

Decomposition, Ignition and Flame Spread on Furnishing Materials

A thesis submitted in fulfillment of the requirement
for the degree of
Doctor of Philosophy

by

Yun Jiang

Centre for Environment Safety and Risk Engineering
Victoria University, Australia

2006

ABSTRACT

The general aim of this research is to find an effective and applicable method for prediction of pyrolysis and ignition of certain furnishing materials in a real fire environment. Current methods for combustion behaviour investigation use standardized bench-scale experiments, such as cone calorimeter, Single Burning Item (SBI) and Lateral Ignition and Flame Transport (LIFT) tests, to extensively and systematically collect data on the ignitability of materials. The test data are useful for classification and evaluation of various building materials, and even for computational schemes. However there are still serious limitations in applying such experimental data directly on to the modelling of ignition and flame spread under real fire environments when complicated geometry and flow conditions are major concern. Meanwhile, current commonly used criteria for determination of ignition of solid fuels were found incapable or inaccurate for the ignition prediction in the complicated environments.

In the current study, certain furnishing materials, timbers, polyurethane foams and fabrics, were chosen for research purposes. Some basic thermal properties of these furnishing materials, such as thermal kinetic parameters and characteristic temperatures, were measured. These thermal properties are critical for a better understanding of thermal decomposition and ignition processes. Then they were applied to heat transfer and thermal analysis through computer modelling to describe the decomposition process. Series of bench-scale tests were carried out to construct a physical platform for modelling and provide test results for validating of the modelling. Through fire modelling, various criteria for ignition were investigated and compared with the test results. Particularly, a gas phase parameter, mixture fraction, was validated against the lean flammability limitation theory and relationship between them was found. Finally, based on the comparison and analysis, a set of robust and accurate criteria, based on the critical mixture fraction, was promoted for ignition and flame spread prediction as well as for improvement of current pyrolysis and ignition models.

Decomposition process of the solid materials was investigated by thermogravimetric analysis (TGA) test. Through current TGA tests, two sets of kinetics were observed in low

and high heating rate ranges. The kinetics obtained from low heating rate is considered close to their intrinsic values. The kinetics obtained from the higher heating rate range is believed to be much more useful and effective in describing the pyrolysis process of real fire conditions. Meanwhile Agrawal's shifting pattern for a linear relationship between heating rate and reaction rate in the high heating rate range was also found for the studied materials. This shifting pattern provides the possibility to apply the "effective" kinetics to further pyrolysis analysis and ignition prediction in real fire conditions.

Atreya's one-step global reaction pyrolysis model was used in the decomposition modelling. A CFD model, Fire Dynamics Simulator (FDS), which is based on Atreya's pyrolysis and heat transfer model, was used to perform the numerical simulation. By applying the "effective" kinetics obtained from previously specified higher heating rate range TGA tests for timber materials, a set of parameters describing the pyrolysis process was then obtained from the simulations. These parameters include surface temperature, surface mass flux, and mixture fraction. The simulated temperatures and mass fluxes match with the data from the bench-scale cone calorimeter tests reasonably well.

Based on the lean flammability theory a critical mixture fraction concept was developed for prediction of ignition phenomenon. Comparing with other commonly adopted ignition criteria, such as critical surface temperature and critical mass flux, the critical mixture fraction approach has the distinct advantage of being able to represent the mixture of pyrolysis product and an oxidant, and the gas phase distribution of combustibles. By carrying out numerical computation via FDS, distribution of the mixture fraction was obtained. A relationship between this critical mixture fraction (at the ignition time determined by previous cone calorimeter tests) and the lower flammable limit (LFL) has been observed. A computation and prediction scheme for ignition of solid fuels was then developed.

Through the study, a practical engineering approach to apply kinetics in the description of decomposition and ignition has been built up. By adopting the critical mixture fraction, the developed computation and prediction scheme is able extended to wider materials and complicated fire environments to achieve a more accurate prediction without extensive bench-scale tests.

ACKNOWLEDGEMENTS

The author wishes to acknowledge:

- The endless support, encouragement and patience from his family.
- The supervision of Professor Ian Thomas and Dr. Yaping He, and also the assistance from all staff at the Centre for Environment Safety and Risk Engineering, Victoria University of Technology.
- Dr Justin Leonard, Division of Building, Construction and Engineering, CSIRO, for his instruction and assistance on operation of cone calorimeter tests.
- Professor Robert Shanks in Applied Chemistry, RMIT University, for providing access to a Thermogravimetric analyser and guidance on the experiments.
- Kevin McGrattan and Simo Hostikka, authors of the Fire Dynamics Simulator, for their instruction on simulation and unpublished key functions of the model.

DECLARATION

I, Yun Jiang, declare that the PhD thesis entitled **Decomposition, Ignition and Flame Spread on Furnishing Materials** is no more than 100,000 words in length, exclusive of tables, figures, appendices, references and footnotes. This thesis contains no material that has been submitted previously, in whole or in part, for the award of any other academic degree or diploma. Except where otherwise indicated, this thesis is my own work.

Signature

Date

TABLE OF CONTENTS

ABSTRACT	ii
ACKNOWLEDGEMENTS	iv
DECLARATION	v
NOTATION	xi
LIST OF ABBREVIATIONS	xv
Chapter 1 INTRODUCTION	1
1.1 Background	1
1.2 Research Requirements for Ignition and Flame Spread Phenomena of Solid Materials	3
1.2.1 Thermal decomposition and kinetics	3
1.2.2 Combustion models and numerical solutions	4
1.2.3 Furnishing materials	6
1.3 Aims of Research	7
1.4 Significance of Research	7
1.5 Research Methodology	8
1.5.1 General methodology	8
1.5.2 Methods involved in key activities	8
1.6 Brief Overview of this Thesis	9
Chapter 2 LITERATURE REVIEW	11
2.1 Background	11
2.2 Fire Models	15
2.2.1 Zone models	15
2.2.2 Field models	18
2.2.2.1 Computational Fluid Dynamics (CFD) basics	18
2.2.2.2 Turbulence	20
2.2.3 Comparison between the zone and field models	21
2.3 Thermal Decomposition	22
2.3.1 Physical and chemical processes	23
2.3.2 Kinetics	25
2.3.3 Decomposition of the furnishing materials	27
2.3.3.1 Pyrolysis and charring of wood	28
2.3.3.2 Role of moisture content	30
2.4 Ignition Controlling Mechanism	31

2.4.1	Auto Ignition	32
2.4.1.1	Solid heating and gasification	34
2.4.1.2	Gas phase reaction	38
2.4.1.3	Ignition time, t_{ig}	40
2.4.1.4	High surface temperature ignition	40
2.4.2	Piloted ignition	41
2.4.3	Ignition criteria	42
2.4.3.1	Critical surface temperature	43
2.4.3.2	Critical mass flux	45
2.4.3.3	Lower flammable limit and possible criteria in gas phase	46
2.5	Flame Spread on Solid Combustible Surfaces	50
2.5.1	Flame spread mechanism	50
2.5.2	Material properties and measurement for the flame spread	53
2.6	Experimental Methods	53
2.6.1	Thermogravimetric analysis (TGA)	54
2.6.2	Cone calorimeter	56
2.6.3	LIFT and SBI	57
2.6.4	Applications of the experimental methods	58
2.7	Unresolved Phenomena and Research Interests	60
2.7.1	Unresolved issues related to current research	60
2.7.2	Research interests and requirements identified for current study	62
Chapter 3	MODELLING OF THERMAL DECOMPOSITION AND IGNITION OF SOLID MATERIALS	64
3.1	Pyrolysis and Ignition Models	64
3.1.1	Classification of pyrolysis models	64
3.1.2	Typical pyrolysis models	66
3.1.3	Criteria of model selection for current research	68
3.2	Atreya's One-dimensional Heat Transfer and Pyrolysis Model	70
3.2.1	Basics of Atreya's pyrolysis model	70
3.2.1.1	Physical model	70
3.2.1.2	Four stages of wood pyrolysis	71
3.2.2	Basic equations and assumptions	73
3.3	Improvements and Applications for Atreya's Model	75
3.3.1	Improvement by Parker	75
3.3.2	Improvement by Ritchie <i>et al.</i>	76
3.4	Calculation for a Studied Material Based on Atreya's Model	78
3.4.1	Thermal properties of studied material	78
3.4.2	Calculation results from Atreya's model	79
3.5	Summary	80

Chapter 4	EXPERIMENTAL DECOMPOSITION STUDY FOR THE FURNISHING MATERIALS	81
4.1	TGA Experiment and its Application	81
4.1.1	TGA apparatus, principle and test procedure	81
4.1.2	Research methodology	83
4.1.2.1	Curve trend and characteristic temperatures	83
4.1.2.2	Kinetics and calculation method	84
4.1.2.3	Concern for test conditions and computation schemes	88
4.1.2.4	Relationships among the parameters	90
4.2	Current TGA Test Results	92
4.2.1	Experimental materials and apparatus	92
4.2.1.1	Details of materials	92
4.2.1.2	Apparatus and test conditions	93
4.2.1.3	Calibration	93
4.2.2	Measurement of thermal characteristics of the materials	93
4.2.2.1	Decomposition process	94
4.2.2.2	Effect of heating rate	97
4.2.3	Thermal dynamic parameters and behaviours	101
4.2.3.1	Activation energy and pre-exponential factor	101
4.2.3.2	Linear relationships and shifting pattern	104
4.2.4	Isothermal test	106
4.3	Summary	108
Chapter 5	CONE CALORIMETER STUDY FOR IGNITION PROPERTIES	110
5.1	Heat Release Rate Measurement	111
5.1.1	Oxygen consumption method	111
5.1.2	Cone calorimeter	112
5.2	Calibration and Operation of Cone Calorimeter	115
5.2.1	Calibration of cone calorimeter	115
5.2.2	Experiment procedure	117
5.2.2.1	Testing materials and preparation	117
5.2.2.2	Testing condition and data sampling	119
5.3	Experimental Results	120
5.3.1	Ignition time	120
5.3.1.1	Tested results	120
5.3.1.2	Linear relationship between $t_{ig}^{-0.5}$ vs radiation	121
5.3.1.3	Determining the critical radiative flux	123
5.3.1.4	Effect of sample thickness	124
5.3.1.5	Comparison with results from others	125
5.3.2	Heat release	125
5.3.2.1	Heat release rate	126
5.3.2.2	Total heat released	130

5.3.3	Mass loss rate and effective heat of combustion	130
5.3.4	Species yield	134
5.4	Surface Temperature Measurement	139
5.4.1	Surface temperature	139
5.4.2	Temperature rising rate	144
5.5	Summary of the Cone Calorimeter Test Results	145
Chapter 6	SIMULATING PYROLYSIS AND IGNITION BY FDS FOR THE WOODS	148
6.1	FDS Modelling for Pyrolysis and Combustion	148
6.1.1	Principle of FDS model	149
6.1.1.1	History of major developments	150
6.1.1.2	Mixture fraction combustion model	151
6.1.1.3	Pyrolysis and charring models in FDS	153
6.1.1.4	Ignition criteria in FDS	154
6.1.2	Treatment of thermal parameters for timber in FDS simulation	155
6.1.2.1	Mixture fraction relation for timber	155
6.1.2.2	Calculation for the thermal dynamic parameters	157
6.2	Setting Up and Running of FDS Simulations	159
6.2.1	General setting	159
6.2.1.1	Simulation domain and grid size	159
6.2.1.2	“Cone” heater	161
6.2.2	Heater temperature and heat flux	161
6.2.3	Cell grid	164
6.2.4	Summary of input parameters in FDS simulation	168
6.3	Simulation Results	169
6.3.1	Observation of initial flame development	169
6.3.2	Surface temperature	174
6.3.3	Heat release rate	175
6.3.4	Mass flux	177
6.3.5	Direct Numerical Simulation	181
6.3.6	Comparison on results from different E and A values	182
6.3.7	Effect of sample thickness and backing material	183
6.4	Distribution of Pyrolysis Products	186
6.5	Summary of the Simulation Results	188
Chapter 7	CRITERIA FOR IGNITION AND DISCUSSION	191
7.1	Further Discussion of Ignition in FDS	191
7.2	Comparison Between the Simulation and Experimental Data	194
7.2.1	Critical ignition temperature	195
7.2.2	Critical mass flux	195

7.2.3	Critical mixture fraction	196
7.3	Special Consideration for the Critical Mixture Fraction	197
7.3.1	Relationship between the critical mixture fraction and the LFL	197
7.3.1.1	Calculation of LFL for timber	197
7.3.1.2	Converting the mixture fraction into volume fraction	198
7.3.2	Discussion for the suggested criterion	200
Chapter 8	CONCLUSIONS AND RECOMMENDATIONS FOR FURTHER RESEARCH	203
8.1	Conclusion	203
8.2	Further Research Recommendations	204
	APPENDIX A. TGA TEST SETTINGS AND RESULTS	206
	APPENDIX B. CONE CALORIMETER TEST SETTINGS AND RESULTS	209
	APPENDIX C. ANALYSIS AND COMPUTATION OF ATREYA'S PYROLYSIS MODEL	216
	REFERENCES	223

NOTATION

A	pre-exponential factor in Arrhenius equation (1/s)
$[A]$	concentration of the reactant A (mol/m ³)
B	body force in momentum conservation equation (N)
c	specific heat (J/kg·K)
c_p	isobaric specific heat (J/kg·K)
c_v	isochoric specific heat (J/kg·K)
C	coefficient for linearized radiative heat transfer (kW/m ²)
C_i	volume percent of fuel, i , in fuel/air mixture
D_p	degree of polymerization, number of monomer units per polymer chain
e	base of natural logarithms
E	activation energy (kJ/mol)
E_{HPM}	heat release per mass unit of oxygen consumed (kJ/kg)
F	external heat flux (kW/m ²)
h	static (thermodynamic) enthalpy (J/kg)
h	heat transfer coefficient (kW/m ² ·K)
H	total enthalpy (J/kg)
H	reaction rate (1/s)
H_{remove}	rate of heat removed from solid surface (W/m ² ·K)
ΔH_c	heat of combustion (kJ/kg)
k	turbulent kinetic energy in k - ϵ equation
k	reaction rate constant (1/s)
L	slab thickness (m)
L	effective heat of gasification (kJ/kg)
L_{phy}	physical length in thermal thickness judgment (m)
$L_{thermal}$	thermal length characteristic in thermal thickness judgment (m)
L_v	heat of vaporization (kJ/kg)
M	mass of material (kg)
MW_i	molecular weight for species i (g/mol)
\dot{m}	mass flow rate (kg/s)
m''	mass flux (kg/m ² ·s)
n	reaction order
p_F	pressure fraction of fuel

q''	heat flux per unit area (W/m^2)
q''_{rad}	external radiation flux (W/m^2)
q''_{rs}	re-radiation flux from the solid surface (W/m^2)
Q'''	critical energy density (kJ/m^3)
r	radius (m)
R	universal gas constant, $= 8.314 \times 10^{-3}$ ($\text{kJ}/\text{mol} \cdot \text{K}$)
$R_{i,cr}$	critical values in ignition criteria for item i , ($i=1, 2, \dots$)
s	solid fuel thickness (m)
s	ratio of consumption rates for the fuel and oxygen in FDS
S	section area (m^2)
S	source or sink in mass conservation equation
t	time (s)
t_{in}	gas induction time (s)
T	temperature (K)
$T_{f,LFL}$	adiabatic flame temperature of a lower flammable limit mixture (K)
u	velocity parallel to the solid surface (m/s)
u_∞	forced flow free stream velocity (m/s)
U	fluid velocity vector (m/s)
v	velocity (m/s)
v_i	stoichiometric coefficient for species i
W	sample weight (kg)
W_∞	final sample weight (kg)
x	fraction of conversion of sample weight
x	coordinate parallel to the solid surface
y	coordinate normal to the solid surface
Y	mass fraction
Z	mixture fraction (kg/kg)
	$Z_{\text{-surface}}$: mixture fraction at surface of solid;
	$Z_{\text{-plug}}$: mixture fraction at the spark plug in cone calorimeter

Greek Symbols

α	thermal diffusivity (m^2/s)
----------	-----------------------------------------------

β	non-dimensional parameter in gas phase ignition analysis, $\beta = T_{\infty} c_p / Y_{F,s} \Delta H_c$
β	linear heating rate (K/s)
Γ	non-dimensional parameter in gas phase ignition analysis, $\Gamma = 4c(E/RT_{\infty})[(2-\beta)/(e^2(1-\beta^2))]$
δ	boundary layer thickness (m)
ε	local energy in k - ε equation
λ	thermal conductivity (W/m·K)
ϕ	combustion efficiency
ϕ	item in measurement of flame heat transfer item
Λ_0	characteristic Damkohler number in the stagnation point flow ignition analysis
μ	molecular viscosity (kg/m·s)
ν	kinematic viscosity (m ² /s)
ρ	density (kg/m ³)
σ	item in momentum conservation equation
σ	Stefan-Boltzmann radiation constant (W/m ² ·K)
σ	non-dimensional parameter in gas phase ignition analysis, $\sigma = \Lambda_0(1 - \exp(-4u_{\infty}t/y))/(cE/RT_{\infty})$

Subscripts

a	active
air	air
c	char
cr	critical
eff	effective
ev	evaporation
f	flame
F	fuel
g	gas
I	initial
ig	ignition

Inert	inert
m	moisture
max	maximum
min	minimum
oxy	oxygen
pd	product
py	pyrolysis
s	surface
samp	sample
solid	solid phase
spec	species
∞	Ambient or final
w	wood

Superscripts

*	Non-dimensional parameter
–	average
”	flux
•	flow rate

LIST OF ABBREVIATIONS

ASTM	American Society for Testing and Materials
CFD	computational fluid dynamics
DNS	direct numerical simulation
DTG	differential thermogravimetric
FDS	Fire Dynamics Simulator, a fire model developed at NIST
FIST	Forced-flow Ignition and flame-Spread Test
FSE	Fire Safety Engineering
FSP	Fibre Saturation Point
FVM	Finite volume method
HRR	heat release rate
HRRPUV	heat release rate per unit volume
LES	Large Eddy Simulation
LFL	lower flammable limit
LIFT	Lateral Ignition and Flame Transport
LOI	lower oxygen index
MF	mixture fraction
MLR	mass loss rate
MW	molecular weight
N-S	Navier-Stokes (equation)
ODE	ordinary differential equations
OFW	Ozawa-Flynn-Wall method
PDE	partial differential equations
PMMA	polymethylmethacrylate
PU	Polyurethane foam
SBI	Single Burning Item
TG	thermogravimetric
TGA	Thermogravimetric analysis
THR	total heat released
VF	volume fraction

CHAPTER 1 INTRODUCTION

1.1 Background

The key to widely and effectively applying performance-based building design and risk assessment is to quantitatively predict fire behaviour and performance of buildings and components. Performance-based building codes have been introduced into more and more countries, including Australia, since the 1990s. Performance-based building design enables engineers to evaluate the performance of buildings and components by considering a wide range of realistic fires. This provides great flexibility for adopting new concepts, materials and technologies in building designs, while simultaneously achieving lower costs and lower risk to life. The performance-based approach is usually achieved by some type of performance-oriented model as a design and assessment tool. CESARE-RISK is such an example (Beck 1998). Among all sub-models in a performance-based building design and risk assessment model, the combustion and fire growth model, which describes the fire origin and development, is the cornerstone. It provides various outputs as critical inputs for other sub-models to assess building damage and risk to life, through barrier failure model, economic model, smoke spread model, and human behaviour and evacuation models. Therefore, a better understanding of real fire development and building performance in fires is a foundation for performance-based design and risk assessment tasks.

Today there are several standardized experimental methods to measure the performance of materials and components in fire environments, as the basis for prediction of fire behaviour.

These experimental methods include:

- bench-scale testing devices, such as the cone calorimeter (Babrauskas 1984) and the Lateral Ignition and Flame Transport (LIFT) (Quintiere 1981)
- middle-scale testing devices, like the Single Burning Item (SBI) (Mierlo 1998), and the furniture calorimeter
- full-scale methods, such as the room/corner burning test and room calorimeter (ASTM 1983).

These methods have been used in many international projects, such as the SBI Round Robin Tests (Mierlo 1997; VTT 1997) and the Cone Calorimeter Inter-laboratory Trials (ASTM 1990). These standardized experimental methods play an important role in establishing databases for assessing material properties, material performance, and combustion behaviour in fire environments.

However, due to the huge variety of building materials and their combinations as building structures and components, it is impossible to test every material and structural configuration in the various scale tests. There are also significant differences between standardized testing conditions and fire environments that occur in buildings, due to the variety and complexity of building geometries and ventilation conditions. Therefore experimental methods cannot be the exhaustive means of investigation of fire performance.

Modelling is another way to study building performance under fire conditions. A fire model is a statement in mathematical language to describe fire phenomena. Fire models now are able to simulate several aspects of fire scenarios (including geometry, ventilation, fuel configuration and even reaction of human beings) over an acceptable modelling duration. Fire modelling is an effective and economical approach for predicting a fire outcome before a fire happens and representing the history of fire development after it happens. During recent decades, fire models have greatly benefited from rapidly developing computer technology. Models available for fire engineers, which were once relatively primitive, are now comprehensive, and can deal with quite complicated phenomena.

There are still many challenges for today's fire models to achieve an applicable and acceptable performance for building fire scenarios (Cox 1994). Firstly the thermal properties of the fuels and other contents or materials in an enclosure must be known for inputting into the models. As indicated by Babrauskas (1996), "the most serious limitation, however, comes from the fact that essential items of fire physics and chemistry are missing from even the best of the existing models." Secondly, the fire models should be robust and usable by fire protection engineers. A good fire model should deal with as many details as possible within an acceptable duration of computation. Finally, prediction of real fires must be validated by experimental results and on-site fire surveys (after a fire incident has happened). Currently adopted ignition criteria are still questionable against on wider variety of fuel materials and conditions. Bridging gaps between current fire models and their

application in fire safety engineering is a critical task for today's fire research and a major aim of this study. To achieve this aim, quantitative analysis of basic aspects involving combustion and development of building fires is essential.

1.2 Research Requirements for Ignition and Flame Spread Phenomena of Solid Materials

As identified in the previous section, ignition and combustion phenomena are major research interests for this study. These phenomena involve basic aspects of physics and chemistry of fire. For example, a spreading flame includes many interactive sub-processes: fluid flow, heat and mass transfer, solid thermal decomposition, gas-phase chemical kinetics, etc. A comprehensive solution for modelling fire behaviours requires extensive knowledge of the phenomena, as well as the application of detailed modelling.

1.2.1 Thermal decomposition and kinetics

Ignition of solid materials can be thought of as a twofold process:

- the decomposition of the solid phase of fuel under an external heating source, and
- the release of volatile products and a gas phase oxidizing reaction.

These two processes are interlaced. When certain ignition criteria are reached, mainly in the gas phase, ignition takes place.

There is a long history of the study of thermal decomposition phenomena of solid fuels, starting with timber and coal. Beyler and Hirschler (2002) give a general and detailed description for the decomposition process of polymers (including timber and coal). A number of physical and chemical processes may be involved in thermal decomposition. These include melting, charring, and vaporization, *etc.* Beyler and Hirschler listed eight generic types of reaction involved in a simple decomposition process. They also indicated that the kinetics describing these reactions could be quite complex and unusable in engineering applications.

Therefore simple overall kinetic expressions are usually utilized as a reasonable engineering approach. It should be pointed out that nearly every current fire model, which deals with ignition and combustion of solid materials, involves simplification of one sort or another (Moghtaderi 2001). The most common assumption in such simplifications is that the reactions can be described by a one-step Arrhenius expression involving the remaining solid mass. However, characterizing those reactions or even defining a simplified overall decomposition process to represent those complicated reactions is still a challenge for today's fire models.

Several experimental methods have been developed for the study of thermal decomposition (Beyler and Hirschler 2002). Thermogravimetric analysis (TGA) is commonly used. The kinetics obtained from TGA tests have been adopted to describe either an overall thermal decomposition process (such as for a timber) or reactions by individual components (such as cellulose, hemicellulose and lignin in a timber) (Baker 1978). This method has been applied in fire safety science and engineering for many years. It is noted that there are still some limitations in this method due to the difference between the test conditions and real fire environments. One major issue is the lower heating rate normally adopted in the TGA tests. The normally adopted heating rate in a TGA test is lower than 30 K/min (0.5 K/s) while the rate of rising of surface temperature can reach a magnitude of 10 to 100 K/s in a real fire scenario (Beyler and Hirschler 2002). Therefore how to apply kinetics from this type of general-purpose chemical analysis test into description of thermal decomposition properly in a real fire condition still remains as one of the major tasks in solid pyrolysis study.

1.2.2 Combustion models and numerical solutions

Combustion models are a group of sub-models in fire models, dealing with various aspects of fire initiation and development. These sub-models simulate the pyrolysis of fuel, charring, ignition, flame spread over a solid surface, pool fire, radiation heat transfer and generation of combustion products. Based on modelling results from these sub-models, the combustion model predicts fire development and outcome, and provides two kinds of major information about a fire: heat release rate and product gases yield. This information is important for assessing either building damage or life safety. Therefore, the combustion model is a critical component within any fire model.

Depending on how many details are included, a combustion model can vary from a very simple, such as a plume model found in some early fire models, to a quite complicated comprehensive model which may include most of the above mentioned aspects of fire physics and chemistry.

Fire models are normally categorised into two types: zone models and field models, and the latter are also known as computational fluid dynamics (CFD) models. The zone models are based on a conceptual representation for the compartment fire process and are good approximations to reality for certain fires. When distinct phenomena are discerned and well isolated, they may provide the ability for better predictions of their roles in the compartment fire system (Quintiere 2002). By contrast, CFD models solve the governing equations by numerical methods and become a general tool for the analysis of the full breadth of fluid flow problems, including those associated with fire. The CFD type fire models are more capable of studying complicated compartment fire problems due to their ability to deal with fine grid details of phenomena, and provide much more accurate prediction for fire development.

However, CFD fire models also have limitations. It is impossible to model all details involved in combustion. First, due to a lack of better understanding of fire phenomena and dynamics, simplification is always necessary. For example, a global reaction is usually chosen to represent a complicated decomposition process. Secondly human expectations from the model usually tend to exceed computational capabilities because of the complexity of compartment fire. Cox and Kumar (2002) provide a simple example. To capture the details of a chemical reaction zone in a fire would require a characteristic mesh size below 1 mm. Such a computational mesh would require computer power and time that are affordable to only a few. In order to obtain solutions with reasonable accuracy and affordable resources, it is necessary to simplify the system of equations by some form of approximation.

Meanwhile for most current pyrolysis and ignition models, no matter what kind of numerical computation schemes adopted, no widely applicable ignition criteria available is a general and serious limitation. Currently adopted parameters, such as critical surface temperature, critical temperature rising rate, and critical pyrolysis rate, have been found

questionable and great variations have been reported for test data. This limitation will be reviewed in detail in next chapter.

To perform a detailed study on pyrolysis and ignition phenomena, including solid phase heat transfer and gas phase distribution, the CFD model is a suitable tool for this research. As mentioned before, choosing the details to be included or excluded is an important task in developing and using fire models. Improving computational schemes to find more efficient numerical solutions is another task. Finally, determining a set of applicable ignition criteria to wide application areas of fire modelling is also a challenge.

1.2.3 Furnishing materials

Furnishing materials often play an important role in a compartment fire. They can be not only the original fuel of fires, but also the means of flame spread in enclosures. Furnishing materials cover a wide range of materials, from natural materials, such as timber and cotton fabrics, to artificial polymers, such as PVC and polyurethane (PU) foam. Timber is often widely used as for structural components as well as for furniture material. Polyurethane foam is extensively used in mattresses and as cushions in sofas and chairs. Fabrics are a common material for covering these objects and as curtains. All these types of materials have been frequently related to fire initiation and flame spread in compartment fires (Ellis 1981; DeHaan 2002).

A great number of research projects have been undertaken on these materials, especially on timbers. These researches will be reviewed in some detail in Chapter 2. However, due to the variety and complexity of these materials, as well as the almost endless combinations of them, there is still much uncertainty remaining in modelling fire behaviours for these materials. In particular, knowledge of ignition criteria for many of these types of materials is quite limited. Therefore, two of each of these materials were chosen for the current research. Thermal decomposition and kinetics of these selected materials will be the key research interest since they determine the ignition phenomenon.

1.3 Aims of Research

The general aim of this research is to develop a new method to quantitatively describe pyrolysis, ignition and combustion processes for several furnishing materials.

By solving uncertainty and requirements that were identified in the previous section, this general aim has been achieved via the following sub-aims:

1. Improve an existing experimental and computational scheme to obtain kinetic data for the studied furnishing materials. The obtained kinetics are able to describe the thermal decomposition behaviour under real fire conditions.
2. Collect thermal properties of the thermal decomposition and ignition processes for the studied materials via various scaled experimental methods. These experimental data were used either to provide input information for further modelling or to validate the simulation results.
3. Identify an appropriate ignition criterion by applying previously obtained thermal properties into a pyrolysis and ignition model via a suitable numerical solution (CFD model).

1.4 Significance of Research

The significance of this research includes the following:

- Different decomposition behaviours under various environmental conditions have been observed for the studied furnishing materials. The conditions and limitations to apply a simplified overall decomposition model are identified. These contribute to a better understanding of the basic thermal decomposition of the materials.
- Applicable thermal kinetics have been obtained for the materials to describe the pyrolysis process in realistic fire conditions. These calculated parameters will enable more accurate modelling results to be generated. This has demonstrated an effective way to apply small-scale, basic thermal testing results into simulation of bench-scale to full-scale tests.
- Ignition and combustion properties under bench-scale tests have been obtained. These results have added to the knowledge database of the studied furnishing materials. The experimental data can be used to validate modelling results.

- A more widely applicable gas phase ignition criterion, critical mixture fraction, for the studied materials has been found which is satisfactory for engineering calculations. The criterion was found related to lean flammability limit theory. This provides the possibility to improve the current pyrolysis and ignition models and extend the application area of the models to more complicated environments accurately.

1.5 Research Methodology

1.5.1 General methodology

The following sequence has been adopted in this thesis, reflecting the generally accepted research methodology:

1. Literature review
2. Review and further development of theoretical modelling of pyrolysis and ignition processes for solid materials
3. Experimental studies of the thermal decomposition and ignition processes of the chosen furnishing materials. These tests include basic kinetic experiments and bench-scale tests for combustion behaviour
4. Computer modelling to simulate decomposition and ignition processes in the test environment
5. Analysis and discussion of ignition criteria leading to the proposal of a more applicable criterion

1.5.2 Methods involved in key activities

The methods adopted for the kinetics calculations are:

- Review and evaluate current experimental methods and calculation schemes for the decomposition and chemical kinetics
- Find some pattern or relationship to enable those parameters, which are used to describe an overall decomposition process, to be applicable in an environment closer to real fire conditions

- Determine the “effective” kinetics for the materials by the identified method

The methods involved in the collection of properties of pyrolysis and ignition processes are:

- Carry out bench-scale fire tests of the materials
- Measure ignition and combustion properties of the materials, especially for those related to ignition criteria
- Identify the factors affecting the ignition process

The methods involved in the evaluation of the pyrolysis model and its numerical solution are:

- Review available mathematical fire models dealing with ignition and combustion. The basic requirements will include a kinetic description for pyrolysis of charring materials, such as timber and fabrics
- Use a CFD model to perform the numerical solution for the mathematical model
- Run extensive simulations of the studied materials to obtain ignition properties, and the discrete relationship between those parameters

The methods involved in ignition criteria study are:

- Link and compare the experimental and modelled ignition properties for the studied materials
- Evaluate various ignition criteria for the materials against the experimental data and lean flammability theory
- Find one or several ignition criteria appropriate for the tested materials and compare and validate with the experimental data and research results obtained by others

1.6 Brief Overview of this Thesis

In line with this approach, this thesis has been organized in the following manner:

Chapter 2 is a general review of areas related to the current research. These include: fire models, thermal decomposition, ignition and criteria, flame spread mechanisms of solids, experimental methods, and thermal properties of the studied furnishing materials. Unsolved problems are also identified to define research areas and tasks.

Modelling for pyrolysis and flame spread on a solid is discussed in depth in Chapter 3. Various fire models involving ignition and combustion are evaluated and compared. Based on comparison and analysis, an appropriate pyrolysis model is then chosen as a prototype for the current research.

In Chapter 4, TGA experiments are carried out to determine the thermal properties of the studied materials. Based on the experimental data, kinetics are calculated for the materials. An application scheme to apply the “effective” kinetics into an environment closer to real fire conditions is then developed.

In Chapter 5, a set of bench-scale tests, cone calorimeter tests, are performed to obtain the ignition and combustion behaviours for the same materials. Some other parameters, such as surface temperature and ignition time that are helpful to validate the pyrolysis model, are also measured from the tests.

In Chapter 6, a CFD fire model is used to simulate the decomposition and ignition processes in a confined environment, simulating the cone calorimeter test. The thermal properties, including the kinetics obtained from the previous TGA tests, are used as input parameters. The simulation results are compared with and then validated by the cone calorimeter test data.

In Chapter 7, several available ignition criteria are compared with each other as well as the experimental data. Through analysis and discussion, a robust ignition criterion is then proposed.

A final summary and conclusion is given in Chapter 8.

CHAPTER 2 LITERATURE REVIEW

This review consists of seven sections. The first section briefly introduces the background of the current research. As indicated in the first chapter the research will focus on solid fuel ignition and combustion phenomena. Section 2.2 outlines computer fire models used in fire engineering. Two main kinds of computer fire models of fire in enclosures (zone and field models) are introduced briefly and compared. Section 2.3 reviews previous major research activities on thermal decomposition of solid materials and various schemes for determining the kinetics of decomposition. A special discussion of the decomposition process of timber is given in this section. The controlling mechanism of ignition of solid fuel is then described in Section 2.4. Major factors related to ignition as well as the criteria of ignition are reviewed. Section 2.5 describes the mechanism of flame spread on solid fuel materials. Experimental methods and their application for obtaining thermal properties and combustion behaviour are discussed in Section 2.6. Unresolved issues in fire modelling, pyrolysis and ignition processes are identified in Section 2.7. Based on this discussion, current research interests and requirements are then determined.

2.1 Background

During the past two decades, performance-based building codes and design practices have begun to be applied in many countries. In Australia, the first performance-based building code was released nearly ten years ago (ABCB 1996). More and more building projects are adopting the performance-based approach and “alternative solutions” are used rather than the deemed-to-satisfy solutions included in the Building Code Australia (BCA) and previous documents. Performance-based design requires quantitative analysis of various aspects and factors that may affect total building performance. In fire safety engineering (FSE), performance-based codes and practice have existed for more than a decade in New Zealand, Australia, Canada, the UK, and Japan, etc (Bukowski and Babrauskas 1990; Snell *et al.* 1993; Richardson 1994).

However there is still a long way to achieve wide application of performance-based design in FSE (Babrauskas 1996; Brannigan 1999). For example, Brannigan indicates that currently

scenario fires (design fires) are usually adopted in fire safety assessment rather than the use of fire scenarios that closely resemble real building environments. This is a serious limitation for assessing building performance in real world fires. Therefore, as identified in Chapter 1, acquiring a solid knowledge of fire behaviour is still a major task for improving the performance-based approach. This knowledge of fire behaviour covers fire origin (thermal decomposition and ignition), development (combustion and flame spread) and outcome (heat release and gaseous species yields).

Fire models, including mathematical, empirical and semi-empirical models, are mathematical statements to represent our theoretical understanding about fire. They are used to simulate or predict a process or phenomena in a fire environment, including fire development and consequences (Cox 1994). Today almost all the fire models available are computer programs. These computer programs perform large numbers of time consuming and lengthy calculations and provide the user with a set of parameters that describe the phenomena or events being simulated. Computer modelling of fire development, smoke and fire spread is a desirable major component in risk assessment models. Fire growth models are used to predict the fire growth characteristics of various fire scenarios in an apartment. The predictions of particular aspects of hazard development include the burning rate, room temperatures, oxygen and toxic gas concentrations, etc. Such data are critical for a risk-cost system model to accurately estimate the expected risk-to-life and fire-cost expectations.

The development of fire models shows progress from simple to complex. The complexity of models has two meanings: detailed phenomena with a smaller magnitude and more aspects of problems being considered and evaluated.

As for the physical magnitude of combustion phenomena, the fire models have progressed from zone models to field models. The zone models divide the whole enclosure into two zones (an upper hot gas layer and a lower cool fresh air layer) and a plume may be also modelled to bring combustion products and entrained air from the lower zone to the upper zone. The thermal properties within these two zones are treated as uniform. The size of the zones may exceed a couple of metres. The field models, which are also called as computational fluid dynamics (CFD) models, divide the enclosure into thousands of cells. The magnitude of the cells can be as small as millimetres, depending on the computational

capability and duration applied to the models. Brief introductions for these two types of fire models will be given in Section 2.2.

As mentioned in Chapter 1, a characteristic mesh size required for a CFD model to capture the details of chemical reaction zone in a fire may be smaller than a magnitude of millimetres. Therefore to study the pyrolysis and ignition processes in details, including gas phase mixing and reaction, CFD models are appropriate and available. A CFD model was then chosen for this research purpose.

As for the fire phenomena embedded within the combustion models, the sophistication of the models has grown rapidly in the past decades. Initially, these models were only able to describe limited phenomena of fires that were observed in fire growth. Gradually, more and more aspects of fire were added. A full picture with certain details for the fires is now appearing (Xue *et al.* 2001). For example the treatment of the fire source in these models developed as following, according to Friedman's international survey of fire models (Friedman 1992):

- Set, in the simplest case, a heat release source and specify the fire base area and pyrolysis rate of the combustible
- Specify a fire with heat release rate varying in a prescribed manner with time
- Add the influence of oxygen concentration on combustion into the calculation according to some formula
- Take radiative feedback into the burning rate calculation
- Set the burning rate according to full-scale experimental results, while bench-scale data can be adopted to predict relevant burning characteristics of the combustibles

Today the treatment of the fire source in fire models has become even more mature. In some complicated combustion models, fire development and outcome are estimated based on computations of complex heat transfer and flame spread rather than simply being specified by users (Atreya *et al.* 1986; Quintiere 1993; Staggs and Whiteley 1999). It is found that a great number of basic quantities are needed to describe more and more phenomena in current fire models. Delichatsios and Saito (1991) provide a list of the quantities needed for a scientific fire model of upward flame spread over a charring surface:

- The ignition parameters (intensity, size, duration)

- Thermal conductivity, density and heat capacity of the virgin material and of the char
- Surface temperature of the pyrolyzing surface
- Surface reflectivity
- Heat of gasification
- Heat of combustion of pyrolysis gases
- Combustion efficiency
- Radiative fraction of flame heat output

It should be noted that this list is not completely definitive. Some other factors/quantities, such as heat of combustion of char and the effect of composite material, may need to be taken into consideration as well.

To achieve an engineering approach for modelling combustion, it is necessary to identify the input quantities and phenomena that are most relevant to fire initiation, development and outcome. Then these quantities and phenomena must be included in models to obtain desirable engineering results. Note that over time, more and more details will be added into these models with an acceptable modelling duration and accuracy. These efforts will enable fire models to deal with more complex and realistic fire situations. Detailed reviews on research activities about pyrolysis, ignition, flame spread over solid fuel are performed in Sections 2.3 to 2.5. Research requirements in those areas for the current study are then identified.

Based on the results of the theoretical study, a series of test methods and devices were developed to obtain the basic properties of materials and to investigate the burning behaviour and fire performance of building and their components. These experimental data are also critical for validation of modelling results. The experimental equipments range from small-scale/bench-scale (such as the TGA, the cone calorimeter and Lateral Ignition and Flame Transport tests) to middle-scale (furniture calorimeter and ISO room tests) and full-scale sizes (doorway and room calorimeter tests). The basic quantities obtained from the small/bench-scale tests are normally used to predict material or component performance in the full-scale tests through theoretic analysis and modelling. The method for predicting ignition time developed by Quintiere and Harkleroad (1984) is such an example.

Since the research interest in the current study is to describe the pyrolysis and ignition processes in detail, only experimental methods relevant to this purpose, normally the small/bench-scale tests, are reviewed. Their major applications are discussed in Section 2.6.

2.2 Fire Models

During the past two decades, a number of reviews on fire models have been made by various researchers. Some of the reviews focused on a comparison and evaluation of the overall ability of the models, like those by Jones (1983), Friedman (1992), Dembsey *et al.* (1995) and Beard (1997). Other reviews concentrated on details of modelling schemes for special phenomena, such as: effect of combustion (Xue *et al.* 2001), pyrolysis of char forming solid (Moghtaderi 2001), the role of condensed phase in polymer combustion (Moghtaderi 2001), and ignition of wood (Babrauskas 2001), etc.

In this literature review, it is not intended to perform an exhaustive review of all the fire models available. However a general description of major types of fire models is given in this chapter. In the next chapter, emphasis is laid on those models related to the current study: pyrolysis and ignition of solid fuels, especially of some types of furnishing materials.

The principle kinds of deterministic models that have been developed are zone and field models. A brief review of these two kinds of models is given in the following sub-sections.

2.2.1 Zone models

A modelling approach for predicting various aspects of fire phenomena in enclosures has been called “zone” modelling. It is based on a conceptual representation of the compartment fire process, and is an approximation to reality. The zone model simply represents the system as two distinct compartment gas zones (Peacock *et al.* 1993):

- an upper, hot volume and
- a lower, cold volume

resulting from thermal stratification due to buoyancy.

Conservation equations (for energy, mass and momentum transport) are applied to each zone and serve to embrace the various transport and combustion processes that apply. The fire is represented as a source of energy and mass, and manifests itself as a plume, which acts as a “pump” for the mass from the lower zone to the upper zone through a process called “entrainment.”

The properties of the upper and lower zones are assumed to be spatially uniform, but can vary with time. Thus, temperature, T , and species mass concentration, Y_i , are properties associated with ideal upper and lower homogeneous layers. The gases in the layers are treated as ideal gases with constants of specific heats c_p and c_v . The pressure in the enclosure is considered uniform in the energy equation, but hydrostatic variations account for pressure differences at free boundaries of the enclosure.

The solution process of the conservation equations is completed by each source or transport term being given in terms of the layer properties. The extent to which source and transport relationships are included reflects the sophistication and scope of the zone model. These source and transport relationships are usually termed “sub-models” and can be subroutines in the computer code of zone model. Due to the limited knowledge of fire behaviour, many assumptions are adopted and many of the sub-models still need further improvement. For example, the mass of fuel supply can be a result of a fire spreading over an array of different solid fuels. However, the fuel properties are still not completely defined or conventionally accepted for fire applications. The main reason for this is that no general exhaustive theory exists for pyrolysis, and theories of flame spread and ignition are couched in terms of effective fire properties. Meanwhile the treatments for mass and heat transports (such as vent flows, various heat transfer, mixing of layers) are still very simple and sketchy in today’s zone models due to complex geometry and fuel configuration (Tanaka 1983; Peacock *et al.* 1991).

A detailed review of the zone models, including the conservation equations and the sub-models can be found in (Quintiere 2002).

The beginnings of zone fire modelling were marked by the fundamental equations published by Quintiere in the mid-1970s (Quintiere 1977). The first pre-flashover zone fire model published was PFIREs by Pape *et al.* (1981). The next publicly accessible model was

HARVARD by Emmons and Mitler (1985). At about the same time the first zone fire model written specially for IBM-compatible personal computers was introduced by Walton (1985).

Several zone models have been developed at the Building Fire Research Laboratory, USA. A summary of those typical zone models is given by Jones (2000). These models include FAST, FIRST, ASET, CCFM, CFAST, FPETool and HARZARD. CFAST is a good example in the way it represents the underlying physics of zone models.

CFAST is capable of predicting the environment in a multi-compartment structure subjected to a fire. It solves conservation equations of mass and energy by using the ideal gas law and relations for density and internal energy. The predictions obtained from these equations are functions of time quantities, such as pressure, layer heights and temperatures. The model calculates the time evolving distribution of smoke and fire gases and the temperature throughout a multi-compartment building during a user-specified fire (Jones and Forney 1990).

An important limitation of CFAST is the absence of a fire growth model. The model utilizes a user specified fire, expressed in terms of time specified rates of energy and mass released by the burning item(s). Such data can be obtained by measurements taken in large- and small-scale calorimeters, or from room burns. However, there are limitations in associating such data for modelling real compartment fires. For example the data obtained from a furniture calorimeter is derived from a “free burning” test, and the test environment is different from real compartment fire conditions (such as radiation feedback from hot upper layer gases) (Jones 2001).

Some major features of CFAST are briefly described as follows (Jones 2001):

- *Fires*: treated as fuel source with a specified releasing rate of combustibles, and the burning rate controlled by oxygen concentration
- *Plumes and Layers*: a plume model is adopted to predict plume entrainment including mass and enthalpy transferring
- *Vent Flow*: two types of vent flows, horizontal and vertical, are determined by pressure difference across a vent based on Bernolli’s law
- *Heat Transfer*: material thermophysical properties are assumed to be constant for convective and radiative heat transfer. This can cause error in gas phase radiative

calculations since the emissivity is a function of the concentration of species of some strong radiators that change as the fire develops

- *Species Concentration and Deposition*: a combustion chemistry scheme based on a carbon-hydrogen-oxygen balance is used to estimate the rate of production of species

It can be seen from the above reviews that zone models are not suitable for the current research purpose. The major limitations of zone models are the lack of descriptions of the fire source and flame spread process, and low accuracy in the computation of mass and heat transfer, especially under complex geometry and environment conditions.

2.2.2 Field models

Field models are complex fluid mechanical models of turbulent flow derived from classical fluid dynamics theory. This type of model solves versions of the fundamental equations of mass, momentum, and energy (Stroup 2002). In order to facilitate the solution of the equations, the compartment is divided into a three-dimensional grid of cells. The field model calculates the physical conditions in each cell as a function of time. The calculations account for physical changes generated within each cell and changes in the cell resulting from changes in surrounding cells.

2.2.2.1 Computational Fluid Dynamics (CFD) basics

Classical fluid dynamics is concerned with the mathematical description of the physical behaviour of fluids (gases or liquids). The equations consist, in general, of a set of three-dimensional, time-dependent, non-linear partial differential conservation equations, referred to as the Navier-Stokes (N-S) equations.

The N-S equation describing the conservation of mass is described by the continuity equation.

$$\frac{\partial \rho}{\partial t} + \nabla \cdot (\rho U) = S \quad (2.1)$$

where:

ρ : local density of fluid, kg/m³

U : fluid velocity vector with components in x , y , and z directions, m/s

S : sources or sinks of mass, kg/m³·s

t : time, s.

Conservations of momentum and energy are given as below, the equations (2.2) and (2.4) respectively:

$$\frac{\partial \rho U}{\partial t} + \nabla(\rho U \bullet U) = B + \nabla \sigma \quad (2.2)$$

where:

$$\sigma = -p\delta + \mu[\nabla U + (\nabla U)^T] \quad (2.3)$$

and,

B : body force, here is due to gravity (buoyancy), N

p : pressure, N/m²

δ : boundary thickness, m

μ : molecular viscosity, kg/m·s

T : temperature, K

$$\frac{\partial \rho H}{\partial t} + \nabla(\rho U H) - \nabla(\lambda \nabla T) = \frac{\partial p}{\partial t} \quad (2.4)$$

where:

H : total enthalpy, J/kg, given as a function of static enthalpy, h , by

$$H = h + \frac{1}{2}U^2$$

λ : thermal conductivity, W/m·K

Analytical solutions of these equations exist for a limited number of special cases that have simple boundary conditions. In their most general form, the N-S equations can not be solved by analytical methods. Therefore, solving the equations usually requires the use of numerical techniques. Computational fluid dynamics (CFD) involves the numerical solution of the N-S equations using computers. Field models solve the fundamental partial differential equations of motion and conservation numerically at a discrete moment in time and point in space. Using a set of grids in three dimensions, the compartment under study is

divided into many small volume elements or cells. The governing differential equations are solved simultaneously for each cell to obtain various parameters.

2.2.2.2 Turbulence

The flows occurring in room fires are turbulent, generating eddies or vortices of many sizes. The energy contained in large vortices cascades down to smaller and smaller vortices, until it diffuses into heat. Eddies exist down to the size where the viscous forces dominate over inertial forces and energy is dissipated into heat. For typical fires, this scale is of the order of a millimetre or so. Using cells of this tiny scale would result in problems that cannot be handled by most computers. As a result, turbulence models have been developed to account for the effect of small-scale fluid motion on the motion in large-scale cells. A turbulence model estimates the effect of small-scale or sub-grid phenomena on motion in the larger scale.

Several turbulence models have been developed. The traditional approaches solve the so-called Reynolds-averaged Navier-Stokes (RANS) equations (Cox and Kumar 2002). The common type of model adopting the format of the RANS equations is the eddy viscosity model which specifies the Reynolds stresses and fluxes algebraically in terms of known mean quantities. The k - ε models, probably the best known and most widely used turbulence models, are examples of eddy viscosity models (Launder and Spalding 1974). This type of model has two additional differential equations per control volume. The first equation governs the distribution of the turbulent kinetic energy k , while the second describes the dissipation of the local energy ε . The equations used in the k - ε model contain several empirical constants, which should be verified when used for new applications to ensure that reasonable results are obtained. Currently, most CFD models use k - ε models to handle the turbulence flow.

An alternative approach is to exploit Large Eddy Simulation (LES) techniques, where the larger turbulent vortices are simulated rigorously (McGrattan *et al.* 1998; Zhou *et al.* 2000). However this approach does not capture the length and times scales associated with the details involved in combustion. Another methodology, direct numerical simulation (DNS), that solves the exact equations rigorously is still under development (McGrattan *et al.* 1998;

Vervisch and Poinso 1998). It needs much larger computer resources and more detailed combustion-reaction information. Generally, with the current widely available computer hardware, simulation involving direct integration of the full Navier-Stokes equations in three dimensions is still not practical.

A detailed review of CFD models can be found in an article written by Cox and Kumar (2002). In that paper, the authors discussed many of the issues involved with a CFD model, such as turbulent flow, combustion, radiant heat transfer, boundary conditions, numerical solution method, validation and some practical applications.

In the next chapter of this thesis, some typical CFD models developed to model pyrolysis and combustion processes will be discussed in detail.

In summary, CFD models are able to simulate complex phenomena in combustion with a relatively small cell size. Adopting some form of appropriate numerical solutions, such as the $k-\epsilon$ models or the large eddy simulation technique for the turbulence problem, accurate results can be obtained within an acceptable computational duration.

2.2.3 Comparison between the zone and field models

Zone models are relatively simple, running rapidly and cheaply. Zone models have the ability to reduce computational complexity of fire growth and smoke spread modelling with a certain level of accuracy. This makes a zone model a handy tool for investigating the hazard of fire in buildings, which deals with hundreds of variables.

Zone models utilize many equations employing empirical relationships and constants obtained from experiments. There are three serious limitations of zone models. The first is that the empirical expressions used to describe physical behaviour in zone models may break down under certain circumstances (e.g., as the geometries become more complex.) The second limitation is that the scale of the combustion behaviours is much smaller than the zones in the zone models, and then the combustion is not properly modelled. The third limitation is that zone models treat each zone as being uniform, and no details within each zone can be analysed.

On the other hand, field models have the potential to be applied to a variety of problems with only minor modifications. Field models are able to estimate detailed velocity and temperature distributions, whereas the zone models only calculate average or maximum temperatures and velocities for a few points in a room. When study interests focus on detailed phenomena, field models are the perfect choice for the modelling tools. For example, plume entrainment, pyrolysis process and flame spread on a solid are just few of the areas that create huge difficulties for the zone models.

Fluid dynamic considerations are automatically built into field models to avoid oversimplified approximations. Field models are used in analysing problems involving far-field smoke flow, complex geometries (e.g., sprinkler links), and impact of fixed ventilation flows (Stroup 2002). Field models have been successfully used to predict special fire behaviours, such as the “trench effect” (Cox *et al.* 1989) and low temperature “islands” (Beard 1992).

This does not mean, however, that there are no unresolved difficulties with this kind of modelling. The application of field models to real fires is still at the preliminary stage, though significant progress has been achieved recently (Babrauskas 2002). The modelling of the complicated combustion process of solids, including the surface temperature and pyrolyzing flux, the near field entrainment and flow, and the process of transition from solid to gas phase, is yet to be adequately incorporated into field models. Meanwhile the simulation accuracy is greatly dependent on a better understanding of various phenomena in detail and appropriate selection of properties for simulated materials.

2.3 Thermal Decomposition

It is necessary to distinguish three commonly confused concepts: thermal decomposition, thermal degradation and pyrolysis. According to definitions given by the ASTM (ASTM_E176), *thermal decomposition* is:

➤ “a process whereby the extensive chemical species change caused by heat,”

and *thermal degradation* is:

- “a process whereby the action of heat or elevated temperature on a material, product, or assembly causes a loss of physical, mechanical, or electrical properties.”

Pyrolysis is a process of chemical decomposition of solid and gaseous products released by effort of heating. In other words, pyrolysis is a special case of decomposition in which gaseous products are released from the decomposition of solid materials.

In a fire situation, thermal decomposition is an important change, which occurs before ignition of solid materials. This decomposition involves physical and chemical changes that usually generate gaseous combustibles vapours (pyrolysis). Normally physical changes, such as melting and charring, can markedly alter the composition and burning characteristics of a material, while chemical processes are responsible for the generation of flammable volatiles. Beyler and Hirschler (2002) provide a detailed description of the physical and chemical processes involved in the decomposition of a polymer.

The thermal decomposition of some identified furnishing material will be investigated in the current research. Major processes affecting the decomposition will be identified. Methods used to describe the decomposition by thermal dynamics will be discussed. All such knowledge is useful for determining the ignition of solid fuels and fire development, since the thermal decomposition affects not only the conditions for ignition but also the supply of combustibles to the fire.

2.3.1 Physical and chemical processes

Solid fuel materials usually undergo both physical degradation and chemical decomposition changes when heat is applied to them. When thermal decomposition takes place a solid material generates gaseous fuel, which can burn above the surface of the material. In order for the process to be self-sustaining, it is necessary for sufficient heat to be fed back to the material to continue the production of gaseous fuel vapors or volatiles. This heat transfer normally comes from the burning gases as well as possible external heat sources.

The various physical processes that occur during thermal decomposition depend on the nature of the material. The common processes are: softening of thermoplastics, melting of

crystalline materials, deformation, etc. Cellulosic materials have been well studied due to their wide application. These materials, due to their structure, may not change state below the temperature at which thermal decomposition occurs. Since water is absorbed physically and chemically, release of water is a change that always occurs during a heating process with a substantial temperature rise. The activation energy for physical desorption of water is 30 to 40 kJ/mol, and the physical desorption starts at temperatures somewhat lower than 100 °C (Beyler and Hirschler 2002).

Another noticeable phenomenon associated with thermal decomposition of some materials is charring. Chars can be formed on many materials, such as cellulose, thermosetting materials and thermoplastics. The physical structure of these chars will strongly affect the thermal decomposition process (Goos 1952). Low density and high porosity chars are good thermal insulators and can significantly inhibit the flow of heat from the combustion flame back to the condensed phase behind it. As the char layer becomes thicker, the heat flux to the un-charred part of the materials decreases, and the thermal decomposition rate is reduced.

The thermal decomposition of solid materials may proceed by oxidative processes or simply by the action of heat. In many solid materials, the thermal decomposition processes are accelerated by oxidants, such as air or oxygen. The minimum decomposition temperatures in the presence of an oxidant are lower than that without the oxidant. Therefore the concentration or presence of oxygen is very important in determining the thermal decomposition rate and mechanisms. The effect of oxygen makes the prediction of the thermal decomposition rate much more complicated, since the prediction of the concentration of oxygen at the solid surface during thermal decomposition or combustion is quite difficult. Some efforts have been made to study the effect of oxygen concentration on the decomposition process (Kashiwagi *et al.* 1985; Brauman 1988; Gijnsman *et al.* 1993).

Kashiwagi and co-workers (1985; 1992) found that a number of material properties affect the thermal and oxidative decomposition of thermoplastics. These properties include molecular weight, prior thermal damage, weak linkages, and primary radicals. Their research also resulted in the development of models for predicting the kinetics of general random-chain scission reaction, as well as for the thermal decomposition of celluloses and thermoplastics.

There are numbers of general chemical mechanisms to describe thermal decomposition of polymers. These can be listed as follows (Beyler and Hirschler 2002):

- random-chain scission
- end-chain scission
- chain-stripping
- cross-linking, etc

Thermal decomposition of a solid material generally involves more than one of these classes of reactions. These general classes may only provide a conceptual framework useful for understanding and classifying solid material decomposition behaviour.

Some materials, especially thermosets and cellulose, have more complex decomposition mechanisms. Indicated by previous researchers (Beyler and Hirschler 2002), polyurethane (particularly flexible foams) can be decomposed by three different mechanisms. One of them involves the formation of gaseous isocyanates, which can then re-polymerize in the gas phase and condense as a yellow smoke. Cellulose, such as wood, decomposes into three types of products:

- laevoglucosan, which quickly breaks down to yield small volatile compounds
- a new solid, char
- a series of high molecular weight semi-liquid materials, known as tars

Since the decomposition processes of polymers are so complicated and there are a great number of unknowns in the processes, identifying the major processes and products is a challenge for the study of decomposition. It is especially true for the kinetic description of the thermal decomposition.

2.3.2 Kinetics

There are several different usages of “kinetics”. Generally, “kinetics” means chemical kinetics, i.e. the reaction rates of chemical processes. In order for a reaction to occur, a certain threshold that should be reached is called the “activation energy”. This activation energy, and other parameters to describe a reaction, such as a pre-exponential factor, are commonly called as “kinetics” by many researchers. This is also the usage in this thesis.

Normally a chemical reaction rate between two reactants, A and B, can be expressed as follow (Beyler and Hirschler 2002):

$$\text{reaction rate} = k[A]^m[B]^n \quad (2.5)$$

where:

k : the reaction rate constant, 1/s;

$[A]$ and $[B]$: are concentrations of the reactants A and B, mol/m³;

m and n : orders of reactions with respect to A and B respectively.

There may be up to eight generic types of reaction involved in decomposition processes. The kinetics describing the process can be quite complex. It is possible to give an expression for the rate of weight loss of solid fuel caused by some relatively simple chemical reactions, such as random-chain initiation and end-chain initiation (Beyler and Hirschler 2002). A simple expression of the rate of weight loss for the end-chain initiation is given as:

$$\frac{dW}{dt} = D_p \cdot (2n) \cdot k \quad (2.6)$$

where:

W : weight;

D_p : degree of polymerization, or number of monomer units per polymer chain;

n : is the number of polymer chains;

k : rate constant for end-chain initiation.

However, the reaction rate constant and reaction order for the expressions are somehow difficult to decide.

From an engineering point of view, the above chemical expressions for the reaction kinetics are either unsolvable or inapplicable. Therefore, for engineering applications, some simplified kinetic descriptions are considered. The general simplification is to use an overall (global) decomposition process to represent the possible multiple reactions existing in the decomposition process of the polymer. This overall decomposition can be one-step (representing one major reaction) or multiple steps (representing a multiple reaction). Moghtaderi (2001) carried out a detailed review of these overall decomposition models.

Details for application of the overall decomposition models will be given in the next chapter where modelling for pyrolysis and ignition processes is described.

The simplest and most commonly adopted assumption for utilizing the simple overall kinetics expressions is that the reactions can be described by a one-step first order Arrhenius expression:

$$k = Ae^{-\frac{E}{RT}} \quad (2.7)$$

where:

k : the reaction rate constant, 1/s;

A : the pre-exponential factor, or frequency factor, 1/s;

E : activation energy, kJ/mol;

R : universal gas constant, = 8.314×10^{-3} kJ/mol·k;

T : reaction temperature, K.

For example, Kashiwagi and Nambu (1992) obtained the overall kinetic constants for the thermal oxidative decomposition process of a cellulosic paper. The predicted decomposition rate matches with the experimental result reasonably well.

The simplified overall kinetic approach, which uses the overall kinetics to describe the reaction, has been adopted for many decomposition models. The key point is how to define the overall reaction and how to obtain the kinetics. A standard kinetic test method is the thermogravimetric analysis (TGA) test, which will be briefly introduced late in this chapter. The efforts to improve the experimental and calculation scheme for the kinetics are further discussed in Chapter 4 where TGA tests are carried out for the studied materials.

2.3.3 Decomposition of the furnishing materials

As mentioned in Chapter 1, furnishing materials play an important role in ignition and combustion of fires in compartments. Six furnishing materials have been chosen for the current research to represent typical materials used in furniture manufacture and inner furnishing. Two are timber: mountain ash (botanical name *Eucalyptus regnans*) and Australian pine (botanical name *Casuarina equisetifolia*); two are fabrics: cotton fabric and

cotton and polyester fabric; and two are polyurethane (PU) foam, standard PU foam and Stamina PU foam. There are a number of papers which report the thermal properties and combustion behaviour of these materials. For cotton materials, these are (Cleary *et al.* 1992; Ohlemiller and Shields 1995), for polyurethane foam (Luo and He 1997; He *et al.* 1999; Walther *et al.* 2000), and for wood (Atreya *et al.* 1986; Li and Drysdale 1992; Moghtaderi *et al.* 1997). However, the pyrolysis of wood is a very complex process due to its composition. It is necessary to discuss various stages of decomposition process of this material individually.

2.3.3.1 Pyrolysis and charring of wood

The physical and chemical changes that occur in the pyrolysis of wood can mainly be considered as charring and gasification. However the reactions involved may be quite complicated. As described by Beyler and Hirschler (2002), there are at least four processes in the decomposition of celluloses, the major component of wood:

1. cross-linking of cellulose chains with the evolution of water (dehydration)
2. unzipping of the cellulose chains to form laevoglucosan from the monomer unit
3. decomposition of the dehydrated products (dehydrocellulose) to yield char and volatile products
4. further decomposition of the laevoglucosan into smaller volatile products, including tars, and finally carbon monoxide

Meanwhile a simple desorption of bound water may be also included in the decomposition process of wood.

Wood consists of approximately 50% cellulose, 25% hemicellulose, and 25% lignin. The decomposition of wood may be treated as the combined decomposition mechanisms for the individual components. It can be observed from the yields of volatile products and kinetic data. When heated, the decomposition temperature ranges for the hemicellulose, cellulose and lignin are 475 to 535 K, 525 to 625 K, and 555 to 775 K respectively. Therefore the decomposition kinetics of a specific species of wood will be determined by its composition. It is also known that the decomposition of lignin contributes significantly to the overall yields of char, and that the lignin fraction supports most of the subsequent glowing combustion. The cellulose fraction contributes most to flaming combustion (Tang 1972).

In the gasification of the solid, only part of the original fuel becomes a vapor and a certain amount solid residue is left. If the residue is carbonaceous, the char is formed on the surface first. When the thermal decomposition of deeper layers of the solid continues, the volatiles produced must pass through the porous char above. The hot upper char layer can cause a secondary reaction in the volatiles. The top char layer can be burnt by an oxidation reaction at a higher temperature. On the other hand, the forming of top char layer can prevent the underlying layers from further thermal breakdown or at least slow the process down. The combination of these factors will be affected by heating conditions and thermal properties of the wood.

Many factors are involved in wood charring. Kanury and Blackshear (1970) checked various physiochemical effects, including diffusion of condensable vapors, internal convection outward, properties of the partially charred wood, kinetics of pyrolysis, and post-decomposition reactions. Lee *et al.* (1977) added other factors to the wood charring, such as external heating rate, total time of heating, and anisotropic properties of wood and char which related to internal flow of heat and gas. Among the factors some characteristics of wood greatly affect the charring rate. These characteristics are density, moisture content, permeability, and chemical composition. Density is recognized as the major factor affecting charring rate. According to Schaffer's study (Schaffer 1967), denser wood has a slower charring rate. A similar relationship was also observed for wider wood species by other researchers (Hall *et al.* 1972). Permeability may be a controlling factor in the movement of moisture, which also affects the outflow of pyrolysis gases (Kanury and Blackshear 1970). The pressure in a heated wood was measured and reported to drop when structure changes were observed (Roberts 1970). The relationship between inner pressure and external radiative flux has been measured and included in Fredlund's theoretical model (Fredlund 1988).

The gaseous pyrolysis products of wood are a complex and highly variable mixture. For instance, the volatile materials detected as products of wood decomposition have been reported as being from 30 up to 200 compounds (Goos 1952; Beck and Arnold 1977). By investigating the composition of pyrolysis products of wood, Abu-Zaid (1988) and Nurbakhsh (1989) found that the total hydrocarbons and carbon monoxide are about 25% (mass fraction) of the total pyrolysed gas. For modelling purposes, the volatiles are normally represented by four major gases H_2 , CO , CH_4 , and CO_2 (Klose *et al.* 2000). Of course this is

a certain degree of simplification. More detailed knowledge about the pyrolysis products may be still required.

2.3.3.2 Role of moisture content

Changes of moisture content in a solid piece of wood involve vaporization and condensation processes. These changes may affect the pyrolysis process greatly, as explained below.

The moisture content in wood exists in two basic forms: (1) bound or hygroscopic water, and (2) free or capillary water. For most wood species the moisture content at the Fibre Saturation Point (FSP) is about 30% while the total moisture content could be as high as 60%. When exposed to fire, the temperature of the wood will rise to a point, near 100 °C, when the moisture starts to evaporate. Since the bound water is adsorbed into the cell walls (at least if the moisture content is below the FSP), evaporation for this portion of water requires more energy than needed to boil free water. During this initial period, most of the heat received by the fuel is consumed by heating and evaporating the free water portion. When the total moisture content of the surface region drops to a level close to the FSP, the evaporation front begins moving into the solid. The water vapor largely migrates toward, and escapes through, the exposed surface. A fraction also migrates in the opposite direction, and re-condenses at a location where the temperature is below 100 °C. The movement of the moisture within the wood has a significant impact on the heat and mass transfer processes taking place within the solid. For example the heat conductivity may increase several times compared to when the wood has a completely “dry” status.

The dryer wood portion further increases in temperature until the fibres begin to degrade. The thermal decomposition of wood starts around 200 to 250 °C. The volatiles that are generated again travel primarily toward the exposed side, but also partly in the opposite direction. They consist of a mixture of combustible gases, vapors of moisture and tars. A solid carbon char matrix remains. The volume of the char is smaller than the original volume of the wood. This results in the formation of cracks, bends and fissures which greatly affect the heat and mass transfer between the flame and the solid. The combustible volatiles that emerge from the exposed surface mix with ambient air and burn in a luminous flame.

Generally, the moisture content and its movement may significantly affect the pyrolysis progress in two aspects: (1) changes in the thermal properties; and (2) overall heat transfer and balance, such as heat of vaporization.

2.4 Ignition Controlling Mechanism

The flaming ignition of a combustible material, the subsequent spread of flames over its surface and the establishment of steady burning are critical processes in the development of a fire. They determine the rate of growth of the fire and the rate of heat release.

A fundamental understanding of these processes is basic to the development of material flammability and combustion test methods. Such tests are used to provide meaningful and reliable information about the behaviour of the material in an actual fire.

There are several ways that a solid combustible can be ignited. The ignition, or combustion reaction initiation of a combustible material, can occur either in the solid or in the gas phases. In fires, the latter (flaming ignition) is the most important since it may lead to the spread of the fire.

The gas phase ignition of a solid combustible is generally a combination of a number of events. The first is exposure to an externally imposed heat flux (radiation and/or convection) that causes gasification of the solid. The second is the presence of conditions (in the gas or external to it) that will lead to the onset of a sustained combustion reaction between the vaporized fuel and the oxidizer gas. If the reaction is initiated by an ignition source (such as open flame, electrical spark, etc) the ignition is normally referred to as piloted ignition. If ignition occurs without a pilot the process is normally referred to as spontaneous or auto-ignition. For this latter type of ignition to occur, the gaseous oxidizer/fuel mixture must be at an elevated temperature. Gas phase ignition caused by a high surface temperature or by a surface reaction, such as smouldering or char oxidation, can also be included in this category.

A detailed description for these two types of controlling mechanisms was given by Fernandez-Pello (1995). Brief descriptions of them are in the following sections.

2.4.1 Auto Ignition

The auto ignition study was based on a simplified experimental ignition model provided by Niioka (1981). See Figure 2.1.

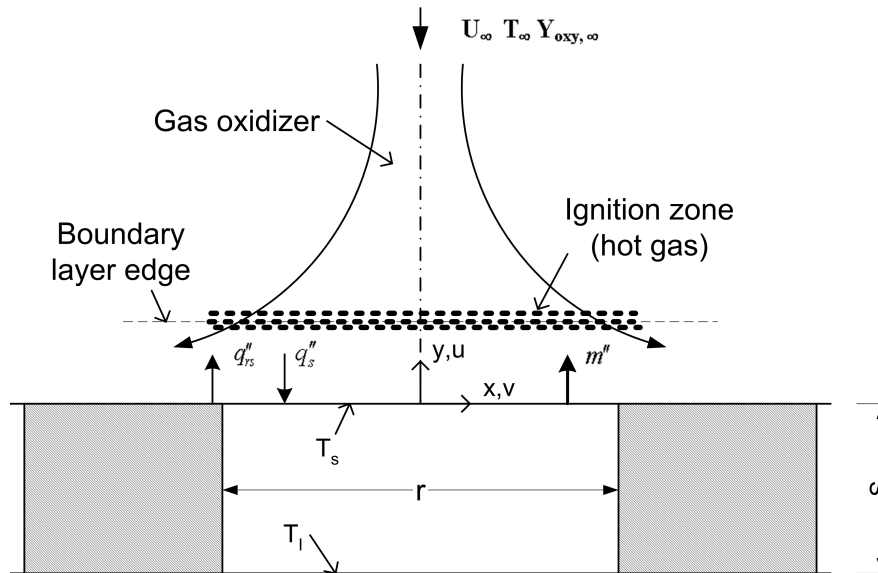


Figure 2.1 One-dimensional experimental ignition model

The physical description of the simplified ignition model can be given as follows. A solid fuel slab with a thickness s and a constant initial temperature T_i is suddenly exposed to a hot, stagnation point gas flow. This hot gas flow consists of oxidizing gas with properties marked as ambient parameters, U_∞ , T_∞ , and $Y_{oxy, \infty}$. This works as an external heat flux and the heat flux is absorbed at the solid surface, which heats the solid and eventually causes it to pyrolyse. The pyrolysed fuel vapour convects and diffuses outwards, mixes with hot oxidizer gas and forms a combustible mixture near the surface. The high gas temperature helps initiation of a gas combustion reaction. If the energy absorbed from the hot gas is high enough to overcome the heat loss to the surroundings, a sustained combustion reaction (flame) will occur over the combustible surface.

By studying various flow velocities and distances to the solid surface, Niioka suggested that two primary mechanisms control the solid fuel ignition process. One is the heating and gasification of the solid and the other is the onset of the gas phase chemical reaction. Some times (t) related to this ignition process are defined as follows:

- the ignition delay time, also shorten as ignition time, t_{ig} , is the time from the sudden exposure of a surface to a hot gas flow at a stagnation point to the onset of combustion
- solid pyrolysis time, t_{py} , related to the heating and pyrolysis of the solid, is the time from the beginning of exposure to the hot gas to the starting of pyrolysis on the solid surface (at pyrolysis temperature T_{py} , (Carslaw and Jaeger 1959))
- gas induction time, t_{in} , related to the onset of the gas phase chemical reaction and also named as gas phase time delay, is the time from starting of pyrolysis of the solid fuel to the ignition.

The gas phase time delay is then decided by two times:

- The flow residence time, which is the time for pyrolysed gas to reach the boundary layer edge, and
- the chemical time, which is the reaction time of the pyrolysis products in the gas phase.

The solid (total) ignition delay time is the sum of the solid pyrolysis time and the gas induction time:

$$t_{ig} = t_{py} + t_{in} \quad (2.8)$$

For example, as the flow velocity is increased the surface heat flux also increases and consequently the time required to heat up and pyrolyse the solid decreases. The influence of this mechanism is graphically represented by the descending pyrolysis time line in Figure 2.2. On the other hand, it is noticed that an increase in the gas velocity results in a decrease of the flow residence time, if compared to the chemical time. This will delay the onset of the chemical reaction and eventually prevent its initiation. The effect of this mechanism can be graphically represented by the ascending line, i.e. the induction time. Therefore, the solid ignition delay time can be decided by the sum of the solid pyrolysis time line and the gas induction time line.

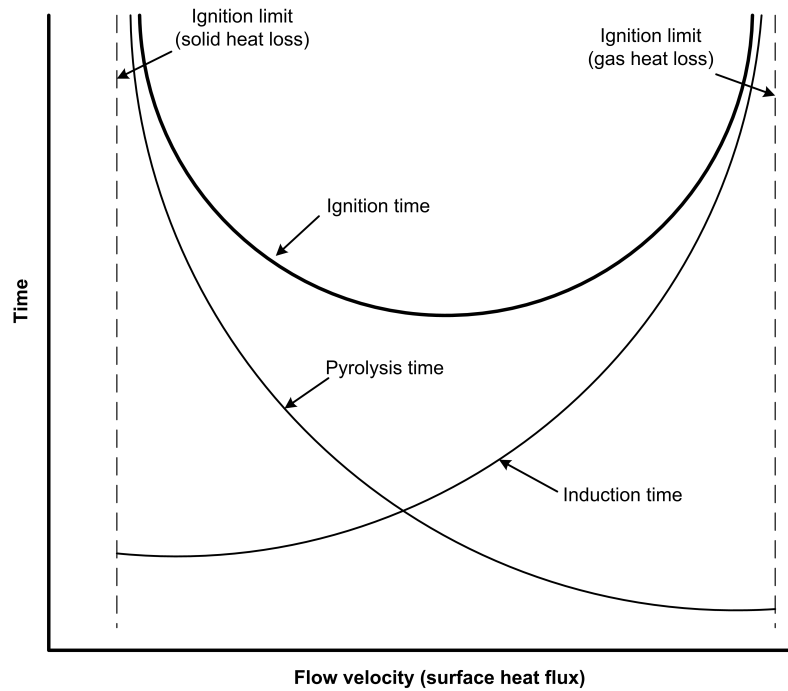


Figure 2.2 Solid ignition controlling mechanisms and ignition time variation

If the gas phase chemical time is very short compared with the flow time, the induction time will also be very small and the solid ignition delay will be controlled by the heat transfer to the solid. This will occur for low flow velocities, and/or high temperature and oxygen concentrations. For high velocities and/or low temperatures and oxygen concentrations, the solid ignition delay will be dominated by the onset of the gas phase chemical reaction. These concepts can be extended to other geometrical configurations and other sources of ignition. For example, the presence of a pilot flame affects the ignition process by locally reducing the gas induction time. The solid heating is consequently the dominant controlling mechanism of the solid ignition process, unless the flow velocity is very large or the oxygen concentration is very low.

2.4.1.1 Solid heating and gasification

Since the oxidizer supplying flow in Figure 2.1 is uniform on the x-axis and the studied part of the solid is limited in the middle of the flow, this physical problem can be treated as one-dimensional. Fernandez-Pello (1995) gave a detailed analysis for this problem and provided the following assumptions and equations. Assumptions adopted in the problem are:

- solid properties are constant

- the pyrolysis occurs at the surface of the solid
- solid pyrolysis is described by a first order Arrhenius law
- the radiation is absorbed and emitted at the surface
- there is no surface oxidation or material charring

The governing solid phase equation for energy is:

$$\rho_s c_s \frac{\partial T_s}{\partial t} + \rho_s c_s \frac{ds}{dt} \frac{\partial T_s}{\partial y} = \lambda_s \nabla^2 T_s - m'' L_v \quad (2.9)$$

where:

mass flux is given by:

$$m'' = A_s \rho e^{\left(-\frac{E}{RT_s}\right)}, \text{ and}$$

ρ_s : density of surface solid, kg/m³;

c_s : specific heat of surface solid, J/kg·K;

T_s : surface temperature, K;

λ_s : thermal conductivity at surface, W/m·K;

L_v : heat of vaporization, kJ/kg;

A_s : pre-exponential factor for the pyrolysis reaction occurring at surface, 1/s;

E : activation energy, kJ/mol;

y : coordinate normal to the solid surface;

s : thickness of the solid, m.

Since the activation energy E is large for most materials, the pyrolysis rate is small for surface temperature lower than a certain value (Williams 1985). Thus it can be assumed that pyrolysis of the solid takes place at the surface and at a constant surface temperature T_{py} , which is defined here as the “pyrolysis” temperature. For a one-dimensional process and for the period prior to pyrolysis initiation ($T_s < T_{py}$), Equation (2.9) is reduced to the heat conduction equation

$$\rho_s c_s \frac{\partial T_s}{\partial t} = \lambda_s \frac{\partial^2 T_s}{\partial y^2} \quad (2.10)$$

A solid is considered thermally thick if its thickness is larger than the thickness of the heat penetration layer (at a particular time). It is considered thermally thin if the temperature

variation across its thickness is negligible. A theoretical judgement can be achieved by the following equation, (Kanury 2002):

$$q''L/\lambda(T_s - T_{s,i}) \ll 1 \quad (2.11)$$

where:

- q'' : imposed flux, W/m²;
- L : slab thickness, m;
- λ : thermal conductivity, W/m·K;
- T_s : surface temperature, K;
- $T_{s,i}$: initial surface temperature, K.

If Equation (2.11) is satisfied, the solid may be considered thermally thin; i.e., a rapid transfer of heat within a material would lead to establishment of a uniform temperature profile. On the contrary, if the left hand of Equation (2.11), the ratio of imposed flux to the conductive flux, is larger than 1, the solid body behaves as thermally thick. The latter can be true either if the solid is physically thick or the thermal length, $\lambda(T_s - T_{s,i})/q''$, is small.

For thermally thick or thin solids, the pyrolysis time can be obtained from solution of Equation (2.10) and the boundary conditions as follows:

for a thermally thick solid:

$$t_{py} = \frac{\pi\lambda_s\rho_s c_s (T_{py} - T_I)^2}{4q_s''^2} \quad (2.12)$$

for a thermally thin solid:

$$t_{py} = \frac{\rho_s c_s L (T_{py} - T_I)}{q_s''} \quad (2.13)$$

where:

- T_I : initial solid temperature, K;
- T_{py} : pyrolysis temperature, K;
- L : solid fuel thickness, m;
- q_s'' : surface heat flux, kW/m².

If the gas phase induction time is very small (low velocity and high oxygen concentration, and high gas temperature or piloted ignition) the pyrolysis time will be nearly equal to the

solid ignition time. Equations (2.12) and (2.13) can be used to predict ignition times as a function of the process parameters.

Because the fuel/oxidizer mixture becomes flammable almost immediately after solid pyrolysis starts, the pyrolysis temperature is often defined as the “ignition” temperature. This definition, though not physically correct, can yield fairly accurate results.

For the thermally thick solid fuel, the solid heating process with the surface heat flux can be expressed as follows, (Arpaci and Larsen 1984):

$$q_s'' = c(\lambda_g \rho_g c_p u_\infty / x)^{1/2} (T_\infty - T_{py}) - q_{rs}'' + q_{rad}'' \quad (2.14)$$

where:

q_{rs}'' : re-radiation from the solid surface, kW/m²;

$$q_{rs}'' = \sigma \varepsilon_s (T_{py}^4 - T_\infty^4)$$

λ_g : gas thermal conductivity, kW/m·K;

ρ_g : gas density, kg/m³;

u_∞ : forced flow free stream velocity, m/s;

x : coordinate parallel to the solid surface (see Figure 2.1);

T_∞ : ambient temperature, K;

q_{rad}'' : external radiation, kW/m²;

σ : Stefan-Boltzmann radiation constant, W/m²·K;

ε_s : surface emissivity.

If it is assumed that the surface temperature is constant and equal to the pyrolysis temperature and that the gas does not emit or absorb radiation, substituting Equation (2.14) into (2.12) gives the solid pyrolysis time:

$$t_{py} = \frac{\pi \lambda_s \rho_s c_s (T_{py} - T_l)^2}{4 [c(\lambda_g \rho_g c_p u_\infty / x)^{1/2} (T_\infty - T_{py}) - q_{rs}'' + q_{rad}'']^2} \quad (2.15)$$

If the heat fluxes at the surface of solid are balanced, or the surface is in thermal equilibrium before the pyrolysis temperature is reached, ignition will not occur. The minimum heat flux for ignition can be obtained by equating the denominator of Equation (2.15) to zero. This is useful for determining a relationship between the minimum heat flux and ignition

temperature (assumed as the pyrolysis temperature), which was raised by Quintiere and Harkleroad (1984) and discussed further in Section 2.4.2.

2.4.1.2 Gas phase reaction

When the ambient oxygen concentration is low or the gas velocity is high, the gas induction time may be significant, and this has to be considered in the prediction of the solid ignition times.

The theoretical modelling of the gas phase reaction includes the solution of the mass, momentum, energy and species equations combined with the chemical rate equations. However, an analytical solution for this problem is not easy to obtain. As discussed earlier in Section 2.3, a common practical method to simplify the solution is the assumption that the gas phase reaction is a single step overall reaction. Then the reaction rate can be described by the Arrhenius equation:

$$k = A_g p_F^n Y_F Y_{oxy} e^{\left(\frac{-E}{RT}\right)} \quad (2.16)$$

where:

k is reaction rate, 1/s, and

A_g : gas phase pre-exponential factor;

p_F : pressure fraction of fuel;

Y_F : fuel mass fraction;

Y_{oxy} : oxygen mass fraction;

n : reaction order number;

E : activation energy, kJ/mol·K;

R : universal gas constant, =8.314×10⁻³ kJ/mol·K;

T : gas temperature, K.

Williams (1985) developed expressions for the critical conditions of ignition and delay time by using the property of large activation energies. Since a large number of the fuels (particularly the hydrocarbon type) have large activation energies, also due to the character of the Arrhenius combustion reaction, the reaction rate is very small for temperatures below a critical value. Thus the solution of the problem can be divided into two solutions: one non-

reactive (frozen solution) and another active that applies to a very small region of the mixture where the temperature is the highest.

A characteristic Damköhler number, Λ_o , is introduced to express the induction time.

$$t_{in} = - \left(\frac{1}{4 \left(\frac{du}{dx} \right)} \right) \ln \left(1 - \frac{\Gamma}{\Lambda_o} \right) \quad (2.17)$$

where

$$\Lambda_o = \frac{A \Delta H_R \rho_g n W_I E Y_{oxy, \infty} Y_{Fs}}{2 c_p R T_\infty^2 \left(\frac{du}{dx} \right)} e^{\left(-\frac{E}{RT_\infty} \right)} \quad (2.18)$$

and

$$\Gamma = 4c(E/RT_\infty)[(2-\beta)/e^2(1-\beta^2)] \quad (2.19)$$

$$\beta = T_\infty c_p / Y_{F,s} \Delta H_c \quad (2.20)$$

where all the variables have same meaning as in previous equations, and

ΔH_c : heat of combustion, kJ/kg;

W_I : initial solid weight, kg;

$Y_{oxy, \infty}$: ambient oxygen mass fraction;

$Y_{F,s}$: surface fuel mass fraction.

The gas velocity gradient parallel to the solid surface, du/dx , is defined as stretch rate (acceleration). It can be seen that as the stretch rate increases the induction time increases and becomes infinite at the value of the stretch rate at which $\Lambda_o = \Gamma$. This also determines the critical Damkohler number for ignition:

$$\Lambda_{o,cr} = \Gamma$$

If the Damkohler number is below the critical value, ignition will not occur. The common reasons are a too low gas temperature, low oxygen concentration and large stretch rate. This critical Damkohler number can be derived from steady-state analysis (Fernandez-Pello and Law, 1982).

For large Damkohler numbers ($\Lambda_o \gg \Gamma$) the gas phase induction time becomes inversely proportional to the Damkohler number, $t_{in} = \Gamma / (4(du/dx)\Lambda_o)$ and becomes negligible. This will occur mainly for high gas temperatures, moderate values of the flow velocity and oxygen concentration. The presence of a pilot flame could be sufficient for this limit because the reaction rate is very sensitive to temperature and only a little fuel vapor is needed to initiate the reaction.

2.4.1.3 Ignition time, t_{ig}

For the simple situation discussed in Section 2.4.1, the solid's ignition delay time (ignition time t_{ig}), is given by the sum of the solid pyrolysis time (Equation (2.15)) and the gas induction time (Equation (2.17)), i.e.

$$t_{ig} = \frac{\pi \lambda_s \rho_s c_s (T_p - T_l)^2}{4 [c(\lambda_g \rho_g c_p u_\infty / x)^{1/2} (T_\infty - T_p) - q_{rs}'' + q_{rad}'']^2} - \frac{1}{4u_\infty / x} \ln \left(1 - \frac{\Gamma}{\Lambda_o} \right) \quad (2.21)$$

More accurate analyses can be developed for other complicated situations by numerically solving both the solid and gas phase governing equations. For example, Wang and Yang (1992) gave such example of the ignition of a polymethylmethacrylate (PMMA) sphere in a forced oxidizer flow.

2.4.1.4 High surface temperature ignition

When a solid fuel slab is heated by an external radiation, the solid surface temperature may reach a high level enough to cause gas phase ignition. This kind of ignition normally occurs best with charring materials because the char layer generated by the initial pyrolysis can reach a very high temperature due to radiation absorption or char oxidation. The high temperature char in fact acts as the ignition source. This ignition process may take place in the initiation of wood fire, especially when a sudden enhancement of solid gasification happens.

The ignition model discussed in the foregoing subsections can be applied to describe this kind of ignition, although the formation of char will affect the solid heating process and some modifications are needed. If the ignition occurs before charring becomes important

(high surface heat flux, low charring materials), the ignition times are short and can be described well by Equation (2.21). Here, ambient temperature T_∞ , i.e. the temperature of the oxidizer flow, will be substituted by the surface temperature of the solid T_s in the induction term, since the surface temperature (char temperature) may be higher than the temperature of the hot gas flow. However, complicated phenomena such as transit from the char surface to flaming are still not understood clearly and are thus impossible to model (Fernandez-Pello 1995).

Some issues related to this problem have been studied. Alvares and Martin (1971) studied how gas properties influence the solid ignition temperature and ignition time. Their research showed that the surface temperature at the time of ignition and the ignition time decrease as the ambient oxygen concentration or the pressure increase. Meanwhile, Ohlemiller and Summerfield (1971) studied in-depth absorption. Kashiwagi (1985) studied the surface oxidation. All these results are helpful to extend the above model and may need to be taken into consideration while modelling heavy charring materials.

2.4.2 Piloted ignition

The piloted ignition phenomenon is similar to the previous problem but there is an extra pilot source present. The pilot source can be a spark plug, a high temperature surface or a flame. The function of this pilot source is to provide sufficient energy to ensure the gas phase chemical reaction reaching ignition.

This ignition problem has been studied by Quintiere and co-workers (Quintiere 1981; Quintiere and Harkleroad 1984). The results for a vertical solid slab heated by a radiative flux are provided as follows. When the ignition is achieved with a pilot flame, the gas induction time is small and the ignition time is very close to the pyrolysis time. The solution of the problem is given by Equation (2.12) where the pyrolysis time can be replaced by the ignition time and the pyrolysis temperature by the ignition temperature.

$$t_{ig} = \frac{\pi \lambda_s \rho_s c_s (T_{ig} - T_I)^2}{4[q_{rad}^n - h(T_{ig} - T_I)]^2} \quad (2.22)$$

where:

h : heat transfer coefficient incorporating the convective and linearized radiation heat transfer, and

$$h = h_{conv} + h_{rad}, \quad h_{rad} = C(\bar{T}_s - T_\infty)$$

h_{conv} : convective heat transfer coefficient, kW/m²·K;

C : coefficient for linearized radiative heat transfer, kW/m²;

\bar{T}_s : average surface temperature, K.

The solid initial temperature has been taken as equal to the ambient temperature and the surface temperature as equal to the pyrolysis temperature.

The minimum heat flux for solid ignition, $q''_{ig,min}$, is the heat flux for the solid surface coming into thermal equilibrium. It can be determined by applying $t_{ig} \rightarrow \infty$:

$$q''_{ig,min} = h_{ig}(T_{ig} - T_l) \quad (2.23)$$

where h_{ig} is heat transfer coefficient at ignition, kW/m²·K.

By investigating the pilot flame ignition of a vertical thick solid exposed to a constant external radiation, Quintiere and Harkleroad gave descriptions of the relationship between pilot ignition and flame spread (Quintiere and Harkleroad 1984). Based on Equation (2.23), they developed a test method, LIFT (Quintiere 1981), for determining one of the flammability characteristics, ignition time. The other critical parameter in this type of ignition is the pyrolysis or ignition temperature. This value can be measured directly by a thin type of thermocouple embedded at the solid surface, or determined experimentally by obtaining the critical heat flux for the ignition, described in Equation (2.23). This critical heat flux can be a radiative flux or a combination of radiative and convective heat fluxes. Details of this method will be discussed later in this chapter.

2.4.3 Ignition criteria

Following a wide study of research results from various researchers, Kanury (2002) summarized the ignition criteria for a solid as follows:

1. $T_s \geq T_{l,cr}$ -- critical surface temperatures (Simms 1963; Martin 1965)

2. $\bar{T}_s \geq T_{2,cr}$ --critical average solid temperature (Simms 1963; Martin 1965)
3. $m''_{py} \geq R_{1,cr}$ --critical pyrolysis mass flux (Bamford *et al.* 1946)
4. $\delta_c \geq \delta_{c,cr}$ --critical char depth (Sauer 1956)
5. $\partial T_g / \partial t \geq R_{2,cr}$ --critical local gas temperature increase rate
6. $\int_i^{\infty} k_i dy \geq R_{3,cr}$ --critical total reaction rate in the boundary layer (Kashiwagi 1974)

where:

T_s and \bar{T}_s : surface and average surface temperatures, K;

$T_{1,cr}$ and $T_{2,cr}$: suggested critical temperatures, K;

m''_{py} : pyrolysis mass flux, kg/m²·s;

$R_{1,cr}$: suggested critical pyrolysis mass flux, kg/m²·s;

δ_c and $\delta_{c,cr}$: char depth and suggested critical char depth, m;

$\partial T_g / \partial t$: local gas temperature increase rate, K/s;

$R_{2,cr}$: suggested critical local gas temperature increase rate, K/s;

$\int_i^{\infty} k_i dy$: total reaction rate in the boundary layer, 1/s;

$R_{3,cr}$: suggested critical total reaction rate, 1/s.

Among these parameters, some are difficult to measure, like the critical gas temperature increase rate and critical total reaction rate (relying on local fuel concentration measurement); some are dependent on other parameters, like the char depth, which is determined by surface temperature. The widely adopted criteria are critical surface temperature and critical pyrolysis mass flux. They have been used in a number of ignition models, and are discussed below. The possibility of applying some gas phase criteria is also investigated in this section.

2.4.3.1 Critical surface temperature

Kanury (1995) suggested that the possibility of an ignition occurring under a given set of conditions is judged by whether the exposed surface will attain a critical ignition temperature. The temperature of the surface at the time of ignition is defined as the ignition

temperature, T_{ig} . He also gave an approximate T_{ig} for a broad range of timbers in a small specimen tested in the vertical orientation as follows:

- | | |
|---------------------------|--------------------------------------|
| For spontaneous ignition: | 600 °C for radiation exposure, |
| | 500 °C for convective exposure; |
| For piloted ignition: | 300 ~ 410 °C for radiation exposure, |
| | 450 °C for convective exposure. |

He also indicated that in spite of significant physical and chemical differences in structure and composition, most organic solids undergo pyrolysis in a rather narrow temperature range of 325 ± 50 °C or 598 ± 50 K.

By studying the ignition of radiantly heated wood in the presence of a small pilot flame, Koohyar (1968) gave the critical temperature of about 600 K, near the pyrolysis temperature. Alvares (1964) indicated that the ignition temperature increases with decreasing irradiance.

Recently, Babrauskas carried out an extensive literature review of the ignition temperatures of timber (Babrauskas 2001). He summarized that piloted ignition at heat fluxes sufficient to cause a direct-flaming ignition normally occurs at surface temperatures of 300 ~ 365 °C (300 ~ 310 °C for hardwoods, and 350 ~ 365 °C for softwoods). The ignition temperature is around 250 °C for wood exposed to the minimum heat flux, which mostly causes a glowing or glowing/flaming combustion. The results for auto-ignition temperatures evidently span a huge range, from 200 to 700 °C while the median values are from 380 to 500 °C.

Babrauskas suggested that following reasons should be considered in relation to these widely differing ignition temperatures:

- The definition of ignition used
- Piloted vs auto-ignition conditions
- The design of the test apparatus and its operating conditions
- Specimen conditions (e.g., size, moisture, and orientation)
- The species of wood

It can be seen that it is difficult to find a widely acceptable and applicable ignition temperature as the ignition criterion for a timber, as all these reasons contribute to wide data

variation. Even for tests carried out in a test apparatus, it is found that the ignition temperature is dependent on a number of parameters. One of these is radiation flux, and the gas phase condition over the solid surface is another. This gas phase condition includes gas flow velocity, oxygen concentration and ambient pressure (Fernandez-Pello 1977; Kashiwagi and Omori 1988; Blasi *et al.* 1989). All these factors must be investigated and evaluated where the ignition temperature is considered as the ignition criterion.

2.4.3.2 Critical mass flux

Compared with the great amount of ignition temperature data, experimental results for critical mass flux are relatively scarce. However, the critical mass flux is suggested by a number of researchers to range from 0.8 to 6 g/m²·s for polymers (Tewarson 1982; Deepak and Drysdale 1983; Rasbash *et al.* 1986; Thomson and Drysdale 1989; Tewarson *et al.* 1999). An example value that Banford (1946) obtained for wood is 2.5 g/m²·s.

It is noticed that the critical mass flux changes when radiative flux and gas flow conditions changes. For example, Yang *et al.* (2003) reported 2 to 4 g/m²·s for the critical mass flux for cherry wood and the value of this mass flux increased as the radiative flux increased.

Another example of varying gas flow conditions is the experimental study of PMMA carried out by Zhou *et al.* (2002). These tests were conducted in the Forced-flow Ignition and flame-Spread Test (FIST) apparatus, which was developed at the University of California, Berkeley (Cordova *et al.* 2001). This apparatus is a derivation of the LIFT apparatus. The gas flow was forced over the sample surface which was heated by a radiative panel. A spark plug was placed 0.5 to 1.5 mm above the PMMA plate. In the tests the researchers found that the critical mass flux increased from 1.5 to 3.0 g/m²·s when the laminar parallel air flow over the surface increased from 1 to 1.7 m/s.

Alvare's research conclusion, which was quoted by Kanury (2002), indicates that the parameters discussed above, like critical temperature, pyrolysis flux and total gas reaction, are not generally acceptable as criteria of ignition. This is because these parameters are all strongly dependent on other factors, such as exposed heat flux, boundary layer height and slab thickness, re-radiative loss and chemical kinetics. As there is not enough detailed

information about these factors, or suitable and effective computation available, they are questionable for adopting as criteria.

2.4.3.3 Lower flammable limit and possible criteria in gas phase

For many years the concept of combustion has been symbolized by the Triangle of Combustion and represented as fuel, heat and oxygen. Further fire research determined that a fourth element, an uninhibited chemical chain reaction, was a necessary component of combustion. Then the fire triangle was changed to a fire tetrahedron (a pyramid) to reflect this fourth element (Haessler 1974), as shown in Figure 2.3. It is known that an uninhibited chemical chain reaction only occurs within certain reactant concentrations. In combustion, these suitable reactant concentrations in gas phase are normally expressed as within a range that was confined by the lower and upper flammable limits. Therefore the fourth element for the combustion tetrahedron was also suggested as an item “Atmosphere” (suitable fuel concentration in a favoured environment).

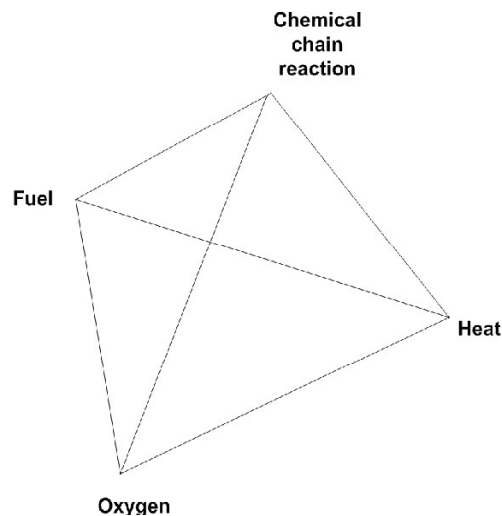


Figure 2.3 Combustion tetrahedron (pyramid)

Some other gas phase parameters, which were based on the concept of above tetrahedron, have also been considered as the criteria of ignition by researchers (Wichman 1986; Kashiwagi *et al.* 1990; Durbetaki *et al.* 1995). Through a verification of these criteria through gas phase ignition experiments, Tzeng *et al.* (1990) found that the fuel concentration at the location of the ignition source and at the time of ignition for all gas phase ignition cases in their study was approximately the same. Zhou and his co-workers

(2002) obtained similar results through both experiments and numerical analysis for ignition of polymer materials. They found that the gas fuel concentration above the solid, which is partially determined by the pyrolysis rate, is more meaningful compared with the critical mass flux. One conclusion that the authors reached is:

“The invariant gas mixture composition at the time of ignition indicates that for ignition to occur a particular stoichiometry must be reached at the pilot location. This critical stoichiometry, most likely related to the lean flammability limit, is obviously a good choice as the ignition criteria.”

One widely adopted concept for assessing the lean flammability limit is the so-called lower flammable limit (LFL). This is the limit of composition within a fuel/diluent mixture which a flame can propagate. It is expressed as a concentration of fuel in a specified oxidant/diluent mixture at a specified temperature and pressure.

Another widely used concept is the limiting oxygen index (LOI) for supporting flame propagation. This is normally defined as the oxygen mole fraction of the oxidant stream at the point of flammability. The LOI can be used to predict the extinction of flame under certain diluted oxidant conditions. Compared to the LOI, the LFL is more useful in evaluating the possibility of ignition in the fuel mixture.

As indicated by Beyler (2002), the ability of a fuel and oxidant pair to react in diffusion flames can be evaluated by examining the flammability of a premixed stoichiometric mixture of the fuel and oxidant. This may be achieved by satisfying Le Chatelier’s empirical rule. Le Chatelier’s rule, which was generalized by Coward *et al.* (1919), is expressed as follows in an ambient atmosphere:

$$\sum_{i=1}^n \frac{C_i}{LFL_i} \geq 1 \quad (2.24)$$

where:

C_i : volume percent of fuel gas, i , in the fuel/air mixture;

LFL_i : volume percent of fuel gas, i , at its lower flammable limit in air alone.

If the indicated sum is greater than unity, the mixture is above the lower flammability limit. This relationship can be restated in terms of the lower flammable limit concentration of the fuel mixture, LFL_F , as follows:

$$LFL_F = \frac{100}{\sum_{i=1}^n (C_{fi} / LFL_i)} \quad (2.25)$$

where C_{fi} is the volume percent of fuel gas i in the fuel gas mixture.

The lower flammability limit at other temperature conditions can be obtained from the above values by applying the critical adiabatic flame temperature at the lower flammable limit. The concept of the critical adiabatic flame temperature came from observation by Burgess and Wheeler (1911). They noted a constancy of the potential heat release rate per unit volume of normal alkane/air lower flammable mixture at room temperature. This observation also implies that the adiabatic flame temperature at the lower flammable limit is a constant, since the heat capacity of the products from complete combustion are almost the same for all hydrocarbons. The details about this concept and its utility exceeds the research area of current study, but can be found in Beyler's paper (Beyler and Hirschler 2002).

Due to the constancy of the adiabatic flame temperature at the lower limit, this concept can be used to predict the effect of variable mixture temperature and diluents. The relation between the LFL and the critical adiabatic flame temperature, $T_{f,LFL}$, is given by the following equation when all the heat released in adiabatic combustion is absorbed by the products of combustion:

$$\left(\frac{LFL}{100} \right) \Delta H_c = \int_{T_i}^{T_{f,LFL}} n C_p dT \quad (2.26)$$

where:

ΔH_c : heat of combustion of the fuel, kJ/kg;

$LFL/100$: mole fraction of fuel;

n : number of moles of products of combustion per mol of fuel/air mixture;

C_p : heat capacity of the products of combustion, kJ/kg·K;

T_i : initial temperature of the fuel/air mixture, K;

$T_{f,LFL}$: adiabatic flame temperature of a lower flammable limit mixture, K.

The heat capacity in Equation (2.26) is a temperature-dependent variable. When an average value of the heat capacity is applied in the above equation, it gives:

$$\left(\frac{LFL}{100}\right)\Delta H_c = nC_p(T_{f,LFL} - T_I) \quad (2.27)$$

Equation (2.27) exists for different initial temperatures. Therefore the following equation applies for LFLs at various initial mixing temperatures.

$$\frac{(T_{f,LFL} - T_{I,1})}{LFL_1/100} = \frac{\Delta H_c}{nC_p} = \frac{(T_{f,LFL} - T_{I,2})}{LFL_2/100} \quad (2.28)$$

Suppose the first initial temperature $T_{I,1}$ is the ambient temperature, then the LFL at another initial temperature $T_{I,2}$ can be calculated from Equation (2.28).

It is postulated that flammability limit is a more appropriate criterion for ignition. Flammability limits are expressed in terms of fuel volume fraction in air. Since mixture fraction is defined as fuel mass fraction and, therefore, fuel volume fraction has one-to-one relationship for any given fuel. The lower flammable limit can be translated to a critical mixture fraction, which is a form of critical gas phase fuel concentration.

The concept and theory of the LFL are simple and the relationship between the LFL and critical mixture fraction is clear. An ideal approach to validate this criterion is to compare a LFL value from the theoretical computation with a fuel concentration value (expressed as the mixture fraction) measured from experiments. However, the direct application of this concept is not so easy. The reason is that the experimental measurement for the mixture fraction of pyrolysis products is restrained by current technology and resources. Therefore investigation of the mixture fraction as the criterion will rely on some type of numerical computations. Such numerical solutions may require advanced computing technology and the availability of more accurate decomposition chemistry, gas phase chemical kinetics and thermal and radiative properties (Zhou *et al.* 2002). This reveals a possible research approach for this study to achieve an applicable criterion, some form of fuel concentration, for complex gas phase conditions.

2.5 Flame Spread on Solid Combustible Surfaces

As mentioned in Chapter 1, flame spread over solids is a key component in a fire model since this will affect the initial fire development and heat release. This has been a subject of interest in both testing and modelling researches.

2.5.1 Flame spread mechanism

Flame spread over a solid combustible surface can be regarded as a continuous pilot ignition process. For the flame to spread, enough heat must be transferred from the flame and/or other heat sources to the unburnt area ahead of the flame front. The vaporized fuel is then diffused and convected away from the surface to mix with the oxidizer. The flammable mixture is formed ahead of the flame edge and is then ignited by the flame.

Flame spread was reviewed in detail by Williams (1976). The fundamental equation for the flame spread is as follows:

$$\rho V_f \Delta h = q'' \quad (2.29)$$

and

$$\Delta h = c(T_{ig} - T_l) \quad (2.30)$$

where:

ρ : density of the medium, kg/m³;

V_f : flame spread speed, m/s;

q'' : net heat transfer, kW/m²;

c : specific heat of the solid or liquid, kJ/kg·K,

T_{ig} : ignition temperature, K; and

T_l : initial surface temperature, K.

Rearranging Equations (2.29) and (2.30):

$$V_f = \frac{q''}{\rho c (T_{ig} - T_l)} \quad (2.31)$$

The problem is essentially about heat transfer. The geometry of the solid, i.e. horizontal or vertical orientation, opposed or concurrent flow, is found to affect the heat transfer, and has been studied extensively (Quintiere 1995).

The heat transfer from the flame to the unburnt combustible ahead is strongly dependent on the orientation of the flame, which in turn is dependent on the characteristics of the gas flow. When the gas flow, either naturally induced or forced, opposes the direction of flame spread, the flow keeps the flame close to the surface downstream of the pyrolysis front. This type of spread is commonly called opposed flow flame spread and natural convection horizontal flame spread is an example. If the gas flow is in the direction of spread, the flame is pushed forward ahead of the pyrolysis region. This type of spread is known as concurrent flame spread and natural convection upward spread of flame is such an example.

Fernandez-Pello *et al.* (1980) studied both opposed flow and concurrent flow flame spreads, and found a similarity between the mechanisms controlling the solid ignition and the flame spread processes. Their experimental results show a relationship between the ignition delay time and the flame spread rate. In the flame spread process, the flame acts as both a heating source for pyrolysis and a pilot for ignition. This suggests that a simplified model of flame spread could be based on the analyses developed for solid ignition (Section 2.4). Since the time for a solid element to ignite is the same as for the flame to propagate to the solid element position, the velocity of flame spread will be given by the ratio of the solid heated length ahead of the pyrolysis front to the solid ignition time. For a comprehensive analysis of flame spread under various conditions, readers are referred to papers by Fernandez-Pello (1995) and Quintiere (1995).

Theories of flame spread have been built up, and a number of models to apply the theories have been published (Drysdale 1999).

Quintiere and Rhodes (1994) developed a model for the combustion of PMMA in the cone calorimeter. The analytical model was based on solutions for one-dimensional unsteady conduction and surface vaporization at a fixed temperature. The burning rate was calculated by the moving vaporizing surface at the fixed vaporization temperature. The flame radiation was calculated by adopting an algorithm for pool fires to obtain the absorption coefficient and mean beam length. This is a relatively simple model, and suitable for plastic material,

such as PMMA, since their vaporization and combustion behaviour is similar to that of a pool fire.

Fernando (2000) developed a CFD-type flame spread model, CESARE-CFD, that was based on a simple combustion model which was combined with a flame spread model (Luo and Beck 1996). This CFD model adopted the basic ignition controlling mechanism described in Section 2.4 and a critical surface temperature was used as the ignition criterion. It used the kinetics obtained from TGA tests to model the pyrolysis of polyurethane (PU) foam with certain assumptions about the decomposition process. The simulated prediction matched favorably with tested flame spread on a PU foam slab in a full-scale room test.

Flame spread on building elements, especially on walls, is an important application area for basic flame spread theory and the material property data obtained from tests. Quintiere suggested a practical approach to predicting material performance (Quintiere 1988). In his study, an analytical method was adopted to create correlations between the theories of ignition, spread and combustion and the tested material data. These properties have been measured for many types of materials, such as thermo-plastics and timber.

Beyler *et al.* (1997) developed a model to describing upward flame spread and fire growth on wall materials. This model includes following sub-models: ignition, material heating, pyrolysis and burning rate, flame spread, and flame and surface heat transfer. In this model, a relatively simple pyrolysis model was adopted which determining the pyrolysis flux by effective heat flux and heat of gasification of the material. The heat transfer was simplified as one-dimensional problem and integral solution was used. The ignition criterion is the critical surface temperature. The material property data, including the thermal inertia, $k\rho c$, ignition temperature, effective heat of gasification, and heat of combustion, were obtained from cone calorimeter tests. This model has been used to predict flame spread behaviour of PMMA, plywood, and vinyl-ester/glass composite, and reasonable agreement with experimental data has been achieved.

Generally flame spread depends on the heat transfer processes at the front of the flame. These transport processes depend on both the fuel material properties and other environmental conditions. Therefore the estimation of flame spread requires specific

material data and complex analysis. The current state of knowledge provides limited formulas and material data to make this estimation.

2.5.2 Material properties and measurement for the flame spread

Since flame spread is a continuous ignition process, the two mechanisms that control ignition, discussed in Section 2.4, can also be assumed to control flame spread. The material properties that are associated with the controlling mechanisms include density, ρ , thermal conductivity, k , specific heat, c , and ignition temperature T_{ig} . These parameters are sometimes treated as parameter groups under specific circumstances. For example, when dealing with thermally thick materials, the predominant parameters are $k\rho c$ and T_{ig} . If the material studied is thermally thin, then parameter group ρc and T_{ig} are important.

For engineering applications of thermal modelling, it is important to develop a practical methodology to estimate these properties. T_{ig} is a critical parameter in the application of both the ignition and flame spread models. As noted earlier, its value can be measured directly with thin thermocouples embedded at the surface of the solid. However, the measurement may not be very accurate because it is difficult to place the thermocouple exactly at the surface, and it may also absorb or emit radiation in a different way from the solid surface itself. Therefore some analytical methods, combined with the experimental data to estimate this parameter, are still necessary.

2.6 Experimental Methods

Experiments or tests play a key role in fire science. Fire may be the first and also the most important tool in history of human beings. It has been utilized for more than thousands of years. However, studies of building fire behaviour, especially the modelling of fires, are still in their early stages. All fire models available for fire engineering users need experimental data or results either as inputs or for validation purposes. First, experiments can introduce concepts and semi-empirical formulas, such as the “zone” concept. Secondly, they also provide necessary data, such as material properties. Thirdly, a model can only be put to practical purposes after being validated by experiments.

Experiments used in fire science can be divided into two categories: bench-scale tests and full-scale tests. Bench-scale tests can provide material properties and their basic behaviour in fires. They are relatively cheap and can be repeated easily. The commonly used small and bench-scale experimental methods and apparatus include Thermogravimetric analysis (TGA), the cone calorimeter, Lateral Ignition and Flame Transport (LIFT), and Single Burning Item (SBI) tests.

On the other hand, middle to full-scale tests can simulate real fire scenarios, measure fire behaviour (mainly the heat release rate), and validate the modelling results. However, they may be expensive. The middle to full-scale test equipment includes the furniture calorimeter (NT FIRE 032), the room calorimeter (ISO 9705), and the room/corner test device (ASTM 1983). The furniture calorimeter enables the study of combustion behaviour of a whole piece of furniture and one example of application of this equipment can be found in research carried out by Babrauskas *et al.* (1982). One example of the full-scale tests is a doorway calorimetry that can be used to measure oxygen concentration profiles across the burn room door (He *et al.* 1998). Another such example is the room/corner test that is used to evaluate the fire performance of wall and ceiling linings from a corner fire. This test method has been standardized by ASTM (ASTM 1983) and ISO (ISO_9705 1993).

The middle to full-scale experimental methods will not be reviewed individually in this literature review since they are not directly related to the current research interest.

2.6.1 Thermogravimetric analysis (TGA)

The thermogravimetric (TG) analyser is now a standard device in chemistry and chemical engineering research. It was first used for analysis of coal burning profiles by Wagoner and Duzy (1976). This test has been established as a routine procedure and is in regular use for assessing the burning characteristics of solid fuel, such as coal products. More recently it has been used to study reaction kinetics (rates) of pyrolysis and combustion (Stanmore 1991).

The TG analyser maintains a desirable thermal condition for a specimen of a very small quantity (less than 20 mg) and a constant supply of a relatively large amount of working gas

so that the diffusion control factor of the reaction can be neglected and hence the reaction kinetics can be analysed. The output from a thermo-balance system is plotted against temperature to obtain the kinetic features of the sample. A detailed description of this device is given in Section 4.1.

Research using the TGA to calculate the kinetics of materials can be found in works by Ramiah (1970), Cordero *et al.* (1989; 1991), Parker and LeVan (1989), and Liu (2000).

Questions have been raised about the direct application of the kinetics obtained from the TGA tests (Schneider 1992; Beyler and Hirschler 2002). Concerns about the traditional TGA method are the low heating rate and large temperature gradients in the specimen. The heating condition monitored is limited to the surface or a shallow depth of the specimen. This may limit the application of the kinetics in flaming combustion conditions.

To eliminate the above problems and obtain applicable kinetics, a number of efforts have been made. Cordero *et al.* (1989) suggested controlling the sample size and heating rate for the TGA tests. Parker (1988) developed a test method to separate the whole set of apparatus into two parts, the TG analyzer (as pyrolyzer) and the catalytic converter (carbon dioxide, water vapor and oxygen analyzers). This was believed to help eliminate the effect from the heating environment (in the pyrolyzer) for the calculation for the kinetics (through the gas analysers). On the other hand, improvements have been also made in the computational scheme for the kinetics. Seungdo and Park (1995) demonstrated the application of high heating rates in TGA tests. They also verified a shifting pattern in reaction rate curves, which was discovered by Ozawa *et al.* (1970) and is capable for calculation of the kinetics. Liu and his co-workers (Liu and Fan 1998; Liu *et al.* 2003) improved the kinetics calculation by illustrating a kinetic compensation effect in the kinetic parameters and developing a method to avoid the presupposition for reaction order, which may introduce errors. Staggs' research (1999) also demonstrated that a global in-depth pyrolysis model using TGA-derived kinetics may be able to predict mass loss rates in bench-scale experiments such as the cone calorimeter tests.

Despite these improvements, a key issue still somehow remains. As discussed in Chapter 1, it is a major challenge to find a relatively simple test method and computational scheme to

obtain “effective” kinetics that can adequately describe the decomposition process under real fire conditions.

2.6.2 Cone calorimeter

The cone calorimeter is the most commonly used bench-scale heat release rate apparatus. It measures the heat release rate (HRR) by utilizing the oxygen consumption principle. It was developed by Babrauskas at the National Bureau of Standards in the 1980s (Babrauskas 1984).

The cone calorimeter simulates the conditions of a piece of fuel exposed to a fire environment. The major measurements include the mass loss rate (MLR), heat release rate (HRR), temperature, species yield, radiation, and so on. The apparatus and test procedure are standardized in the USA (ASTM_E1354-04 2004) and internationally (ISO_5660-1 2002).

The cone calorimeter can be used to measure certain quantities in the testing conditions. These quantities include heat release rate, ignition time, heat of combustion, etc. These measured quantities are used to predict fire behaviour in a full-scale or compartment environment. Detailed information about this bench-scale experimental device and its operation is included in Chapter 5. There is a great wealth of literature in regard to the cone calorimeter and its applications in fire research. Only a few articles that clearly relate to the current research interest are reviewed below.

Grexa and co-workers carried out a series cone calorimeter tests on wood products (Grexa *et al.* 1996; Grexa *et al.* 1997). The major measurements in their tests were HRR, total heat released (THR), and ignition time (t_{ig}). A number of thermal properties were then derived from those basic measurements, such as critical heat flux q_{cr}'' by Janssens’ method (Janssens 1991), thermal inertia $k\rho c$ and heat of ignition ΔH_{ig} . The effects of wood species and timber surface orientation (alone or cross-sections) in the cone calorimeter tests were investigated by Harada (2001). While most of experimental data available were obtained from the along-texture section samples, a slower combustion (longer t_{ig} and smaller HRR at the same external radiation level) was observed for the cross-texture section samples. Tests

for the thermal plastic material PMMA were carried out by Tsai *et al.* (2001) and Zhou *et al.* (2002). It was found that ignition process depends not only on PMMA pyrolysis but also on gas phase reaction (i.e. it is affected by gas flow conditions, which matches previous analysis for ignition). As a thermal thick material, a linear relationship between $1/\sqrt{t_{ig}}$ and \dot{q}_{rad}'' was observed from the tests for the PMMA.

By running Round-Robin type international or inter-laboratory tests (ASTM 1990), errors in the material property measurement from the cone calorimeter, which are associated with device and operation differences, can be reduced greatly.

Meanwhile the combustion process in the cone calorimeter has been modelled by a number of researchers (Staggs and Whiteley 1999; Bilbao *et al.* 2001; Janssens *et al.* 2001). Some reasonable simulation results have been obtained. In general, the standardized testing condition and environment makes the cone calorimeter a useful device for measuring material properties and to validate ignition models.

More cone calorimeter experimental results, especially for those materials identical or similar to the furnishing materials used for this research will be discussed later in Chapter 5.

2.6.3 LIFT and SBI

LIFT (ASTM_E1321-90 1990) is a flame spread test resulting from Quintiere's research (Quintiere 1981). This device has been used to measure the "effective" properties for ignition and flame spread, including $k\rho c$ and T_{ig} . Measurements from LIFT are normally combined with other bench-scale test results, such as those from the cone calorimeter, to predict full-scale and real fire environment behaviour. Some applications of results from this testing can be found in the literature (Quintiere and Harkleroad 1984; Delichatsios 1999; Zhou *et al.* 2002).

The SBI test (prEN_13823 2002) is a new fire test method developed for the Euroclass system. The test is based on a fire scenario of a single burning item located in a corner

between two walls covered with the lining material to be tested. The SBI test can be used for the classification of construction products.

Measurements from the SBI test include the heat release rate and the smoke production rate. Observation of flame spread can also be made, but only to the extent of recording the time taken to reach the extreme edge of the sample. These data are used to produce derivative indices, such as FIGRA (Fire Index Growth RAte) and SMOGRA (SMOke index Growth RAte), for classification. These two indices express the rates of growth of the heat release rate and the smoke production rate.

Modelling and experimental studies have been carried out for the relationship between the SBI test and the cone calorimeter test (Messerschmidt *et al.* 1999; Hakkarainen and Kokkala 2001). It was found that by using cone calorimeter tests, the number of SBI tests required could be reduced greatly without additional data or material parameters. For example, the results from a single cone calorimeter test are useful for predicting peak heat release rates in a number of SBI tests (Messerschmidt *et al.* 1999).

2.6.4 Applications of the experimental methods

This section describes the methods that may be used or have been developed to obtain several thermal parameters, by the above experimental methods.

The “effective material fire properties” for modelling flame spread can also be measured by a number of test procedures. The lateral ignition and flame spread (LIFT) apparatus is one such example (ASTM_E1321-90 1990). The effective properties obtained from this method include: $k\rho c$, T_{ig} and Φ (a measurement of the flame heat transfer under conditions of opposed flow natural convection in air).

The ignition temperature can also be measured in cone calorimeter tests following an experimental procedure suggested by Quintiere and Harkleroad (1984). A series of cone calorimeter tests were carried out to determine the minimum radiative flux required for a kind of fuel ignited. The minimum radiative flux is decided by the radiative flux when an

asymptotic curve of ignition time is extended to the infinite (normally 600 seconds is used). The experimental results are illustrated in Figure 2.4. Then Equation (2.23) is applied to calculate the ignition temperature when the heat transfer coefficient at ignition h_{ig} is known or can be determined from other methods.

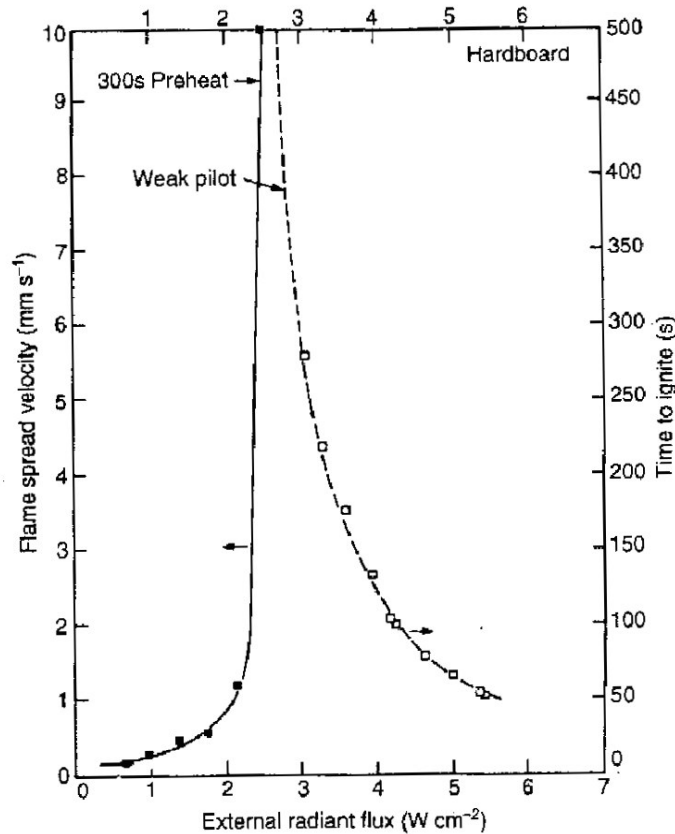


Figure 2.4 Experiments for obtaining ignition temperature (quoted from work of Fernandez-Pello (1995))

The heat of combustion, ΔH_c , can be determined from the cone calorimeter test (using measured heat release rate and a mass loss rate) by a procedure suggested by Janssens (1992). The calculation of effective heat flux for a thermally thick solid was modified by extensive numerical simulation results.

There are other parameters not related to the current study and thus not discussed in this thesis. Table 2.1 below briefly summaries the major properties of solid combustible materials and the measuring devices.

Table 2.1 Major parameters and measuring methods

Parameters	Measuring apparatuses
Ignition temperature, T_{ig}	cone calorimeter or LIFT
Thermal inertia, $k\rho c$	as above
Lateral flame spread parameter	LIFT
Minimum temperature for lateral spread, $T_{s,min}$	as above
Heat of combustion, ΔH_c	cone or bomb calorimeter
Effective heat of gasification, L	cone calorimeter
Heat release rate per unit area, Q''	as above
Activation energy, E , & pre-exponential factor, A	TG analyser

However, it should be noted that the capability of a bench-scale test apparatus to reproduce end-use conditions of tested materials and correspondence of test conditions with fire environment is not yet very clear. Originally the heat release rate of common combustible building and furniture materials was believed to be sensitive to the heating condition. It is technically difficult to run cone calorimeter tests at very weak levels of radiation (say, less than 10 kW/m^2 for timber materials) which is still meaningful in flame spread for fire safety. Meanwhile, the heat release rate obtained from the cone calorimeter at a level of external heat flux of 25 kW/m^2 or lower is considerably lower than that obtained at an identical heating condition in full-scale or medium-scale heat release measurement. While the bench-scale test results were difficult to apply to such situations, basic pyrolysis analysis (based on the kinetics from TGA tests) and heat transfer calculations may be able to contribute to the solution of this kind of problem.

2.7 Unresolved Phenomena and Research Interests

Unresolved issues based on the literature review and discussion in the previous sections were summarized in this section. Interested areas and requirements were then identified to achieve the specified research aims described in Chapter 1.

2.7.1 Unresolved issues related to current research

Providing enough accurate information to describe fire development is necessary in performance-based fire safety and risk assessment practice. It is also a requirement for development of today's fire models. This task requires a better understanding of fire itself. For example, the heat release rate is the single most important variable in describing fire hazard (Babrauskas and Peacock 1992). The prediction of HRR has experienced continuous improvement during the last decades as fire models have developed. As reviewed previously, this improvement started from prescribing input data for the HRR, to perform basic calculations for simple fuel configuration, such as pool fuel, wood crib or polyurethane foam, and then estimating real-scale HRR based on bench-scale test results. The limitation of this latter scheme is numbers of uncertain and then assumptions existed when applying the bench-scale HRR values to the prediction of real-scale HRR.

Recently prediction of HRR based on a combustion model, which combined with computation from a flame spread model, has been adopted into a number of fire models (Drysdale 1999). However, serious limitations still exist for applying the theories into real flame spread prediction as a number of assumptions and empirical correlations have to be embedded into the models. Examples include the NRCC-VUT (He 1996) and FIRST (Mitler and Rockett 1987), etc. Even for a CFD model, which has the ability to describe the combustion process in detail, the flame spread modelling is still relatively crude. There are a number of reasons. First, most CFD models have only one-dimensional heat transfer ability for the solid (Quintiere and Rhodes 1994; McGrattan *et al.* 2000). A number of simplifying approximations for the geometry and heat transfer conditions are normally made to make a flame spreading problem theoretically 'tractable'. This often limits the usefulness of the models. Secondly, modelling of flame spread on a solid greatly depends on ignition properties of the material, such as ignition temperature. Such critical data are still very limited for widely used materials (Babrauskas 2001). Finally heat transfer in real fire conditions is very complicated and very fine resolutions of grid in CFD models are required. This limits the engineering applications of most of today's computer models. Reasonable accuracy can only be achieved by modelling more details about the combustion phenomena with a robust numerical scheme.

Fire model developers are currently making improvements for numerical schemes aiming to deal with complicated heat and mass transport, and to shorten the simulation duration. Some progresses have been achieved recently. Therefore the research task of this study returns to

the area identified in Chapter 1: the basic phenomena within the pyrolysis, ignition and flame spread processes.

The basic theories and experimental methods for measuring quantities related to these processes have been developed as reviewed in previous sections. There are still unresolved issues, which have been identified in this literature review related to the current research aims. These can be listed as follows and some are similar to those summarized by T'ien (2002):

1. Lack of detailed chemical kinetic information for the combustion of solids. This includes both the solid thermal decomposition processes and the oxidizing kinetics of the pyrolysis gases.
2. The application to a real fire condition of the kinetics obtained from the normal TGA test method and computational scheme is still questionable.
3. Solid phase processes, for the studied materials, may include charring, bubbling, cracking and smouldering. Whether these events should be incorporated into the model may depend on their importance to a particular problem.
4. The common ignition criteria for solid materials are still to be validated in complicated geometry conditions. The criterion associated with gas phase fuel either does not exist or is difficult to compute.

Meanwhile, lack of knowledge of widely used materials, even for commonly used furnishing materials, impedes their applications in fire models. This is partly due to insufficient applicable experimental data, and partly due to inadequate models (methods) to interpret the available data. For example, the kinetics of the thermal decomposition processes of the furnishing materials selected in the current study are either not known or there is great variation in the available experimental data.

2.7.2 Research interests and requirements identified for current study

According to the unresolved issues identified above, the interests of the current research will focus on pyrolysis analysis and ignition processes. The objective of the study is to verify the critical mixture fraction as an ignition criterion, which will be applied in an engineering approach for prediction of combustion and flame spread. The methodology is to use a

combined experimental and numerical simulation approach. The better understanding of pyrolysis progress enables describing pyrolysis and ignition in detail by suitable kinetics and modelling. By applying those pyrolysis details a robust CFD fire model will be improved to generate engineering satisfactory prediction of ignition based on the critical mixture fraction criterion. The requirements for achieving this aim include the following:

- Better understanding of the decomposition process of studied materials under different environments
- Improvement of the TGA test method and computational scheme to obtain the “effective” kinetics which are able to describe the decomposition process in real fire environments
- Modelling the pyrolysis process with major phenomena for the studied materials. (Detailed requirements for the modelling will be discussed in the next chapter.)
- Applying the above, modelling results into a CFD model to simulate pyrolysis, ignition and combustion processes in a carried out bench-scale test, cone calorimeter environment
- Studying the ignition criteria by validating various possible parameters from the modelling against the data from the experiments; calculating the gas phase fuel concentration (the mixture fraction) via CFD modelling and obtaining the critical value at the ignition time which determined by the bench-scale tests
- Validating a relationship between the critical mixture fraction and the lower flammable limit. Developing a gas phase criterion that based on the lean flammability limit theory and applying it onto complex environmental conditions.

CHAPTER 3 MODELLING OF THERMAL DECOMPOSITION AND IGNITION OF SOLID MATERIALS

This chapter deals with modelling of decomposition process, including theoretical analysis and numerical modelling. Based on analysis and comparison for available pyrolysis models, one of the models that meets research requirements will be chosen as a prototype for further modelling. This chapter consists of five sections. The first section describes pyrolysis models in general. Criteria for choosing a pyrolysis model are developed. Section 3.2 discusses Atreya's pyrolysis model in detail. Basic equations for the heat transfer and charring processes are presented. Section 3.3 introduces the major improvements for the Atreya's model made by other researchers. A simple theoretical calculation is performed for one of the studied materials, mountain ash, in Section 3.4. Section 3.5 gives a brief summary of this chapter.

3.1 Pyrolysis and Ignition Models

As reviewed in Chapter 2, a substantial number of experimental and modelling researches have been carried out to study the pyrolysis of a charring solid. The primary objective of these experimental works has been identified as obtaining thermal quantities, such as chemical kinetic data, heat of pyrolysis as well as pyrolysis mass fluxes. The primary objective of pyrolysis modelling is to predict pyrolysis and ignition behaviours of both full-scale and real fires based on measured thermal quantities.

3.1.1 Classification of pyrolysis models

During the past 30 years, a number of pyrolysis models have been developed (Moghtaderi 2001). These models, according to the technical basis adopted to describe the conversion of virgin fuel into volatiles and char residues, can be classified into the following categories:

1. simple thermal models, including
 - algebraic and analytical models

- integral models
2. comprehensive models, including
- analytical models
 - numerical models

In the thermal models, the basic assumption is that pyrolysis occurs when the temperature reaches a so-called “pyrolysis temperature”. With this assumption the problem is greatly simplified and only basic energy balance needs to be solved.

Algebraic and analytical thermal models ignore most of the chemical and physical processes involved in order to reduce the complexity of the solution. For example the mass flux is expressed as a function of location of the pyrolysis front (where surface temperature reaches the pyrolysis temperature). The applicability of this type of model is limited due to the fact that it is incapable of providing a comprehensive solution for detailed outputs. Models developed by Mikkola (1991) and Kanury (1994) are a few examples of this type of models.

Integral thermal models employ numerical solution techniques to solve temperature distribution and mass flux. It can take many physical phenomena into consideration. However, like all thermal models, the integral model neglects chemical kinetics and is again based on the critical temperature criterion. By reducing the partial differential equations (PDE) for energy conservation into ordinary differential equations (ODE), the integral thermal models are relatively simple, easy to use, and computationally economic. However the accuracy for the results is not as high as that of PDE methods. Moghtaderi *et al.* (1997), Spearpoint and Quintiere (2000; 2001) give examples of thermal integral models.

The critical pyrolysis temperature criterion used in the thermal models is equivalent to assuming that chemical processes are much faster than diffusion processes. This has been discussed in Section 2.4. Since the ignition temperature is assumed to be the pyrolysis temperature, (i.e. $t_{ig} = t_{py}$), the gas phase induction time is ignored. However for common solids the global pyrolysis is controlled by chemical kinetics at low temperatures and by diffusion at high temperatures. A building fire may occur over a wide range of temperatures (between 450 – 1000 °C), both diffusion and chemical kinetics should be taken into consideration. This sets the underlying principle of comprehensive models.

In comprehensive models, chemical processes are normally based on first order kinetic schemes. According to the schemes adopted, the models can be categorized as follows:

1. one-step global
2. one-stage multi-reaction
3. two-stage semi-global

The items “step” or “stage” deal with the number of stages involved for a virgin fuel to decompose into products. For example, “one-step” means that the conversion performs directly without middle products being considered. The terms of “global” or “multi-reaction” deal with how to treat the pyrolysis energies. For example the global scheme calculates an activation energy to represent the combination effect of all sub-reactions, whereas activation energies for a number of major reactions are calculated separately in the multi-reaction. In a two-stage semi-global scheme, an activation energy is used for all sub-reactions in one of the two stages.

An example of the development of the comprehensive model may be found in an improved version of Kung’s model (Kung 1972). Kung’s original model incorporated features like variable thermo-physical properties and convective heat transfer. Kung’s model was further developed to account for the porous structure of some solids (DiBlasi 1993), structure changes (Parker 1985) and effect of moisture content (Atreya 1984; Moghtaderi *et al.* 1998).

According to a review given by Moghtaderi (2001), the typical kinetics for one-step global pyrolysis of cellulose have been reported by many researchers. The activation energy ranges from 33.4 kJ/mol to 166.4 kJ/mol, and the pre-exponential factor from 0.1 to 6.8×10^9 1/s.

Other examples of the comprehensive models are Atreya’s one-step global model (Atreya 1984), Parker’s one-stage multi-reaction model (Parker 1985), DiBlasi’s two-stage semi-global reaction model (DiBlasi 1993).

3.1.2 Typical pyrolysis models

As mentioned above, Quintiere’s integral thermal model was applicable for the one-dimensional unsteady conduction problem (Quintiere and Rhodes 1994; Spearpoint and

Quintiere 2001). It has all of the major features described previously. For example, the surface pyrolysis was triggered at a fixed pyrolysis temperature. It is suitable for predicting pyrolysis process of thermoplastics, such as PMMA. With some modifications, it has been applied to model the wood pyrolysis in a cone calorimeter environment (Spearpoint and Quintiere 2001). A degree of agreement to the experimental data has been achieved. However the application of this model to a situation consisting of complicated physical and chemical reactions is still questionable since the simulated details in pyrolysis are limited.

Janssens developed a comprehensive pyrolysis model for the investigation of wood structure performance exposed to fire (Janssens 1994; 2004). The model is based on one-dimensional heat transfer analysis in the wall and assumes a zero value for the heat of pyrolysis. Moisture content was taken into consideration but not the moisture movement to the cold side. The significant feature of this model is that it takes char contraction into account. This function was achieved by adopting a sub-model named CROW (Charring Rate Of Wood). The CROW model is based on White's correlation (White and Nordheim 1992) for charring rate under standard fire conditions, according to the ASTM E119 test. Generally this model provides an ability to predict the charring rate of wood exposed to the specified fire conditions. Additional comparison and validation are needed to extend its application range.

Yuen *et al.* (1997) developed a three-dimensional mathematical model for studying pyrolysis of wet wood. This model includes detailed considerations of evaporation of moisture, anisotropic and variable material properties, and pressure-driven internal convection of gases in wood. The 3-D modelling capability enables it suitable for prediction the pyrolysis of a wooden cube inside a furnace under various temperatures. The pyrolysis reaction is modelled by a first-order Arrhenius reaction. Totally six first-order reactions representing the competing thermal decomposition reactions of various constituents have been formulated in the computational code for future applications.

The kinetics for the pyrolysis of the single constituent (in a beech wood) was obtained from a research conducted by Bonnefoy *et al.* (1993). The kinetics was determined by a method of best fit of mass loss to the experimental results for the wooded cube heated in a furnace. The obtained values for the kinetics are $E = 125$ kJ/mol and $A = 1.25 \times 10^8$ 1/s. Yuen *et al.* found that the computed mass loss is lower than the experimental data within the first 35

seconds in a 973 K environment. According to the researchers, the use of the single kinetic reaction for the modelling is the reason. It is known that competing primary reactions due to the different major constituents (i.e., cellulose, hemicellulose and lignin) and secondary reactions exist in wood pyrolysis (Bradbury *et al.* 1979). They believed that the prediction might be improved by modelling the multiple competing reactions. The method to determine the kinetics for the total 6 reactions corresponding to the major constituents was developed by Alves and Figueiredo (1989) which conducting series isothermal TGA tests. However, no applicable results have been published for adopting such method due to the complication of simulating those reactions properly under various heating conditions.

Atreya's one-dimensional heat transfer pyrolysis model is a comprehensive one-step global reaction model. It is based on Atreya's earlier research on wood pyrolysis and horizontal flame spread (Atreya 1984). This model solves the heat conduction equation with locally varying density, thermal properties and reaction rates to compensate for char formation. With continuous improvement by the author and other researchers, it has the built-in ability to model most aspects of pyrolysis phenomena, such as charring, moisture content, etc. Some developments of this model have been performed and several applications of this basic pyrolysis model have been published, which will be further reviewed later in Section 3.3.

3.1.3 Criteria of model selection for current research

As indicated in the review performed by Moghtaderi (2001), the major weakness of the current thermal model is the lack of detailed chemical pyrolysis expression and poor accuracy in predicting details related to chemical pyrolysis. For example, the integral thermal model could not accurately predict the onset of pyrolysis. This is because the initiation of pyrolysis that occurs at a low temperature range is controlled by chemical kinetics rather than thermal transport. However, this does not mean that the most complicated comprehensive models, such as two-stage multi-reaction and two-stage semi-global, are automatically the best. It is because that there are a great number of details about the semi-reactions which are still unknown or difficult to describe. For example, in the previous isothermal TGA tests developed by Alves and Figueiredo (1989), the temperatures to separate various reactions are difficult to determine. To handle a huge number of details

in today's pyrolysis models is either impossible or unnecessary. Modelling is simplification. As identified in the literature review, a solution for engineering applications is to include enough major phenomena and appropriate details about the phenomena but with a robust kinetic mechanism.

Meanwhile, when heat transport details, such as surface radiative heat loss, are taken into consideration, the difference between experimental data and integral model's prediction will be increased dramatically (Moghtaderi 2001). These shortcomings led to the elimination of the thermal models from consideration as a modelling tool for pyrolysis and ignition.

To meet the research requirements specified in Chapter 1, a set of criteria for choosing the pyrolysis and combustion model was identified by the author. Except for normal requirements like high accuracy and sufficiently fast computational speed, the following criteria are of major concern:

- including major pyrolysis details, such as charring, moisture content, etc
- presenting multiple ignition criteria such as critical surface temperature and critical mass loss flux
- the ability to obtain distribution of gas phase products
- the ability for users to intervene, especially with the kinetics, is highly desirable, as this will provide the possibility to model more closely the materials studied in this thesis.

Among these criteria, user control of kinetics is essential for the current research and the description of gas phase fuel distribution is a preference.

Against the selection criteria above, Atreya's model comes out as the most satisfactory candidate. Atreya's model includes the key functions in the study of pyrolysis. The one-step global pyrolysis model makes it a suitable engineering tool. Various improvements, especially a robust numerical computational scheme in a computer model (McGrattan *et al.* 1998), have been achieved recently. This computer model has been widely applied in FSE. When balancing the advantage of robust computational ability and the disadvantage of a lack of minor phenomena, the author believes that Atreya's model is a suitable prototype for modelling pyrolysis and ignition processes. Therefore this computer model based on Atreya's model was chosen in this research. Further discussion of Atreya's model is presented in the following section.

3.2 Atreya's One-dimensional Heat Transfer and Pyrolysis Model

Based on the basic pyrolysis process described in the literature review, Atreya developed a one-dimensional heat transfer and pyrolysis model (Atreya 1984). The major content of this model is presented briefly in this section.

3.2.1 Basics of Atreya's pyrolysis model

3.2.1.1 Physical model

The physical configuration of the system is illustrated in Figure 3.1.

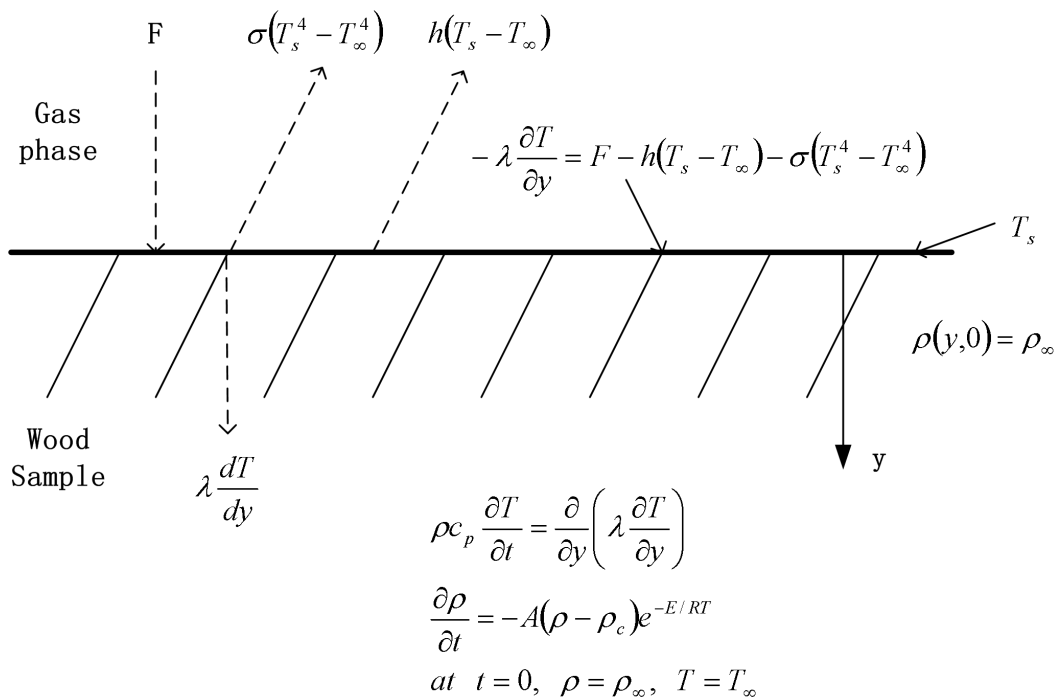


Figure 3.1 Physical configuration of the case being studied

Definitions for the variables used in Figure 3.1 are as follows:

F : total cold wall heat flux, kW/m²;

T : solid temperature, K;

T_s : surface temperature, K;

T_∞ : ambient temperature, K;

t : time, s;

- h : convective heat loss coefficient, $\text{kW/m}^2\cdot\text{K}$;
 e : base of natural logarithms;
 A : pre-exponential factor, $1/\text{s}$;
 E : activation energy, $\text{kJ/mol}\cdot\text{K}$;
 R : universal gas constant, $=8.314\times 10^{-3} \text{ kJ/mol}\cdot\text{K}$;
 λ : conductive coefficient, $\text{kW/m}\cdot\text{K}$;
 c_p : specific heat of solid, $\text{J/kg}\cdot\text{K}$;
 ρ : solid density of fresh solid, kg/m^3 ;
 ρ_c : density of char, kg/m^3 ;
 ρ_∞ : density of solid at ambient environment, kg/m^3 ;
 σ : Stefan-Boltzmann radiation constant, $\text{W/m}^2\cdot\text{K}$;
 y : coordinate normal to the solid surface.

This physical problem can be described as below. A solid fuel slab, wood in Atreya's research, initially at equilibrium with the surrounding atmosphere, is subjected at $t = 0$ to a constant incident radiative heat flux F . It is assumed that the gas phase is inert (no oxidative effects) and that the influences of solid-phase cracking, shrinkage, surface regression, and grain direction are negligible. The interaction between F and the gaseous products of pyrolysis is also neglected. Thus, F is assumed to be the time-average radiative heat flux reaching the surface. The wood is assumed to be nondiathermic and opaque to the incident radiative flux.

3.2.1.2 Four stages of wood pyrolysis

There are four stages of the wood pyrolysis process, as shown in Figure 3.2.

The initial heating phase, herein called the "inert heating stage", is characterized by the heat of the surface to T_{py} , the pyrolysis temperature, which is defined as the value of T at the inception of pyrolysis. No chemical reactions occur in this stage, and since the material is considered dry (i.e., there is only bound or hygroscopic water, see Section 2.3.3.2), there are no effects of moisture. The change in density is negligible until the solid temperature is close to the pyrolysis temperature.

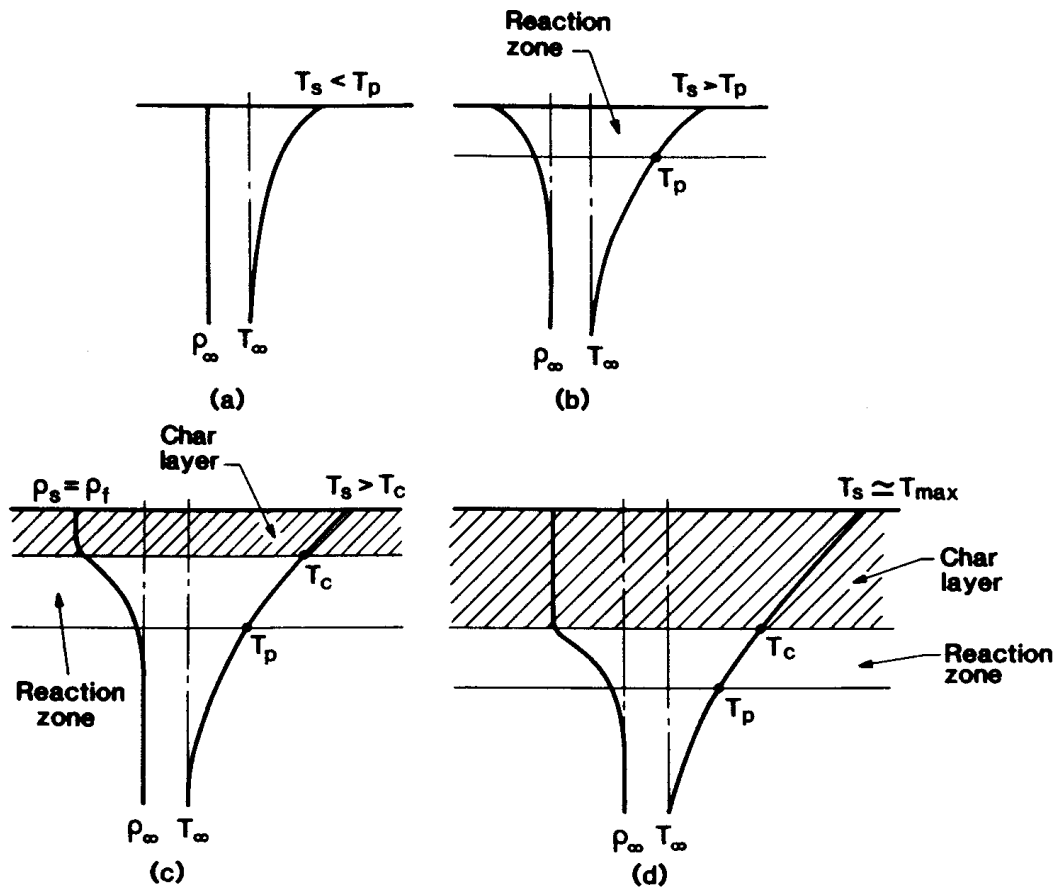


Figure 3.2 Stages of wood pyrolysis

In the next heating phase (the initial pyrolysis stage or the transition regime) the initial release of volatiles from the surface coincides with the formation of a pyrolysis front. In this phase a rapid rise in the volatile mass flux is observed, and heat losses from the surface by convection and re-radiation become important. The surface temperature and the volatile mass efflux continue to increase until a thin char layer forms.

In the char layer, the temperature is defined as charring temperature, T_c . In this heating stage (thin char) the mass flux reaches its maximum value.

The final heating stage (thick char) is characterized by a gradual decline in mass flux, m'' , and a correspondingly gradual increase in the char layer thickness. The expected time span of each of these four stages is illustrated qualitatively in the m'' versus t plot of Figure 3.3.

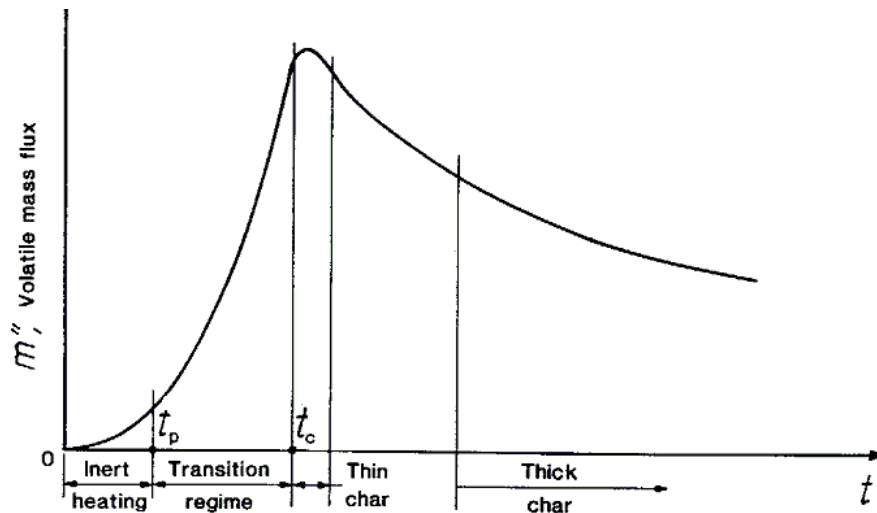


Figure 3.3 Pyrolysis regimes in a qualitative plot of the volatile mass flux versus time (source: Atreya (1984))

3.2.2 Basic equations and assumptions

Three important assumptions were made in Atreya's study. The first assumption is that the thermal interactions between the volatile gases and the reacting material can be neglected. It is known that the generation of volatile gases inside the solid sample can produce high pressures (up to 0.3 atm (Lee *et al.* 1976), depending on the wood porosity). And they force the volatiles toward both directions, to the hot char layer and to the interior of the solid condense, only to be subsequently re-gasified. The net heat transfer between the volatiles and the hot char, whose magnitude is measured by the quantity $c_{p,g}(T_s - T_c)$, ($c_{p,g}$ is the specific heat of the volatiles), is ignored for two reasons. First, for small char layer thickness, $c_{p,g}T_c(T_s/T_c - 1)$ is negligible because $(T_s/T_c - 1)$ is far less than 1. Second, when the char layer thickness is large, and T_s/T_c far larger than 1, most of the volatiles are issued through cracks, which were observed in the char layer before ignition in most experiments (Goos 1952; Tang 1972). This makes the net heat transfer between volatiles and char negligible. The effects of condensation and re-gasification are also ignored since the temperature gradient is decreased down from the surface and these effects will be very weak while volatiles are releasing.

The second assumption is that the chemical processes occurring in the decomposition of "dry" wood to char can be modelled by a single, one-step rate equation containing three fixed parameters, the char density ρ_c , the pre-exponential factor A , and the activation energy

E. This assumption is an idealization of the actual process since wood decomposes in a complex manner, producing hundreds of compounds. However, there is presently much controversy concerning its precise nature and no generally accepted reaction pathway, analogous to those used to model gas phase reactions, has yet been developed.

The third assumption is that the heat of pyrolysis, ΔH_{py} , in Atreya's original model is negligible. As discussed by Atreya (1984), there is much confusion about this term. Reported values vary between 750 J/g (endothermic) and -18800 J/g (exothermic). The exothermicity apparently arises from secondary reactions between the oxygen and the hot char, or the pyrolysis gases. However, the net exothermicity of the process must be relatively small, since thermal runaway (i.e., explosion) has never occurred during wood pyrolysis. An estimate for the upper bound of ΔH_{py} is $c_p(T_{py}-T_\infty) \approx 0$ (418 J/g), which is the sensible heat required to raise 1 g of wood to its pyrolysis temperature. Thus, $\Delta H_{py} < 418$ J/g could lead to thermal runaway. Therefore, Atreya argues that whether exothermic or endothermic, ΔH_{py} is generally much smaller than the thermal diffusion term in the equation for the conservation of energy (see Figure 3.1), and $\Delta H_{py} \approx 0$ is assumed here. This assumption has been employed by previous researchers (Atreya 1984; Parker 1985).

With the above assumptions, the model equations and boundary conditions describing the pyrolysis of wood can be reduced to those shown in Figure 3.1. The density and thermal conductivity of timber are all functions of solid temperature. If it is also assumed that the thermal conductivity is proportional to the density, i.e., $\lambda = \rho k$, where $k = \text{constant} = \lambda_\infty / \rho_\infty$, then the equations from this figure can be re-written as follows. It is noted that all the variables in following equations have same definitions as in Figure 3.1.

Heat transfer equation at surface:

$$-\lambda \frac{\partial T}{\partial y} = F - h(T - T_\infty) - \sigma(T^4 - T_\infty^4) \quad (3.1)$$

Within the solid:

Energy:

$$\rho c_p \frac{\partial T}{\partial t} = \frac{\partial}{\partial y} \left(\lambda \frac{\partial T}{\partial y} \right) \quad (3.2)$$

$$\text{Decomposition:} \quad \frac{\partial \rho}{\partial t} = -A(\rho - \rho_c)e^{-E/RT} \quad (3.3)$$

$$\text{Mass:} \quad \frac{\partial m}{\partial y} = \frac{\partial \rho}{\partial t} \quad (3.4)$$

Boundary and initial conditions:

$$\begin{aligned} T(y,0) &= T(\infty,t) = T_\infty \\ \rho(y,0) &= \rho_\infty \\ -\rho \frac{\partial T}{\partial y}(0,t) &= T_\infty - \Gamma(T_s - 1) \end{aligned} \quad (3.5)$$

where:

T_s : surface temperature, K;

m : mass of the solid, kg;

$\Gamma = hT_\infty/F + (\sigma T_\infty^4/F)(T_s + 1)(T_s^2 + 1)$, the linearized convective and radiative heat losses term.

The derivation for the critical parameters, such as pyrolysis temperature, pyrolysis time, charring temperature, charring time, and mass flux at different stages, are presented in Appendix B.

3.3 Improvements and Applications for Atreya's Model

Major improvements to Atreya's model were made by Parker (1989), Steckler *et al.* (1994), and Ritchie *et al.* (1997). The improvements include incorporation of charring properties, backing substrate, and moisture content, etc. The works of Parker and Ritchie *et al.* are described in the following two sub-sections.

3.3.1 Improvement by Parker

In his numerical scheme, Parker (1985) divided the fuel slab into thin isothermal slices, and calculated mass flux on each slice. The total mass loss was summed from all the slices. The shrinkage was calculated from the char contraction coefficients. Moisture content was taken into account in the energy equation. The ignition criterion was the critical mass flux, set as

2.5 g/m²·s, excluding the release of moisture. When the calculation results were compared with cone calorimeter testing data, a reasonable agreement was achieved (Parker 1992).

3.3.2 Improvement by Ritchie *et al.*

Ritchie's modified model (Ritchie *et al.* 1997) includes descriptions for conduction of heat to the back substrate materials, the evaporation of moisture and the decomposition of the virgin wood into gas phase fuel products and char. In other words, Atreya's third assumption was eliminated. The time lag for the movement of gases products within the solid, which is caused by the obstacles, is ignored. This assumption results in an instantaneous release of the gaseous products.

On the surface, the governing equation for energy (Equation (3.2)) is detailed as below:

$$\bar{\rho}c \frac{\partial T}{\partial t} = \frac{\partial}{\partial y} \left(\lambda_w \frac{\partial T}{\partial y} \right) + \frac{\partial \rho_w}{\partial t} [\Delta H_{py} - C_1(T - T_\infty)] + \frac{\partial \rho_m}{\partial t} [\Delta H_{ev} - C_2(T - T_\infty)] \quad (3.6)$$

where:

ρ_w : the total density of the wood, kg/m³;

ρ_m : the moisture density, kg/m³;

ΔH_{py} and ΔH_{ev} : the heat of pyrolysis of wood and the heat of evaporation of water, kJ/kg;

λ_w : conductivity for the wood, W/m·K, and determined by Equation (3.7);

C_1 and C_2 : coefficients and given by Equations (3.8) and (3.9);

$\bar{\rho}c$: average density and specific heat for pyrolysis process, kg/m³, and

T_∞ : ambient temperature, K.

The boundary condition on the wood surface is due to radiation and convection, and reaches a balance as follows:

$$-\lambda_w \frac{\partial T}{\partial y} \Big|_{solid} = q_{rad}'' - \lambda_g \frac{\partial T}{\partial y} \Big|_{gas} \quad (3.7)$$

where:

q_{rad}'' : the net radiative heat flux on the surface, kW/m², and

λ_g : conductivity for the gas phase, $\text{W/m}^2\cdot\text{K}$.

The two coefficients C_1 and C_2 are defined as

$$C_1 = \frac{\rho_{w0}\bar{c}_{p,w0} - \rho_{wf}\bar{c}_{p,wf}}{\rho_{w0} - \rho_{wf}} - \bar{c}_{p,g} \quad (3.8)$$

$$C_2 = \bar{c}_{p,m} - \bar{c}_{p,g} \quad (3.9)$$

where:

ρ_{w0} and ρ_{wf} : densities of the virgin wood and the char respectively, kg/m^3 ;

$\bar{c}_{p,w0}$ and $\bar{c}_{p,wf}$: average specific heats of the virgin wood and the char during the pyrolysis period respectively, $\text{kJ/kg}\cdot\text{K}$;

$\bar{c}_{p,g}$ and $\bar{c}_{p,m}$: average specific heats of the gaseous products and the moisture during the pyrolysis period respectively, $\text{kJ/kg}\cdot\text{K}$.

Inside the solid timber, the pyrolysis rate is modelled as a first order Arrhenius reaction:

$$\frac{\partial \rho_w}{\partial t} = -\rho_a A e^{-E/RT} \quad (3.10)$$

where:

ρ_a : density of the active wood, kg/m^3 ;

A : the pre-exponential factor, $1/\text{s}$, and

E : the activation energy, $\text{kJ/mol}\cdot\text{K}$.

As a simplification, equation (3.10) is only applied after the wood temperature reaches 100°C . The evaporation of moisture is assumed to consume all the available energy while the wood reaches the evaporation temperature, T_{ev} . The evaporation rate is given by following equation:

$$[\Delta H_{ev} - C_2(T - T_\infty)] \frac{\partial \rho_m}{\partial t} = -\frac{\partial}{\partial y} \left(\lambda_w \frac{\partial T}{\partial y} \right) \Big|_{T=T_{ev}} \quad (3.11)$$

The thermal properties of the wood during the moisture releasing and charring processes are calculated by the following equations:

$$\bar{\rho c} = (\rho_a c_{p,w0} + \rho_c c_{p,wf} + \rho_m c_{p,m})$$

$$\lambda_w = \lambda_{w0} \left(\frac{\rho_a}{\rho_{w0}} \right) + \lambda_{wf} \left(\frac{\rho_c}{\rho_{wf}} \right) \quad (3.12)$$

$$\rho_a = \rho_{w0} \frac{\rho_w - \rho_{wf}}{\rho_{w0} - \rho_{wf}}$$

$$\rho_c = \rho_w - \rho_a$$

where the thermal properties of the virgin wood and the char, $c_{p,w0}$, $c_{p,wf}$, λ_{w0} and λ_{wf} are functions of local temperature and have been described by other researchers (Hostikka 2002).

Combined with the gas phase sub-model, Ritchie's global analytical model was used to predict the Douglas fir burning in bench-scale tests (Ritchie *et al.* 1997) and reasonable agreement has been achieved.

3.4 Calculation for a Studied Material Based on Atreya's Model

3.4.1 Thermal properties of studied material

The selection of appropriate material properties and pyrolysis kinetics is a very difficult task. Some of the properties were measured from the experiments described in previous chapters, but most of the values were sourced from published results. Where no data for the identical testing materials are available, parameters extracted from similar materials are included. The pre-exponential factors and activation energies were verified with the experimental data obtained in the current study. The thermal properties for one of the tested woods, mountain ash, are listed in Table 3.1.

Table 3.1 Thermal parameters for the studied timber, mountain ash

Parameter	Value	Unit	Source
ρ_c	146.5	kg/m ³	Measured by the author
ρ_w	681.3	kg/m ³	Measured by the author
λ_{w0}	$3.054 \times 10^{-7} T_{\infty} + 3.62 \times 10^{-5}$	kW/m·K	(Hostikka 2002)
$c_{p,\infty w}$	$0.01 + 0.0037 T_{\infty}$	kJ/kg·K	(as above)
α_{∞}	1.94×10^{-7}	m ² /s	(as above)
ΔH_{ev}	125.6	kJ/kg	(as above)
\bar{T}_s	$(T_{\infty} + T_{ig})/2$	K	$T_{ig} = 350$ °C was chosen for normal timber materials

The inputs for Atreya's model are given in Table 3.2. The evaluation of these input parameters is included in Appendix C.

Table 3.2 Inputs for calculation by Atreya's model

L	7.38×10^{-4} m
τ	2.81 s
F	50 kW/m ²
A	1.21×10^8 1/s
E	140.2 kJ/mol
Γ	0.4

3.4.2 Calculation results from Atreya's model

Manual calculation was performed following a procedure provided by Atreya, which is listed in Appendix C, and results are presented therein. A plotting for the non-dimensional mass flux curves is also shown in Figure 3.4. The variables shown in this figure are non-dimensional mass flux, m^* , and non-dimensional time, t^* .

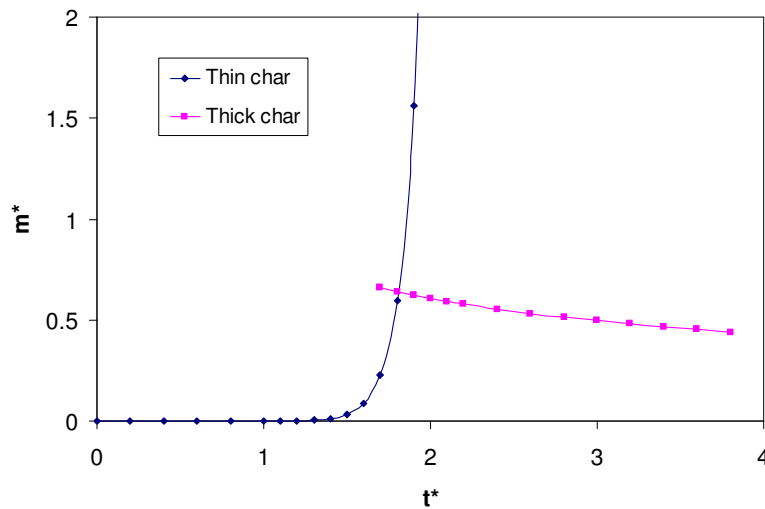


Figure 3.4 Non-dimensional mass flux for mountain ash under 50 kW/m²

Compared with Atreya's calculation result for inputs of a construct timber fuel, (shown in Appendix C), current calculation results for mountain ash has a similar trend in mass flux plotting. It is shown that in the thin char pyrolysis stage, the mass flux increased by an exponential curve following the Arrhenius equation. As the pyrolysis process changed into

the thick char stage, the increased thickness of the charring layer starts impeding the heat and mass transferring through the charring layer. Therefore the mass flux curve decreased from its peak value. This mass flux plotting can be used later to compare with the Fire Dynamics Simulator (FDS) model's simulation results.

3.5 Summary

A combustion model is a critical component in a fire model. A practicable combustion model should be able to model pyrolysis and ignition phenomena properly. All available pyrolysis models are simplified descriptions for the pyrolysis process. Some are quite simple while some are relatively complex and able to deal with detailed phenomena and reactions. An engineering approach can be achieved by balancing the details a model can handle and the computational ability available. Combined with the research aims specified in Chapter 1, a set of criteria for selecting pyrolysis models for this research has been identified.

Major types of existing pyrolysis models have been discussed in this chapter. Atreya's one-dimensional heat transfer and pyrolysis model was chosen as modelling tool according to the criteria developed. Atreya's model, including its physical problem, assumptions, basic equations and theoretical calculation, has been discussed in detail. Major improvements for the model by a number of researchers have also been presented. These improvements involve a numerical scheme, shrinkage of wood during combustion, moisture content, etc.

Following Atreya's model, theoretical calculation was also performed for mountain ash, one of the furnishing materials under study. The calculation mass flux matches the trend from Atreya's original results.

CHAPTER 4 EXPERIMENTAL DECOMPOSITION STUDY FOR THE FURNISHING MATERIALS

This chapter involves the application of the basic thermal experiment, the TGA test. The test method and computational scheme for obtaining decomposition kinetics are examined and improved according to the basic analysis for decomposition that was performed in Chapter 2. Then this modified scheme is used to obtain the “effective” kinetics for the studied materials.

Three sections are included in this chapter. The first section introduces the test device, its principle and test method. The computational scheme for the kinetics is also analysed and improved. In Section 4.2, the test procedure and test results for the materials included in the current study are presented and discussed. The last section, Section 4.3, summarises the test results and their potential application.

4.1 TGA Experiment and its Application

As reviewed in Chapter 2, the TG analyser is a commonly used tool for basic thermodynamic studies due to its wider temperature testing range and environmental gas control capability. It is easy to analyse the thermal pyrolysis processes of solid materials under confined environments. This experimental device and computational schemes have been widely adopted by researchers to determine kinetics for various materials.

4.1.1 TGA apparatus, principle and test procedure

The TGA analyser was designed to investigate the thermal characteristics of a tiny amount of samples. It consists of:

- a radiant heating chamber (furnace)
- a quartz reactor
- a temperature controller
- a precision balance

- a gas feeding system
- an acquisition data set

An illustration of the major structure of the TG analyser is shown in Figure 4.1. The sample to be tested is exposed to thermal radiation in a platinum basket and the temperature is continuously recorded by a chromel-alumel thermocouple (0.1 mm bead) placed under the basket with a 0.1 mm gap. A precision balance (accuracy 0.1 to 1 μg) allows the sample weight to be measured while a continuous air flow establishes the proper reaction environment. The gas flow also carries away the volatilisation products, thus minimizing any secondary reaction activity. The testing procedures involve either constant temperature ramp or constant temperature experiments. The sample size and heating condition can be chosen so as to avoid significant deviation with respect to the desired temperature value. The process can also be carried out with a continuous control of the sample temperature through variation of the intensity of the applied radiative heat flux.

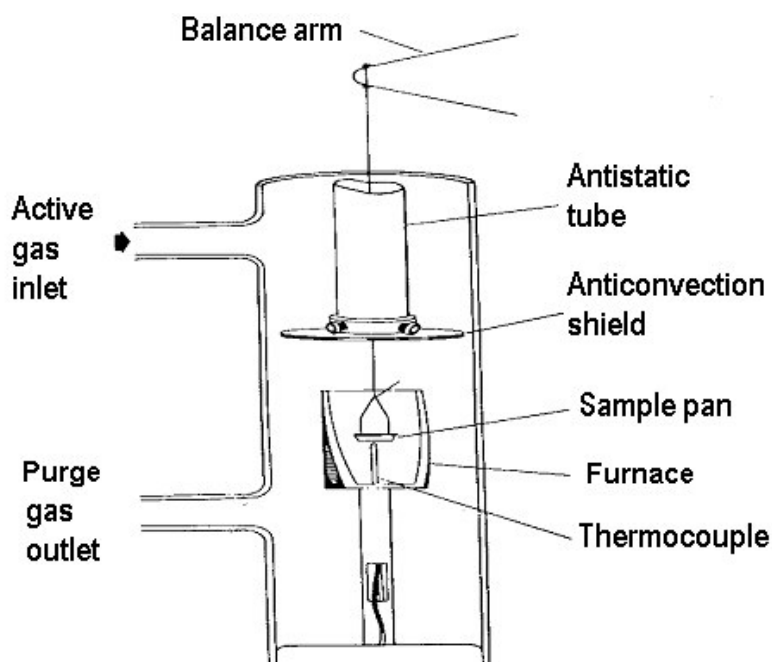


Figure 4.1 Illustration of a TG analyser

One standard usage of the TG analyser is the so-called “dynamic” or “non-isothermal” experiment. In this kind of experiment, a sample is heated at a desired heating speed, normally a constant heating rate or a linear time-temperature curve. The heating rate can

vary from 0.05 K/min to 200 K/min. Much higher heating rates, up to 100 K/s, may be achieved by using special techniques.

Alternatively, the isothermal experiment can be conducted. Samples are first heated to the required temperature very quickly, at a rate higher than 700 K/min. Then the sample mass and mass loss rate can be monitored at the required temperature for a specified time duration.

Both dynamic and isothermal methods can be used in oxidative or inert gas flow environments. The test results from these methods can be used for calculation of the kinetics. The computational methods are discussed in the following sub-section.

4.1.2 Research methodology

From the TGA test, two kinds of plots are available. One is the plot of sample weight (or weight fraction) against temperature: the thermogravimetric (TG) curve. The other is a plot of the rate of sample weight loss against temperature: the differential thermogravimetric (DTG) curve. Obtained under a set of standard conditions, the TG and DTG curves provide information of the combustion reactivities of the fuel from the onset of oxidation to complete burn-out (Wagoner and Duzy 1976). Meanwhile other parameters, such as the kinetics of a reaction, can be derived from these curves (Seungdo and Park 1995).

4.1.2.1 Curve trend and characteristic temperatures

The TG and DTG curves were at first used to present burning profiles of fuels. The “burning” process is generally characterized by several events (Wagoner and Duzy 1976). For example, in an oxidizer flow environment TG test for coal, as well as for many other solid fuels, the following events may occur. The initial mass loss rate peak in a DTG curve at temperatures below 100 °C corresponds essentially to the release of moisture. The rate then falls at about 200-300 °C. This is caused by oxygen absorption by the solid before subsequent combustion. The main combustion peak is usually preceded by a small peak or shoulder which is partly attributable to volatile release. Then the mass loss rate reaches a peak value (MLR_{max}) and the corresponding temperature is the peak temperature (T_{max}).

An example of TG/DTG plotting for a timber material can be found in Figure 4.2.

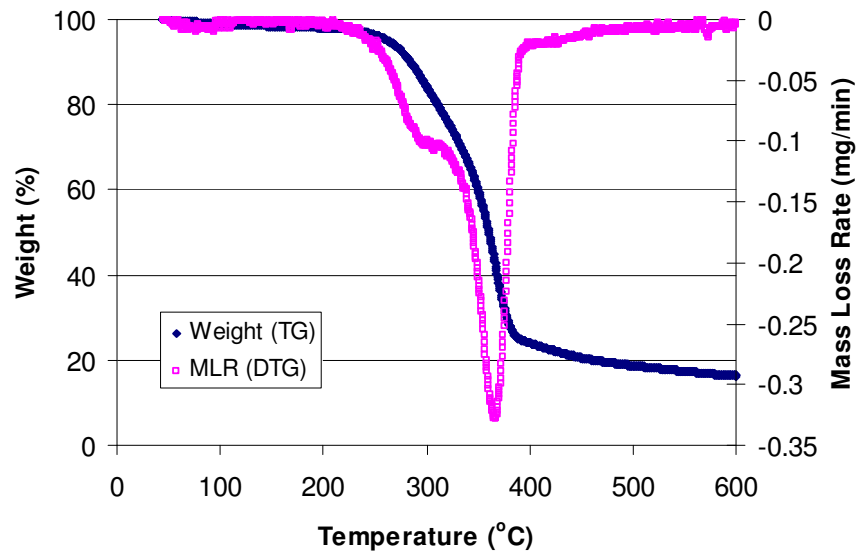


Figure 4.2 A typical TG (WT curve) and DTG (MLR curve) plotting

The peak temperature T_{max} can be used to assess the relative combustibility. A higher T_{max} is indicative of a less reactive fuel, and vice versa.

4.1.2.2 Kinetics and calculation method

In many kinetic formulations of solid state reactions, it has been assumed that the isothermal homogeneous gas or liquid phase kinetic equation can be applied (Baker 1978). An expression of Arrhenius equation for a one-order kinetic reaction has been shown in Section 2.3.2. Generally, for a single kinetic reaction, a DTG curve (as expressed as conversion rate H (dx/dT)) can be represented by the following Arrhenius equation based on reaction order (Seungdo and Park 1995):

$$\frac{dx}{dT} = \frac{A}{\beta} e^{\left(\frac{-E}{RT}\right)} (1-x)^n \quad (4.1)$$

where:

x : weight fraction of conversion, and

$$x = \frac{W_I - W}{W_I - W_\infty}$$

W : sample weight, g;

W_I : initial sample weight, g;

W_{∞} : end sample weight, g;

T : sample temperature, K;

A : pre-exponential factor, 1/s;

β : heating rate, K/s;

E : activation energy, kJ/mol;

R : universal gas constant, $=8.314 \times 10^{-3}$ kJ/mol·K;

n : reaction order.

At the peak temperature T_{max} , differentiating the right hand side of Equation (4.1) with respect to temperature yields zero:

$$\frac{E}{nRT_{max}^2 (1 - x_{max})^{n-1}} - \frac{A}{\beta} e^{\left(\frac{E}{RT_{max}}\right)} = 0 \quad (4.2)$$

where:

T_{max} : temperature at peak conversion rate, K;

x_{max} : sample weight fraction of conversion at peak conversion rate.

A great number of methods have been developed to compute kinetics from the TGA tests. The first example was illustrated here. The peak temperature (T_{max}) and corresponding maximum sample weight fraction of conversion (x_{max}) and the maximum conversion rate (H_{max}) can be utilized to estimate the activation energy and pre-exponential factor of a reaction. Substituting Equation (4.1) into Equation (4.2) yields the expression for the activation energy and the pre-exponential factor

$$E = \frac{nRT_{max}^2 H_{max}}{1 - x_{max}} \quad (4.3)$$

and then replacing Equation (4.3) into Equation (4.2)

$$A = \frac{H_{max} \beta e^{\left(\frac{E}{RT_{max}}\right)}}{(1 - x_{max})^n} \quad (4.4)$$

where H_{max} is the peak conversion rate, $H_{max} = \left(\frac{dx}{dT}\right)_{max}$.

If the reaction order, n , is known, then the activation energy, E , and the pre-exponential factor, A , can be estimated from experimental measurements of T_{max} , H_{max} and x_{max} .

To obtain those three parameters, Coats-Redfern method has been reported as the most frequently used (Vyazovkin and Wight 1998). Equation from the Coats-Redfern method was given as follow:

$$\ln\left(\frac{f(x)}{T^2}\right) = \ln\left[\frac{AR}{\beta E}\right] - \frac{E}{RT} \quad (4.5)$$

where $f(x)$ is a function that represents the reaction model. When Arrhenius equation was assumed, expression from Equation (4.1) can be applied, $f(x) = (1-x)^n$.

Therefore Equation (4.5) can be rewritten as

$$\left[\frac{1 - (1-x)^{1-n}}{1-n}\right] \frac{1}{T^2} = \frac{AR}{\beta E} e^{\frac{-E}{RT}}, \quad (n \neq 1) \quad (4.6)$$

$$\frac{-\ln(1-x)}{T^2} = \frac{AR}{\beta E} e^{\frac{-E}{RT}}, \quad (n = 1)$$

A plot of $\ln[-\ln(1-x)/T^2]$ vs $1/T$ (for $n=1$) or $\ln\{[1-(1-x)^{1-n}]/[(1-n)T^2]\}$ vs $1/T$ (for $n \neq 1$) gives a straight line of slope $-E/R$. The pre-exponential factor A can be calculated from the intercept of this straight line. The reaction order, n , was then determined from a series of values that can give the best fit to the plots, i.e. the one generates smallest relative standard deviation.

Another widely adopted method is the so-called Ozawa-Flynn-Wall (OFW) method (Ozawa 1970) which was based on traditional multiple heating rate technique. It has the advantage without supposition of the reaction order n .

By linearizing Equation (4.1) the following form is obtained:

$$\ln\left(\beta \frac{dx}{dT}\right) = \ln[A(1-x)^n] - \frac{E}{RT} \quad (4.7)$$

This equation can be further reduced with Doyle's approximation (Doyle 1962):

$$\ln f(x) = \ln(AE/R) - \ln \beta - 5.33 - \frac{1.05E}{RT} \quad (4.8)$$

where $f(x)$ is a function of reaction model.

At each conversion level (x), the item $[\ln f(x) - \ln(AE/R) + 5.33 - 1.05E/R]$ is constant. A plot of logarithm heating rate ($\ln \beta$) vs reciprocal temperature ($1/T$) will yield a slope of

$1.05E/R$. By running multiple various heating rate tests, the values of activation energy, E , can be computed at different sample fractions of conversion. This is the so-called OFW method. An illustration of the application of the OFW method is given in Figure 4.3. Each line in the figure was generated by a conversion level x under various heating rates.

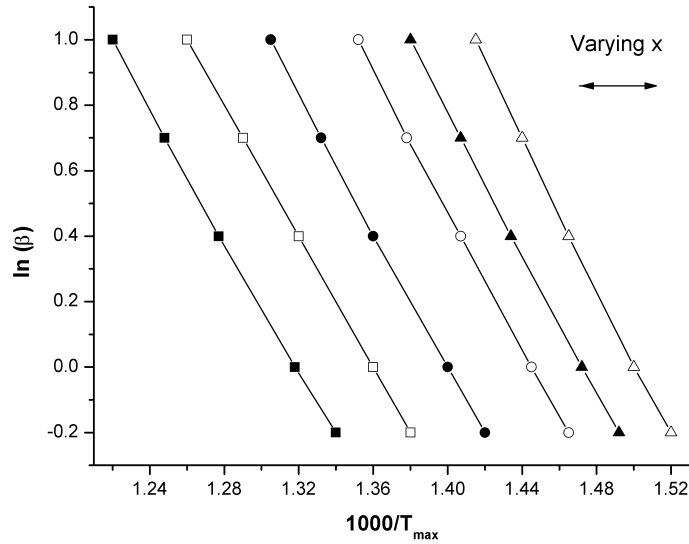


Figure 4.3 OFW plotting of heating rate, $\ln(\beta)$, vs temperature, $1/T$, for various conversion fraction, x

Furthermore, a special format of OFW method can be developed. Based on an observation by Flynn and Wall (1966), for each peak in a DTG curve the x_{max} would rarely vary with heating rate. Therefore the activation energy computed by a single mass conversion fraction x_{max} was used for the reaction. This method could be considered as a special case of the OFW equation. From Equation (4.4), following expression exists for different heating rate.

$$\ln \beta = \ln \left[\frac{A(1 - x_{max})^n}{H_{max}} \right] - \frac{E}{RT_{max}} \quad (4.9)$$

Applying Equation (4.9) to two different heating rates, the activation energy can be obtained by T_{max} , H_{max} and β from the two tests:

$$E = R \left(\frac{T_{max 1} \cdot T_{max 2}}{T_{max 1} - T_{max 2}} \right) \ln \left[\left(\frac{\beta_1}{\beta_2} \right) \left(\frac{H_{max 2}}{H_{max 1}} \right) \right] \quad (4.10)$$

Comparing above three methods, the method expressed in Equation (4.3) and (4.4) has an advantage of requiring only single running of test at a heating rate. The disadvantage is that

the reaction order has to be estimated first. The estimation of the reaction order may affect the accuracy of the obtained kinetics. Coats-Redfern method can calculate all the parameters from a single test. However relatively complex mathematic computation is required. The calculated results rely on the step of reaction order in the trial. The OFW method has the advantage of not relying on the supposition of the reaction order n . By comparing nearly 20 typical computing models for kinetics, Carrasco (1993) found that OFW method has satisfactory high accuracy. The special format OFW method has similar accuracy while the peak conversion rate and peak temperature are required. Furthermore, the OFW computing scheme can provide additional benefit. The kinetics obtained from a wide heating rate range can be verified by the linearity of the plotting. For example, for a peak conversion fraction (x_{max}), if two or more slopes (presenting the activation energy) were observed from the $\ln\beta$ vs $1/T_{max}$ curve, different decomposition behaviours may exist under different heating conditions. In the current study, the Coats-Redfern method was used to calculate kinetics under very low heating rate, from 5 to 10 K/min, and therefore compared with results from others. The OFW method was used to check decomposition behaviour and compute the kinetics under relatively high heating rates for the studied materials.

4.1.2.3 Concern for test conditions and computational schemes

When the TGA test is used to study chemical and physical processes of solid samples, one of the main drawbacks concerning solid phase chemistry is that a large part of the analyses has been carried out in the presence of serious heat and mass transfer limitations. For inert atmospheres, these mainly arise from the large sample size, so that significant temperature gradients are established along the sample and the activity of secondary reactions is not negligible. In the presence of oxidants, the process is further complicated by the strong exothermicity of the combustion reactions. So that, apart from the wide variability of the thermal conditions, the response time of the measuring devices may become too long compared with the characteristic times of process evolution. Therefore some methods and configuration are necessary in order to minimize these effects.

The configuration of the sample, the thickness and size, plays an important role, along with the heating conditions. DiBlasi *et al.* (1999) found for a powdered wood sample that ignition is a function of number of factors, such as sample size, heating rate, final heating

temperature, as well as gas flow condition. The sample size they suggested to avoid ignition is between 2 to 25 mg. Either the heating rate or the final heating temperature has to be controlled depending on the type of wood species.

Parker improved the TGA test method by introducing an extra oxygen analyzer to calculate kinetics (Parker 1988). The test device and method have been briefly introduced in Section 2.6.1. This method is believed to eliminate the temperature gradient on the sample in a TGA environment.

Some other efforts focused on improving kinetic computational schemes by TGA data. Schultz *et al.* (1989) improved the calculation method by carrying out isothermal tests. Kinetics were calculated through the Arrhenius equation by using measured reaction rate and pyrolysis temperature. This isothermal test method is believed to eliminate temperature lag complications.

The measured temperature inside the TG analyser was expected to differ from the real temperature of the sample specimen due to the placement of the thermocouple. The measured temperature is approximately in parity to the real temperature and the difference may be proportional to the heating rate applied. The error in temperature measurement will be translated into errors in the estimated parameters such as onset and maximum temperatures. However, it is expected that the rate of temperature rise of the specimen would closely follow the rate of measured temperature rise, i.e. a similar temperature difference between the measured and real sample temperatures exists over the whole heating process. ASTM also gives a normal temperature measuring error range of 20 °C (ASTM_E1582 2000). As such, the quantities that are determined by a linear relationship (the slope) of the heating rate and the measure reaction rate would be less sensitive to errors in the temperature measurement. Seungdo and Park (1995) found that kinetic values are more sensitive to slopes in the plotting of peak temperatures and peak reaction rates, not the peak values themselves. This indicates that the kinetics may be less affected by the error in temperature measurement.

As indicated in Section 2.3.2, the activation energy, one of the major parameters of kinetics, is a material property and its intrinsic value believed to be independent on reaction conditions, for example the heating condition. To obtain this intrinsic value above efforts

have being made to improve test method. However, due to limitations exist in every test method, only “perfect” values, which being considered very close to the intrinsic value but approximate expression, can be achieved. To obtain this “perfect” kinetics, small size and tiny amount of specimen should be tested under very low heating rate.

On the other hand, the “perfect” kinetics was computed from test data according to various reaction models. For the same decomposition process, kinetics obtained by different reaction models may vary. As studied by Vyazovkin and Wight (1998), major issues in computing schemes are as follows:

- Arrhenius equations may be meaningfully applicable only to reactions that take place in a homogeneous environment
- For non-isothermal TGA tests, solid decomposition processes ordinarily show multi-step kinetics that readily change with heating condition.

It’s further argued that there are serious limitations to apply those “perfect” kinetics directly into description of decomposition of solid materials in real fire conditions. In real fire environments, the “drawbacks” existed in TGA tests are always present, such as temperature gradient, heat and mass transfer within the solid. The so-called “perfect” kinetics are either difficult to obtain or unhelpful in describing the decomposition in a real fire. In a later part of this chapter, the author will provide more evidence from analysis of computed activation energies to support this argument.

Therefore, the author aimed to obtain some kind of simplified kinetics, “effective” value, which is suitable to describe decomposition process in a simplified modelling scheme, as discussed in Section 3.1. This engineering approach for pyrolysis research is for solving real fire problems with enough physical and chemical details by the applicable kinetics. In late sections of this chapter, kinetics obtained from normal and the improved schemes will be presented for further pyrolysis modelling.

4.1.2.4 Relationships among the parameters

There are two commonly used approximations for the parameters. From Doyle’s (1962), one expression is provided as below:

$$\begin{aligned}
 n = 1; \quad \ln \beta &= \ln\left(\frac{AE}{R}\right) - \ln H_{\max} - 5.33 - 1.05\left(\frac{E}{RT_{\max}}\right) \\
 n \neq 1; \quad \ln \beta &= \ln\left(\frac{AE}{R}\right) + \ln\left(\frac{n}{H_{\max}} - n + 1\right) - 5.33 - 1.05\left(\frac{E}{RT_{\max}}\right)
 \end{aligned} \tag{4.11}$$

Kissinger (1957) assumed the followings:

$$\begin{aligned}
 n = 1; \quad x_{\max} &= 1 - 1/e \\
 n \neq 1; \quad x_{\max} &= 1 - n^{1/(1-n)}
 \end{aligned} \tag{4.12}$$

By introducing those approximation schemes into Equations (4.3) and (4.4), Seungdo and Park (1995) gave the following equations:

$$\frac{\partial T_{\max}}{\partial \beta} = \left(\frac{1.0516}{R\beta}\right)\left(\frac{E}{\xi^2}\right) > 0; \tag{4.13}$$

$$\frac{\partial H_{\max}}{\partial \beta} = -\left(\frac{1.8085R}{e\beta}\right)\left(\frac{\xi}{E}\right) < 0; \tag{4.14}$$

where

$$\xi = \ln\left(\frac{AE}{R\beta}\right) - 5.3305.$$

$$\begin{aligned}
 n = 1; \quad H_{\max} &\approx \frac{E}{eRT_{\max}^2}; \\
 n \neq 1; \quad H_{\max} &\approx \frac{En^{n/(1-n)}}{RT_{\max}^2}
 \end{aligned} \tag{4.15}$$

From Equation (4.15), the following equation can be obtained:

$$\frac{1}{T_{\max}} \approx \left(\frac{eR}{E} H_{\max}\right)^{0.5} \tag{4.16}$$

Substituting Equation (4.16) into Equation (4.9) yields:

$$\ln \beta \approx \ln\left[\frac{A(1-x_{\max})^n}{H_{\max}}\right] - \sqrt{\frac{eE}{R}} \cdot H_{\max}^{0.5} \tag{4.17}$$

From Equation (4.13) and (4.14), it can be seen that the peak temperature increases with the increased heating rate, but the peak conversion rate follows the reverse trend. Meanwhile,

linear relationships are expected between the peak conversion rate and inverse square of the peak temperature, between $\ln\beta$ and $H_{\max}^{0.5}$ (from Equation (4.16) and (4.17)). These theoretical relationships are helpful to validate and group the experimental data.

4.2 Current TGA Test Results

In this section, specifications of the tested materials and experimental equipment are described. The basic thermal decomposition processes from the TGA tests are presented. Finally, the calculated thermal dynamic parameters for the tested materials are given.

4.2.1 Experimental materials and apparatus

4.2.1.1 Details of materials

The tested materials included charring and non-charring materials. They were polyurethane (PU) foams, fabrics, and woods. Stamina, (a brand) PU foam is manufactured by Dunlop and has a density between 29 to 35 kg/m³. Details of the tested materials are listed in Table 4.1. All densities listed were measured after 48 hours conditioning at 50% relative humidity and 25 °C. The fabric samples were cut into a round shape with a diameter of 3.5 mm. The woods were chipped into slices of 3×3 mm with various thickness from 0.2 to 0.5 mm to obtain different sample weights. The PU foams were prepared as 3×3×2 mm dices. The sample weights varied between 0.5 to 3 mg.

Table 4.1 Properties of the tested materials

Materials	Description	Density (kg/m ³)
Hardwood	mountain ash	681.3
Pinewood	Australian pine	440.7
Standard PU foam	A23-130	22.8
Stamina PU foam	HR32-80	31.2
Cotton (fabric)	100% cotton	0.42 (kg/m ²)
Cotton & polyester (fabric)	45% cotton and 55% polyester	0.37 (kg/m ²)

4.2.1.2 Apparatus and test conditions

The experimental apparatus was a PerkinElmer TGA-7 analyser in the Applied Chemistry Department, RMIT University, Australia. For the description of this apparatus, refer to Section 4.1. In all tests the standardized flow rate was set at 200 ml/min.

The heating rates investigated were from 5 to 200 K/min in the dynamic experiments. A constant temperature heating process, isothermal scanning, was also carried out. A gas feeding system can provide varying gas flows, from inert to oxidizing atmospheres. In these experiments, pure nitrogen and air flow were used.

4.2.1.3 Calibration

Calibrations for the TG analyser were performed for weight and temperature. While there are no standards for those calibrations, it is a usual way to follow standard procedures provided by the manufacturer. Since the calibration of weight is relatively simple, only calibration of the temperature was described below.

Standard ferromagnetic samples with different Curie points were used in the temperature calibration (Brown 1988). Those samples were placed in the balance and a magnet outside the furnace alerted the total weight of the sample. When the temperature increased above the characteristic Curie point of the specimen, they lost their ferromagnetic properties and were no longer attracted by the magnet. This resulted in a sudden change in weight. The use of number of ferromagnetic materials extends the calibration over a wide temperature range. By checking recorded temperature against the characteristic temperatures of those calibration specimens have, temperature lag can be then obtained. The supplied ferromagnetic samples and their characteristic temperatures are Ni (355.5 °C) and Perkalloy (596.0 °C). This calibration was carried out before changing heating rate. The temperature lag was found less than 2 to 20 K for heating rates ranging from 10 to 100 K/min, which met the requirement from the manufacturer (Perkin_Elemer 1991).

4.2.2 Measurement of thermal characteristics of the materials

Presented in this part are the decomposition processes of the testing materials as well as the basic thermal characteristics such as mass loss rate, conversion rate and peak temperature.

4.2.2.1 Decomposition process

Figure 4.4 shows the TG and DTG curves for all six materials tested in the air flow at a heating rate of 10 K/min. There is a moisture release phase under 160 °C for the woods and fabrics, which shows in the DTG curves as the first small peak. Above this temperature, there is one pyrolysis reaction for both woods and the cotton fabric, and two reactions for the other materials.

In the temperature range from 500 to 600 °C, there is another “reaction” for both woods. This reaction is attributed to combustion of the charring residue, and is verified by comparing the DTG curves in air and nitrogen flow conditions. Figure 4.5 (a) and (b) shows the difference between these two gas flow conditions under a 20 K/min heating rate. It is found that under the nitrogen flow condition, the second major peak in the DTG curve disappears. The residue of sample weight (shown in the TG curves) under nitrogen flow is about 10%, compared with almost zero for that under air flow. Meanwhile, for the combustion of char under air flow the condition may also be affected by the heating rate, which will be discussed in the following section. The DTG curve for cotton fabric also shows a single peak. The approximate single peak pattern enables the one-step global pyrolysis model, which was discussed in Chapter 3, to be applied to these materials.

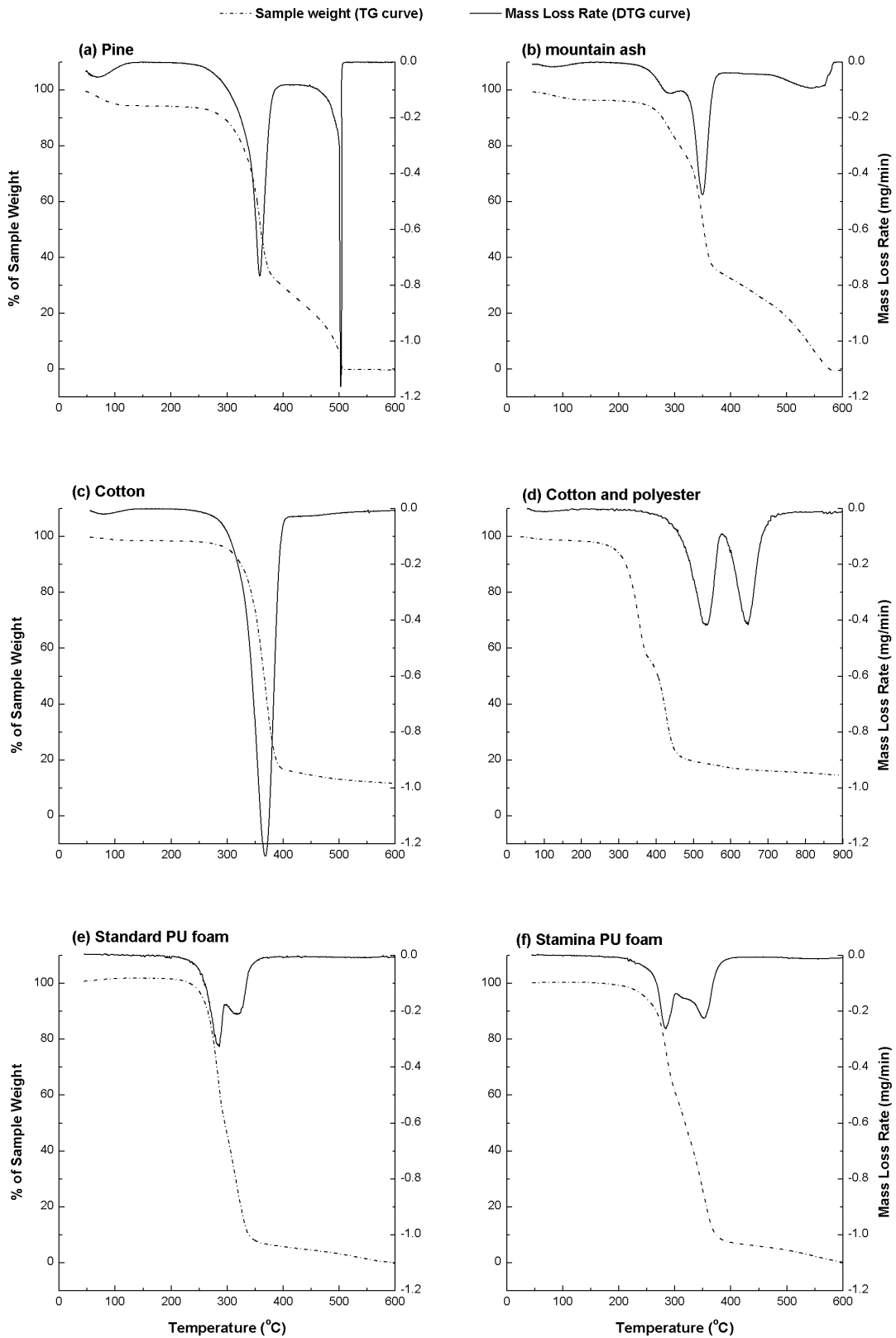


Figure 4.4 TG and DTG curves on 10 K/min heating rate under air flow

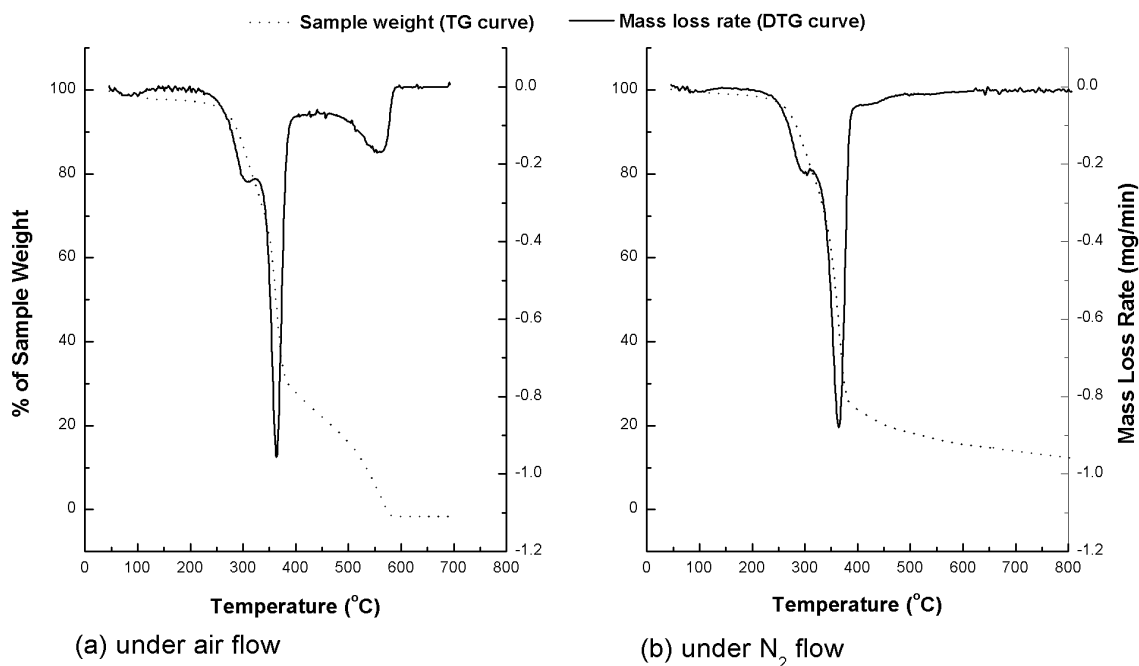


Figure 4.5 TG and DTG curves for mountain ash under 20 K/min heating rate

The double reaction in the DTG curves in the cotton and polyester test (in Figure 4.4 (d)) is a result of the presence of two components, cotton and polyester. Comparing the DTG curves for the cotton (Figure 4.4 (c)) and the cotton and polyester fabrics (Figure 4.4 (d)), it is found the first peak in DTG curve for the cotton and polyester has a similar temperature range with the peak of the cotton. Thus the first peak in the cotton and polyester test is attributable to the decomposition of the cotton component.

Some characteristic temperatures, T_{max} , and maximum mass loss rates, MLR_{max} , for the cotton fabric, mountain ash and the standard PU foam at various heating rates are listed in Table 4.2. These results average values from 3 tests. A full list of all the TGA tests, including other materials under study, can be found in Appendix A.

It can be seen from the Table 4.2 that for shown materials, under two types of gas-flows, the peak mass loss rate and corresponding peak temperature increased as the heating rate increased. Normally the tests in the air flow have lower peak temperature but higher mass loss rate than that of in the nitrogen flow under same heating rate. The standard PU foam shows two peak mass loss rates in most tests except the low heating rate in the nitrogen flow.

Table 4.2 Peak temperatures and mass loss rates

Material	Gas flow	Heating rate (K/min)	$T_{\max,1}$ (°C)	$MLR_{\max,1}$ (mg/min)	$T_{\max,2}$ (°C)	$MLR_{\max,2}$ (mg/min)
Cotton	Air	10	367	1.24	- [#]	-
		50	440	6.36	-	-
		150	480	11.27	-	-
	N ₂	10	394	0.75	-	-
		20	401	1.62	-	-
Mountain ash	Air	10	350	0.48	-	-
		50	470	1.53	-	-
		200	516	6.36	-	-
	N ₂	10	366	0.33	-	-
		30	369	1.24	-	-
Standard PU foam	Air	10	285	0.34	312	0.22
		50	381	0.63	452	0.54
		200	417	1.27	470	1.74
	N ₂	20	309	0.22	-	-
		30	313	0.31	358	0.42

[#] -: means that no second reaction was observed.

4.2.2.2 Effect of heating rate

The effect of heating rate can be seen from plotting of the conversion rate vs sample temperature under various heating rates, in Figure 4.6 to Figure 4.9.

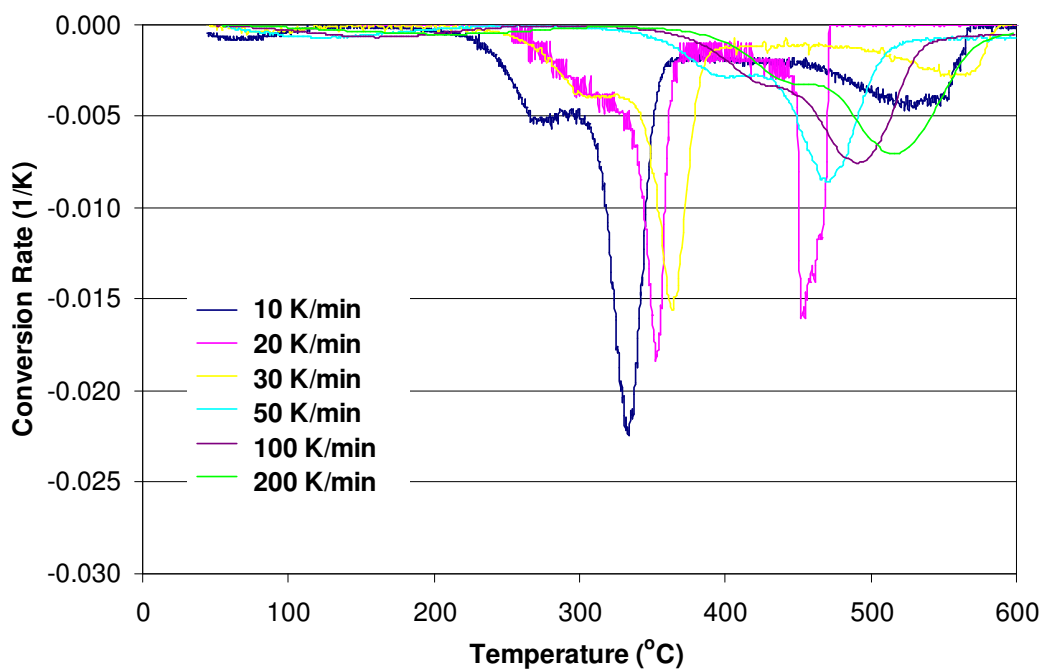


Figure 4.6 Conversion rates for the mountain ash under air flow and various heating rates

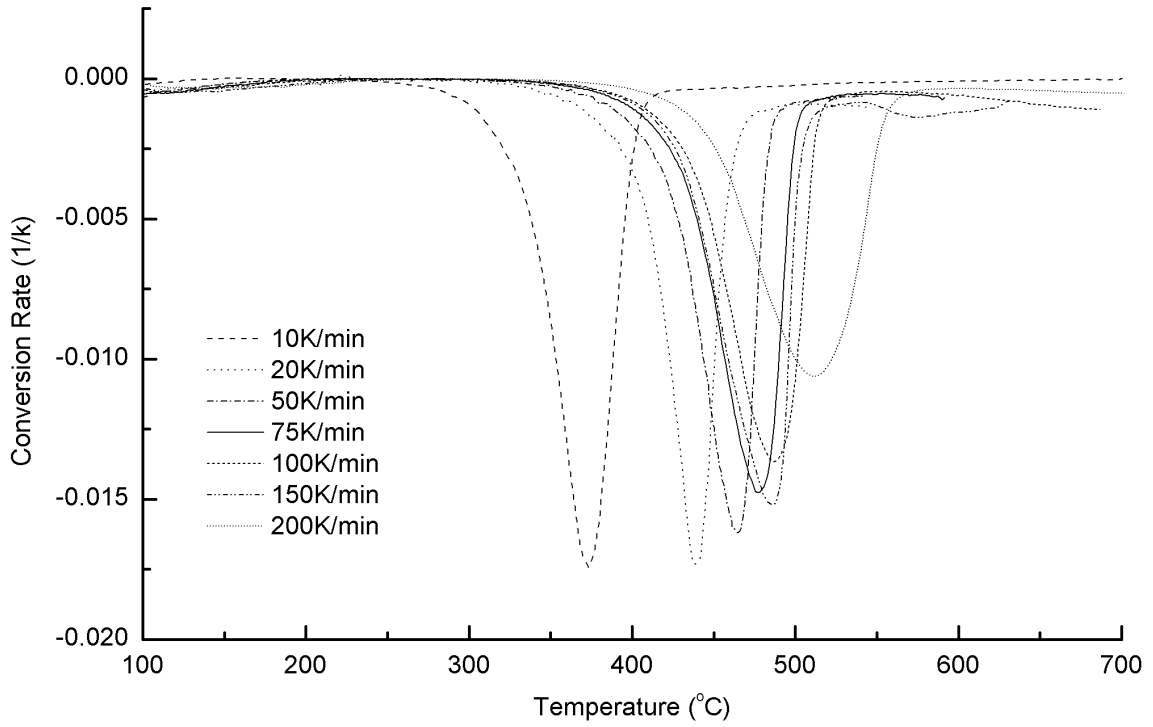


Figure 4.7 Conversion rates for the cotton under air flow and various heating rates

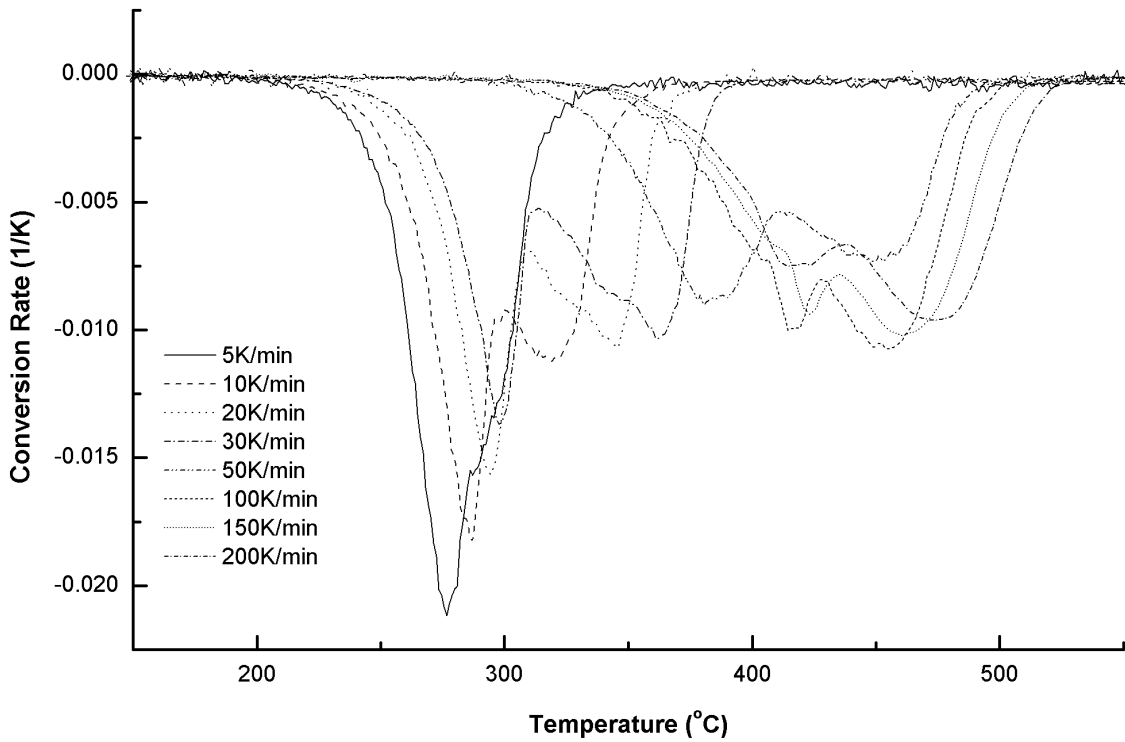


Figure 4.8 Conversion rates for the cotton and polyester under air flow and various heating rates

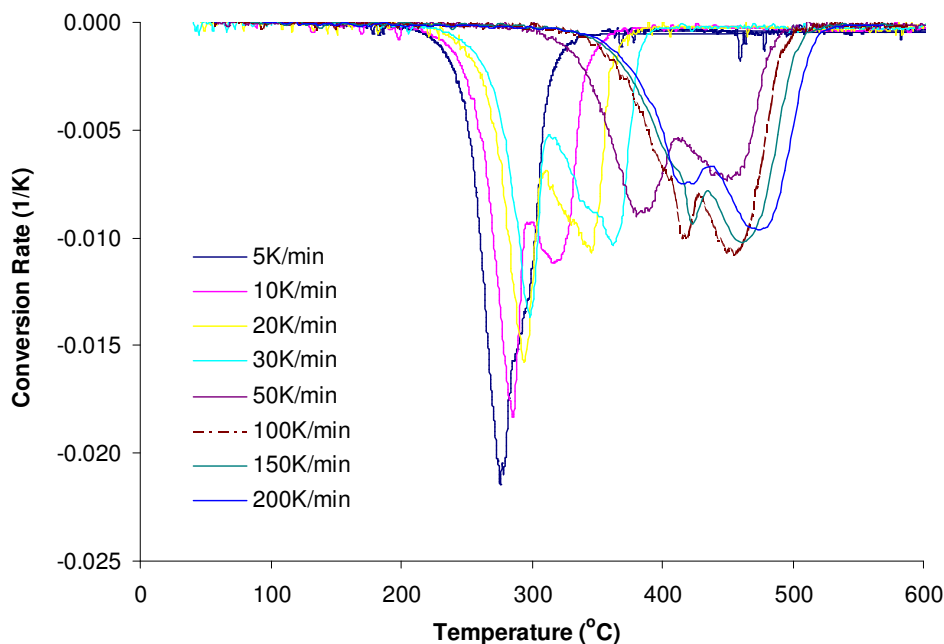


Figure 4.9 Conversion rates for the standard PU foam under air flow and various heating rates

For those materials that can be described by a single reaction, such as the woods and the cotton, the peak conversion rate decreased and peak temperature increased with the increasing heating rate. In fact, the above results were true for all peak temperatures and the first peak conversion rates of all the materials tested under both nitrogen and air flow conditions. This observation matches the previous theoretical analysis (Equation (4.13) and (4.14)), as well as Seungdo and Jae's experimental results (1995). As indicated in Section 4.2.2.1, the second peak in mountain ash's DTG curve under air flow is caused by combustion.

For the multiple reaction materials, the cotton and polyester and the standard PU foam, the trend in the DTG curves under varying heating rates is quite different. For the standard PU foam, the second peak conversion rate increases and becomes the dominant, under a high heating rate range (from 50 to 200 K/min), when heating rate increased (Figure 4.9). The conversion rate for the second peak for the cotton and polyester is quite stable in the low heating rate range (from 10 to 50 K/min), but decreased in the high heating rate range (from 50 to 200 K/min) as the heating rate increased (Figure 4.8). This means that the effect of the first reaction (i.e. the height of the first peak in the DTG curves) becomes gradually weaker and the effect of the second reaction becomes stronger. This can be verified by activation

energy computation, which will be shown in Section 4.2.3.1, as well as Agrawal's results (Agrawal 1992) which will be explained below. Some material has a higher activation energy E for the first reaction followed by a lower E for the secondary reaction, such as the standard PU foam shown in Table 4.3. For this type of material, Agrawal indicated that the first peak conversion rate decreased and then is followed by a slowly increasing rate of volatile evolution, which was limited by the low E reaction. At a high heating rate range, the speeds of both the first peak height decreasing and the second peak height increasing become slower as the heating rate increases. This shifting relation is helpful for predicting the decomposition process under a high heating rate range, which is closer to real world fire conditions.

Changes of the peak mass loss rates (MLR_{max}) followed the opposite trend of that of the peak conversion rates. For example, a comparison between Figure 4.4 (b) and Figure 4.5 (a) indicates that the mass loss rates of the mountain ash increased as the heating rate increased. The peak mass loss rates of all testing materials increased with an increasing heating rate as shown in Appendix A. However, the peak conversion rate decreased as the heating rate increased, which can be observed from Figure 4.6 to Figure 4.9. The relationship between parameters of conversion rate (dx/dT) and reaction rate (dx/dt) is derived from the following equations, while heat rate $\beta = (dT/dt)$:

$$\frac{1}{W_I - W_\infty} \frac{dW}{dt} = \frac{dx}{dt} = \frac{dT}{dt} \cdot \frac{dx}{dT} = \beta \frac{dx}{dT} \quad (4.18)$$

or, at the peak temperature condition,

$$\left(\frac{dx}{dT} \right)_{max} = \frac{1}{W_I - W_\infty} \left(\frac{dW}{dt} \right)_{max} = \beta H_{max} \quad (4.19)$$

where W_I and W_∞ are sample weights at initial and end conditions of a test.

It has been seen that the peak mass loss rate value, $\left(\frac{dW}{dt} \right)_{max}$ (i.e. MLR_{max}), is determined by

the product of β and H_{max} . Even though H_{max} (peak conversion rate $\left(\frac{dx}{dT} \right)_{max}$) may decrease

(for example, for the standard PU foam, those H_{max} shown in Figure 4.9) with increasing β and the end result in βH_{max} increases (MLR_{max} in Table 4.2). This result is consistent with the observations of other researchers (Agrawal 1992; Seungdo and Park 1995).

4.2.3 Thermal dynamic parameters and behaviours

4.2.3.1 Activation energy and pre-exponential factor

The calculation of the pre-exponential factors (A) and the activation energies (E) using the Coats-Redfern method for the studied materials are listed in Table 4.3. The tested heating rate was 10 K/min.

Table 4.3 Pre-exponential factors and activation energies for the testing materials

Testing material	Gas flow	Reaction	A (1/s)	E (kJ/mol)
Cotton	Air	1st	2.6×10^{15}	207.3
	N ₂	1st	4.2×10^{22}	268.4
Pinewood	Air	1st	8.9×10^8	132.8
	N ₂	1st	2.9×10^{11}	161.8
mountain ash	Air	1st	6.7×10^{11}	177.4
	N ₂	1st	2.4×10^{20}	195.7
Cotton & polyester	Air	1st	2.4×10^{10}	149.3
Standard PU foam	Air	1st	3.9×10^{15}	210.0
		2nd	1.8×10^3	67.1
	N ₂	1st	2.5×10^{22}	287.7
Stamina PU foam	Air	1st	3.7×10^{10}	81.8
		2nd	7.1×10^{13}	87.3

The OFW method was also used to check decomposition behaviours under various heating condition, and compute kinetics. It was found that the slope in the $\ln\beta$ vs $1/T$ plot varied, i.e. two different slopes exist in the $\ln\beta$ vs $1/T$ plot, for example in Figure 4.10 for the cotton fabric. This is a direct evidence to show that different kinetics dominate the decomposition in these ranges. Therefore two sets of thermal decomposition kinetics can be obtained for each material studied under different heating rates, and the one from lower heating rate range are similar to that computed from the Coats-Redfern method. Two reasons may cause this result: errors in temperature measurement or different decomposition behaviour.

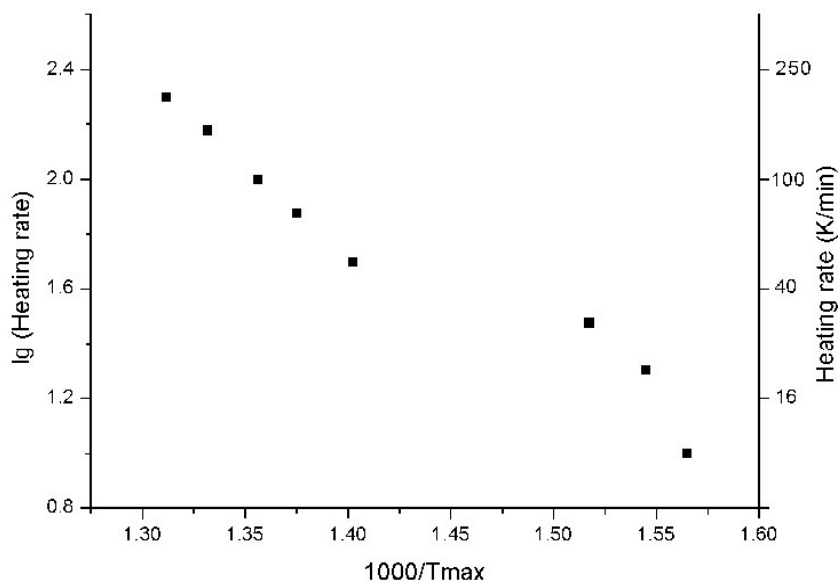


Figure 4.10 Plotting of $\lg\beta$ vs $1000/T_{max}$ for the cotton fabric

As discussed in the previous section, the temperature measurement error may exist in tests of various heating rates. The error in the peak temperature measurement will affect the accuracy of kinetics, which were obtained by the single running method (as in Equation (4.3) and (4.4)). In a normally adopted low heating rate range (from 5 to 30 K/min), the sets of kinetics obtained from different heating rates also varied. Therefore very low heating rate (10 K/min) was adopted in current study to obtain a set of “perfect” kinetics.

When the OFW method was used to obtain the kinetics, it calculates the linear relationship over the heating rates. It was found while the temperature measurement error exists in all heating rates, it has a minor effect on the slope (activation energy). The kinetics calculated by the OFW method were mainly determined by the moving trend of the peak parameters. Therefore, it is believed that OFW method is able to generate more accurate results if a linear relationship exists.

Different decomposition behaviours of these materials under various heating rates do exist. As discussed in Section 2.3, there may be a number of reactions in a decomposition process and several sub-reactions in a reaction. All these reactions and sub-reactions have different behaviours under various environments and the biggest factor that affects the decomposition behaviour most is the heating rate. Since the studied materials are all composite, the overall reaction to describe the decomposition is determined by a combination of individual

reactions and sub-reactions. Therefore the order and positions of the reactions and sub-reactions are varied as the heating rate changes. These changes may then affect the kinetics under different heating rates.

Kinetics calculated from the OFW method for the high heating rate range (50 ~ 200 K/min) were shown in Table 4.4. From Table 4.3 and Table 4.4, it can be seen that as the heating rate is increased, the calculated activation energy of the first reaction decreased for all the materials under both inert and oxidising flow conditions. The tested materials have lower calculated activation energy under the air flow condition than that under the inert flow. This matches with the lower peak temperatures under the air flow environment compared to those of the nitrogen environment, as listed in Table 4.2. Of the multi-reaction materials, the calculated activation energy of the Standard PU foam for the first reaction drops dramatically from a low heating rate to a high heating rate and the activation energy of the second reaction increases gradually. This means the second reaction takes control of the decomposition process under high heating rates.

Table 4.4 Pre-exponential factors and activation energies for heat rate range (50 ~ 200 K/min)

Testing material	Gas flow	Reaction	A (1/s)	E (kJ/mol)
Cotton	Air	1st	3.5×10^8	128.1
	N ₂	1st	9.6×10^{14}	142.3
mountain ash	Air	1st	1.2×10^8	140.2
Cotton & polyester	Air	1st	5.3×10^5	95.7
Standard PU foam	Air	1st	2.1×10^3	68.3
		2nd	5.5×10^5	95.9
Stamina PU foam	Air	1st	3.5×10^{10}	75.8

While no data for identical materials is available from literatures, the following experimental results from others are still helpful for an approximate comparison. For wood species the activation energy and the pre-exponential factor of the pyrolysis process are typically in the order of 10^2 kJ/mol and 10^8 1/s, respectively (Moghtaderi 2001). Since

wood-based fuels are composed of approximately 50 - 60% cellulose by mass, many kinetic characteristics of cellulose pyrolysis are common to all biomass and wood-based type fuels according to Antal and Varhegyi (1995). However a wide range of kinetics are reported for cellulose in a one-step global pyrolysis process. For example, the activation energy ranges from 70 to 200 kJ/mol and the pre-exponential factor in a range from 6.8×10^3 to 4.7×10^{12} 1/s, (Barooah and Long 1976; Gullet and Smith 1987; Cordero *et al.* 1990; Antal and Varhegyi 1995; Lyon and Janssens 2005). The variation for this single major component of wood is believed to be caused by the experimental conditions (Vovelle *et al.* 1984). Some other examples for woods are as follows. Cordero *et al.* (1991) obtained an E value of 83 kJ/mol for sawdust of Aleppo pine under a heating range from 5 to 20 K/min. Atreya suggested an E value of 126 kJ/mol for pine wood (Atreya *et al.* 1986). For the standard PU foam, Luo and He (1997) obtained an activation energy of 170 kJ/mol under a testing condition of 20% O₂ flow and 30 K/min heating rate. Similar values were reported and adopted by a number of other researchers (Chang *et al.* 1995; Fernando 2000).

Compared with the above experimental data, the test results from the current study, with a lower heating rate range, fall into the reported ranges with reasonable agreement.

4.2.3.2 Linear relationships and shifting pattern

Three reasonably linear relations were observed among three types of parameters: heating rate, peak temperature and peak rate in $\ln\beta$ vs T_{max}^{-1} , $\ln\beta$ vs $H_{max}^{1/2}$, and H_{max} vs T_{max}^{-2} plots. Figure 4.11 to 4.13 show two of these relations for some of the studied materials, since the third relation can be derived from the first two. The linear relationships agree with the previous theoretical analysis, as presented in Equation (4.15) and (4.16).

Notably, the $\ln\beta - T_{max}^{-1}$ plot, which is used to obtain kinetics such as activation energy, has the highest linearity in comparison with other two plots. The linear plots for PU foams are broken into a low heating rate range (10 to 30 K/min, corresponding to $\ln\beta$ from 2.3 to 3.4) and a high heating rate range (50 to 200 K/min, corresponding to $\ln\beta$ from 3.9 to 5.3) (Figure 4.13). As discussed previously, this is caused by different decomposition mechanisms on the different heating rate ranges. For the single reaction materials, the linearity on both heating rate ranges is similar, while the linearity is much higher on the first

heating rate range for the multi-reaction materials. The linearity for all materials tested in the current study, varying between 0.975 and 0.998 for the $\ln\beta - T_{max}^{-1}$ plot, are slightly lower than that of the rubbers tested by Seungdo and Parks (1995).

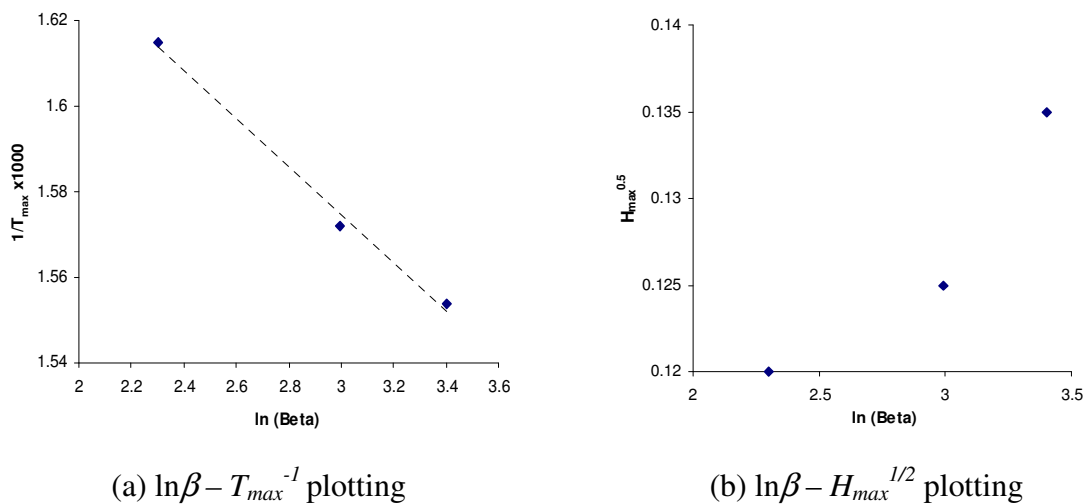


Figure 4.11 Linear relationships for the mountain ash under lower heating rate range

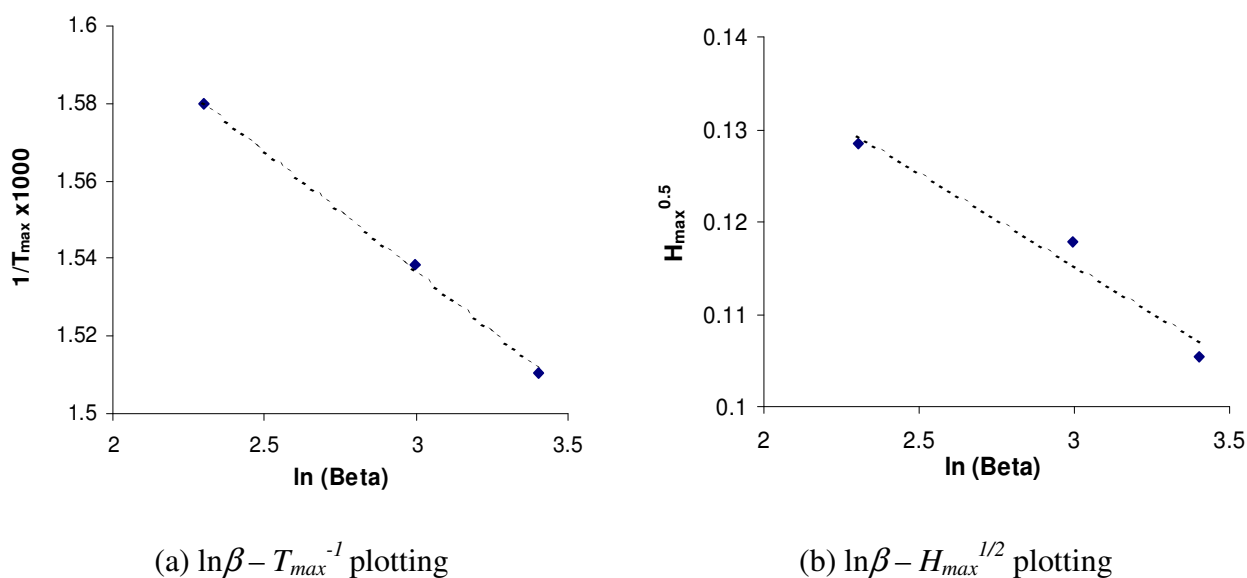


Figure 4.12 Linear relationships for the pine under lower heating rate range

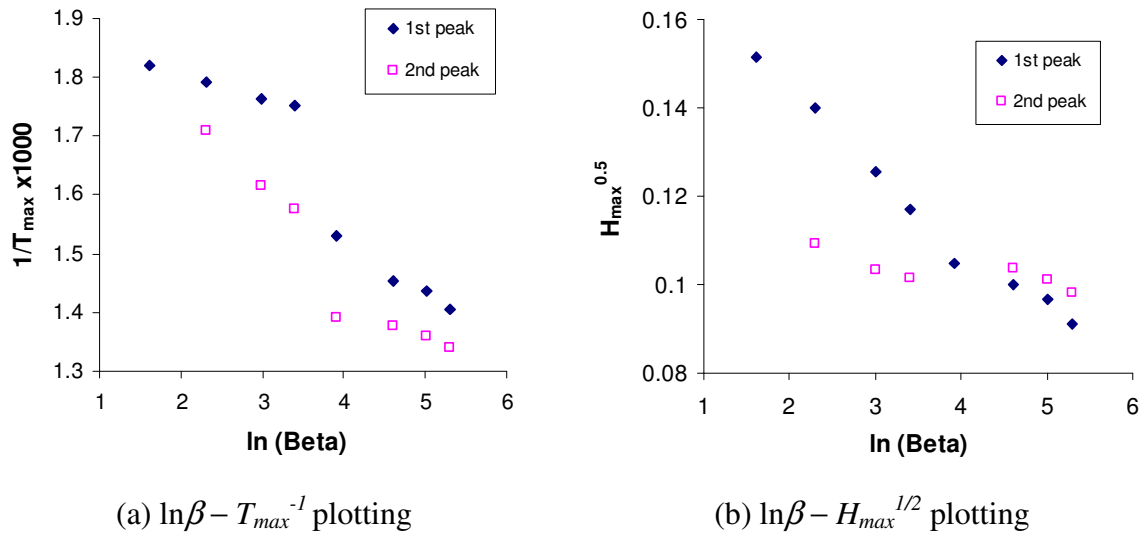


Figure 4.13 linear relationships for the standard PU foam under two heating rate ranges

In the current study, these linear relations were observed on a wider heating rate range, especially at the high heating rate range. This is especially meaningful since the slope of the linear curve of $\ln\beta - T_{max}^{-1}$ plotting represents the activation energy. This shifting pattern, extending the linear relationship to the higher heating rate range, is a clue to the application of the thermal kinetics obtained from the range to real fire test environment, such as the cone calorimeter test.

4.2.4 Isothermal test

Isothermal tests for the studied materials were also carried out to investigate the pyrolysis processes under so-called “isothermal” (constant temperature) conditions. It is helpful to investigate the temperature at which pyrolysis starts. This identified temperature can be used to validate modelling pyrolysis temperatures in Chapter 6.

Shown in Figure 4.14 are mass loss rate curves for mountain ash under various temperature conditions. Both sample weight and mass loss rate curves for the standard PU foam under different external temperature conditions are presented in Figure 4.15.

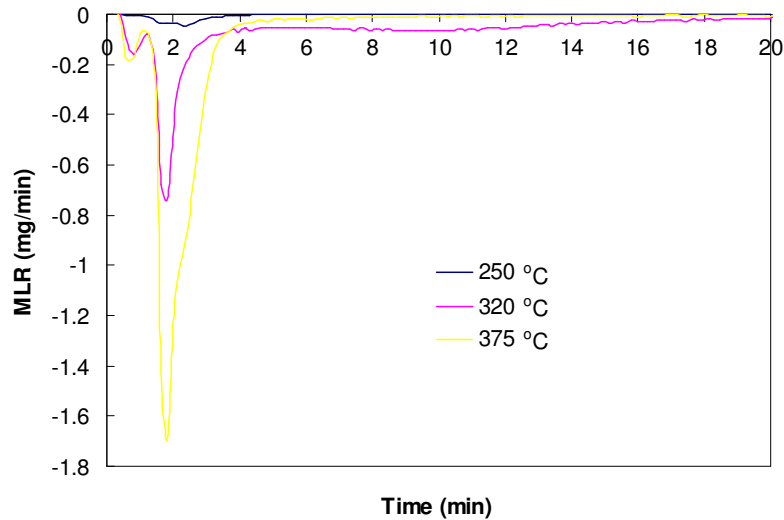


Figure 4.14 Mass loss rates for mountain ash under different temperature environments

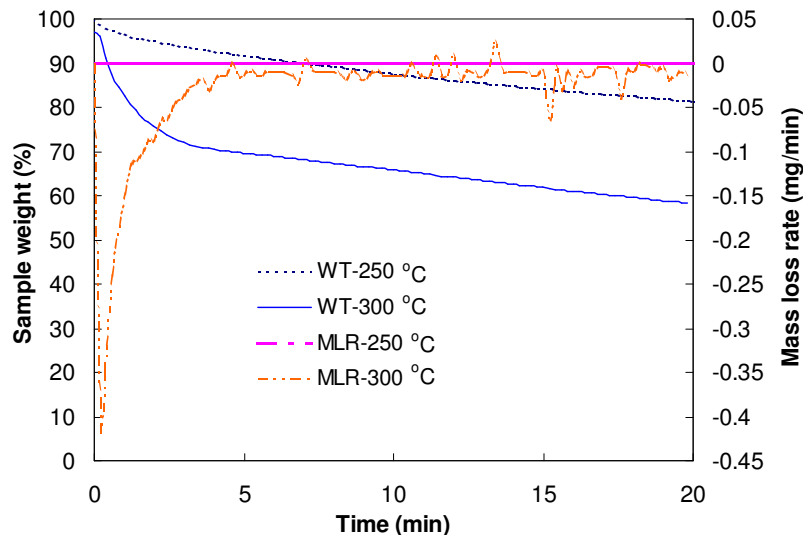


Figure 4.15 Isothermal sample weight and mass loss rate curves for the standard PU foam

It can be seen that for the mountain ash, the onset pyrolysis temperature is slightly below 250 °C (in Figure 4.14), since a very low mass loss rate exists at this temperature. It was seen that a small peak appeared in the first 1 to 2 minutes, which is believed to be caused by the release of the moisture. When the isothermal temperature increased from 320 °C to 375 °C, the mass loss rate nearly doubled. However the times to the peak mass loss rates under various temperatures were almost identical.

From Figure 4.15, it was found that the pyrolysis temperature for the standard PU foam under the isothermal condition is between 250 °C and 300 °C. At 250 °C, the mass loss rate

was almost zero during the whole testing duration, but there is a significant mass loss at 300 °C. The sample weight change under the 250 °C isothermal condition is resulted from the release of moisture. The total mass lost during the whole test is relatively small, less than 20% of the sample mass.

4.3 Summary

To obtain kinetics to describe the pyrolysis process of the studied materials properly, detailed analysis of the TGA test procedure and computational scheme were performed. A series of TGA tests were carried out under both dynamic and isothermal conditions. The data from the tests were used to obtain the desired kinetics in two computing methods. By analysing the test conditions and linear relationships among the obtained parameters, the computed kinetics from the higher heating rate range were believed to be suitable to model decomposition happening in an environment close to real fires.

The Coats-Redfern method was used to calculate “perfect” kinetics at low heat rate as a usual scheme. Applying the one-step overall Arrhenius pyrolysis equation, the OFW method was chosen to compute kinetics through multiple heating rate dynamic tests. The benefits from the OFW method include higher accuracy and validation ability for the computed kinetics.

Several factors that may affect the test results were identified. The error in temperature measuring was found to be controlled by generalizing the test procedure. More importantly it was found that the calculated kinetics were less sensitive to the peak temperature but sensitive to the linear slope in the $\ln\beta$ vs $1/T_{max}$ plotting. The temperature gradient within the sample was not considered by the author as a major issue, since an even greater gradient exists in the real decomposition environment. When the usage of these “effective” kinetics is to model decomposition in real fire situations, the concern becomes how to obtain the kinetics in a similar heating condition. Furthermore the kinetics obtained from a very slow heating rate are of questionable while were uses in the application to a real fire problem.

Through the tests, parameters of the decomposition process under various heating rates (from 5 to 200 K/min) were obtained. It was noted that the thermal decomposition processes

for the timbers and cotton could be treated approximately as a one-step overall reaction, while there were two peaks (i.e. two reactions) in decompositions of the PU foams and the cotton and polyester fabric. These different decomposition characteristics must be taken into consideration when the pyrolysis model is chosen or when simplifications are made.

Two different kinetics values were obtained by OFW method from two heating rate ranges (by two different slopes) for the tested materials. By analysing the test procedure and features of the OFW method, the author believed that there are two different decomposition behaviours in the lower (10 to 30 K/min) and higher (50 to 200 K/min) heating rate ranges. The theoretical basis for this judgement was that discussed in previous chapters: that multiple reactions or sub-reactions have different behaviours under different heating conditions. The kinetics obtained from the TGA test were all based on a certain degree of simplification, i.e. how many steps and reactions will be used to describe the decomposition (Moghtaderi 2001). When a one-step overall pyrolysis model was chosen for the current modelling, the kinetics obtained from a heating condition, which was closer to that in real fires, was more applicable. This judgement has to be validated by later modelling and experimental results.

Linear relationships were observed among a number of parameters that can be found from either theoretical analysis or test results from others. These linear relationships, especially in the $\ln\beta$ vs T_{max}^{-1} plot, which was used to obtain the activation energy, were also found shifted into that higher heating rate range for the studied materials. This indicates a possibility of applying the “effective” kinetics obtained from the higher heating rate range into an even higher rate, which is closer to that in real fire conditions.

CHAPTER 5 CONE CALORIMETER STUDY FOR IGNITION PROPERTIES

As reviewed in Chapter 2, the cone calorimeter test provides an ideal physical platform for the study of pyrolysis and ignition phenomena. In its confined environment, effects of various factors, such as radiative flux and gas flow condition, can be well isolated and identified. Measured parameters from the tests are useful for not only predicting full/real-scale fire performance but also validating modelling results. Therefore a series of tests were carried out for the studied materials in the cone calorimeter, and major results are presented in current chapter.

This chapter includes 5 sections. The first section introduces the principle of oxygen consumption theory for heat release computation and one of the applications of this theory in the cone calorimeter. The experiment and calibration procedures are described briefly in Section 5.2. Major testing results, including ignition time, heat release rate and mass loss rate, under different radiation levels are presented in Section 5.3. In Section 5.4, the measured surface temperatures of the specimen are compared with theoretical calculations as well as published experimental results. Finally, a brief summary of the test results is given in the last part, Section 5.5.

5.1 Heat Release Rate Measurement

Heat release rate is the primary parameter that contributes to compartment fire hazard from burning materials. The importance of heat release rate in the fire hazard assessment was first recognized three decades ago by Smith (1971). At Ohio State University, Smith also developed one of the first bench-scale heat release rate test methods. As indicated by Janssens (1995), the importance of the heat release rate can be explained as follows. First, heat release rate is directly related to mass loss rate. The toxic fire hazard of a material is a function of the release rate of toxic gases, and the toxic gas release is the product of total mass loss rate and yield of the gases. Second, the heat released by a material burning in a compartment results in a temperature rise of the hot layer gases as well as that of compartment walls and ceiling. The radiation feeding back from the hot gases and surfaces

to the fuel surface increases the mass loss flux. This means that the heat release will greatly affect fire development. As illustrated by Babrauskas and Peacock (1992), fire hazard is most sensitive to changes in the heat release rate of the burning fuel.

In the past half-century, mostly since the 1970s, a number of reaction-to-fire test methods have been developed to measure the heat release rate. A detailed review for the development of these methods can be found from one of Janssens' articles (Janssens 2002). These test methods vary widely in concept and features. They can be sorted into the following four catalogues:

- Sensible enthalpy rise method (Smith 1972);
- Substitution method; first implemented at Factory Mutual Research Corporation, (Thompson and Cousins 1959);
- Compensation method, developed at the National Bureau of Standards (Parker and Long 1972) and Stanford Research Institute (Martin 1975);
- Oxygen compensation method (sourced from Thornton (1917)).

The usage of the first three methods is limited due to their disadvantages. The major problems in practical implementation of them include temperature delay, thermal lag, and complexity in controlling. The oxygen compensation method was further improved as the oxygen consumption method. It is the most accurate and convenient way to measure the net heat release rate. Problems due to thermal lag are eliminated. It can be applied to both bench-scale and large-scale tests.

The oxygen consumption method has been proven to be a robust and versatile method with reasonable accuracy for engineering studies (Huggett 1980). It can be used to study the dynamic combustion behaviour of flammable materials in controlled or uncontrolled environments. Therefore the oxygen consumption method was chosen in the current research.

5.1.1 Oxygen consumption method

The cornerstone of the oxygen consumption method was laid by Thornton (1917). He indicated that for a large number of organic liquids and gases, a more or less constant net

amount of heat is released per unit mass of oxygen consumed for complete combustion. Huggett (1980) found this was also true for organic solids, and further obtained an average value for the constant of 13.1×10^3 kJ/kg of oxygen consumed. Thornton's observation implies that it is sufficient to measure the oxygen consumed in a combustion system in order to determine the net heat released. An equation illustrating the relationship between the oxygen consumed and heat released was given as:

$$q = E_{HPM} (\dot{m}_{air} Y_{oxy,air} - \dot{m}_{pd} Y_{oxy,pd}) \quad (5.1)$$

where:

E_{HPM} : heat release per mass unit of oxygen consumed ($\approx 13.1 \times 10^3$ kJ/kg),

\dot{m}_{air} : gas flow rate of air (l/s),

\dot{m}_{pd} : gas flow rate of combustion products (l/s),

$Y_{oxy,air}$: mass fraction of oxygen in the combustion air (0.232 kg/kg in dry air),

$Y_{oxy,pd}$: mass fraction of oxygen in the combustion products (kg/kg).

Some concerns have to be solved before this equation can be applied. For example, the mole fraction of oxygen that was measured in oxygen analyzers must be converted into a mass fraction of oxygen in the gas sample. Water vapour needs to be removed from the sample before it passes through the analyser, so that the resulting mole fraction is on a dry basis. Such issues have been well addressed and solved in the standard of applying this method (ISO_5660-1 2002).

5.1.2 Cone calorimeter

An apparatus that utilises the oxygen consumption principle to measure heat release rate is the cone calorimeter. The cone calorimeter was developed at the National Bureau of Standards (now renamed as NIST) by Babrauskas in the early 1980s (Babrauskas 1984). It is presently the most commonly used bench-scale heat release rate measuring apparatus. The apparatus and test procedure are standardized in the USA (ASTM_E1354-04 2004) and internationally (ISO_5660-1 2002). The principle construction of a cone calorimeter is illustrated in Figure 5.1.

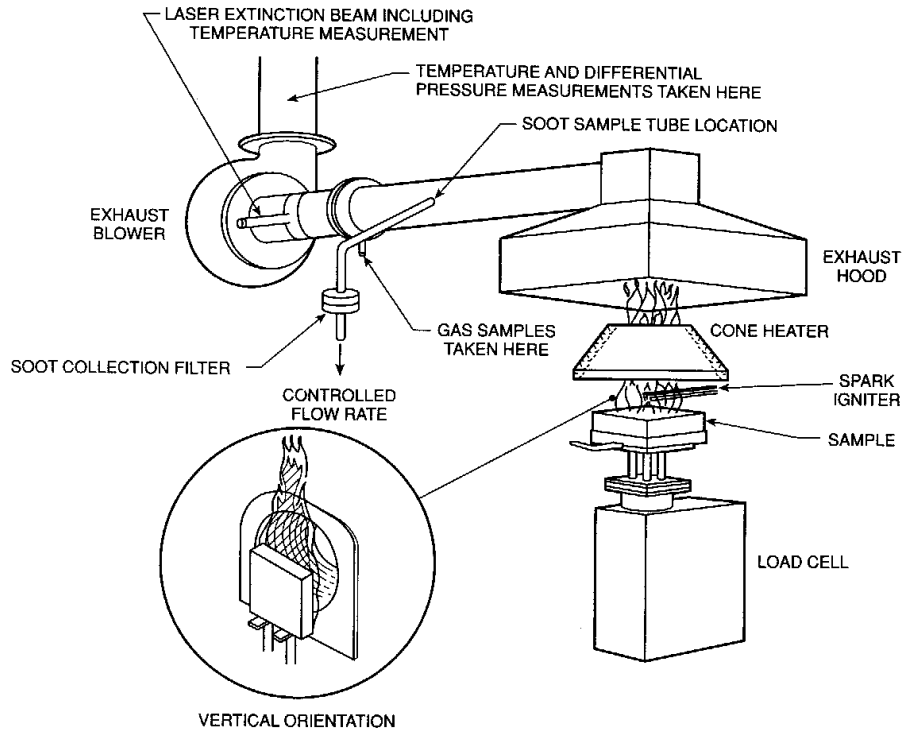


Figure 5.1 Illustration of cone calorimeter

A sample material is placed on a load cell which measures the mass in real time. An electrical cone shape heater provides a uniform external heat source to cause thermal decomposition and vaporization of the sample material. In the case of piloted ignition tests, an electric spark is used as the ignition source above the sample. In the case of non-piloted ignition tests, the ignition of flaming combustion relies on sufficient heating of the sample and vapor by the cone heater. The product gas mixture is controlled by an exhaust hood and its flow rate. Temperature and chemical composition of the gaseous product are measured.

The configurations of a standard cone calorimeter are as follows:

- *Cone heater*: consists of a 5 kW electrical heating element, which can provide uniform radiation up to 100 kW/m^2
- *Spark igniter*: an electric spark as the ignition pilot
- *Specimen holder*: holds specimen size of $100 \times 100 \text{ mm}$ and can be mounted in horizontal and vertical orientations
- *Load cell*: used to measure mass changing of the specimen
- *Oxygen analyzer*: high accuracy for oxygen concentration measurement, typical noise level is 20 ppm

- *Air flow*: a high temperature duct fan allows flow rate adjusted between 10 and 32 l/s
- *Additional measurements*: most cone calorimeters include instruments for measuring smoke obscuration and concentration of soot, carbon dioxide, carbon monoxide, water vapor and other gases.

Depending on the instruments installed, parameters that can be measured as functions of time from the cone calorimeter may include:

- Heat release rate
- Total heat released
- Mass loss rate
- Effective heat of combustion
- Ignitability
- Smoke and soot yields
- Toxic gases yields.

The effective heat of combustion (EHC) is derived from the measured heat release rate per unit exposed area (kW/m^2), q'' , and mass flux (i.e. mass loss rate per unit exposed area) ($\text{g}/\text{m}^2\cdot\text{s}$), m'' , by the following equation:

$$\Delta H_{c,eff} \equiv \frac{q''}{m''} \quad (5.2)$$

Therefore a combustion efficiency, ϕ , of a material in cone calorimeter testing conditions can be calculated from following equation:

$$\phi = \frac{\Delta H_{c,eff}}{\Delta H_c} \quad (5.3)$$

where ΔH_c is the theoretic heat of combustion.

The cone calorimeter tests for the current research were carried out in the Centre for Environment Safety and Risk Engineering (CESARE), Victoria University of Technology, Australia. A Dual Analysis cone calorimeter was used, which was made by Fire Testing Technology (FTT) Limited, England. The oxygen analyser is a Servomex 1440C Gas Analyser. More details about this equipment are listed in Table 5.1.

Table 5.1 Specifications of FTT's cone calorimeter

ITEM	SPECIFICATIONS
Heater	Cone type, 5 kW
Heat flux	0 to 100 kW/m ²
Specimen size and orientation	100 mm×100 mm, Horizontal & vertical
Load cell measuring capacity	500 g, and up to 1300 g for horizontal
Load cell tare capacity	2.0 kg
Load cell resolution	0.1 g
Ignition	Electric spark
Exhaust fan	0 to 0.045 m ³ /s
Oxygen analyzer detect range	0 to 100%

5.2 Calibration and Operation of Cone Calorimeter

5.2.1 Calibration of cone calorimeter

In the cone calorimeter tests, meticulous operation, routine maintenance, and calibration are essential for obtaining accurate results. The operation and routine maintenance are described in the operation manual (FTT 1998).

The calibration procedures include a number of daily calibrations, such as those for gas analysers, load cell, gas flow rate, heat flux meter, thermocouples, etc. The details of these calibrations are detailed in the operation manual and standards (AS/NZS_3837 1998; FTT 1998; ISO_5660-1 2002). Among the calibrations, checking for the orifice flow constant, (calibration constant, named *C* factor), was carried out daily by a methanol burning. This check verifies not only the oxygen analyser, but also the integrity of the gas sampling system, thermocouples, orifice plate and pressure transducer circuits. When a burner is being supplied with methane (purity ≥99.9%) at a flow rate of 16.76 l, equivalent to 10 kW, the actual methane flow rate is given in Equation (5.4). Using the basis of 50.0×10³ kJ/kg as the net heat of combustion of methane and the specific constant for methane, 12.54×10³ instead of the general constant 13.1×10³, basic Equation (5.1) will be expressed as following equation (5.5), while q'' is 10 KW.

$$V = 16.76 \left(\frac{101.3}{P} \right) \left(\frac{T}{273} \right) \quad (5.4)$$

$$C = \frac{7.25 \times 10^{-2} \sqrt{\frac{T_c}{\Delta P}} - (1.105 - 1.5 X_{O_2})}{0.2095 - X_{O_2}} \quad (5.5)$$

where:

X_{O_2} : the oxygen concentration,

T_g : the gas temperature in the test meter (K),

T_{sta} : the stack temperature (K),

P : the gas pressure in the test meter (kPa)

ΔP : the stack orifice differential pressure (Pa)

V : the flow rate of methane (l/min).

The obtained orifice coefficient should be between 0.040 and 0.046 according to the manual of the cone calorimeter (FTT, 1998).

Before the normal testing, a burning of a piece of PMMA was also carried out daily under an external radiation of 50 kW/m^2 . This test can calibrate heat release rate as well as the heater radiation, smoke yield and yields of various gases. A typical running result for the heat release rate of PMMA is shown in Figure 5.2.

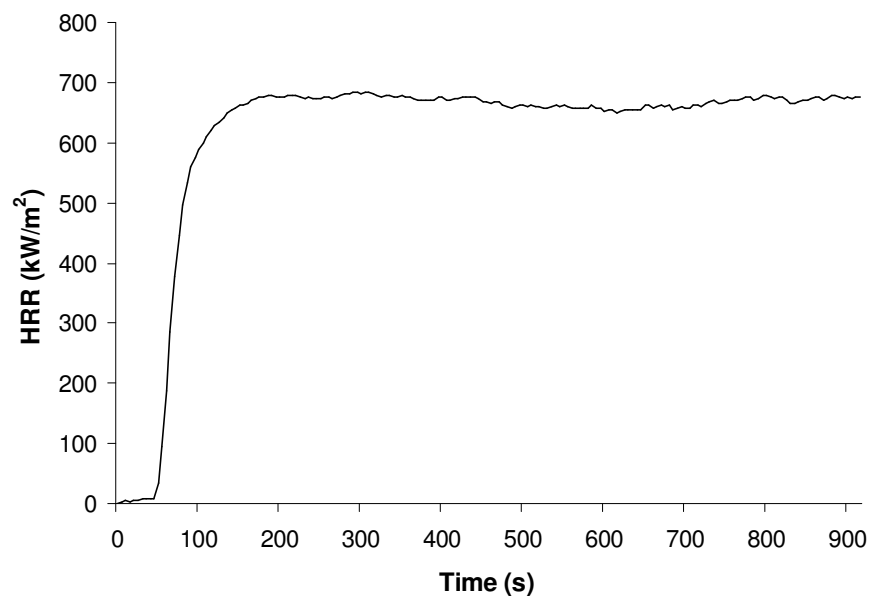


Figure 5.2 Calibration by PMMA burning

Meanwhile, another calibration method, Heat Release Rate calibration, developed for a project of interlaboratory-calibration, was also adopted for comparison. In this calibration,

methanol (99.8% of purity, H₂O < 0.1%) was burnt in a set of 4 tests (50 ml, 100 ml, 150 ml, and 200 ml respectively) to decide the *C* factor. An initial value of *C* factor (*C_i*) was used to obtain the total heat released in the cone calorimeter tests. Then an amended value of the *C* factor can be calculated by following formula (Equation (5.6)).

$$C = C_i \times V \times d \times 19.94 / THR \quad (5.6)$$

where:

V: volume of methanol,

d: density of methanol (0.791kg/l),

19.94: the net heat of combustion of methanol (MJ/kg), and

THR: calculated total heat release from cone calorimeter tests (MJ/kg).

Average the four results to get final *C* factor. The standard deviation should be within 2%. Compared the *C* factors obtained from methane test and methanol test, the difference is within 1.5%, which shows a good operation condition of the used cone calorimeter.

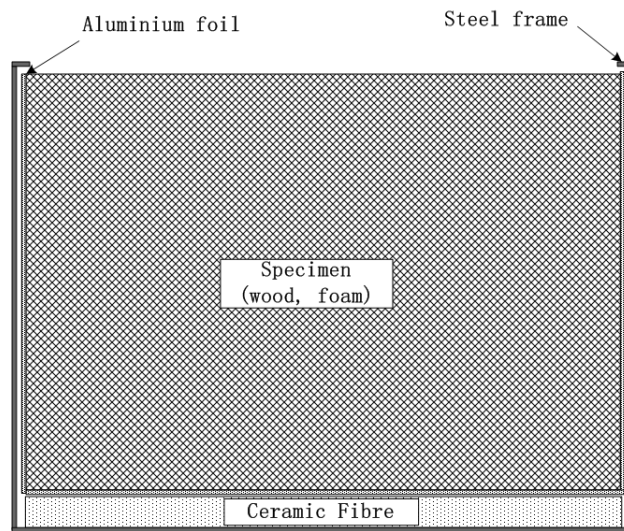
5.2.2 Experiment procedure

5.2.2.1 Testing materials and preparation

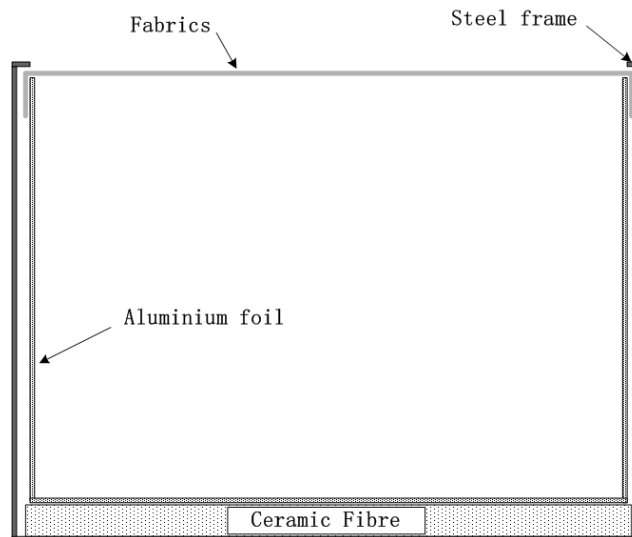
The furnishing materials in the current cone calorimeter tests are the same as those used in the TGA tests (Chapter 4). Their properties were listed in Table 4.1.

For the timber materials, two thicknesses, 32 mm and 14 mm, were tested. For the PU foams, tests were carried out with 50 mm and 25 mm thicknesses. The top area of these samples was 100×100 mm.

For the wood and PU foam specimens on tests, the side faces and bottom were wrapped with aluminium foil, and a 13 mm thickness of ceramic fibre was put under foil for thermal insulation, see Figure 5.3 (a). The fabrics, cut into 120×120 mm, were suspended by an empty aluminium foil frame, as shown in Figure 5.3 (b). Meanwhile, certain combinations of the furnishing materials, mainly adding fabrics on the top of the polyurethane foams, were also tested, following the configuration of a previous test in CSIRO (He *et al.* 1999).



(a) wood and foam specimens



(b) fabric specimen

Figure 5.3 Section views of the specimens in the sample holder

Before the tests, all specimens were conditioned in a condition chamber with a temperature of 23 ± 1 °C and relative humidity of $50 \pm 2\%$ for more than 48 hours, according to the ISO 5660-1 standard. Under such conditions, the mass variations for the woods and fabrics are less than 0.1% per 24 hours, and no mass change were observed for the PU foams.

The moisture content in the timber materials was also measured. After conditioning as above, they were placed in an oven and heated up to 100 °C. The weight change was monitored every 24 hours. The change in the average density and the average moisture

content are shown in Figure 5.4. It can be seen that after 48 hours of heating the density of the sample became constant and the moisture content for the mountain ash was therefore measured as 8.5%.

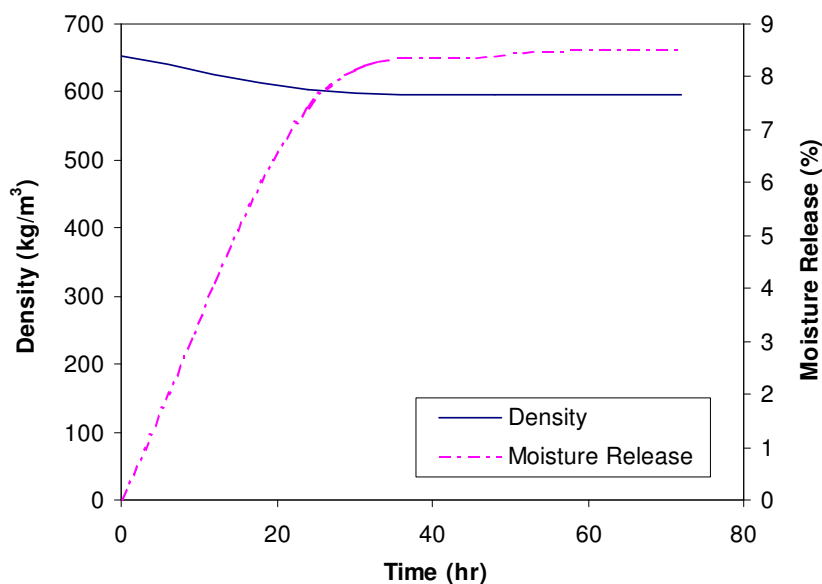


Figure 5.4 Moisture content changing curve for mountain ash

5.2.2.2 Testing condition and data sampling

All the materials were tested in the horizontal orientation, with an air flow rate of 24 l/s. Radiation levels ranged from 10 kW/m² to 100 kW/m². Both spark piloted and non-piloted methods were tested. The exposed areas of the samples were 0.0089 m² with a standard steel frame.

The scrubbed method was used for all the tests. In the scrubbed method, all the water and CO₂ content were removed from the sampling gas before it was pumped to the oxygen analyser. An illustration of the gas flow is given in Figure 5.5, and followed the requirements discussed in Appendix D of AS/NZS 3837:1998.

In accordance with the test standard for the cone calorimeter, the tests under each condition were repeated at least 3 times to obtain average values, while the differences of the measured heat release rates during the 180 seconds from the ignition for the 3 runs were less than 10%.

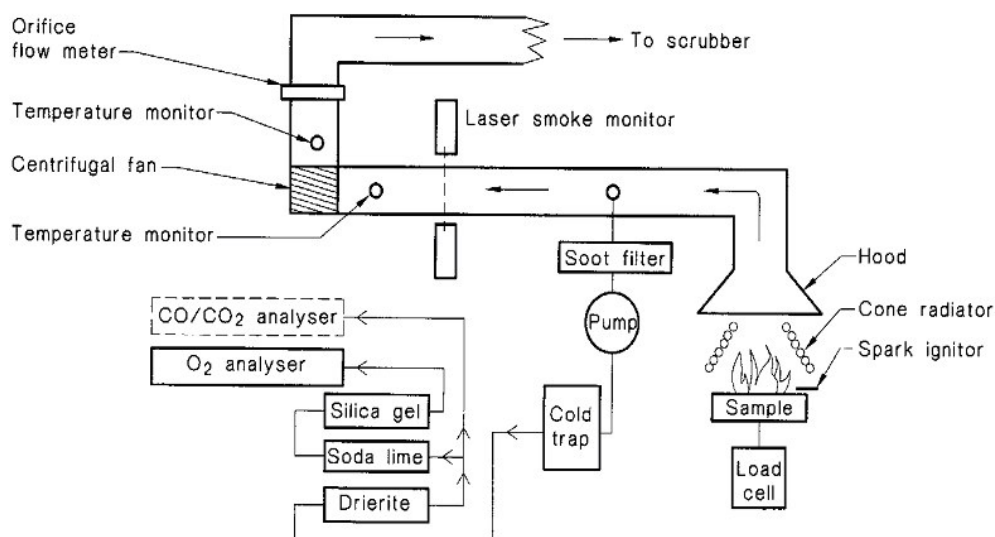


Figure 5.5 Illustration of gas sampling in cone calorimeter

The ignition time was determined manually by observing a sustained ignition, rather than a brief, non-sustained flash. The end of the test was decided by the moment of flame out plus an extra 2 minutes, according to the ISO-5660 standard. All the other testing parameters were recorded automatically by a special software, WinCone4.2, which was developed by the FTT and bundled with the cone calorimeter device.

Tables that listed all the tests conducted are included in Appendix B.

5.3 Experimental Results

5.3.1 Ignition time

5.3.1.1 Tested results

The average ignition times of the tested materials under different radiation levels and sample thickness are listed in Table 5.2. When estimated accuracy of the time measurement is approximately within second, the calculated average values were shown with one decimal.

Table 5.2 Ignition time (in seconds) and standard deviations of the tested materials under different conditions

Material	Thickness	Radiation (kW/m ²)										
		10	20	30	40	50	75	Piloted				
		Yes	Yes	No	Yes	No	Yes	No	Yes	No	No	
mountain ash	32 mm	NA	SM	NA	153.2 (63.5)	NI	53.0 (7.5)	61.3 (6.1)	27.0 (3.2)	36.2 (7.9)	10.7 (2.1)	
	14 mm	NA	NA	NA	98.3 (11.4)	NA	NA	NA	29.3 (2.1)	55.0 (12.5)	NA	
Pine wood	32 mm	NA	SM	NA	96.3 (27.2)	NI	35.0 (1.7)	65.7 (26.0)	19.3 (2.1)	30.5 (5.0)	8.0 (1.0)	
Cotton	1 layer	NI	59.0 (7.0)	NI	22.3 (1.5)	28.3 (5.9)	15.3 (1.2)	18.3 (2.5)	11.3 (1.5)	12.0 (1.0)	7.3 (0.6)	
Cotton & Polyester	1 layer	NI	34.7 (1.2)	NI	17.3 (1.5)	18.3 (1.5)	8.7 (1.5)	12.7 (0.6)	6.3 (0.6)	7.7 (2.3)	5.3 (0.6)	
Stamina PU foam	50 mm	41.3 (3.5)	8.0 (2.6)	NI	6.0 (2.0)	26.7 (8.4)	4.0 (1.0)	17.0 (5.3)	1.0 (0.0)	10.3 (5.7)	2.7 (0.6)	
	25 mm	NA	NA	NA	7.7 (3.8)	46.3 (16.0)	NA	NA	3.7 (1.5)	4.7 (1.2)	NA	
Standard PU foam	50 mm	NI	8.0 (3.2)	NI	3.3 (0.6)	21.0 (5.2)	2.0 (1.0)	8.0 (5.3)	1.7 (0.6)	4.5 (2.4)	1.3 (0.6)	

- Notes: 1. The ignition times are average values from at least 3 tests. The standard deviations are listed in brackets.
2. NA: not tested at such condition.
3. NI: no ignition taking place.
4. SM: smouldering and difficult to determine ignition time.

It was noted that under 75 kW/m² the ignition times of the piloted and non-piloted tests were almost identical for most of the tested materials. Therefore only the non-piloted results are presented in the last column of Table 5.2.

5.3.1.2 Linear relationship between $t_{ig}^{-0.5}$ vs radiation

A linear relationship between the $t_{ig}^{-0.5}$ vs radiation for the thermally thick materials has been reported by Delichatsios (1999). By applying the previous judgment for the thermally thin or thick materials in Section 2.4.1.1, judgments for the studied materials were performed. Table 5.3 shows the thermal length characteristic, $L_{thermal}$ and physical length, L_{phy} , for the studied materials.

Table 5.3 Thermal length characteristics for the studied materials

Material	Heat flux (W/m ²)	T _s -T _{sl} (K)	Conductivity (W/mK)	L _{thermal} (m)	L _{phy} (m)
timber	20000	300	0.15 ^{#1}	0.00225	0.032
fabric		280	0.1 ^{#2}	0.0014	0.001
PU foam		300	0.026 ^{#3}	0.00039	0.05

Note: A relative low radiation was chosen;

The temperature differences for the surface temperatures were determined from ambient to ignition of the materials;

Data source of the thermal conductivities:

#1: average from SFPE Handbook (2002)

#2: Lawson and Pinder (2000)

#3: Mukaro *et al.* (2003)

It was found that the timber and PU foams could be considered as thermally thick at various radiations, since their thermal length characteristics are much smaller than their physical length (thickness). On the contrary, the fabrics can be considered as thermally thin due to their larger thermal length characteristics compared to their physical length. The estimation result for the fabrics matches the experimental results carried out by Flesischmann and Chen (2001). They investigated 14 different fabrics, including 100% cotton and 51% polyester and 49% cotton, and found that above 15 kW/m² radiative flux, a good correlation existed between $1/t_{ig}$ versus q''_{ev} , which is observed for thermally thin materials. Therefore all the fabrics should be considered as thermally thin.

From the current tests, a linear relation was found between $1/t_{ig}^{1/2}$ and q''_{ev} for the timber and PU foams (see Figure 5.6) since they were all thermally thick materials based on the above calculations. It was interesting to note that the same trend was also seen for the fabrics, the cotton and the cotton and polyester, although they were normally treated as thermally thin materials. This may be explained by the configuration of fabric samples in the tests. The fabrics were suspended over a volume full of air which is a poor heat conductor with a thermal conductivity of 0.025 W/m·K. Therefore, there was little heat lost through the back side, or the empty side, of the sample. The thin fabrics then behaved like a thermally thick material.

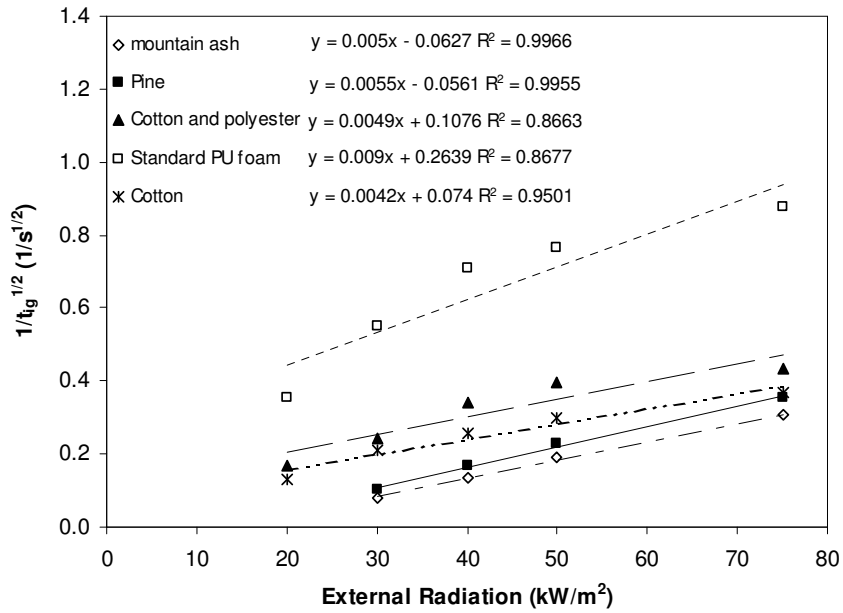


Figure 5.6 Relation between ignition time and external radiation

5.3.1.3 Determining the critical radiative flux

The critical radiative flux, which was defined in Chapter 2 as the minimum radiative flux required for ignition to occur, was not measured in the current experiments. However it can be determined approximately by a method, which was developed by Quintiere (Quintiere and Harkleroad 1984) and discussed in Chapter 2, Figure 2.4. A Quintiere chart of the ignition time applied for the mountain ash is shown in Figure 5.7.

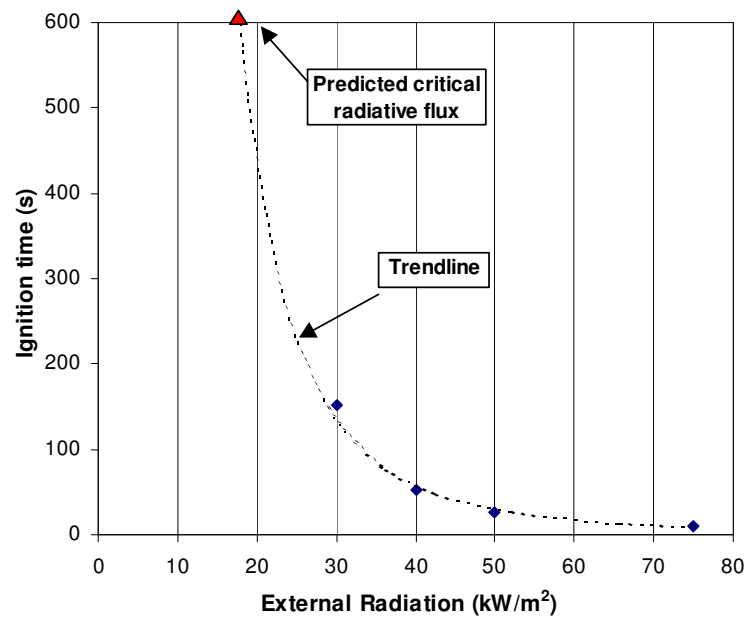


Figure 5.7 Ignition times and trend-line for the mountain ash

By extending the trendline of the curve of ignition time back to 600 seconds, the critical radiative flux for the mountain ash was then estimated approximately as 17 kW/m^2 . This critical radiative flux can be used to predict ignition surface temperature, as discussed in Section 2.4.2.

This estimated critical radiative flux could be validated indirectly by the following methods. The first one is observation from the tests. The smouldering combustion always occurred at 20 kW/m^2 radiation but not at 10 kW/m^2 for the mountain ash. Secondly it can be validated by an empirical equation given by Babrauskas (2001), which was derived from a great number of cone calorimeter tests for wood. The details of this comparison can be found later in Section 5.3.1.5.

5.3.1.4 Effect of sample thickness

It was found that for the mountain ash, varying the sample thickness had different effects on the ignition time under different radiation fluxes. The ignition time becomes shorter as the sample thickness (as well as the sample mass) decreases under low radiation flux ($<30 \text{ kW/m}^2$). On the contrary, under high external radiation, the ignition times for various thicknesses were similar (piloted ignition) or the ignition time for a thinner sample became longer (non-piloted ignition).

Ignition of solid fuel is greatly dependent on the sample surface temperature. Under low external radiation conditions, the surface temperature rise is controlled by conduction as well as external radiation. The time to heat a thinner sample is shorter than that for a thicker one. Therefore the thinner sample reaches a certain surface temperature quicker which results in a shorter ignition time. Under high external radiation conditions, the heat flux wave within the solid reaches to the back of sample much quicker and bounces back due to the effect of the insulation material. This bounced back heat wave may speed up the forming of a thicker char layer. As discussed in Section 2.3.3, the thicker char functions to impede the heat flux flow in and the gas pyrolysis products out of the solid. Therefore a longer ignition time may exist where thickness is reduced. This phenomenon can be also found from experimental results by others (Harada 2001).

5.3.1.5 Comparison with results from others

For the pine wood, the measured results are similar to Delichatsios' cone calorimeter experimental results (Delichatsios 1999). In his piloted experiments, the ignition times for a 19 mm thick pine wood are 132 s and 22 s under 30 kW/m² and 50 kW/m² radiation levels respectively.

The tested results can be validated against even wider experimental data by a correlation developed by Babrauskas (2001). For the piloted ignition, an estimated rule for radiant heating ignition of wood is:

$$t_{ig} = \frac{130 \rho^{0.73}}{(q_{ev}'' - q_{cr}'')^{1.82}} \quad (5.7)$$

where:

t_{ig} : ignition time, s;

q_{ev}'' : effective radiation flux, kW/m²;

q_{cr}'' : critical radiation flux, kW/m²;

ρ : sample density, kg/m³.

Checking the current tested results against Equation (5.7), a quite good agreement was obtained. For example, applying a critical radiation flux of 17 kW/m² obtained from Figure 5.7 for the mountain ash, the measured ignition times from Table 5.2 for the timbers match the above relationship reasonably well, as shown in Table 5.4.

Table 5.4 Comparison of ignition times from current tests and Babrauskas' equation for mountain ash

		Radiative flux (kW/m ²)		
		30	50	75
Ignition time (s)	Tested	153.2	27.0	10.7
	Estimated	142.9	26.2	9.4

5.3.2 Heat release

In this section, experimental results for two types of heat release parameters, the heat release rate (HRR) and total heat released (THR) are presented.

5.3.2.1 Heat release rate

The heat release rate curves for the various tested materials under various test conditions are shown in Figure 5.8 to Figure 5.12. The presented curves were picked up from one of those 3 runs that had a closest peak value to the averaged peak value.

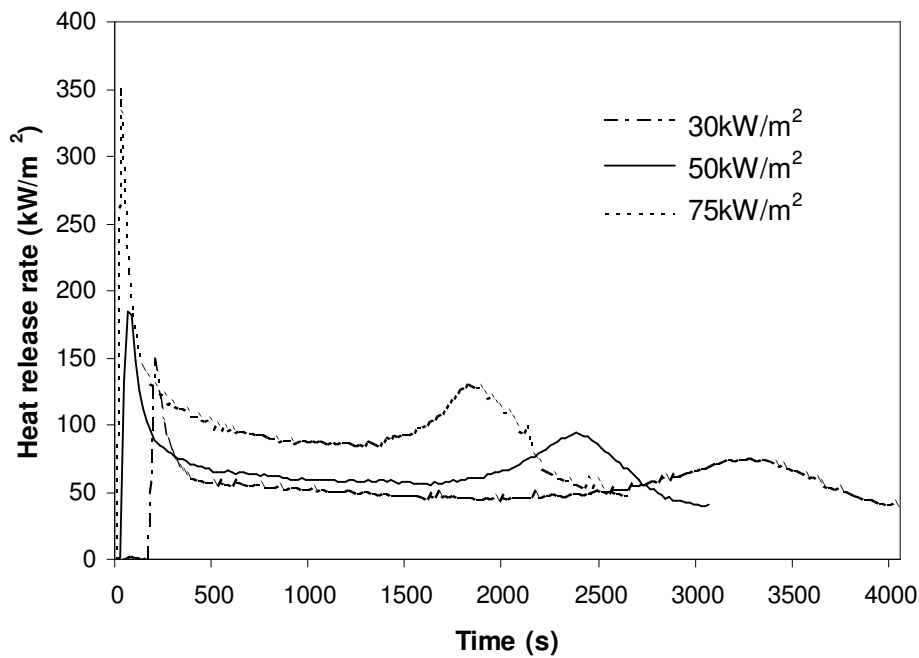


Figure 5.8 Heat release rate of mountain ash from piloted tests

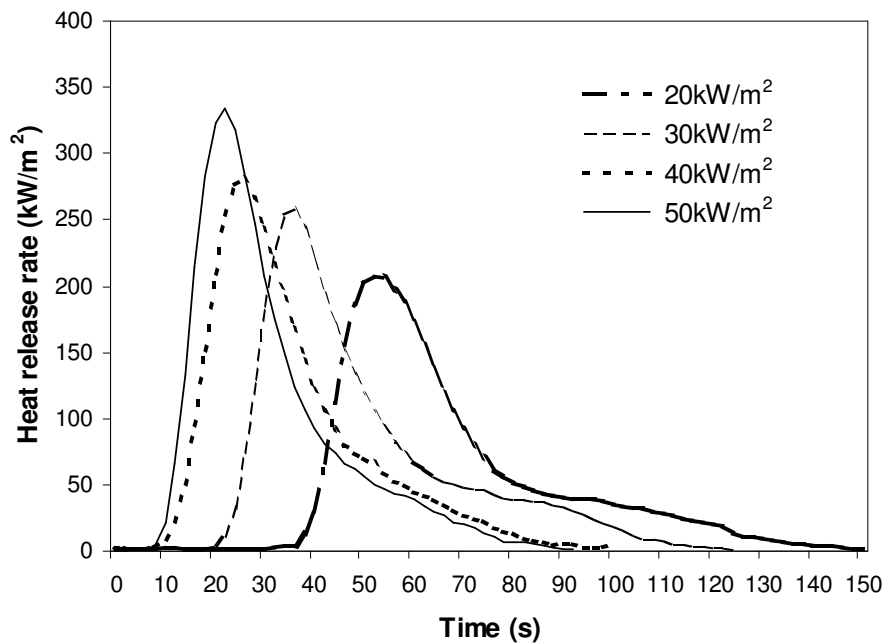


Figure 5.9 Heat release rate of cotton and polyester from piloted tests

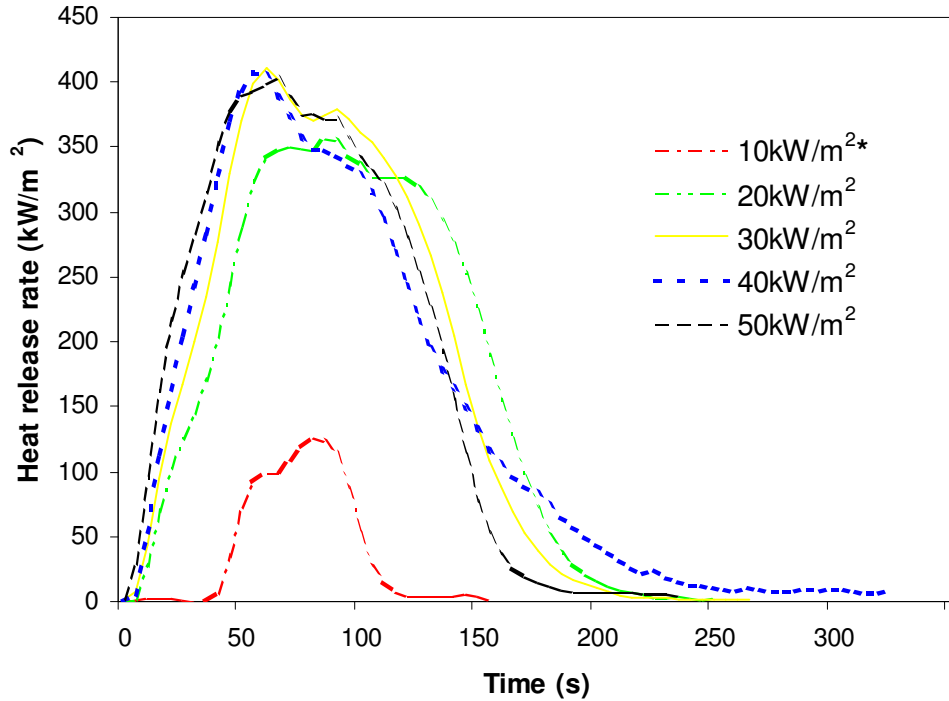


Figure 5.10 Heat release rate of Stamina PU foam from piloted tests (* smouldering and flame-out during the tests)

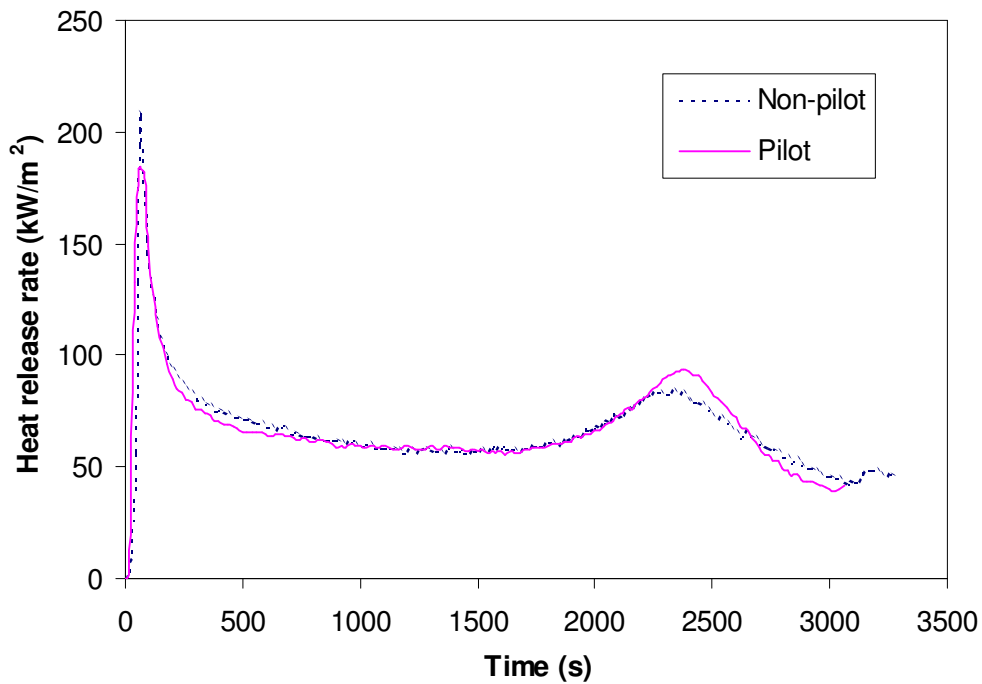


Figure 5.11 Piloted and non-piloted HRR curves for mountain ash under 50 kW/m²

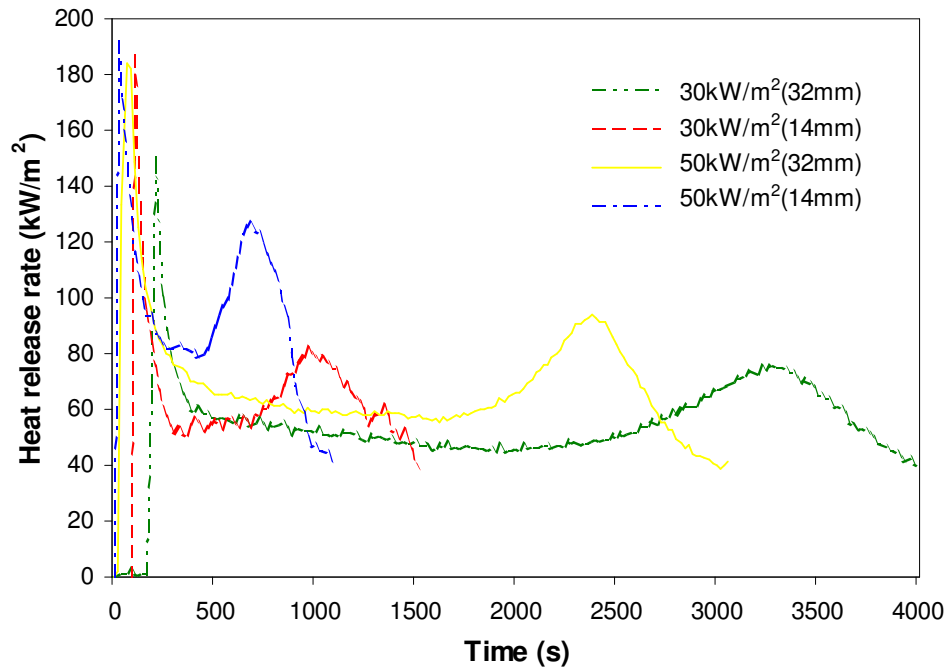


Figure 5.12 Effect of different thicknesses on HRR for mountain ash

There are two obvious peaks shown in the mountain ash's curves (Figure 5.8). The first peak corresponds to combustion of all the available combustible gas mixture, which was generated before the ignition. After the ignition occurred, the top-charring layer becomes thicker and thicker, which weakens the heat transfer downward and obstructs the pyrolysate from escaping upward. As discussed in Chapter 2 and the previous section, for a thermally thick material, the inside temperature of the sample increases rapidly due to the "bounced back" heat front. When the inside temperature reaches above the vaporization temperature of water and the pyrolysis temperature of the timber, the vaporization and pyrolysis processes occur within the sample. The generating of those gasified products results in high pressure building up inside which will cause cracking. The exposure of inner virgin material contributes to the forming of the second peak in HRR curves. This phenomenon was previously observed and explained by a number of researchers (Tran 1992; Grexa *et al.* 1997; Harada 2001). It was also proved by these researchers through tests without an insulation material present. In that type of tests, the second peak did not appear since the sample holder behaved as a heat sink and no high pressure was built up within the sample.

For the fabric materials, the peak value of the heat release rate increases (and needs less time to reach the peak) when the external radiation is increased (Figure 5.9). However, the

total heat release involved in the combustion period under various radiation conditions are very similar except for the lowest radiation level, 20 kW/m^2 , see Figure 5.13.

For the polyurethane foams, the peak HRR and the time to reach the peak are almost independent of the external radiation heat flux unless it is below 20 kW/m^2 . The lowest radiation used for the polyurethane foam was 10 kW/m^2 , and this is obviously close to the critical radiation flux. All three tests under this radiation flamed out (extinguished) during the tests. Therefore a lower peak HRR and a shorter combustion period were observed for this testing condition (Figure 5.10).

Excluding the period leading to ignition, the curve shapes for both piloted and non-piloted tests are very similar for each of the tested materials. An example is given in Figure 5.11 for the mountain ash. Under high radiation levels, the two curves obtained from piloted and non-piloted combustions were almost identical.

The effect of sample thickness on the HRR curve shapes and peak values depends on the external radiation conditions, as shown in Figure 5.12. Under high radiation, varying of thickness has less effect on the value of the first peak in the HRR curve. Under low radiation, the thinner sample has a higher value for the first peak. As explained previously, the first peak is greatly determined by the initial heating conditions. Under high radiation, the sample was heated rapidly and the time for the first peak to occur is relatively short. The conductive heat losses through the samples are relatively small and the difference between the thicknesses is also small. Therefore similar surface temperature profiles on various thickness samples result in similar first heat release peak behaviour (value and time occurred).

Under lower radiation, the role of heating of the samples is obviously slower. Over the longer heating period before the ignition, the difference of heating effort for different sample thickness is significant. The thinner sample will reach a higher surface temperature much more quickly due to its smaller mass.

As for the second peak, the thinner samples reach the “cracking” condition (as discussed previously) more quickly. Therefore the times to the second peak were reduced significantly under various radiation condition levels.

5.3.2.2 Total heat released

Total heat released (THR) is another key parameter. Shown in Figure 5.13 are examples of the total heat release histories of the cotton and polyester under various radiation levels. It can be seen that the total heat released during combustion is virtually identical except under the lowest radiation condition. Under the lowest radiation the combustion efficiency is relatively low which will be shown in next sub-section.

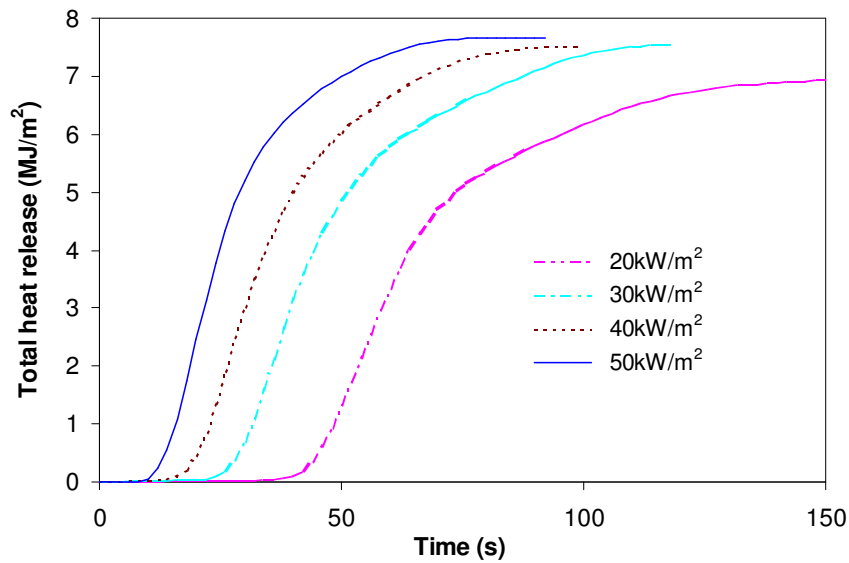
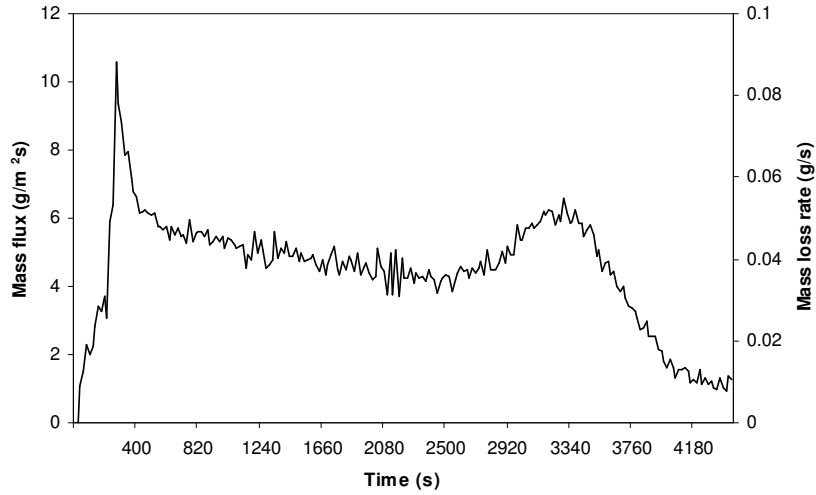
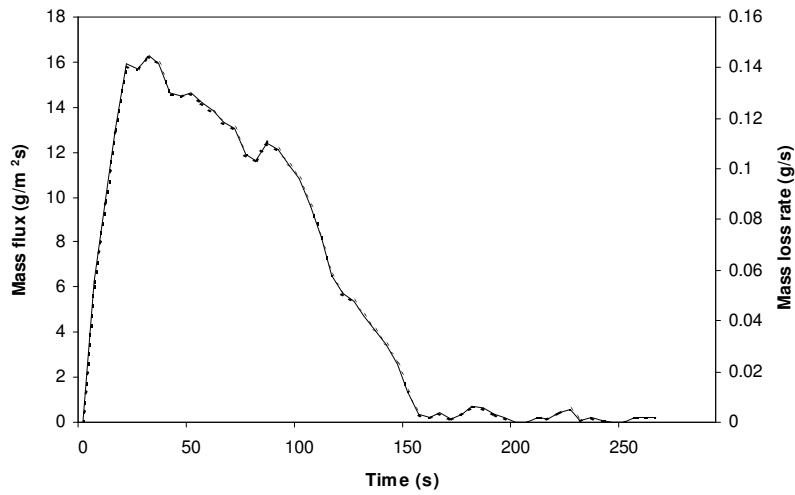
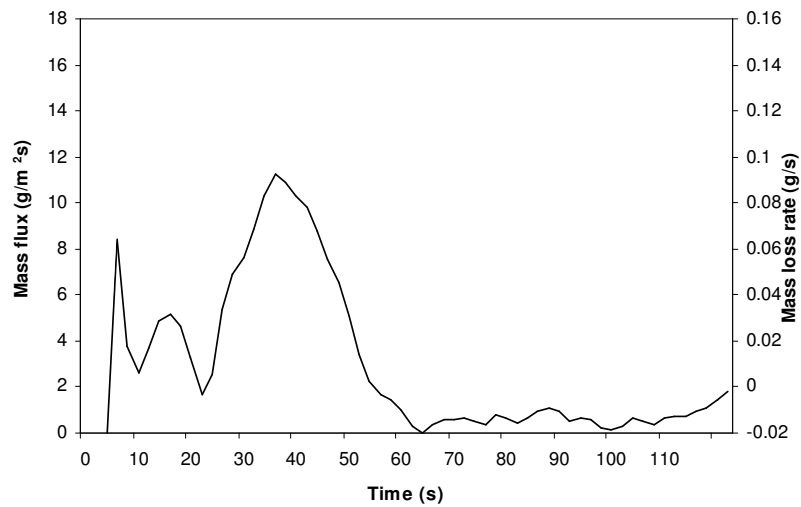


Figure 5.13 THR of the cotton and polyester under various radiation conditions

The total heat release from each cone calorimeter test can be found in Appendix B.

5.3.3 Mass loss rate and effective heat of combustion

The mass loss of a specimen is a direct measure of its pyrolysis. Figure 5.14 to 5.16 show the mass loss rate (MLR) and mass flux curves for the wood, PU foam and fabric under different radiation levels. The shapes of the MLR curve for the thermally thick materials are similar to the corresponding heat release rate curves, shown from Figure 5.8 and Figure 5.12.

Figure 5.14 Mass loss of mountain ash under 50 kW/m² pilotedFigure 5.15 Mass loss of Stamina PU foam under 50 kW/m² pilotedFigure 5.16 Mass loss of the cotton and polyester under 50 kW/m² piloted

As described earlier in this chapter, the effective heat of combustion can be calculated from HRR and MLR data from Equation (5.2). Figure 5.17 shows an example for the mountain ash under 50 kW/m^2 .

The combustion efficiency can be approximately estimated by Equation (5.3). The theoretical heat of combustion can adopt an average value, 20 MJ/kg , which is suggested by the SFPE Handbook for normal timber materials. Then the combustion efficiency is computed. The EHC measured varies from test to test as well as at different stages of a single burning. For the test shown in Figure 5.17 the combustion efficiency is estimated approximately 50% for most of the testing period. The first peak that exceeds 20 MJ/kg may be caused by combustion of accumulated gas phase pyrolysis products and then it does not correspond exactly to the mass loss rate at that moment.

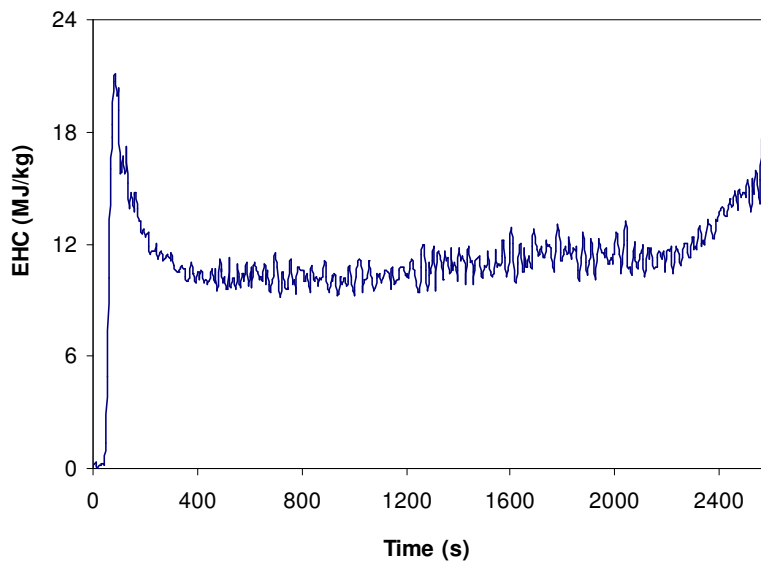


Figure 5.17 Effective heat of combustion for the mountain ash under 50 kW/m^2

It was also found that for the tested timber materials a small peak exists in the MLR curves before ignition occurred except for that under very high radiation levels ($> 75 \text{ kW/m}^2$). Figure 5.18 provides some examples, which show partial enlarged MLR curves for the mountain ash under various radiation levels. In this figure, the small peak can be observed in the MLR curves under 30 and 50 kW/m^2 radiation levels.

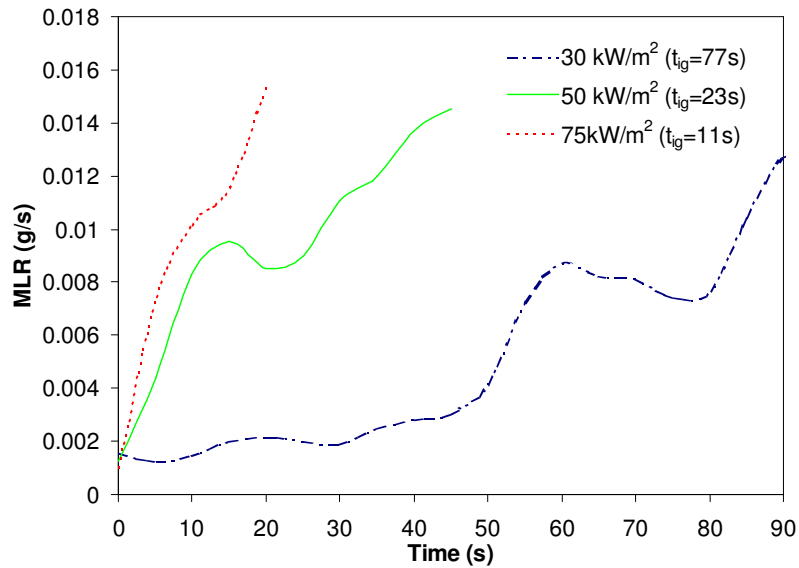


Figure 5.18 Small peaks in the MLR curves for mountain ash under various radiation levels

This phenomenon has been reported by other researchers. For example, similar results can be found from cone calorimeter test data of the Worcester Polytechnic Institute (WPI) for a wide range of wood-based materials (WPI). From their results it is known that for a very thin sample (3 mm in their tests) this phenomenon would not happen under various radiation levels.

This can be explained by the basic charring process and Atreya's theoretical analysis that were presented in Chapter 2 and 3. It is known that the mass loss before ignition was affected by the release of both moisture and pyrolysis products, including inert gases. When a thick char layer formed before ignition under lower radiation levels, it reduced the release rates by obstructing the heat and mass transfers. Then the mass loss rate curves drop until the pyrolysis generating and moisture releasing rates increased again by a higher surface temperature. Under very high radiation levels or for a very thin wooden sample, the possibility for the thicker char forming before the ignition is quite low. Therefore no such obvious peak in the MLR curve before ignition can be observed. Watt gave a similar explanation for this phenomenon (Watt *et al.* 2001).

To investigate effort of the moisture in the mass loss rate, some tests with "dried" timber samples were conducted. The timber samples are mountain ash which were dried in an oven with 100 °C temperature setting for over 100 hours. The moisture release (weight loss) is

approximate 9% and stable sample mass was observed after 72 hours. Show in Figure 5.19 are MLR curves from tests of those “dried” mountain ash compared with result from normal conditioned sample.

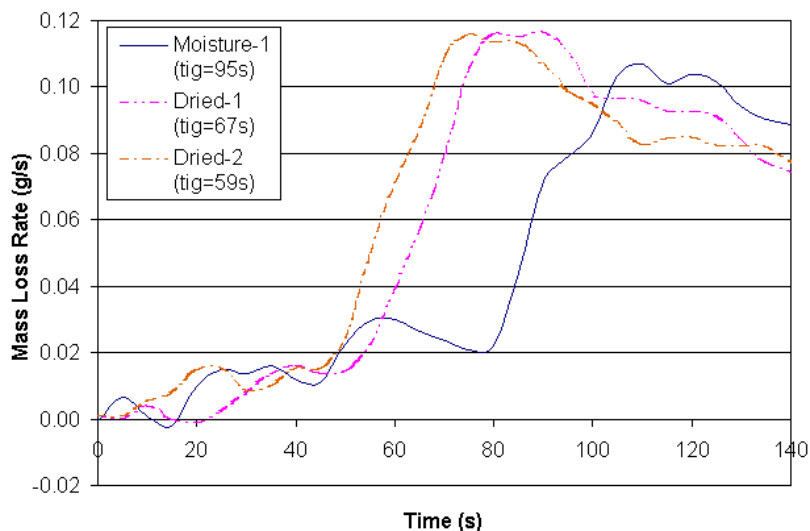


Figure 5.19 Comparison of MLRs from moisture and dried mountain ashes under 30kW/m^2

It's noticed that earlier ignition was achieved from those tests of the “dried” samples. The small peak value of mass loss rate before the ignition still exists but with lower value. This lower mass loss rate consists pyrolysis products, including inert gases. It's also noted that moisture release exists in the whole heating process even for the “dried” samples since total water content, including free and bound waters, in timber can reach 60% of total mass, according to discussion in Section 2.3.3.2. When moisture in upper layer was evaporated at the early heating stage, the moisture inside the sample specimen was keeping heated and evaporated towards both sides of the sample as the heating front moving in. Converting values from above graph into mass flux, approximate 0.009 m^2 top surface area of the sample, the moisture release before the ignition from the “moisture” samples can reach a rate of couple of grams per square metre.

5.3.4 Species yield

The CO and CO₂ yields were also measured in the cone calorimeter experiments. The measured results for these parameters greatly depend on the determination of end points for data collection and calculation. So far no universally accepted method for data treatment is

available in the literature. From previous TGA experiments and theoretical analysis, it is found that the fraction of conversion of sample mass at maximum conversion rates is almost constant. This has been adopted to develop a special OFW method to compute kinetics in Section 4.1.2.2. In the current cone calorimeter experiment, a similar trend was also observed for the fraction of sample mass, although the fractions varied with the level of external radiation. For example, the fractions of sample mass consumed for the second peak heat released for the mountain ash under 30 kW/m^2 and 50 kW/m^2 are about 67% and 66% respectively. Shortly after that point (from a point of mass fraction of 72%) the yields of CO and CO₂ keep increasing sharply. The CO yield information associated to the peak HRRs have been submerged by this sharp increasing. An example of CO yield for the mountain ash under 50 kW/m^2 was shown in Figure 5.20. Since this sharp increase of CO and CO₂ yields may be caused by incomplete combustion as well as noise of mass measurement under a very low mass loss rate, the peak yield values for the mountain ash were only calculated until 70% of the sample was consumed. These data are shown in Table 5.5.

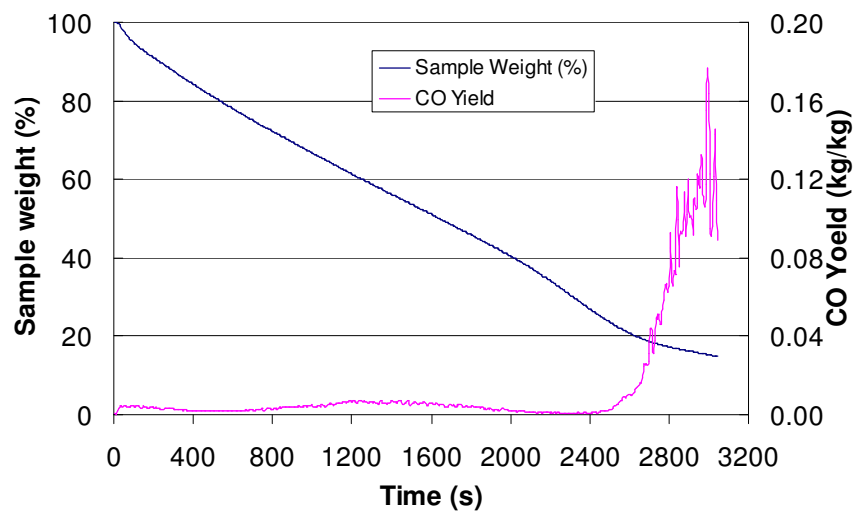


Figure 5.20 Relation between mass loss and CO yield for the mountain ash

For the average yields, $Y_{spec,ave}$, the data generated by the cone calorimeter software is evaluated using the following formula:

$$Y_{spec,ave} = \frac{\sum_{i=1}^n Y_{spec,i}}{n} = \frac{\sum_{i=1}^n \frac{\Delta m_{spec,i}}{\Delta m_{samp,i}}}{n} \quad (5.8)$$

where:

$Y_{spec,ave}$: average yield of a species (kg/kg);

$Y_{spec,i}$: measured species yield at i th time step (kg/kg);

n : number of measuring point;

$\Delta m_{spec,i}$: incremental of a species production rate at the measuring point i , (kg/s);

$\Delta m_{samp,i}$: incremental of the sample mass loss rate at the measuring point i (kg/s).

It can be seen from Equation (5.8) that the accuracy of the average yield of species may be affected by both accuracy of the gas analyzer ($\Delta m_{spec,i}$) and the noise of each measurement step of sample mass ($\Delta m_{samp,i}$). For example, the average CO yields for the mountain ash under 30 kW/m² and 50 kW/m² radiation levels are 0.023 and 0.014 kg/kg respectively. These values are much higher than those reported by other researchers which is shown in the later part of this section. Therefore another improved method was introduced by the author as in the following equation.

$$Y_{spec,ave} = \frac{\int_0^{t_{end}} \dot{m}_{spec} dt}{M} \quad (5.9)$$

where:

\dot{m}_{spec} : species generating rate (kg/s);

t_{end} : end of the period for sampling (s);

M : total mass loss of the sample (kg) .

The total mass loss, M , can be measured accurately at the end of a test.

An expression for the Y_{spec} at any given time can be given. Equation (5.9) is a special case. Now the accuracy of the average yields only depends on the resolution of the gas analysers. The effect of the mass measuring noise is eliminated. The average yields of CO and CO₂ for the mountain ash, stamina PU foam and cotton and polyester are listed in Table 5.5. Figure 5.21 shows a comparison of these two different gas curves, gas production rate and gas yield, for the mountain ash under 30 kW/m². Therefore, in the later part of this section, the gas yields from the combustion are provided by the gas production rate.

It can be seen from Table 5.5 that average yields of CO and CO₂ from the fabric and polyurethane foam are quite stable under various radiation and pilot conditions. For the

timber material, a similar trend exists under the piloted ignition condition. However, a higher radiation level produces much higher combustion efficiency and more complete combustion which generates less CO and more CO₂.

Table 5.5 Yields of CO and CO₂ (kg/kg) for testing materials

Material	Gas	Value type	At 30 kW/m ² radiation		At 50 kW/m ² radiation	
			Piloted	Non-piloted	Piloted	Non-piloted
mountain ash (70% consumed)	CO	Max	0.048	NI	0.0079	0.0059
		Aver.	0.0104	NI	0.0034	0.0028
	CO ₂	Max	1.46	NI	1.75	1.76
		Aver.	1.036	NI	1.15	1.17
Cotton & Polyester	CO	Aver.	0.043	0.05	0.045	0.049
	CO ₂	Aver.	1.87	1.86	1.87	1.88
Stamina PU foam	CO	Aver.	0.025	0.026	0.031	0.029
	CO ₂	Aver.	2.05	2.07	1.99	2.03

NI: no ignition took place.

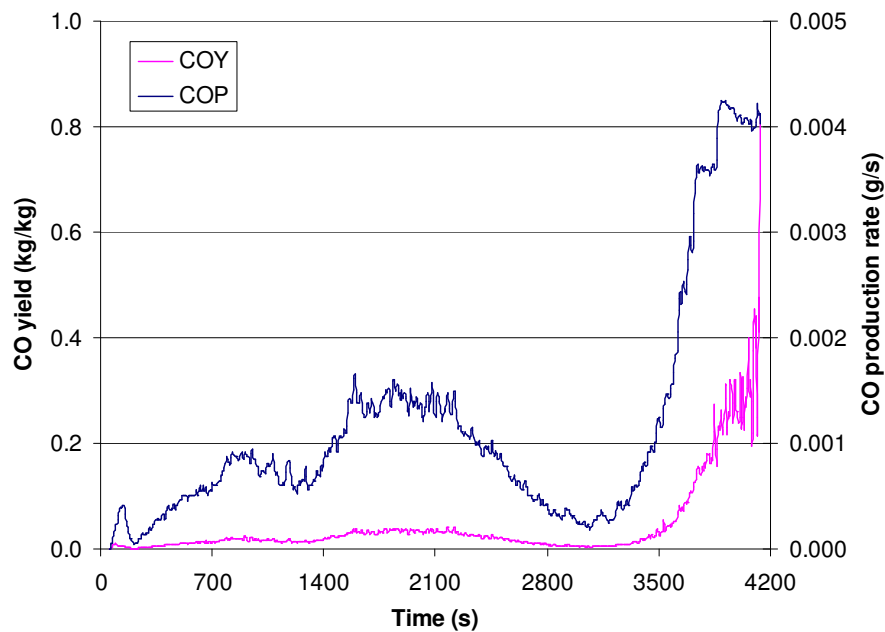


Figure 5.21 Comparison of CO yield and production curves for mountain ash (piloted combustion under 30 kW/m²)

The measured CO yield results matched other experimental data reasonably well when the improved method was adopted. For example, Babrauskas (1992) provided typical average CO yield test data from various cone calorimeter experiments as follows:

- Douglas fir: 0.003 to 0.005 (35 to 75 kW/m²)
- Rigid PU foam: 0.04 to 0.08 (35 to 75 kW/m²).

It can be seen that with one exception (the CO yield of the 30 kW/m² test, which is slightly higher), all other tested data matched with the results provided by Babrauskas quite well.

The full histories of CO and CO₂ production rates for the cotton and polyester, Stamina PU foam and pine are shown in Figure 5.22 to 5.24 respectively.

By studying the gas release rate curves, it was found that CO₂ release rates have similar shapes as that of HRR curves. This can be explained because CO₂ is a complete combustion product and is greatly determined by the fuel burning rate, which is normally measured by the HRR. As for the CO production rate, the latter peak value reflects a great degree of incomplete combustion, which is quite normal at the final stage of timber combustions. Number test results showing a similar feature can be found from the cone calorimeter tests carried out by WPI for various timber based materials (WPI).

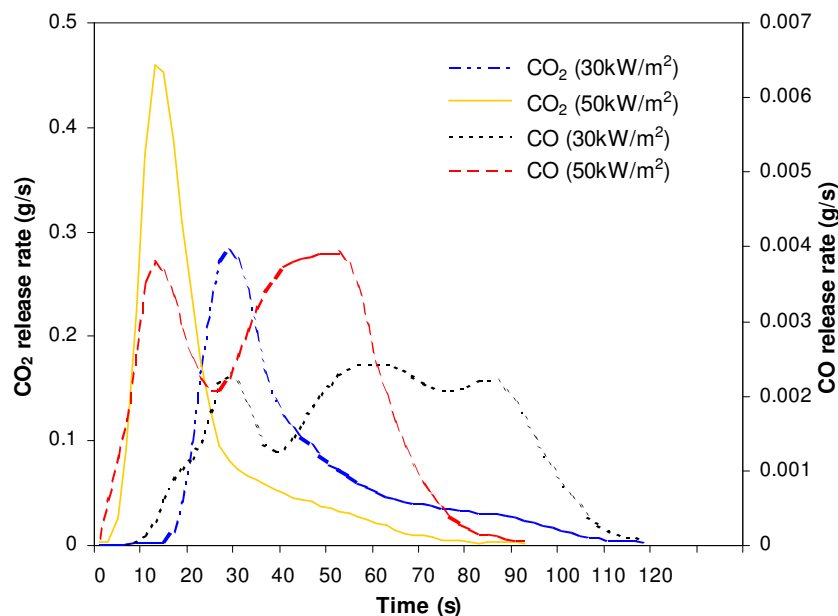


Figure 5.22 Gas release rates from the cotton and polyester

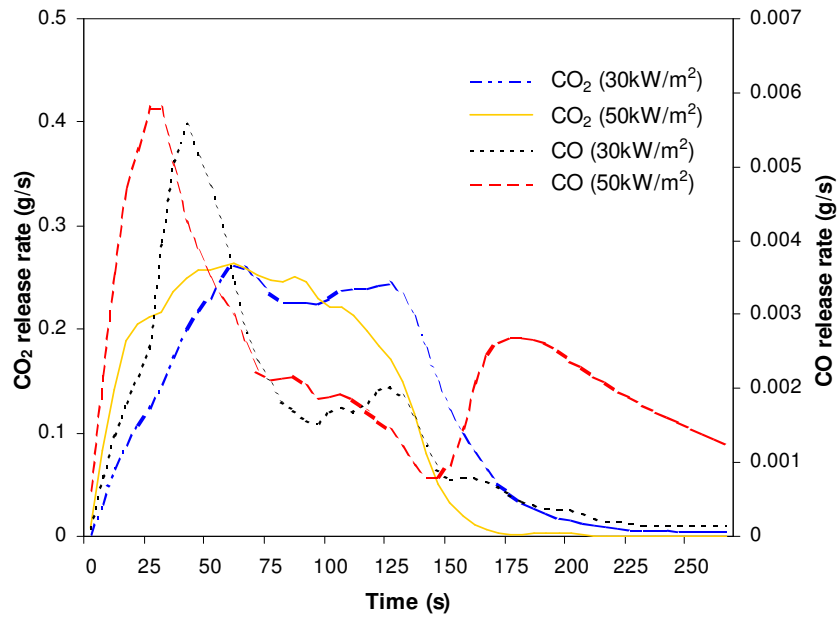


Figure 5.23 Gas release rates from the Stamina PU foam

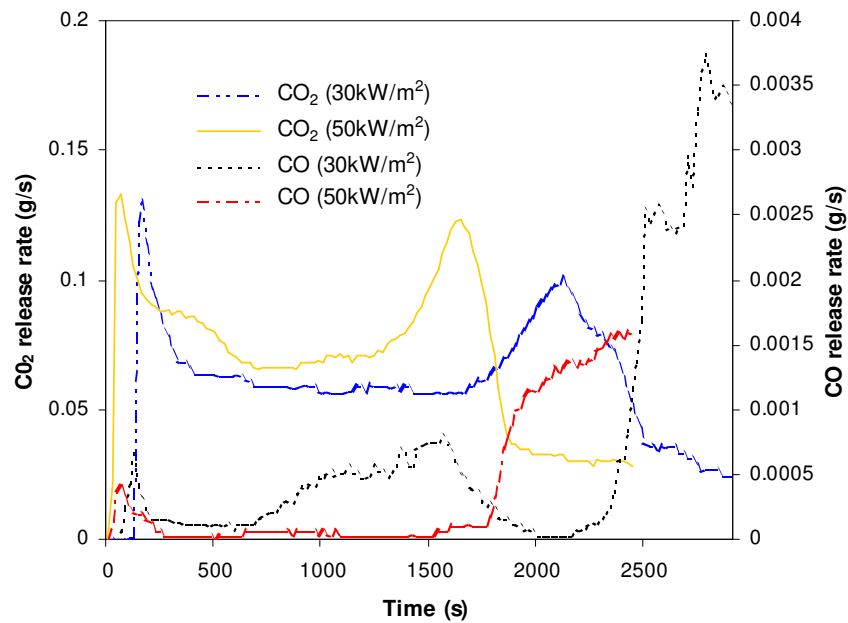


Figure 5.24 Gas release rates from the pine

5.4 Surface Temperature Measurement

5.4.1 Surface temperature

As discussed in Section 2.4.3.1, the surface temperature, especially the temperature at which ignition occurred, is a very important parameter, which has been adopted as a criterion for ignition. Therefore, in the current cone calorimeter tests, the surface temperature of some of the materials was measured.

For woods and fabrics, this surface temperature was measured by using 0.1 mm thermocouples. The configuration of the installation of the thermocouple is shown in Figure 5.25 for the woods. The thermocouple was pushed into the sample along the texture to obtain good contact. Variation in the installation may result in a tiny gap between the sample surface and the top of the thermocouple. This gap (d) was estimated to be within 0.1 mm. For the fabrics, the thermocouples were sewn into the texture to obtain good contact.

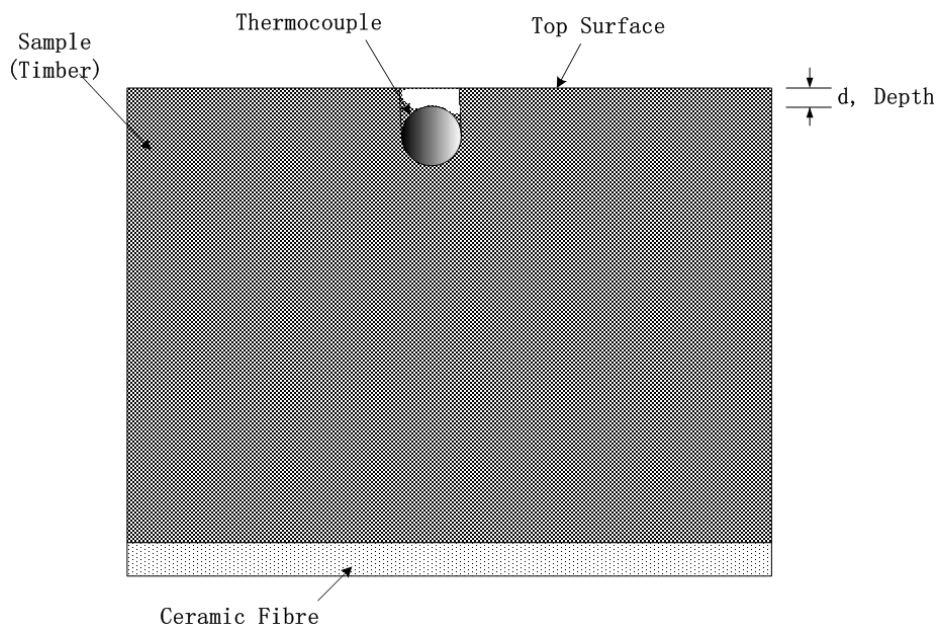


Figure 5.25 Installation of thermocouple on the surface of wood

Some surface temperature measuring results are shown in Figure 5.26 and Figure 5.27. Note that a number of tests were conducted for each test condition and the temperature curves presented in these figures are the results of the tests in which ignition times best matched with average ignition time.

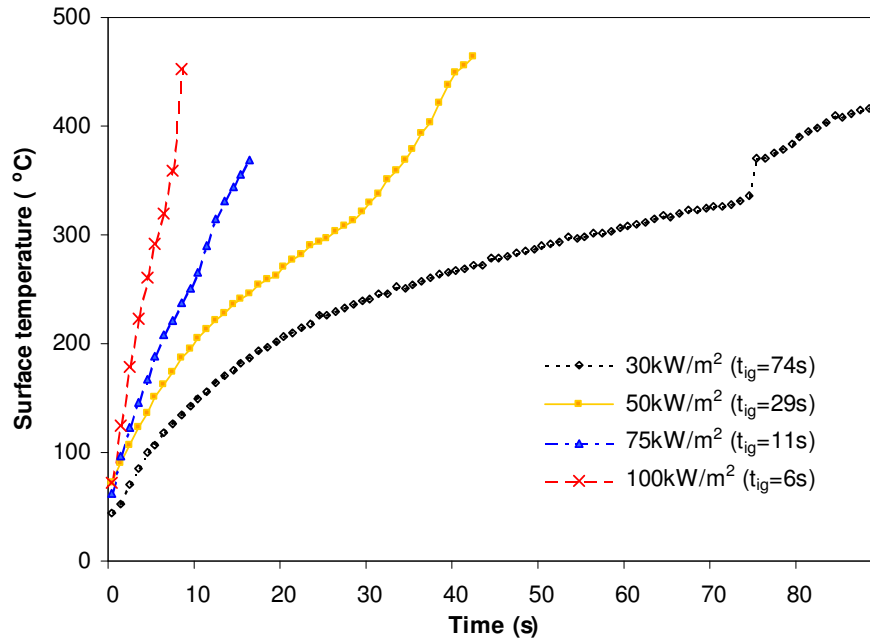


Figure 5.26 Surface temperatures of the mountain ash

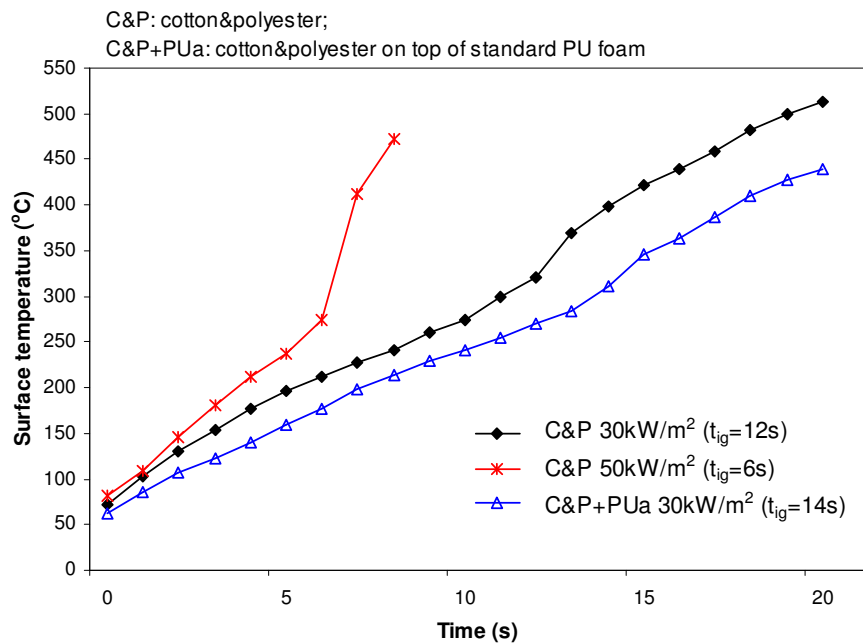


Figure 5.27 Surface temperature of the cotton and polyester and the standard PU foam

Due to the different thermal radiation absorption coefficients of the thermocouple and the samples, the thermocouple temperature reading may be slightly different from the temperature of the sample. The thermocouples were pressed into the timber specimens without additional fixing. The thermocouples usually detach from the surface of the samples shortly after ignition takes place.

The error in surface temperature measurement was not able known exactly. However it can be estimated from following aspects. First, the limit of error of used type of thermocouples (K type from Omega Engineering Inc.) is approximately 2.2 °C or 0.75% of measuring range. So the error from thermocouple itself is below than 4.0 °C before ignition (<400 °C) of the tested timber materials. Second part of the error comes from the different emissivities of timber and thermocouple. According to research by Urbas and Parker (2005), the latter part of error can be eliminated by maintaining a good contact between the thermocouple and specimen. Results from another two non-contact surface temperature measuring technologies are normally adopted for comparison purpose. One is using infrared pyrometer, which has error limit in an order of 10K within 1200 K range. The other is by thermographic phosphor, which has an accuracy of the order 1 ~ 5 °C. By checking temperature profiles from the various technologies, it's noticed that when the good contact was secured which is the case before ignition, temperature measured from thermocouple for timber materials matches with results from other two techniques quite well. Reported temperature difference is within 10 °C (Omrane *et al.* 2003; Urbas *et al.* 2004). Therefore the total error of surface temperature measured by thermocouple can be estimated within 10 ~ 20 °C.

The temperature readings from the thermocouples became inaccurate after ignition took place, due to the detachment of the thermocouple from the surface and enhanced radiation contributed by the flame. The measured surface temperatures at the moment of ignition for the mountain ash are shown in Figure 5.26. When the radiation flux drops from 100 kW/m² to 30 kW/m² the measured surface temperature at the time of ignition increased from approximate 290 to 320 °C. These values and the trend match experimental data from other researchers. For example, Yang *et al.* (2003) measured surface temperatures of 290, 300 and 310 °C for radiations of 50, 40 and 30 kW/m² respectively for beech wood. Tzeng *et al.* (1990) found that the surface temperatures at ignition for a wide range of woods, maple, red oak, poplar and mahogany, are quite close within a temperature range from 580 K to 660 K (307 to 387 °C) under external radiation from 21 kW/m² to 36 kW/m². A trend that surface temperature at ignition decreases with the increase of the external radiation level was found for all the tested materials, such as shown in Figure 5.26 and Figure 5.27. This trend is different from some reports but in agreement with others (Moghtaderi *et al.* 1997; Bhargava *et al.* 2001).

In the results for the fabrics (Figure 5.27) another configuration was added, i.e. fabric was placed on top of the PU foam. Comparing the results from the single fabric configuration and the combination of fabric and PU foam, similar temperature rising trends were observed. With the PU foam covered by the fabric, the surface temperature of the fabric was about 20 °C lower due to the heat transfer to the PU foam.

The possible temperature difference caused by various installation depths of the thermocouple was investigated. Figure 5.28 shows the temperatures at different depths from a test on the mountain ash under 40 kW/m² radiation. From the results shown, it can be estimated that the temperature measuring error caused by the different depths (not more than 0.1 mm) will be within 10 to 20 °C under the test condition.

As for the possible difference between the temperature measured by the thermocouple and the sample surface temperature, Urbas and Parker (1993) carried out an investigation on Douglas fir in a cone calorimeter environment. By comparing results from thermocouple and infra-red pyrometer measurements, they found that an accurate measurement can be achieved when a good contact between the thermocouple and the surface maintained, and the thermocouple was not located in the proximity of a fissure.

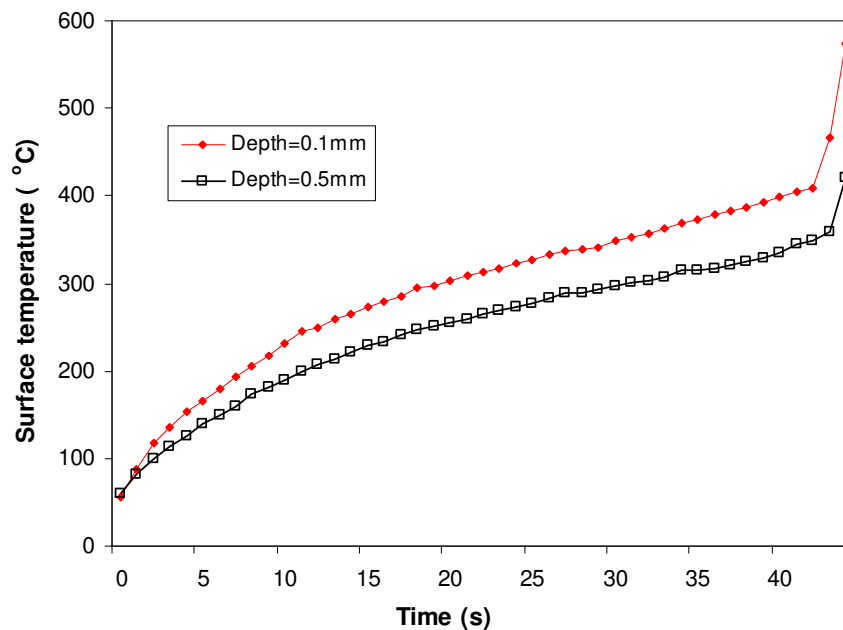


Figure 5.28 Surface temperatures of the mountain ash at different depths under 40 kW/m²

The average surface temperatures at ignition and standard deviation for the mountain ash is given in Table 5.6. In the table average values of critical mass flux and its deviation are also shown.

Table 5.6 Average critical surface temperature and mass flux for mountain ash

External Radiation (kW/m ²)	Thickness (mm)	T _{ig} (°C)	STDEV of T _{ig}	Mass Flux _{cr} (g/m ² s)	STDEV of Mass Flux _{cr}
30	32	330	2.5	6	0.004
50	32	334	5.1	8	0.005
75	32	290		10	

5.4.2 Temperature rising rate

Temperature rising rate is an important parameter since it determine the heating condition greatly. As discussed in Chapter 2, different heating conditions may cause different pyrolysis behaviours. Shown in Figure 5.29 and Figure 5.30 are rising rates of the surface temperatures for some tested materials are. These temperature rising rates are to be compared with the heating rates in the TGA tests.

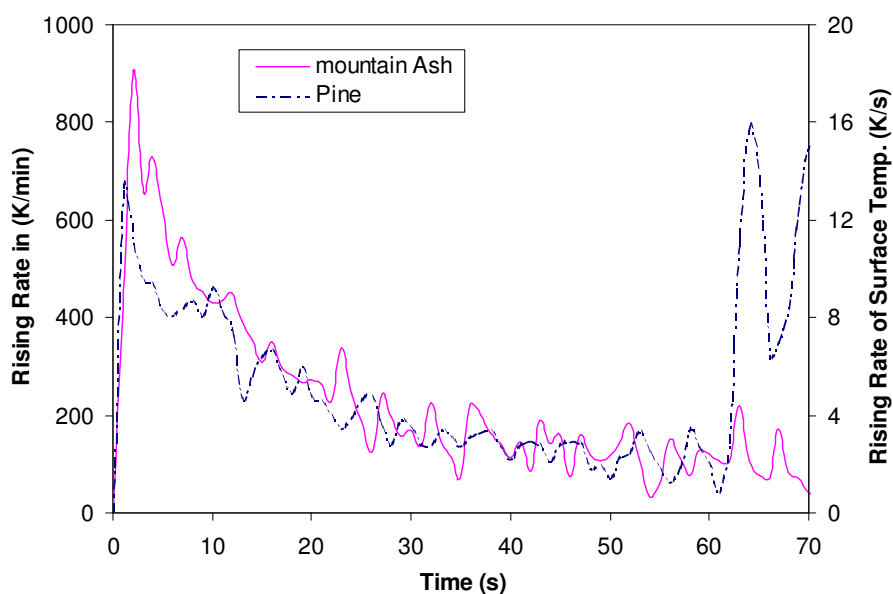


Figure 5.29 Surface temperature rising rates for the timbers under 30 kW/m²

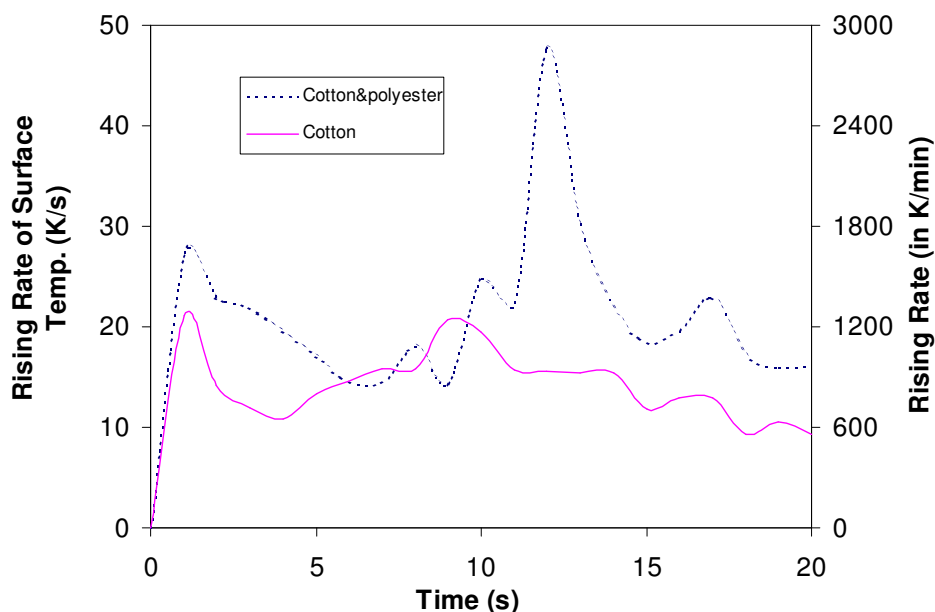


Figure 5.30 Surface temperature rising rates for the fabrics under 30 kW/m^2

It was found that the average rate of temperature rise for timber materials under 30 kW/m^2 radiation is close to the maximum heating rate in the TGA equipment used previously. The temperature rising rates for wood under high radiation (50 kW/m^2), or for fabrics under all radiation conditions, are several times higher than the maximum heating capacity of the TGA. This indicates a necessity for applying the kinetics obtained from the high heating rate TGA tests and further extending the linear shift pattern to higher heating rates.

5.5 Summary of the Cone Calorimeter Test Results

The cone calorimeter tests were carried out for the studied materials with external radiative flux ranging from 10 to 100 kW/m^2 . Major parameters, including ignition time, heat release rate, mass loss rate and surface temperature, were measured. These parameters provided key information for describing the ignition and combustion phenomena in the cone calorimeter environment and are useful for predicting full/real-scale fire behaviour. More importantly, as discussed at the beginning of this chapter, the test provided a physical platform for the models to model on and target results to follow. In other words, these parameters are critical for the modelling of the thermal decomposition process as well as the improvement of ignition criteria.

The ignition time was measured under various radiation levels and ignition assisted methods for all materials. Normally the ignition times under non-piloted conditions are longer than that of piloted conditions. When radiative flux increased up to 75 kW/m^2 , the difference in the ignition times between piloted and non-piloted methods for all the testing materials becomes too small to identify.

Meanwhile an interesting phenomenon between the ignition time and sample thickness was noticed. A longer ignition time was found for a thinner mountain ash sample under the 50 kW/m^2 radiation level. This is believed to be caused by a thicker char layer formed in the thinner sample which obstructs the release of pyrolysis gases. Even though this phenomenon only exists in a few cases, it is worthy of further experiment and modelling.

As a major targeting parameter for modelling research of ignition, the variation from the tests for the ignition time will become a bigger issue. It was found that the non-piloted tests had a higher variation for ignition times. Meanwhile the variations of the ignition time measurement increased when the radiative flux decreased, for all the tested materials. The high variation of the ignition time is usually associated with high variation in other measured parameters, such as HRR and mass loss rate. It is expected that predicting the ignition time under lower radiation levels and non-pilot conditions will be a challenge for any ignition and combustion model.

A critical radiative flux was derived from the ignition time data by the Quintiere chart for the mountain ash. This critical radiation, besides being able to predict ignition surface temperature by the equation developed by Quintiere, was also used to validate the ignition times via the empirical equation suggested by Babrauskas. The predicted ignition times matched reasonably well with the measurement from the current tests.

Another major output from the cone calorimeter, the HRR curves, was also measured. The repeatability of the HRR curves, which can be verified by the raw data presented in Appendix B, met with requirements of the ISO-5660 standard. For the timber materials there are two peaks in the HRR curves. The latter resulted from the exposure of inner virgin materials to the radiative flux. Comparing the piloted and non-piloted methods, they have similar HRR curves except that a higher first peak value existed in the piloted test condition.

The mass loss rate curves have similar shapes with the HRR curves from the same test for the tested materials. It was found that there is a small peak before the ignition in MLR curves under certain radiation levels for the timber materials. By conducting tests with “dried” specimen, composition of the mass flux was verified consisting pyrolysis products and moisture before the ignition. This local peak is formed by effect of impeding mass release by a gradually formed thicker char layer. When the radiative flux reaches up to 75 kW/m^2 , this peak disappears due to the faster heating process.

The species yields for CO and CO₂ were also monitored. When the CO₂ has a similar curve shape with that of HRR and MLR, the CO curve is quite distinctive from other curves. Normally multiple peaks can be found in the CO release curve. A data processing technique was improved to eliminate the errors in average species yields measurement. This error was introduced by mass measurement under a very low mass loss rate.

Surface temperature was measured by thermocouples during the current tests. The measured values, for example the ignition temperature of the timber materials, are similar to the measurements obtained by others. Since surface temperature, especially up to the moment of ignition, plays a critical role in pyrolysis and ignition processes, current measurements are useful to validate later computer modelling results.

CHAPTER 6 SIMULATING PYROLYSIS AND IGNITION BY FDS FOR THE WOODS

Through the research discussed in the previous chapters, the following results have been achieved. The TGA test method and the computational scheme for the kinetics have been improved, and kinetics from traditional scheme and the “effective” kinetics for the studied materials have been computed. The “effective” kinetics are believed to be more suitable to model the decomposition in real fires. The ignition and combustion tests in the cone calorimeter have been conducted and major parameters for describing the ignition and combustion processes have been measured and several phenomena related to the ignition have been identified. Enough information is now available to carry the modelling of pyrolysis and ignition processes on to the physical platform. The simulation work will be presented in this chapter. The simulation results, including the major critical parameters at ignitions determined by the cone calorimeter tests, will be used to compare with the experimental data. This comparison will be helpful for validation of various commonly adopted ignition criteria and development a possible gas phase criterion in next chapter.

This chapter includes 5 sections. In the first section, a computer model, the Fire Dynamics Simulator (FDS), which employs Atreya’s one-dimensional heat transfer equations to model the pyrolysis process, is introduced. Its principle and major features are presented and discussed. Then the calculation process of pyrolysis and thermal parameters for the timber materials are given in Section 6.2. The simulation results are shown in Section 6.3. The mixture of pyrolysis products and oxidants, and distribution above the solid surface are simulated and analysed in Section 6.4. Finally, a brief summary of the simulation results is given in the last section of this chapter.

6.1 FDS Modelling for Pyrolysis and Combustion

As discussed in Chapter 3, Atreya’s one-step mathematical pyrolysis model has been adopted for the current study. Based on one set of selection criteria identified by the author, FDS, a CFD computer model which employs Atreya’s heat transfer pyrolysis model (McGrattan 2004), was selected as a numerical computational tool. FDS has the major

desired features required by the research, as identified in Section 3.1.3, and is able to generate both solid and gas phase results for the study of ignition criteria. Aimed at solving practical fire problems in fire protection engineering, it provides the capability to study fundamental pyrolysis and fire dynamics. This model has been adopted by a number of fire researchers and engineers on fire problems of various scales (Chow and Yin 2002; Hamins *et al.* 2004; Hietaniemi *et al.* 2004).

6.1.1 Principle of FDS model

Not long ago it was believed by many experts that computer models were not particularly helpful for real fire scenario simulation due to their limited computational capability (Cox 1994). As a result of the continuous upgrading of the computational power of modern computers and development in modelling methodology, today's fire models have reached a new level. FDS is a leader of these models and is believed to be capable of predicting fire growth and spread (Babrauskas 2002).

FDS was developed by the Fire Research Division, National Institute of Standards and Technology (NIST), of the US Department of Commerce and released publicly in 2000 (McGrattan *et al.* 2000). The current version of FDS is 4.0.5 (McGrattan and Forney 2005). FDS is a computational fluid dynamics (CFD) model of fire-driven fluid flow. It solves a form of the Navier-Stokes equations numerically for low-speed, thermally-driven flow with an emphasis on smoke and heat transfer from fires. The turbulence is treated by means of the Smagorinsky form of Large Eddy Simulation (LES) which has been briefly discussed in Section 2.2. It is also possible to conduct a Direct Numerical Simulation (DNS) if a fine enough numerical grid is adopted. A mixture fraction combustion model is used in FDS to calculate combustion rate and all of the major products. It solves radiative heat transfer by the equation using a Finite Volume Method (FVM) technique. The simulation results are visually presented by the SmokeView software which was also developed by the same authors (Forney and McGrattan 2004).

Details of the FDS model can be found in its manual and technical guide. Some major features will be further discussed later in this chapter. A brief overview of its history and major features are presented as follows.

6.1.1.1 History of major developments

In FDS v1, radiative fluxes were computed with a Monte Carlo style ray-tracing from the burning particles to the walls. This model neglected gas-to-gas and wall-to-wall interactions, and performed poorly for a fire scenario with very hot gas layers or surfaces (Floyd *et al.* 2003).

In FDS v2, a new combustion model and a new radiation model were added. The new combustion model was a mixture fraction model modified to work on the coarse grids which were often used in FDS simulation. It built a tracking ability for major species, and also for minor species once appropriate state relationships could be developed. The new radiation model was based on the Finite Volume Method (Raithby and Chui 1990). It allowed FDS to model gas-to-gas and gas-to-surface radiation heat transfer.

In FDS v2.2, a sub-combustion model was introduced temporarily to control modelling of the pyrolysis process by modifying the kinetics for the studied materials. This function resulted from cooperating research between the NIST and VTT (Technical Research Centre of Finland) (Hostikka 2002).

A multi-blocking grid system was introduced in FDS v3.0 to enable different grid resolutions within a computational domain. This feature is useful in handling cases where the computational domain is not easily embedded within a single mesh. It is also useful for achieving fine grid resolution for interesting sub-domains while obtaining acceptable computational speed by setting other sub-domains with coarse grid resolutions.

A beta version of v4.0 was first released on January 2004 and the formal version was made available in August 2004. The new features in FDS v4 related to the pyrolysis process are as follows.

- A char model has been implemented in which a thin pyrolysis front is tracked inside a solid fuel. This front separates virgin fuel from the changed portion. The details of the pyrolysis model with charring will be described later in this section.
- The pyrolysis kinetics, activation energy E and pre-exponential factor A , can be calculated by a default method or input by users for various types of fuel, which will be described later in detail.

- Temperature-dependent material properties can be prescribed for solids in input files. This function can be applied in the char model to set properties of both virgin and charred fuels as a function of temperature.

6.1.1.2 Mixture fraction combustion model

The foundation of the mixture fraction combustion model is based on the following key assumption (McGrattan 2004):

The large-scale convective and radiative transport phenomena can be simulated directly, but physical processes occurring at small length and time scales must be represented in an approximate manner.

The actual chemical dynamics that control the combustion energy release in fires are not fully understood. Even if they were known, the spatial and temporal resolution limits imposed by both present and foreseeable computer resources make it very difficult to get a detailed description of the combustion. Thus, in FDS, the combustion is assumed to be mixture-controlled. This implies that all the production of species of interest can be described in terms of a single mixture fraction Z . The mixture fraction is a conserved quantity representing the fraction of material at a given point that originated as fuel.

The relations between the mass fraction of each species and the mixture fraction are known as “state relations” in FDS 4 (Appendix C.7) (McGrattan and Forney 2005). These state relations can be calculated from the chemical composition of the fuel. The oxygen mass fraction in the state relation provides the information needed to calculate the local oxygen mass consumption rate. The form of the state relation that emerges from classical laminar diffusion flame theory is a piecewise linear function. This linear function will be used to determine the full history in a state relation chart, such as in Figure 6.1. Then the local heat release rate is computed from the local oxygen consumption rate at the flame surface by the oxygen consumption method used in the cone calorimeter.

Generally, a combustion reaction can be expressed as follows:



where the values of v_i are the stoichiometric coefficients for species i , including the fuel, oxygen and products in the overall combustion process.

The mass consumption rates for fuel and oxidizer have the following relation:

$$\frac{\dot{m}_F}{v_F MW_F} = \frac{\dot{m}_{oxy}}{v_{oxy} MW_{oxy}} \quad (6.2)$$

where MW_F and MW_{oxy} are the fuel and oxygen molecular weights.

The scalar parameter, mixture fraction Z , is defined as:

$$Z = \frac{sY_F - (Y_{oxy} - Y_{oxy,\infty})}{sY_{F,I} + Y_{oxy,\infty}} \quad (6.3)$$

where:

$$s = \frac{v_{oxy} M_{oxy}}{v_F M_F} = \frac{\dot{m}_{oxy}}{\dot{m}_F} \quad (6.4)$$

s : the ratio of oxidizer and fuel consumption rates in a stoichiometric reaction;

Y_i : the mass fraction of species i ;

$Y_{F,I}$: the fraction of fuel in the fuel stream from a fuel/pyrolysis source;

Y_{oxy} : the mass fraction of oxygen, and

$Y_{oxy,\infty}$: the ambient oxygen mass fraction.

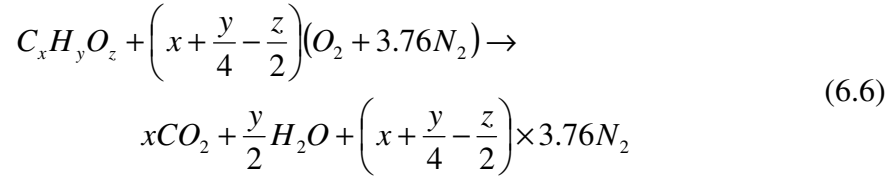
Therefore, the mixture fraction value will be 1 in a region containing only fuel, and 0 where the oxygen mass fraction takes its undepleted ambient value, $Y_{oxy,\infty}$. Therefore the fuel mass fraction is zero, and will vary between 0 and 1 between such regions.

It is assumed in the mixture fraction model that the chemical reaction between the consumed fuel and oxidizer occurs so rapidly that the fuel and oxidizer cannot co-exist. This means that the fuel and oxidizer simultaneously vanish at a flame surface:

$$Z = Z_f; \quad Z_f = \frac{Y_{oxy,\infty}}{sY_{F,I} + Y_{oxy,\infty}} \quad (6.5)$$

where Z is the mixture fraction, a distribution function in space and time.

For a normal oxygen containing hydrocarbon fuel, $C_xH_yO_z$, its ideal reaction in the normal atmospheric environment is expressed as follows:



The ideal mixture fraction for the fuel is the “ideal” fuel/air ratio for the reaction, and this calculation is given as:

$$Z_{F,ideal} = \frac{mass_F}{mass_{total}} = \frac{mass_F}{mass_F + mass_{air}} = \frac{C_xH_yO_z}{C_xH_yO_z + \left(x + \frac{y}{4} - \frac{z}{2}\right)(O_2 + 3.76N_2)} \quad (6.7)$$

where:

$$mass_F = x \cdot MW_C + y \cdot MW_H + z \cdot MW_O ;$$

$$mass_{air} = \left(x + \frac{y}{4} - \frac{z}{2}\right)(2MW_O + 3.76 \times 2MW_N) ;$$

MW_C , MW_H , MW_O , and MW_N are molecular weights for elements C , H , O and N respectively.

This ideal mixture fraction will be used to determine the turning point in the state relation chart and therefore further determine all the combustion products as functions of the mixture fraction Z .

6.1.1.3 Pyrolysis and charring models in FDS

The heat transfer and pyrolysis in a charring fuel are described by a one-dimensional model which was originally developed by Atreya and described in Section 3.2. To perform a numerical solution, further simplification was made. The pyrolysis is assumed to take place over an infinitesimally thin front. The model includes the conduction of heat inside the solid, the evaporation of moisture and decomposition of the virgin material to gaseous fuel and char. The volatile gases are instantaneously transported to the surface.

Based on the improvement made by Ritchie *et al.* (1997), the basic governing equations including consideration of moisture release were shown as Equations (3.6) to (3.9). The pyrolysis rate of the material was modeled with a single step first order Arrhenius reaction:

$$\dot{m}'' = A(\rho_{solid,I} - \rho_c)e^{-E/RT} \quad (6.8)$$

where:

A : pre-exponential factor, m/s;

$\rho_{solid,I}$: initial solid density, kg/m³;

ρ_c : density of char, kg/m³;

E : activation energy, kJ/mol·K;

T_s : surface temperature, K.

The A and E are chosen so that the pyrolysis takes place very close to the desired pyrolysis temperature for the solid fuel. The thin pyrolysed front is moving inside the material. The velocity of the front, v , is given by

$$v = \frac{\dot{m}''}{(\rho_{solid,I} - \rho_c)} \quad (6.9)$$

6.1.1.4 Ignition criteria in FDS

The ignition criteria are not directly documented in FDS. One convenient method to “judge” the ignition is via visual observation by the software SmokeView. The parameters normally provided in FDS to form the “isosurface” are heat release rate per unit of volume (HRRPUV) and mixture fraction. There should be some internal criteria (not discovered and controlled by users at the moment) for these parameters to present the flame. While FDS does not give criteria of ignition directly and leaves great flexibility for users to pick up some suitable parameters for the prediction purpose, discussion of ignition phenomena will start from the available parameters in FDS: the HRRPUV and mixture fraction.

When these two parameters were used for the visual observation, there are some limitations. First, the observation of flame is just an “apparent” method. When different values of parameters were set up, the shape as well as the moment of flame appearing will vary largely. Secondly, the observations by different parameters for a simulation may be different.

Therefore, in current thesis, the ignition determined by visual observation in FDS will be treated as “apparent ignition” and only used for comparison purpose. The detailed discussion of limitations of a critical HRR as the criterion of ignition will be further performed in Section 7.1. All the ignition parameters in simulation will be extracted at the moment of ignition decided by previous corresponding cone calorimeter tests.

The combustion model adopted in FDS is a mixture fraction model. When Atreya’s pyrolysis model was used in FDS, the pyrolysis rate of solid fuel can be obtained through modelling. The mixture fraction is able calculated from the pyrolysis rate by equations in Section 6.1.1.2. Therefore current author assumes that the criteria of ignition in FDS are mainly related to the mixture fraction. This assumption of value in the simulation domain has also been verified by personal correspondence (McGrattan 2004). While a critical mixture fraction is a materials property under certain pyrolysis conditions, this supposed criterion needs to be further studied and the prediction of ignition in FDS can be improved.

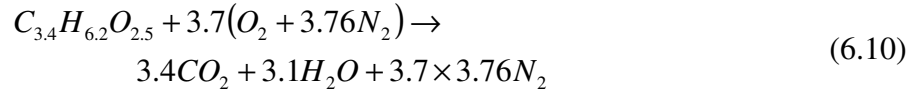
To find a more suitable criterion for the studied materials, particularly the mixture fraction, is one of the major aims of the current research. Therefore, in the later stage of this thesis, all possible criteria of ignition in FDS will be investigated in detail. These criteria include critical surface temperature, critical mass flux, critical heat release rate, and the mixture fraction.

6.1.2 Treatment of thermal parameters for timber in FDS simulation

Calculations of the mixture fraction and thermal dynamic parameters for the current studied timber materials are described in the following sections.

6.1.2.1 Mixture fraction relation for timber

Even though the compounds of timber material are very complex, as indicated in Section 2.3.3.1, certain simplifications must be made for modelling study. A typical expression for the chemical compound for timber material is $C_{3.4}H_{6.2}O_{2.5}$ (Ritchie *et al.* 1997) which was adopted in the FDS model. Applying Equation (6.6) to this expression, the reaction is given as follows:



The ratio of consumption rates for the fuel and oxygen, s , can be calculated from Equation (6.4).

$$s = \frac{v_{oxy}M_{oxy}}{v_F M_F} = \frac{3.7 \times 32}{87} = 1.36$$

Substituting the s value and $Y_{oxy,\infty} = 0.233$ into Equation (6.3) yields the expression of mixture fraction for timber:

$$Z = \frac{1.36Y_F + 0.233 - Y_{oxy}}{1.36Y_{F,I} + 0.233} \quad (6.11)$$

The ideal mixture fraction for timber, $Z_{wood,ideal}$ which is the stoichiometric ratio of fuel to air, is calculated using Equation (6.7).

$$\begin{aligned} Z_{wood,ideal} &= \frac{mass_{wood}}{mass_{wood} + mass_{air}} \\ &= \frac{87}{87 + (3.4 + \frac{6.2}{4} - \frac{2.5}{2})(32 + 3.76 \times 28)} = 0.12 \end{aligned}$$

The state relations for wood were then determined from Equation (6.10) and shown in Figure 6.1. It is noted that at $Z=0$ (no fuel present), the mass fractions of all gases are obtained from composition of the atmosphere, and at $Z=1$, only fuel is present. At the ideal mixture fraction, $Z=0.12$, the fuel and oxygen have been used up, and only combustion products are present. At the two regions between these three points ($Z=0, 0.12$, and 1) linear relationships exist for all reactants and products, as indicated previously.

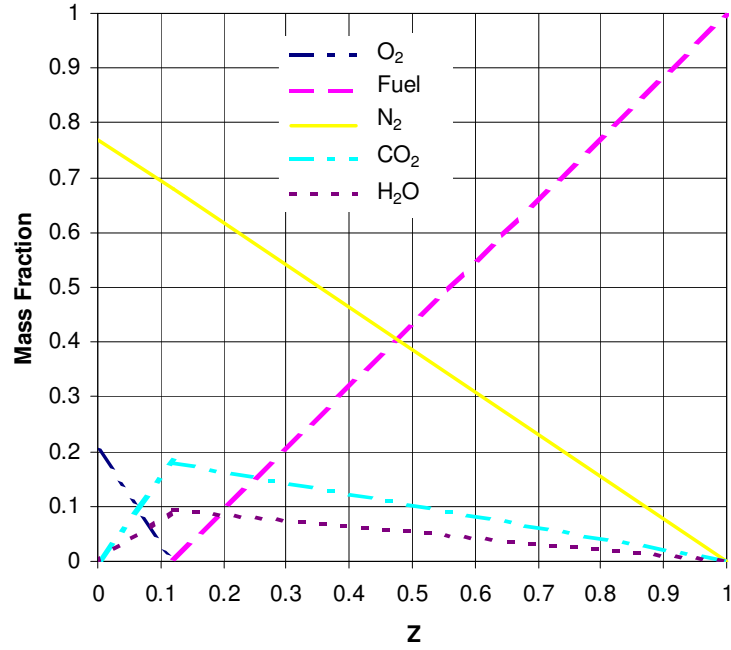


Figure 6.1 State relations for wood

6.1.2.2 Calculation for the thermal dynamic parameters

FDS adopts a pyrolysis model as presented in Section 4.2.2.2. Solid fuels are treated as either thermoplastics or charring materials. Thermoplastic materials are assumed to pyrolyse at the surface and charring materials at a pyrolysis front that propagates through the solid. The burning rate (pyrolysis rate) for these two types of solids is given by Arrhenius' equation as follows:

$$\text{For the thermoplastic} \quad m'' = A\rho_s e^{-E/RT} \quad (6.12)$$

$$\text{For the charring material} \quad m'' = A(\rho_s - \rho_c)e^{-E/RT} \quad (6.13)$$

where:

A : pre-exponential factor, m/s;

E : activation energy, kJ/mol;

ρ_s : the surface density, g/m³;

ρ_c : the char density, g/m³;

T_s : the surface temperature, K;

R : universal gas constant, 8.314×10^{-3} kJ/mol·K;

m'' : mass flux, g/m²·s.

There are two methods to calculate these parameters in FDS. They are described below, using charring materials as an example.

The default method in FDS is to use a set of given values, $2.6E8 \text{ kg/m}^2\cdot\text{s}$ for product of the pre-exponential factor A and solid density, and $20 \text{ g/m}^2\cdot\text{s}$ for the critical mass flux (Hostikka 2004). The ignition temperature for the specific material is provided by the user via the database file. Then the activation energy is calculated through the above formula (Equation (6.13)) at ignition point.

$$E = RT_{ig} \ln\left(\frac{m''_{cr}}{A(\rho_s - \rho_c)}\right) \quad (6.14)$$

With heat transfer calculation, this computed activation energy is then used to calculate the pyrolysis rate as well as the mixture fraction. When the ideal mixture fraction value is reached in the simulation domain, ignition takes place immediately.

An alternative method is to supply values of the E and A as inputs. The values can be obtained from other sources, such as the TGA tests. Then from Equation (6.13), mass flux is calculated by the kinetics as a function of the surface temperature. Ignition takes place when the ideal mixture fraction is reached at some point in the computational domain.

The first method relies on the input of three parameters, A , m''_{cr} and T_{ig} , which are difficult to obtain from experiments. FDS applies a fixed pre-exponential factor to the whole range of materials, which is questionable since A is strongly material-dependent as demonstrated in Table 4.3 of this thesis and in the work of Moghtaderi (2001).

The difficulty for the second method is the determination of E and A . Although these parameters can be obtained from the TG analyser, the application of these basic thermal kinetic parameters in real fire modelling is still very limited. Generally, as discussed in Section 4.2.3, the difference between fundamental thermal dynamic testing conditions and real fire scenarios, both in bench and full scales, is the first concern in applying these kinetics (i.e. E and A). Secondly, large variations in the values of these parameters have been reported from different researchers using different testing equipments and test methods even for a single material (Hostikka 2002). Thirdly, lack of validation of those parameters in

complicated fire scenarios, mainly through lack of suitable calculation tools/computer models, impedes their application (Hostikka 2002).

It is necessary to note that the values of the basic thermal parameters, T_{ig} and m''_{cr} , adopted in FDS, are suggested for general evaluation purposes only. They may not be applicable to a specific material and fire scenario without validation (Hostikka 2004).

Simulation results obtained by adopting the above two methods are compared in the following section.

6.2 Setting Up and Running of FDS Simulations

General information of the cone calorimeter tests that their settings were followed up in FDS simulations were described in Chapter 5. Represented here are configurations of the simulation domain.

6.2.1 General setting

6.2.1.1 Simulation domain and grid size

A computational domain 400 mm wide by 400 mm long by 500 mm high was used for FDS simulations of the cone calorimeter combustion region (Figure 6.2). An air flow upward through the domain at a flow rate of 24 l/s was specified using a vent at the top of the domain. The four vertical glass walls were adopted as a boundary condition following the physical configuration of the cone calorimeter. An open boundary condition was specified at the bottom to allow a free flow of air into the domain.

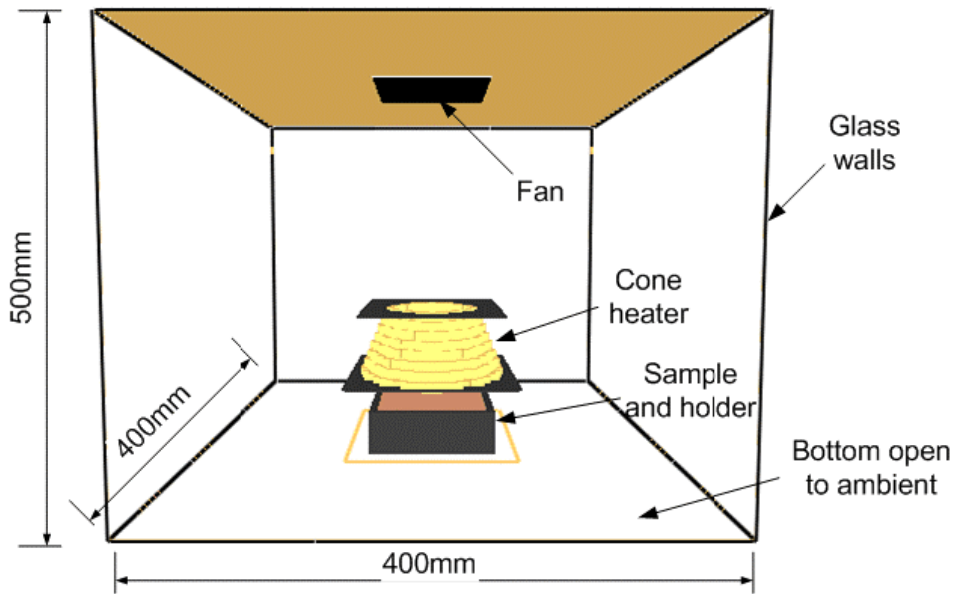


Figure 6.2 Simulation domain for the cone calorimeter situation

The multi-blocking technique was adopted. A grid size of $3 \times 3 \times 2$ mm was applied to a volume including the sample and the heater ($150 \times 150 \times 100$ mm) and the remaining part of the domain has a resolution of $5 \times 5 \times 5$ mm. The selection process for the grid resolution is discussed in Section 6.2.3. An illustration showing the grid is given in Figure 6.3.

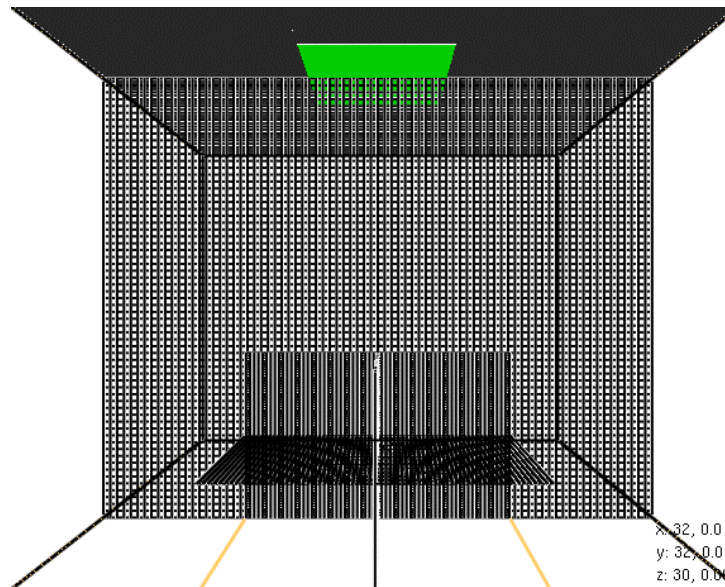


Figure 6.3 Grids for the simulation domain

6.2.1.2 “Cone” heater

The cone heater was represented by a stair polygon shape heater due to the FDS limitation that all objects in a domain must be rectangular. The height of each level of steps is 6 mm. Figure 6.4 shows an illustration of the heater’s structure. The effect of the stair polygon shape heater on the radiation heat transfer is discussed in following section.

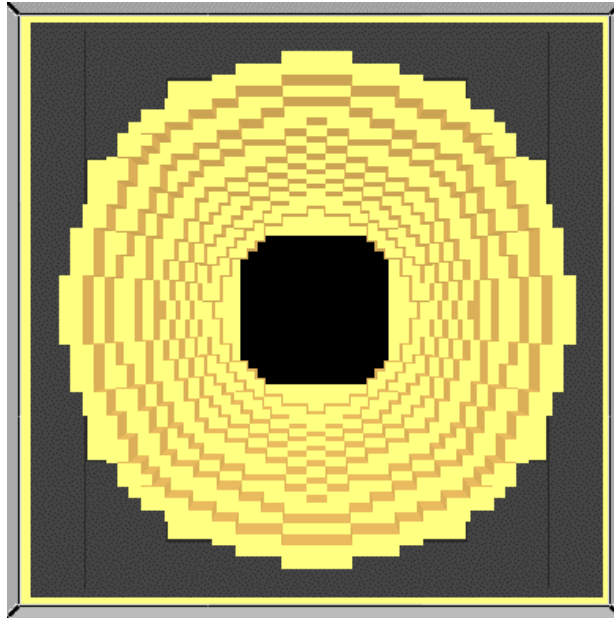


Figure 6.4 Bottom view of the stair shape heater

6.2.2 Heater temperature and heat flux

The input temperature value for the heater in the simulation was determined by trial and error. A heater temperature value was selected when it produced the desired heat flux at the sample surface.

The radiative heat flux at the surface of the sample was obtained by placing heat flux gauges at the desired locations on the sample surface. To investigate the uniformity of surface radiation, surface temperatures at various locations on the surface were also measured in the simulation. The radiation and temperature distribution at different distances along an axial symmetry in the domain are shown in Figure 6.5 and Figure 6.6. In these two figures, the rapid rises for radiation and temperature curves at about 22 seconds were caused by ignition

of the simulated timber sample when more radiative heat was fed back from the flame to the surface of the sample.

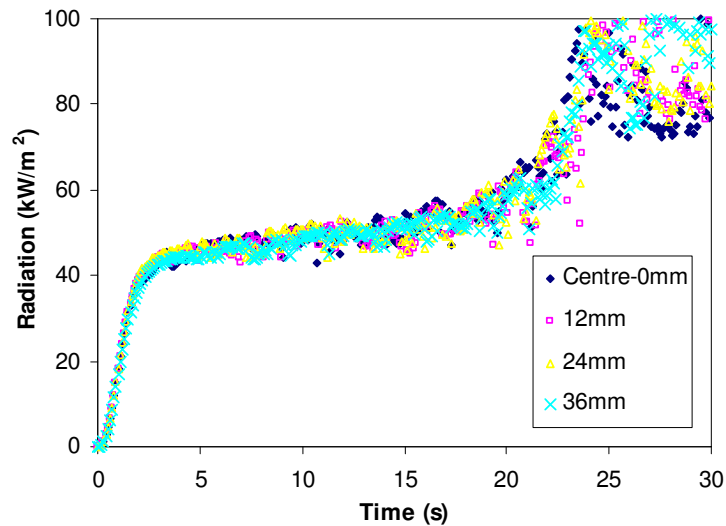


Figure 6.5 Axial distribution of radiation level

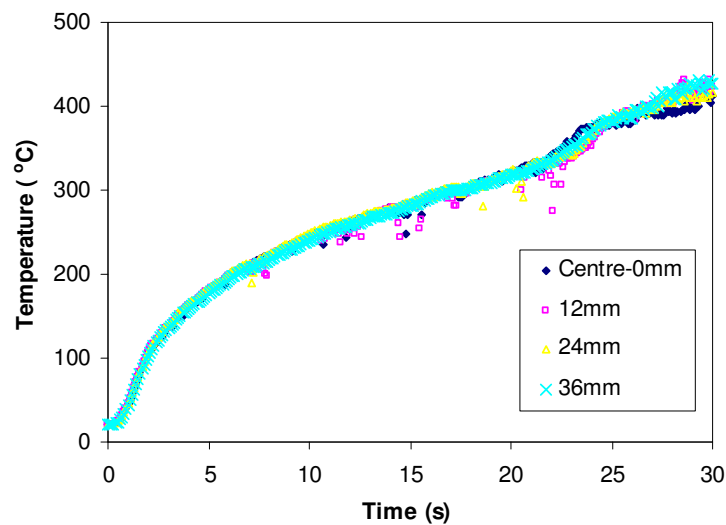
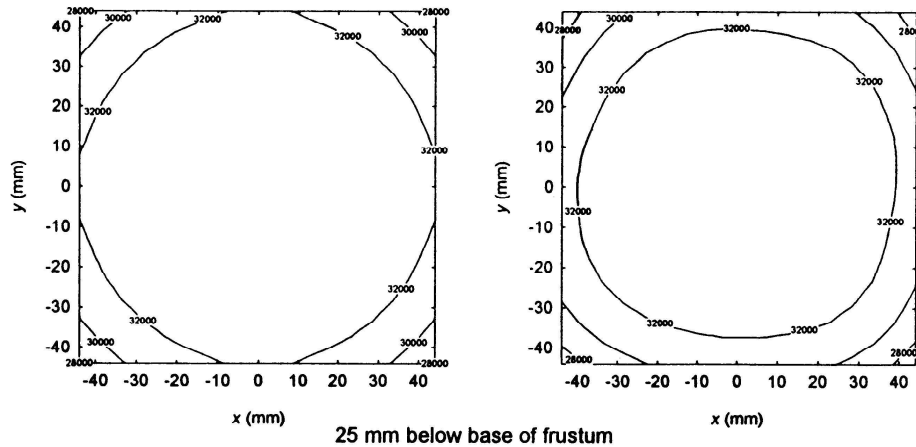


Figure 6.6 Axial distribution of surface temperature

However, the symmetry of the radiation and temperature of the sample surface was only approximate. Wilson *et al.* (2003) studied surface radiation distribution in the cone calorimeter. Their theoretical calculation and measurement by radiative flux gauges are shown in Figure 6.7. The cone heater surface temperature was set to 650 °C. The radiative flux on the central part of the sampling area, which was 25 mm below the bottom of the heater, was measured as 32.7 kW/m². The unit for the contour curves shown in the figures

was W/m^2 . Followed the experimental set up, the surface radiation under same heater temperature was monitored in a FDS simulation, shown in Figure 6.8.



(a) Theoretical

(b) Measured

Figure 6.7 Theoretical and measured irradiance distributions for the cone calorimeter (source: Wilson *et al.* (2003))

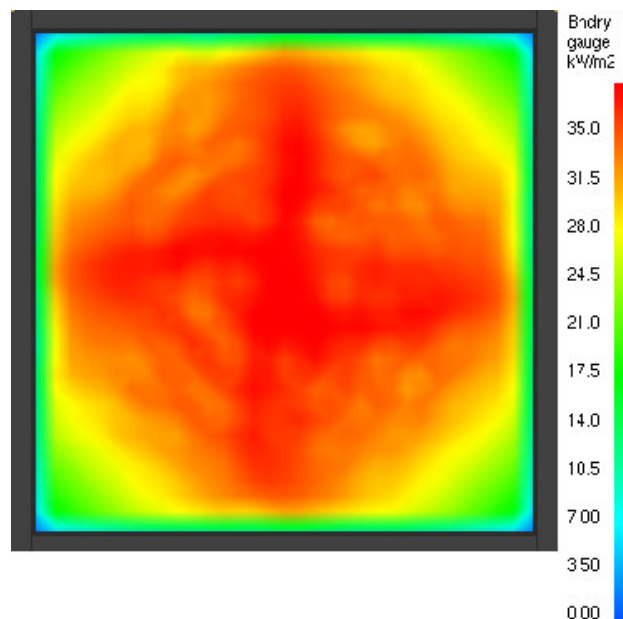


Figure 6.8 Boundary output for surface radiation

It is found that the boundary radiative flux contour on the surface of the sample did not show perfectly circular shapes. Compared between these figures, it is obvious that the radiative heat flux at the edge areas is lower than the experimental value. While the pyrolysis process in the central area is the major concern of ignition study and the heater

temperature was calibrated by the central radiation, lower values obtained for these global parameters, such as HRR, may occur in the simulation.

6.2.3 Cell grid

Grid dependence is an issue that needs to be addressed when using numerical simulation methods (Cox and Kumar 2002). A number of studies on this issue have been done by researchers for various fire source and geometry conditions (Friday and Mowrer 2001; Heskestad 2002; Ierardi and Barnett 2003).

In the current research, grid sensitivity studies were performed. The grid was systematically refined until the output quantities did not change appreciably with each refinement. A set of preliminary simulations was carried out to decide the appropriate grid settings for the FDS model. The simulations were divided into two steps. In the first step, only change of grid on direction of axis Z was applied. Settings of this part preliminary simulation are shown in Table 6.1. After that, horizontal grid was investigated in the second step by fixing grid on Z axis at a value determined in the step one. Table 6.2 shows settings for the second step simulations. It is noticed that the height of the 2nd sampling point above the sample surface could not be exactly identical under various vertical grid resolutions. Therefore, differences of those values were reduced to minimum by choosing a proper height.

Table 6.1 Settings for the first step preliminary simulations

Simulation code	Grid resolution (mm)		Distance between heater and sample (mm)	1st sampling point	Height of 2nd sampling point (mm)
	Vertical (z axis)	Other axes			
RES-V1	1	3	30	Surface	15
RES-V2	2	3	30	Surface	16
RES-V3	3	3	30	Surface	15
RES-V5	5	3	30	Surface	15

Table 6.2 Settings for the second step preliminary simulations

Simulation code	Grid resolution (mm)		Distance between heater and sample (mm)	Sampling point
	Horizontal Axes	Vertical (z axis)		
RES-H1	1	2	30	Surface
RES-H2	2	2	30	Surface
RES-H3	3	2	30	Surface
RES-H4	4	2	30	Surface

The sample material is pine wood and the default material property inputs given by the FDS in the database were adopted. Parameters were monitored at two sampling points (one on the sample surface and another in the space above the sample) to check both solid and gas phase heating effects. The parameters monitored include temperature, radiative flux, mass loss flux, and fuel concentration (expressed as the mixture fraction (Z)). These parameters were sampled at second intervals until ignition occurred. Table 6.3 shows some results from the first step preliminary simulations.

As shown in Figure 6.9 and Figure 6.10, histories of the simulated surface temperature and mass flux in the cone calorimeter situation were obtained in different cell resolution settings. The parameters were obtained at the point 1, centre of a pine wood sample surface.

Table 6.3 Major results from the first step preliminary simulations

Grid (mm)	At 5s				
	T ₋₁ (°C)	Radiation ₋₁ (kW/m ²)	Mass flux ₋₁ (kg/m ² s)	T ₋₂ (°C)	Z ₋₂ (kg/kg)
1	207.5	67.6	2.9E-06	119.0	1.4E-05
2	210.2	58.8	3.5E-06	118.9	1.7E-05
3	243.5	57.1	4.4E-06	111.8	2.2E-05
4	215.2	56.3	5.8E-06	89.5	4.2E-05
5	197.7	51.8	3.2E-06	25.5	2.6E-06
	At 10s				
	T ₋₁ (°C)	Radiation ₋₁ (kW/m ²)	Mass flux ₋₁ (kg/m ² s)	T ₋₂ (°C)	Z ₋₂ (kg/kg)
1	299.4	84.1	5.0E-04	164.8	2.0E-03
2	303.3	70.0	5.9E-04	184.4	2.2E-03
3	272.1	68.9	8.2E-04	200.6	3.0E-03
4	318.6	71.9	1.3E-03	233.8	5.8E-03
5	296.5	56.5	4.1E-04	157.1	2.6E-03
	At Ignition				
	t _{ig} (s)	T _{ig,-1} (°C)	Mass flux ₋₁ (kg/m ² s)	T ₋₂ (°C)	Z ₋₂ (kg/kg)
1	11.0	320.0	1.3E-03	200.4	4.5E-03
2	10.9	320.7	1.3E-03	195.5	3.9E-03
3	10.5	290.2	1.3E-03	210.3	3.9E-03
4	10.0	318.6	1.3E-03	233.8	5.8E-03
5	11.8	321.7	1.3E-03	169.5	4.6E-03

Note: T , t and Z are temperature, time and mixture fraction respectively;
₋₁, at point 1 (on the sample surface);
₋₂, at point 2 (above the sample surface).

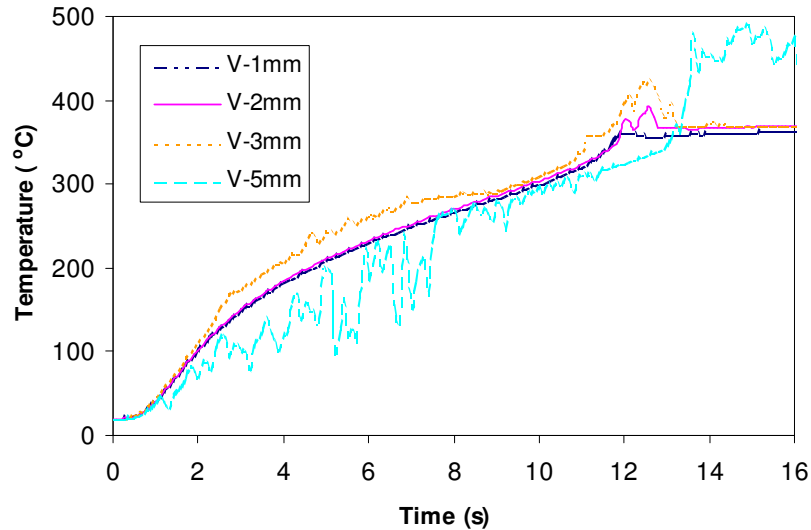


Figure 6.9 Surface temperature from various vertical grid resolutions (pine, 50 kW/m²)

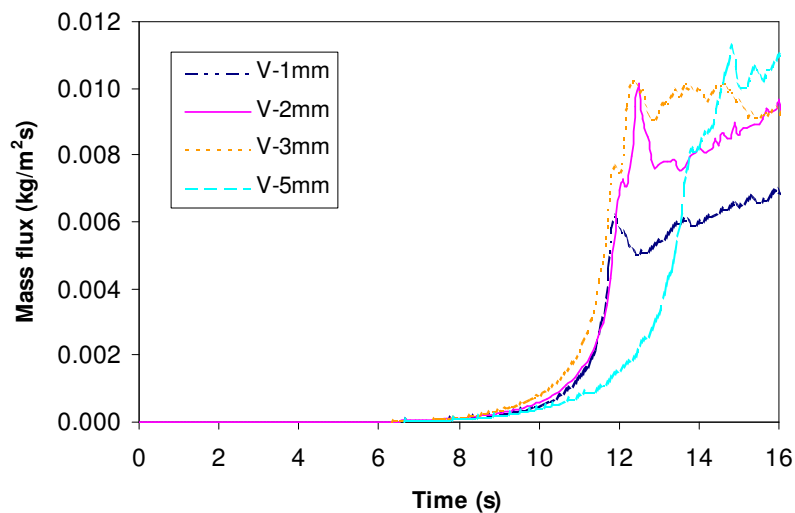


Figure 6.10 Mass flux from various vertical grid resolutions (pine, 50 kW/m²)

From the above tables and figures it can be seen that differences for all the simulated parameters between 1 mm and 3 mm vertical grid resolutions are relatively small, especially between those with 1 mm and 2 mm resolutions, except for the time after 11 seconds – the moment of the “apparent ignition” occurred. Two key parameters for the pyrolysis process from those two resolutions, surface temperature and mass flux, match quite well with each other during the pyrolysis process. In regard to the gas phase, the values for the mixture fraction, which is a critical parameter in FDS to describe pyrolysis, were also very close to each other for the 1 mm and 2 mm grids, at 10 seconds and the moment of the “apparent ignition” as shown in Table 6.3. Considering the simulation time for 1 mm grid is about 16

times longer than that for 2 mm resolution, the 2 mm grid resolution was chosen in all simulations to achieve a good balance between satisfactory simulation accuracy and acceptable simulation time.

Major comparison results of the second step simulation, varying grid resolutions horizontally, are shown in Figure 6.11 and Figure 6.12. The differences of monitored surface temperature and mass flux between 2 and 3 mm grid resolutions are relatively small. Similar consideration exists for the 1 mm horizontal grid resolution as that for the vertical values. Therefore, 3 mm horizontal grid resolution was chosen in all the late simulations.

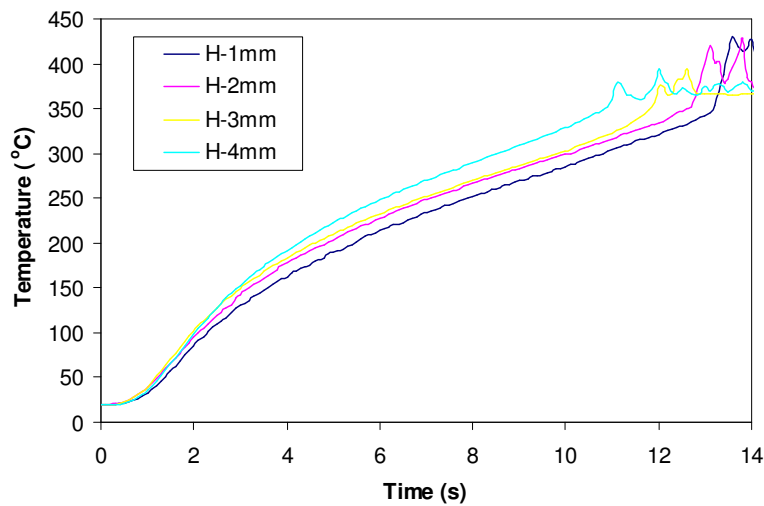


Figure 6.11 Surface temperature from various horizontal grid resolutions (pine, 50 kW/m²)

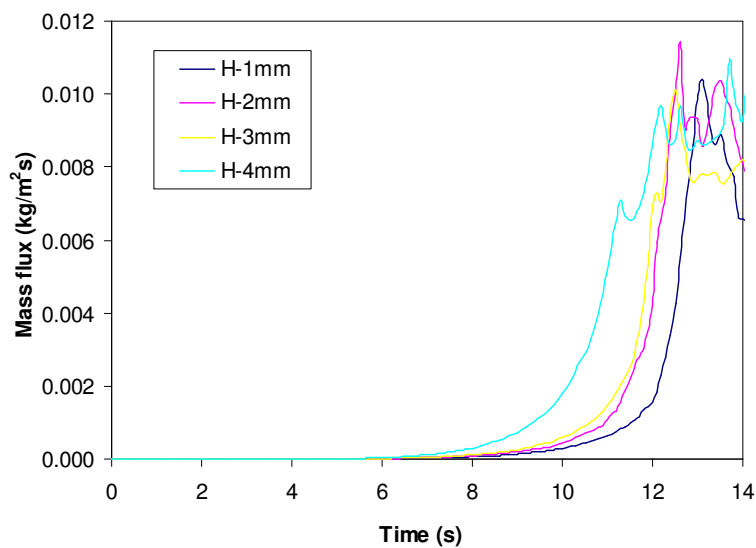


Figure 6.12 Mass flux from various horizontal grid resolutions (pine, 50 kW/m²)

6.2.4 Summary of input parameters in FDS simulation

A summary of major inputs and settings in the simulations are shown in Table 6.4. As measured in the cone calorimeter tests (see Section 5.2.2), the moisture content of 8.5% was adopted for the mountain ash in these simulations. Densities of the wood and char were adopted from the measurements made in the cone calorimeter tests. The heater temperature was set to achieve the desired radiation levels in the table by the method introduced in Section 6.2.2. The default values for E and A were generated by the model according to the first method described in Section 6.1.2.2. Other E and A values for mountain ash were obtained from the TG tests, both lower and higher heating rates, shown in Table 4.3 and Table 4.4. For the pine, the obtained kinetics of from the lower heating rate range are close to the values from Atreya's study (Atreya 1984). Therefore values of E and A suggested by Atreya, $5.1E+11$ 1/s and 126 kJ/mol for the A and E respectively, were used for the pine in the current simulations. Those values were also adopted in FDS as default values (Hostikka 2004). The ignition temperature was the default setting in FDS. Two thicknesses of the sample were simulated. Besides the parameters listed here, values for all the other parameters, such as heat of combustion, heat conductivity, were adopted from the FDS database for the woods.

Table 6.4 Major inputs and settings for simulations

Simulation code	Minimum Grid (mm)	Material	External Radiation (kW/m ²)	E (kJ/mol)	A (1/s)	T _{ig} (°C)	Thickness (mm)
SIMU-01	3x3x2	mountain Ash	30	140.2	1.2×10^8		32
SIMU-02				177.4	6.7×10^{11}		32
SIMU-03			50	140.2	1.2×10^8		32
SIMU-04				177.4	6.7×10^{11}		32
SIMU-05				140.2	1.2×10^8		14
SIMU-06				Default	Default	390	32
SIMU-07				Default	Default	350	14
SIMU-08			75	140.2	1.2×10^8		32
SIMU-09				177.4	6.7×10^{11}		32
SIMU-10		Pine	30	126	5.1×10^{11}		32
SIMU-11			50	126	5.1×10^{11}		32

6.3 Simulation Results

Following the configuration described in Section 6.2 (including Table 6.4), a series of simulations were carried out to simulate the pyrolysis process for timber. Major simulation results are shown as below and some comparisons are given between the simulations and the cone calorimeter test results. The kinetics adopted were the “effective” values obtained from higher heating rate range, i.e. 140.2 kJ/mol and 1.2×10^8 1/s. Simulation results from these kinetics were illustrated in following sub-sections unless specified.

6.3.1 Observation of initial flame development

Although in a cone calorimeter test it is possible that combustion can start anywhere on a timber surface due to non-uniform properties of the specimen, it was observed that the first flame always appeared near the centre of the sample surface in the FDS simulations. The initial development of the flame on the sample surface is shown in Figure 6.13 for the mountain ash under 30 kW/m^2 . The parameter used to represent the flame is the heat release rate per unit volume, HRRPU. The time interval between these pictures is 0.5 s.

Sets of photos taken from the piloted cone calorimeter tests using the mountain ash are shown in Figure 6.14 for 30 kW/m^2 radiation level and in Figure 6.15 for 50 kW/m^2 radiation level. The camera speed used was 15 frames per second (approximate as an interval of 0.06 s).

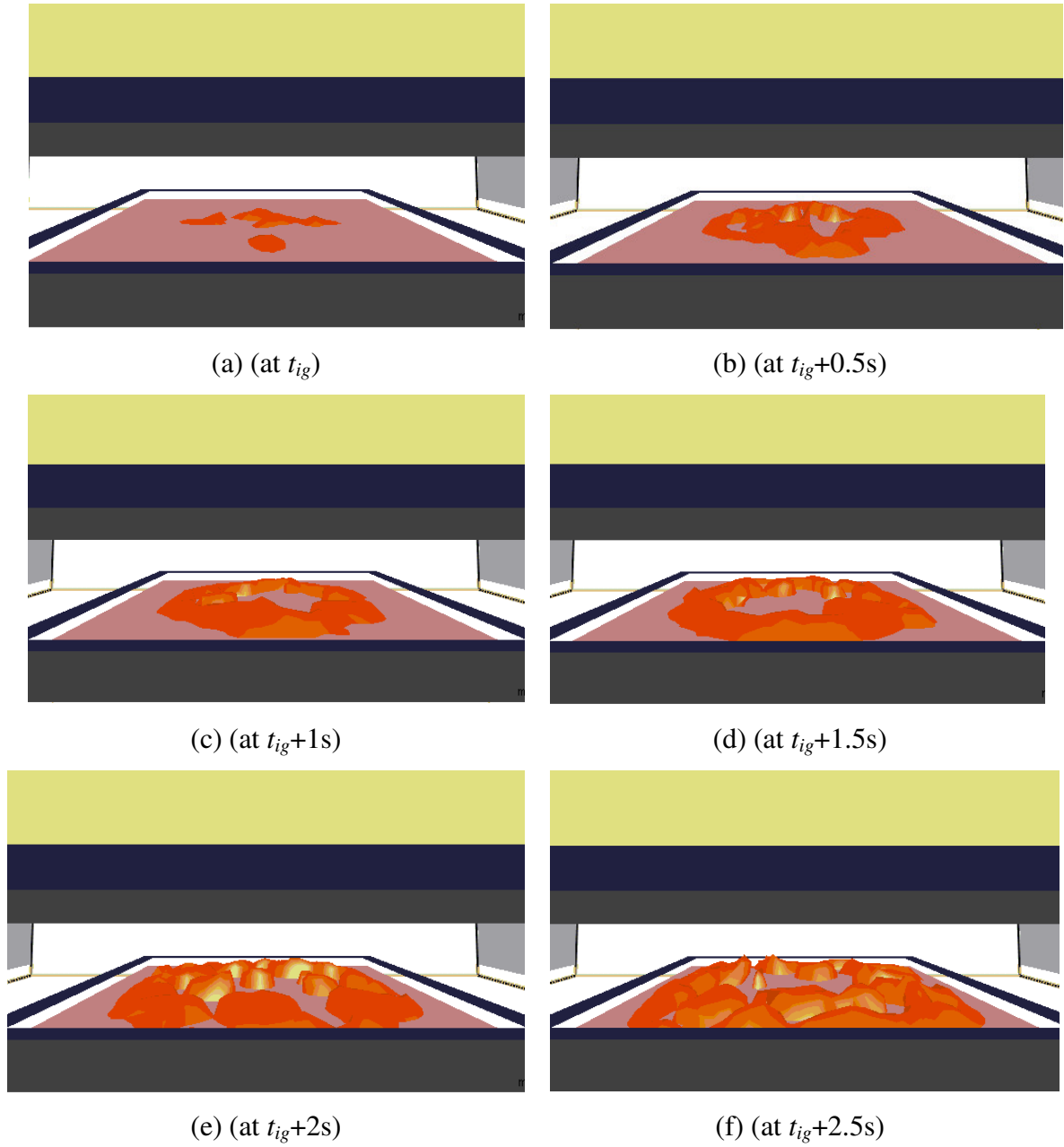


Figure 6.13 Simulated flame development for the mountain ash under 30 kW/m^2

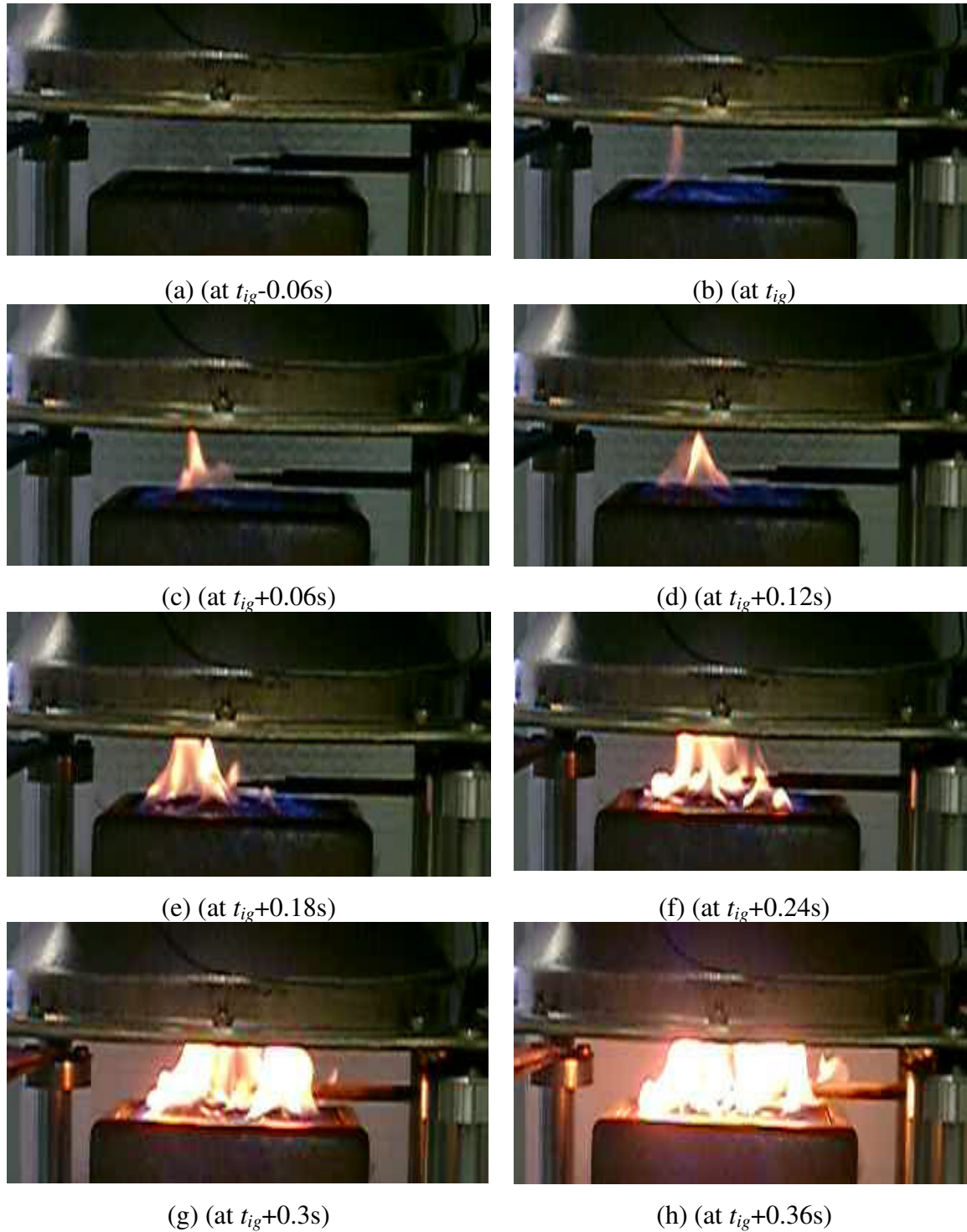


Figure 6.14 Flame development in test from the mountain ash under 30 kW/m^2

Notes for Figure 6.14:

- (a): before ignition, pyrolysis products was observed within the gas stream
- (b): initial flame appeared on the surface
- (c) ~ (e): flame spread on the surface
- (f) ~ (h): flame fully developed

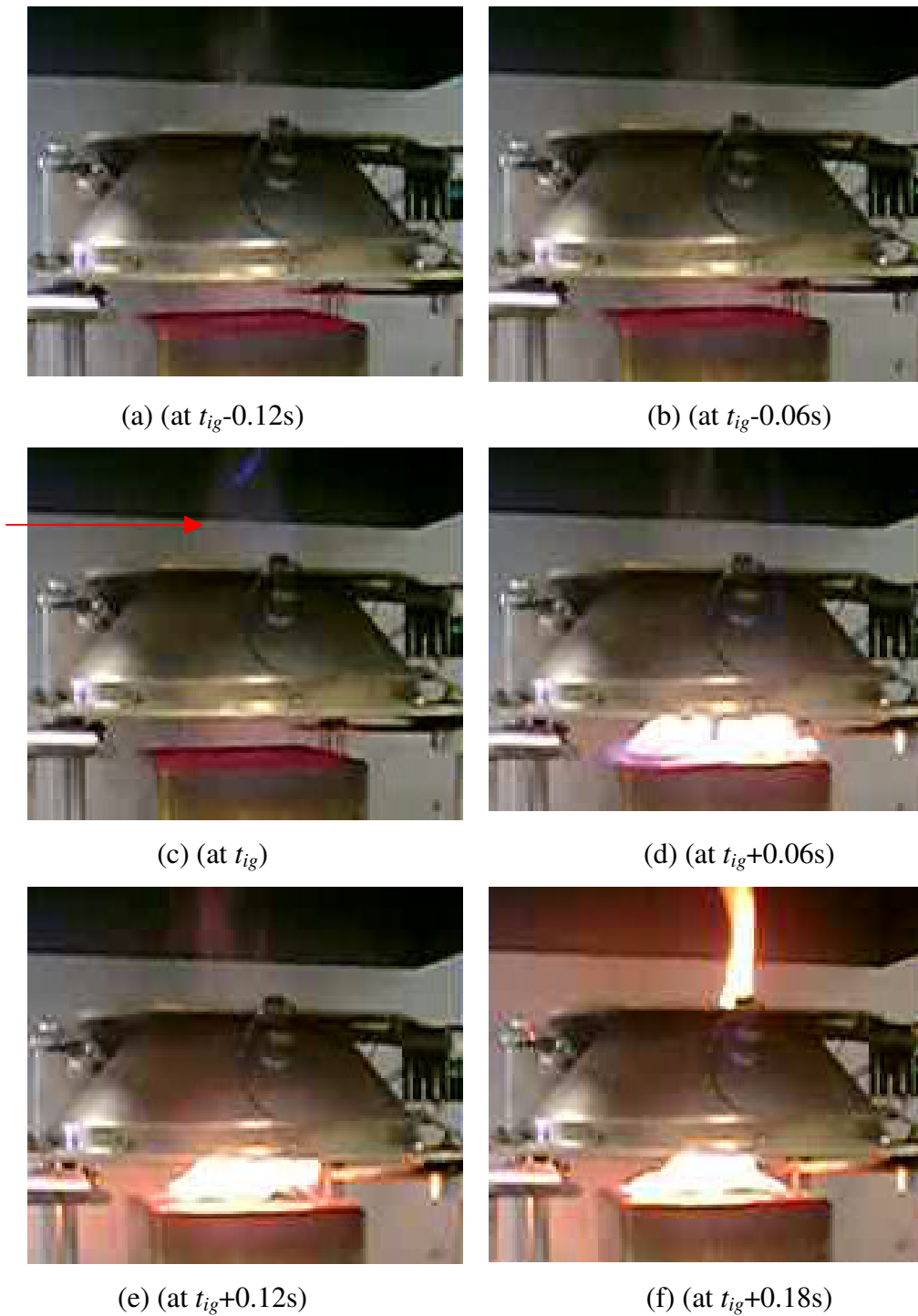


Figure 6.15 Flame development in test from the mountain ash under 50 kW/m²

Notes for Figure 6.15:

- (a) ~ (b): moments before ignition, pyrolysis products appeared within the flow stream with a higher concentration level compared to the 30 kW/m² in test
- (c): initial gas phase flash (colored blue and as indicated by an arrow), the first flash occurred above the cone heater in the gas phase
- (d) ~ (f): flame fully developed without obvious surface spreading

From above illustrations it can be seen that the general trends of flame developing in the modelling match roughly with the real observation. However a perfect matching in flame shape and development is either difficult or unnecessary. The simulated flame shape provides only a visual observation of contour of heat release rate since the chosen value to display the flame will affect flame shape greatly. Meanwhile, there are still some discrepancies and limitations in FDS simulation. First, the initiation of combustion in simulation always occurs in the centre of upper sample surface. In reality, the first flash can appear on any point of upper sample surface, even in the gas phase as that discussed below. Second less gas phase combustion (shown as the flame height in Figure 6.13 (e) and (f)) in simulation was observed compared to that in test (shown as in Figure 6.14 (g) and (h)). The reason to cause this difference is the mixture controlling mechanism (infinite fast mixture speed) in FDS. Thirdly, the HRRPUV used to form the flame contour is also affect the flame appearing and its shape greatly, as discussed in the last sub-section.

One interesting phenomenon is that the initial flash appeared just above the heater in the test under 50 kW/m^2 radiation (Figure 6.15(c)). It is speculated that this was caused by different conditions at top of heater and spark plug. As discussed in Section 2.4.3, key factors for an ignition occur include fuel, oxygen, heat and atmosphere. Therefore for a piloted ignition in cone calorimeter environment can be simplified as suitable fuel concentration and enough temperature at the spark plug location. This suitable fuel concentration should be between the lower and upper flammable limits. In the cone calorimeter, the solid surface was heated by the radiative flux from the heater and generated pyrolysed products. When the pyrolysis rate increased quickly before ignition (under a high radiative flux) and a small volume of pyrolysed products with the suitable fuel concentration rise up rapidly, the pulsing spark may miss out this volume. This phenomenon is really possible when turbulent flow exists above the solid surface. Then the spark plug becomes surrounded by rich fuel stream (above the upper flammable limit). Above the top of the heater, the pyrolysis stream has more chance to mix with fresh air and fell into a suitable range for combustion again. The gas has been also heated up enough when it passed through the heater. Then ignition occurred. This observation matches with the phenomenon that there is a small peak in the mass loss rate measurement for the mountain ash in the cone calorimeter test in Figure 5.14. It is also accord with the theoretical explanation made in Chapter 5 for presence of the peak. As discussed before, for the timber materials, the mass flux before the ignition, which includes the release of moisture and inert gases, is relatively high.

6.3.2 Surface temperature

The surface temperature was monitored in all simulations. Shown in Figure 6.16 to Figure 6.18 are simulated temperatures at the central point on the mountain ash sample surface at different radiation levels, compared to that measured in the cone calorimeter tests. The simulated critical surface temperatures, i.e. the surface temperature at the ignition times, are shown in Table 6.5 and Table 6.6 for the mountain ash and pine respectively.

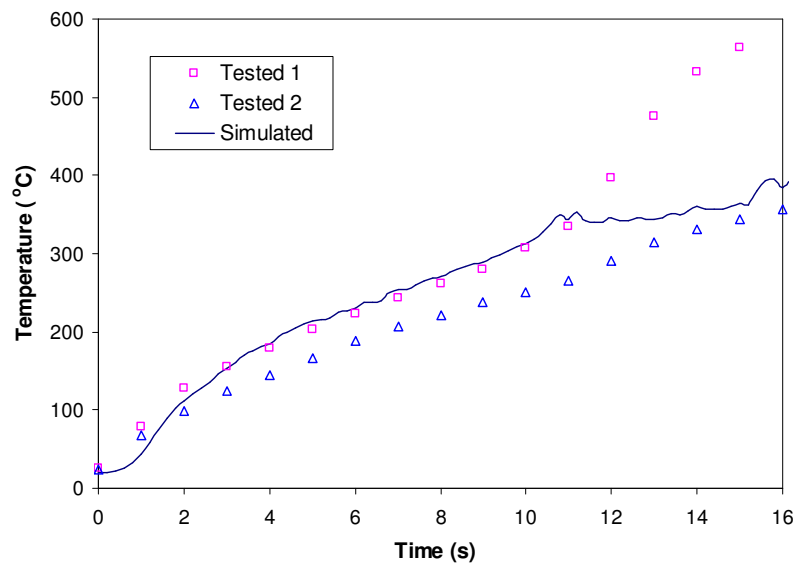


Figure 6.16 Measured and simulated surface temperatures under 75 kW/m^2 (Average tested $t_{ig}=10.7 \text{ s}$, $T_{ig}=290 \text{ }^\circ\text{C}$)

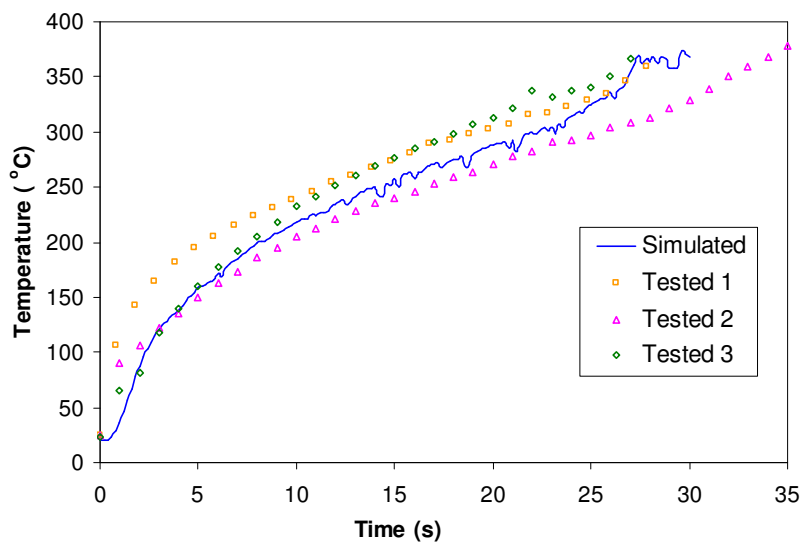


Figure 6.17 Measured and simulated surface temperatures under 50 kW/m^2 (Average tested $t_{ig}=27.0 \text{ s}$, $T_{ig}=334 \text{ }^\circ\text{C}$)

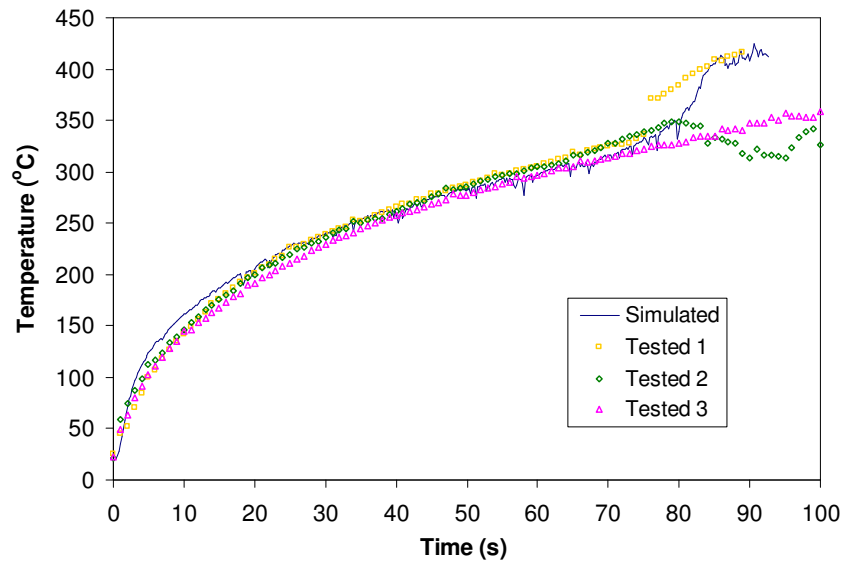


Figure 6.18 Measured and simulated surface temperatures under 30 kW/m^2
(Average tested $t_{ig}=153.2 \text{ s}$, $T_{ig}=330 \text{ °C}$)

6.3.3 Heat release rate

Figure 6.19 and Figure 6.20 show the simulated heat release rate curves of the mountain ash under 50 kW/m^2 and 75 kW/m^2 in comparison with the test values. These experimental results were obtained from the cone calorimeter tests shown in Chapter 5. The full combustion history for the mountain ash normally lasts thousands of seconds. Due to the limitation of computational power, it is nearly impossible to simulate the whole history of combustion by using current grid settings. Therefore a coarser grid resolution, $3 \times 3 \times 4 \text{ mm}$, was adopted for the long simulation under 75 kW/m^2 . The simulated combustion periods were 150 and 2200 seconds for the radiative conditions of 50 kW/m^2 and 75 kW/m^2 respectively.

It can be seen that simulated curves have similar onset times of ignition and trends to the experimental results, except for the second peak in the HRR curves. The times for the first peak in both simulations and tests agree with each other. However by observing the HRR curve in the long simulation, the second peak did not appear. This may be explained by the fact that the FDS model does not have the capability to simulate certain changes in real timber burning, such as bend and crack. As discussed in Section 2.3.3.2, these changes

normally increase the external surface area and expose inner unburnt virgin parts to the radiative flux that all contribute to a higher burning rate and form the second peak.

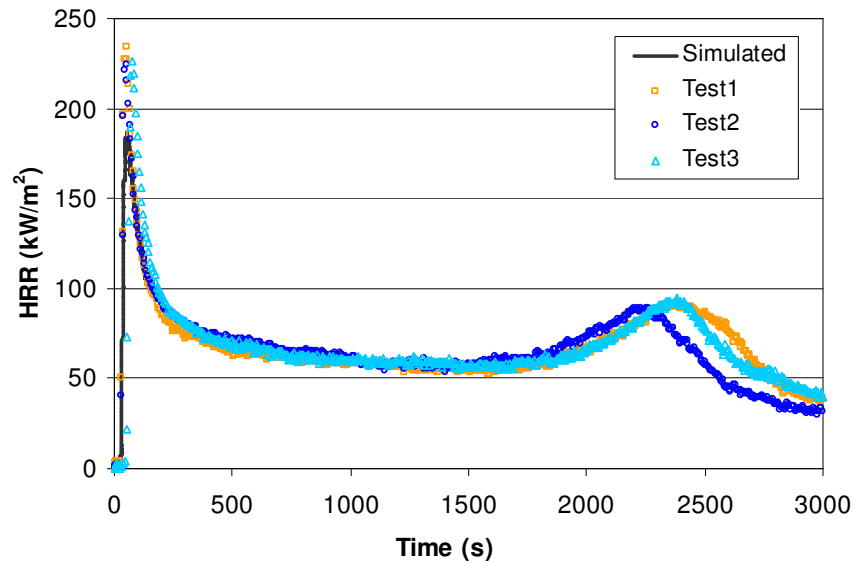


Figure 6.19 HRR curves under 50 kW/m² for the mountain ash

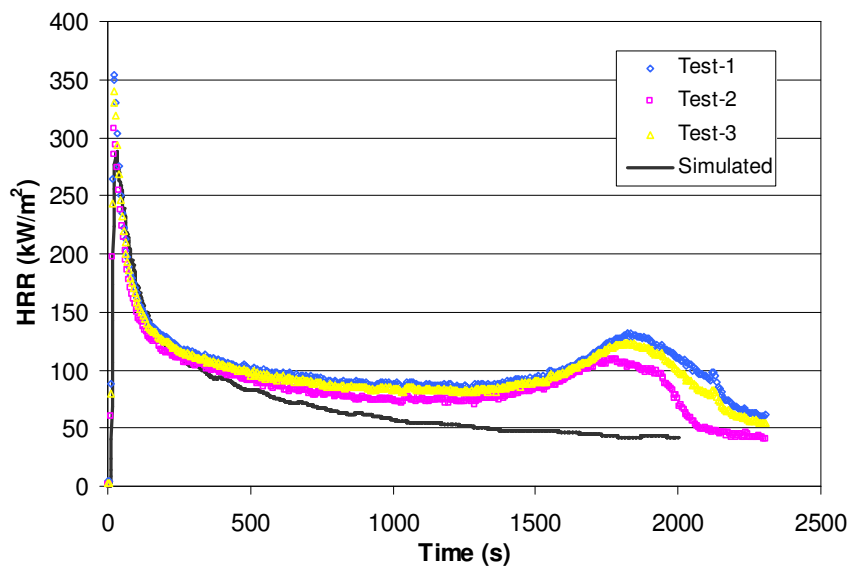


Figure 6.20 HRR curves under 75 kW/m² for the mountain ash

It is clear that the simulated peak and average values of the HRR are lower than the test results. There are a number of reasons contributing to this difference. The first is the different heating conditions in the simulation and in the test. As mentioned in Section 6.2.2, the radiation around the outer area is lower than that of the central area of the sample

surface. While the temperature of the stair-step shape heater was determined to ensure a specific radiative flux was received at the central point of the surface, the total radiative heat flux applied to the sample in the simulation is lower than that in the real test under the “same” radiative flux settings. This can be observed from Figure 6.7 and Figure 6.8. Secondly, it results from the limitation of FDS to simulate the charring process in detail. The charring sub-model in FDS is not sophisticated enough to simulate complicated details in the charring process, such as contraction, surface recession, moisture vaporization and cracking, etc. As mentioned in the literature review (Section 2.3.3.2), these phenomena usually result in an enhancement of exposure of inner fresh solid and heat transfer that contribute to a higher combustion rate and a higher heat release rate (Jonsson and Pettersson 1985).

6.3.4 Mass flux

The simulated critical mass fluxes (i.e. the mass flux at the “ignition” occurred, the ignition times were obtained from the cone calorimeter tests) are listed in Table 6.5 and Table 6.6 for the mountain ash and pine respectively. Shown in the tables included surface temperature at the “ignition”.

Table 6.5 Major inputs and results for simulation for the mountain ash

Simulation code	Settings & Tested						Results	
	External Radiation (kW/m ²)	E (kJ/mol)	A (1/s)	T _{ig} (°C)	Thickness (mm)	t _{ig} (s)	T _{ig} (°C)	Mass Flux _{cr} (g/m ² s)
SIMU-01	30	140.2	1.2x10 ⁸		32	153.2	326	1.0
SIMU-02		177.4	6.7x10 ¹¹		32		331	1.3
SIMU-03	50	140.2	1.2x10 ⁸		32	27.0	334	1.3
SIMU-04		177.4	6.7x10 ¹¹		32		342	1.5
SIMU-05		140.2	1.2x10 ⁸		14		337	1.2
SIMU-06		Default	Default	390	32		320	1.3
SIMU-07		Default	Default	350	32		283	1.4
SIMU-08	75	140.2	1.2x10 ⁸		32	10.7	343	1.6
SIMU-09		177.4	6.7x10 ¹¹		32		352	1.7

Note: All simulation parameters are calculated for the central point of the sample surface.

Table 6.6 Major inputs and results of simulation for the pine

Simulation code	Set-up					Results	
	External Radiation (kW/m ²)	Thickness (mm)	E (kJ/mol)	A (1/s)	t _{ig} (s)	T _{ig} (°C)	Mass Flux _{cr} (g/m ² s)
SIMU-10	30	32	126	5.1x10 ¹¹	98.3	365	1.1
SIMU-11	50	32	126	5.1x10 ¹¹	19.3	354	1.2

Figure 6.21 to Figure 6.23 show the initial part of mass flux curves for the mountain ash from 30 kW/m² to 75 kW/m² radiative fluxes. These simulated results are also compared with those obtained from the cone calorimeter tests. Mass flux from “dried” timber tests were also shown for the 30 kW/m² and 50 kW/m² radiative fluxes.

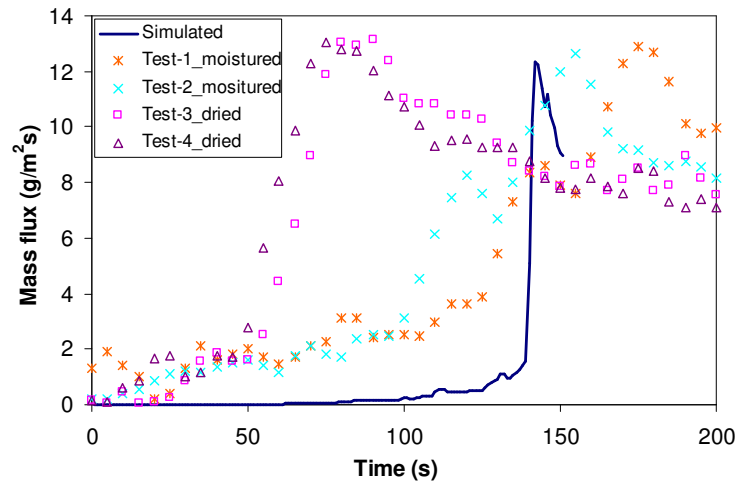


Figure 6.21 Simulated mass flux for the mountain ash under 30 kW/m² compared with test data

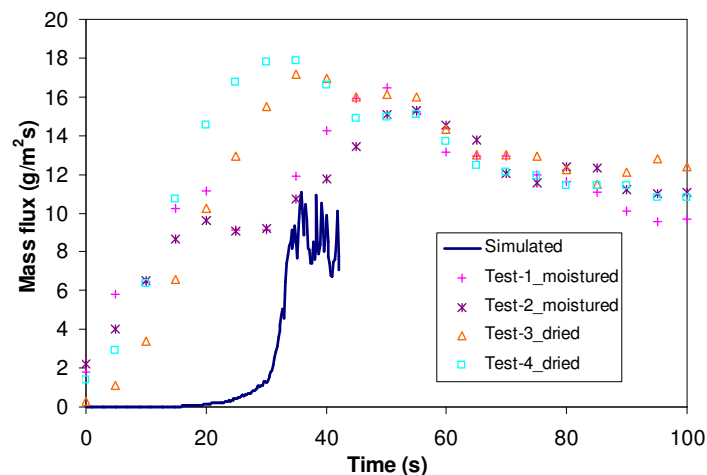


Figure 6.22 Simulated mass flux for the mountain ash under 50 kW/m² compared with test data

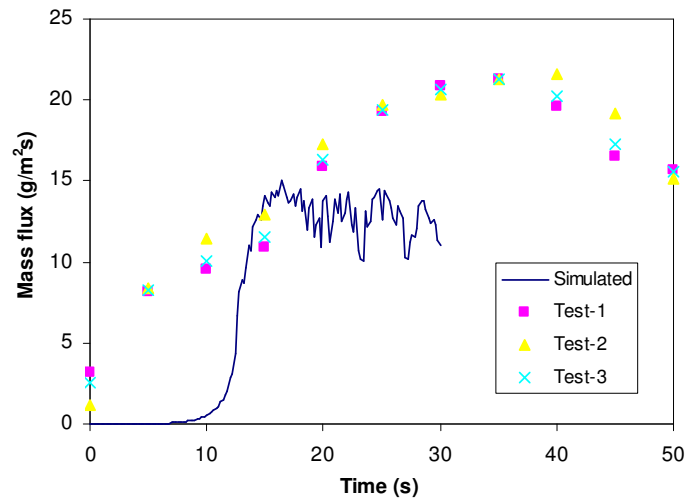


Figure 6.23 Simulated mass flux for the mountain ash under 75 kW/m^2 compared with test data

It is noticed that the simulated mass flux curves have a sharp rise starting from about $1.5 \text{ g/m}^2\cdot\text{s}$ rising to $15 \text{ g/m}^2\cdot\text{s}$ within approximately 2 seconds. Such rapid rises occurred in all simulations. This rise is resulted from increased radiative flux feedback from the sustained combustion followed the ignition. The onsets of the rising under different radiative fluxes have similar values, ranging from 1.0 to $1.6 \text{ g/m}^2\cdot\text{s}$. Other researchers (Deepak and Drysdale (1983), Drysdale and Thomson (1989), and Tewarson *et al.* (1999)), have reported a range from 0.8 to $6.0 \text{ g/m}^2\cdot\text{s}$ for this onset mass flux for timbers. Detailed data from others' results have been reviewed in Section 2.4.3.2. The critical mass flux at the “ignition” increased slightly as the external radiative flux increased. This trend matches with the observation of others (Kanury 2002; Yang *et al.* 2003).

The relationship between the critical mass flux and air flow rate through the simulated domain has been also investigated. Simulated critical mass fluxes, surface temperatures and mixture fractions at the centre of surface under 50 kW/m^2 with various duct air flow rates are shown in Table 6.7.

Table 6.7 Effect of various air flow rates

Flow rate (l/s)	T_{ig} ($^{\circ}\text{C}$)	Mass flux _{cr} ($\text{g/m}^2\cdot\text{s}$)	Mixture fraction _{cr} (g/g)
96	343	1.3	0.027
24	332	1.2	0.024
6	326	1.1	0.022

It is noted that T_{ig} and critical mass flux increased as the air flow rate increased. That means that under a higher air flow rate, the cooling effect on the sample surface and diluting effect for the gas phase fuel concentration all become stronger. Therefore required surface temperature and mass flux are higher compared to that at lower flow rate condition. However the values of the mixture fraction keep stable under various duct air flow rate.

The change in the critical mass flux caused by the air flow rate changing is relatively smaller, compared with the results obtained by Zhou *et al.* (2002). This is because under the current configuration of the simulation domain (modelling a cone calorimeter situation), the air flow velocity just above the sample surface (within 15 mm including the spark plug location) does not change much when the total air flow rate through the top duct varies from 4 to 96 l/s. This feature can be validated by the flow patterns under various vent flow rates that are shown in Figure 6.24. However the general trend for the critical mass flux is still slightly increased when the duct flow rate increased. This trend matches both modelling and experimental results obtained by Zhou *et al.*

In the FIST tests carried out by Zhou *et al.* (described briefly in Section 4.2.2.2), it was found that when air flow velocity over a sample surface increased from 1.0 to 1.7 m/s, the critical mass flux increased from 1.5 to 3.0 g/m²·s for a laminar parallel flow, radiative heated PMMA object. In the cone calorimeter situation, air flow has a quite different pattern compared with the laminar parallel flow pattern in the FIST experiment. In the current FDS simulations, both laminar and turbulent flows exist in the domain simultaneously. The gas flow velocity above the sample is approximately between 0.2 to 0.5 m/s under various total duct flow rates. This estimation can be proved from Figure 6.24 and also from measurements and simulations by Tsai *et al.* (2001). Under this lower flow rate condition, the effect from the changing gas flow velocity on the surface cooling is lower. Therefore the changing of velocity may have less effect on the critical mass flux.

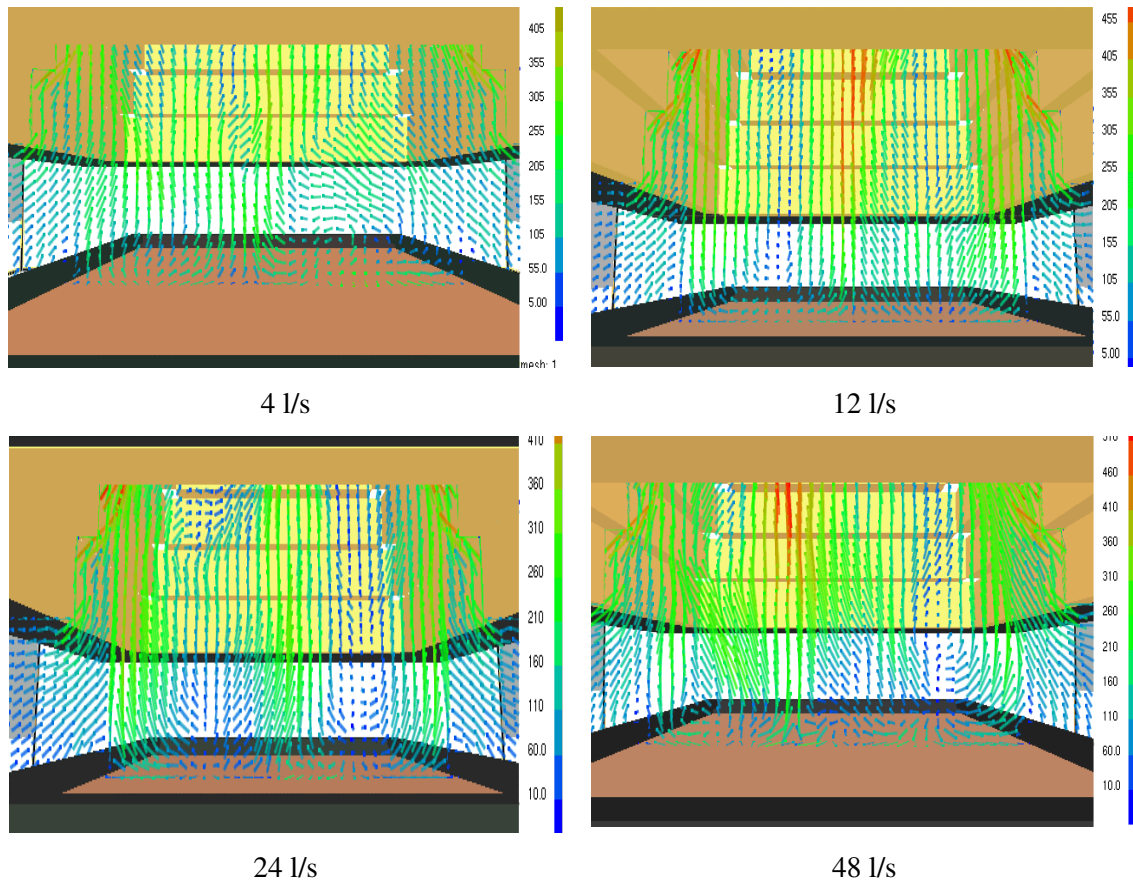


Figure 6.24 Flow velocity ($\times 10^{-3}$ m/s) under 50 kW/m^2 with various duct flow rates

6.3.5 Direct Numerical Simulation

The direct numerical simulation (DNS) computational scheme was also investigated for the mountain ash. The domain dimensions, heater temperature set-up and sample properties remained exactly the same as those in the LES simulations. A grid resolution of $3 \times 3 \times 1$ mm for the volume including the heater and sample was adopted to form a finer grid resolution which is generally required in DNS simulations.

Shown in Figure 6.25 are the surface temperature and mass flux curves obtained from a DNS simulation under 50 kW/m^2 radiation condition, compared with the LES scheme. It can be seen the DNS generates slightly higher initial surface temperature and mass flux. At the ignition (27.0 s) the surface temperature in LES simulation becomes higher than that in DNS simulation. This is caused by an earlier ignition determined by internal criteria in FDS in the LES simulation. Generally the parameters from these two schemes at ignition are relatively close.

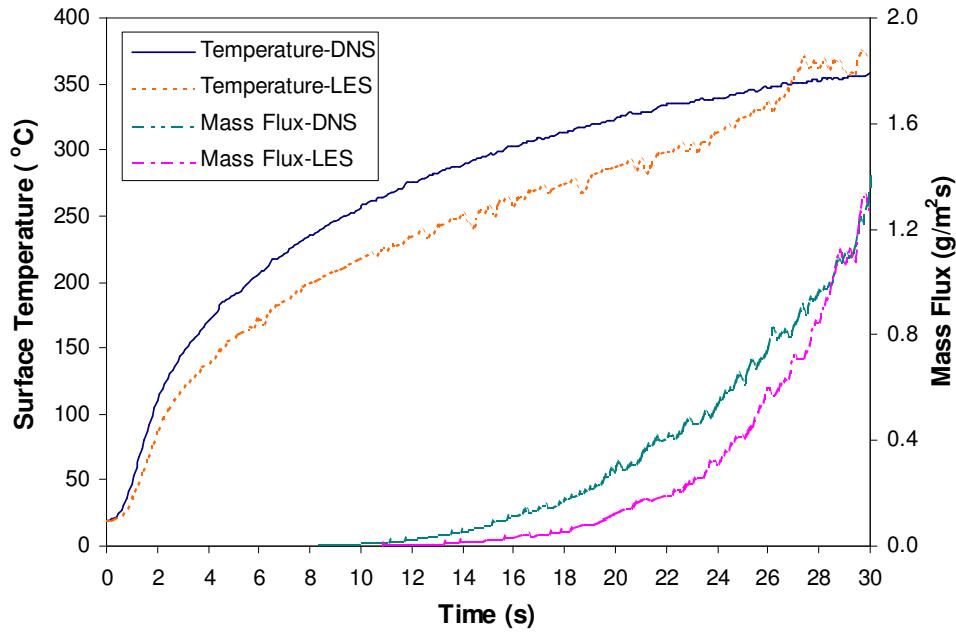


Figure 6.25 DNS results for the mountain ash under 50 kW/m^2

The computational time required for the DNS computation is approximate 6 times longer than that of LES method. Therefore, the DNS method was not used for other simulations in current study.

6.3.6 Comparison on results from different E and A values

The major simulated parameters from adopting different E and A values are compared with that from the tests, shown in Table 6.8. Ignition times determined by the cone calorimeter tests and FDS simulations are all listed for comparison. It is found that ignition parameters, such as critical surface temperature, critical mass flux and ignition time, are affected greatly by the values of the E and A .

Adopting the “effective” kinetic parameters E and A can generate quite good simulated results for the ignition parameters (except a little higher surface temperature at 75 kW/m^2). Applying the “perfect” kinetics obtained from normal used lower heating rates generated slower pyrolysis and ignition processes, and only applicable to the low external radiation condition. On the other hand, if the default computational scheme in FDS was adopted, shown for 75 kW/m^2 as an example, the simulated critical surface temperature and mass

flux are much higher than the experimental data. This can be explained by the earlier ignitions (earlier than that in the tests) occurred in the simulation (see from the column shows ignition time determined by FDS). This result also approved the necessarily to adopt kinetics from the improved TGA test method and computation scheme when detailed pyrolysis is to be studied in FDS.

Table 6.8 Comparison of effect of different E and A values for the mountain ash

Settings			Simulation Results			Test Results	
Radiation (kW/m ²)	E (kJ/mol)	A (1/s)	t_{ig} (s)	T_{ig} (°C)	Mass Flux _{cr} (g/m ² s)	$t_{ig}^{\#}$ (s)	T_{ig} (°C)
30	140.2	1.2×10^8	153.0	326	1.0	110.0	330
	177.4	6.7×10^{11}		319	0.9	131.3	
50	140.2	1.2×10^8	27.0	337	1.3	26.7	334
	177.4	6.7×10^{11}		326	1.1	29.5	
75	Default	Default	10.7	356	1.8	7.8	290
	140.2	1.2×10^8		343	1.6	11.4	
	177.4	6.7×10^{11}		334	1.3	12.8	

Note: $t_{ig}^{\#}$ is obtained from simulations (“apparent ignition” time).

6.3.7 Effect of sample thickness and backing material

The effects of sample thickness and backing insulation materials were investigated by a set of simple simulations. Spruce was used in the simulation and the material properties in the database file for the Spruce in FDS were adopted. This means that the default scheme for the E and A values was applied. Four thicknesses were checked: 28 mm (marked as “thick1”), 12 mm (marked as “thick2”), 8 mm (marked as “thin1”) and 4 mm (marked as “thin2”). A flat hot plate provided two levels of uniform radiative fluxes, 68 and 53 kW/m². The major observations are as follows.

Figure 6.26 provides temperature curves of the “thick1” and “thick2” samples under the 68 kW/m² radiation. Under the same radiative flux, the surface temperatures of the various sample thicknesses are the same, no matter if an insulation material is present or not. A sample temperature 1 mm below the surface remains identical with and without the insulation material. A thicker sample (“1mm-thick1” in the figure) has a higher inside sample temperature at 1 mm deep when the back of the sample was exposed, since the heat flux within the thinner sample is easily lost from the exposed back.

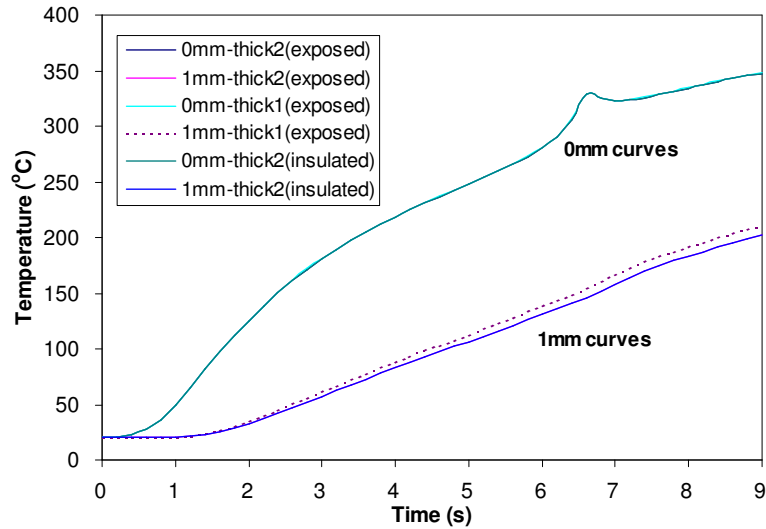


Figure 6.26 Simulations for the spruce under 68 kW/m^2

The effect of the thickness was also checked on the thinner samples, “thin1” and “thin2”. The selection of these thicknesses was based on the cone calorimeter results from the WPI, which have been discussed in Chapter 5. The thickness that may cause different behaviours was around 5 mm from those reported data. Shown in Figure 6.27 are inside temperatures (at 1 and 4 mm) monitored from the simulations with the insulation backing material.

It was noted that with the insulated backing material, the thinner sample has higher inside sample temperatures. However the temperature difference at 1 mm deep for the whole simulation duration is quite small. In fact the temperature difference at 1 mm deep is also very small before the “apparent ignition” in FDS occurs (at 6 seconds).

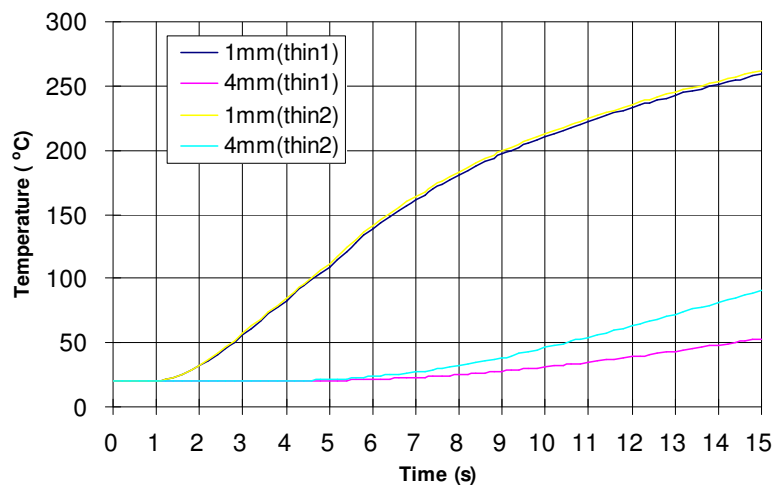


Figure 6.27 Simulations for the thinner spruce samples under 53 kW/m^2

Shown in Figure 6.28 are the temperature and surface mass loss rate curves from simulations for the thinnest sample (“thin2”) under the two radiation levels (“HRR-H” as 68 kW/m² and “HRR-L” as 53 kW/m²). The “apparent ignition” times for the two simulations are 6 and 9 seconds respectively. The surface temperatures at the ignitions are identical (around 300 °C). However the inside temperatures at ignition are different: lower external radiation generates a higher inside temperature (150 °C vs 110 °C) since a longer “ignition” time exists. Therefore a higher mass loss rate was generated from the lower radiation level at “apparent ignition”.

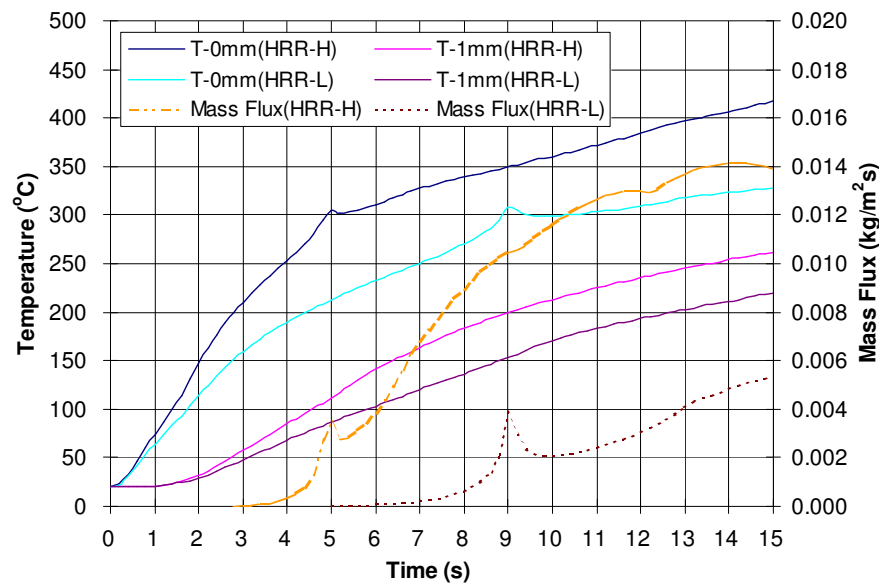


Figure 6.28 Simulation for the spruce under various radiation levels

Heating effect on the studied timbers with various backing materials in the current cone calorimeter environment was also investigated. Temperature profiles at different depths, including on bottom surface as 32 mm, from a pine specimen heated under 30 kW/m² were shown in Figure 6.29.

It can be seen that temperature rises were observed within the specimen, but not at back of the specimen. With tested sample thickness, there is no significant temperature difference from different backing conditions before the ignition occurred, even for this slow heating scenario. Therefore, for a purpose of studying pyrolysis and ignition processes by FDS simulation, there is no significant effect of selection of the backing materials. However, when a full history of the combustion of the timber specimens is a research interest (as in

Section 6.3.3), setting of different backing condition may be critical. For such simulations, “Insulation” was set to follow the cone calorimeter testing condition.

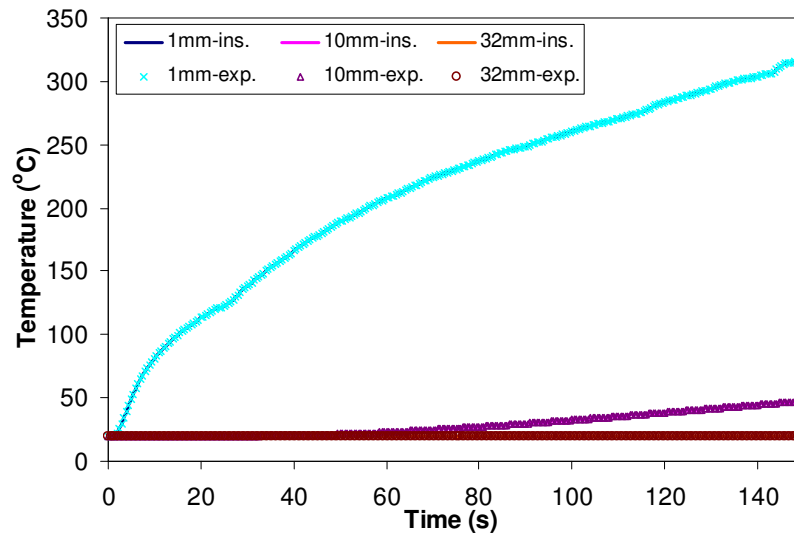


Figure 6.29 Simulated temperatures of a pine specimen under 30 kW/m^2

6.4 Distribution of Pyrolysis Products

“Current filed models are based on one form or another of the ‘mixed is burnt’ hypothesis” (Baum 2002). For example, in the FDS, a mixture fraction variable is used to characterize combustion, by terminating burning at a preset minimum oxygen concentration. Above that preset concentration, the burning rate is controlled by the rate that oxygen mixes into the flame zone (McGrattan 2004).

Meanwhile, as discussed in Section 2.4.3, the gas phase concentration is of interest for the current ignition criteria study. Therefore the gas phase distribution of pyrolysis products, which is represented as the mixture fraction in FDS, requires to be investigated. For this purpose, distribution of the mixture fraction was also studied through FDS simulation.

As illustrated in Figure 6.30 the mixture fraction was monitored at different locations above the solid surface in the cone calorimeter. Location 1 is the location of the spark plug.

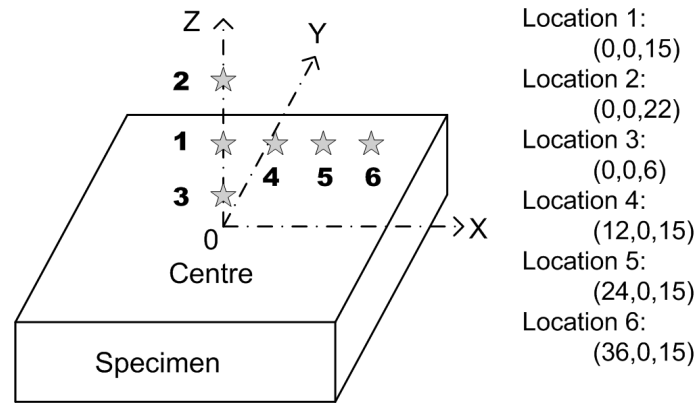


Figure 6.30 Locations of the mixture fraction monitored (distance in mm)

The vertical and horizontal distributions of the mixture fraction under 50 kW/m^2 for the mountain ash are shown in Figure 6.31 and Figure 6.32 respectively. It is noted that the average ignition time is 27.0 seconds from the tests.

Closer to the surface, a higher mixture fraction was monitored in the simulation (as shown in Figure 6.31). Since the pyrolysed stream sources from the solid surface and mixes with air along the rising path, the highest fuel concentration (highest mixture fraction value) is expected at the surface. The mixture fraction curves at different heights have similar trends. They all start increasing rapidly at about 25 seconds and reach a peak value at approximately 27 seconds (the time ignition took place). When nearly all the pyrolysed products were consumed immediately after ignition, the mixture fraction curve drops and rise up again which was controlled by the surface pyrolysis rate.

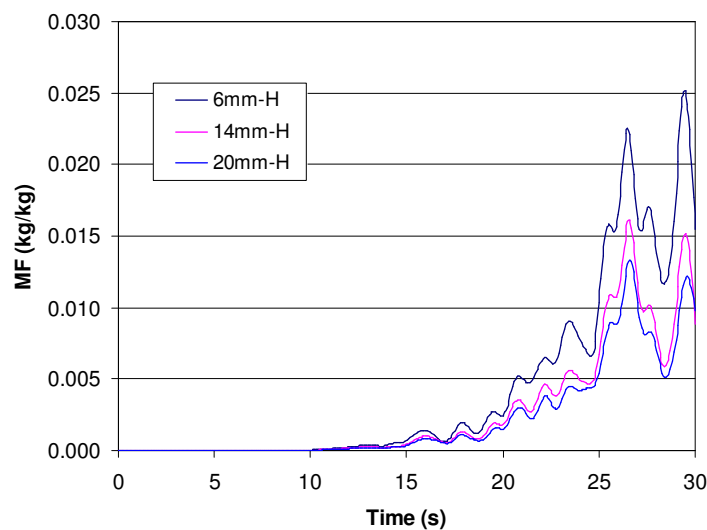


Figure 6.31 Vertical distribution of the mixture fraction at 50 kW/m^2 for the mountain ash

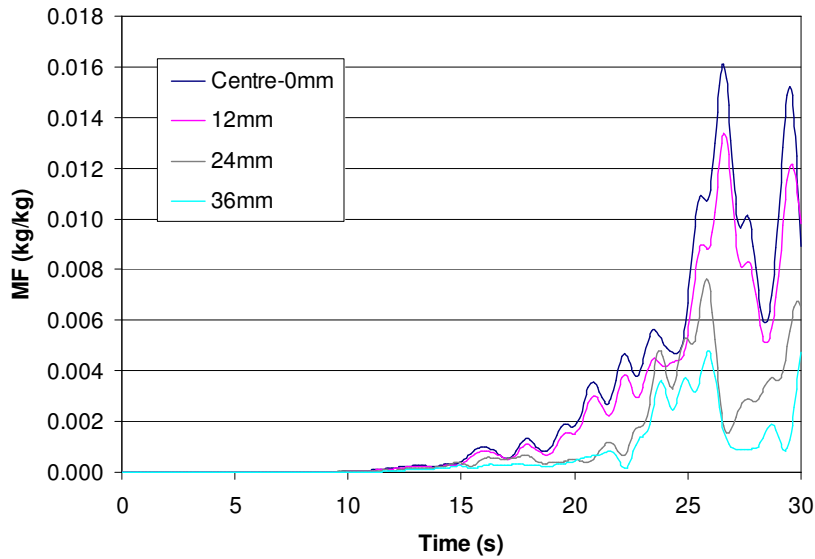


Figure 6.32 Horizontal distribution of the mixture fraction at 50 kW/m^2 for the mountain ash

Checking the horizontal distributions in Figure 6.32, the mixture fractions, within 12 mm of the centreline are higher than that from the edge points. This is caused by a higher central pyrolysis rate which was resulted from higher external radiative flux, and lower dilution with fresh air. The higher radiative flux on the central area of solid surface has been shown in Section 6.2.2.

These trends shown in the figures also exist in simulations for all other simulated materials and radiative conditions. From these trends, following pattern exists: the higher mixture fraction can be monitored along the centreline and the highest value is obtained at the surface of the sample. This result will be used in the ignition criteria study in the next chapter.

6.5 Summary of the Simulation Results

The pyrolysis and ignition processes in the cone calorimeter tests were successfully simulated in FDS by applying the “effective” kinetics obtained from the improved test method and the computational scheme of the TGA test. The most simulated parameters for describing timber ignition, such as ignition time and surface temperature, match with the experimental results reasonably well. It has been shown that by using appropriate material

properties obtained from the TGA experiments, FDS, adopting Atreya's pyrolysis model, is able to simulate the heat transfer, pyrolysis and ignition phenomena for timber in the cone calorimeter environment.

Among the thermal properties of the simulated timber materials, the activation energy E and the pre-exponential factor A are the most critical ones. It was found that a set of the values obtained from the previous TGA tests under higher heating rates, as so-called "effective" kinetics, generated satisfactory simulation results, particularly for the ignition time and ignition surface temperature.

Geometric parameters also affected the simulation results. The constructed heater was able to generate the desired radiative flux at the centre of the sample surface. This ensured the ignition phenomena (which occurred in the central area first in the simulation) was simulated properly.

Resolution of the grid plays an important role in the accuracy of the simulation. A grid size of $3 \times 3 \times 2$ mm was found to get a balance best between higher accuracy and faster simulation speed for the cone calorimeter situation.

The simulated surface temperatures in the central area prior to ignition are slightly higher than those measured in the experiments. The simulated temperatures fall into a range, from 280 to 350 °C, that was reported by many other researchers. As the radiation level increases the surface temperature at ignition decreases. This trend matches partially the current experimental results and has been reported by other researchers.

The HRR curves from the simulations have similar trends to that of the tests, except for the absence of a second peak in the simulation. The times for the first peaks are also similar to the tested results. FDS can not simulate the second peak because the phenomena that cause it, such as crack and bend of the sample, have not been built into the model. The predicted HRR levels are lower than the values from the tests. The lower HRR level is caused by lower radiative heat flux on the edge of the sample in the simulation.

The mass flux curves in the simulations have approximate ranges for peak values with those tested. However the simulated mass flux values before ignition are much lower than that from the tests, because no moisture and other inert gases were included into this mass flux in the FDS.

FDS is able to simulate the heat transfer within the sample and the effects of the sample thickness and insulation backing material. For example, higher inside sample temperatures were generated in a thinner sample, compared to a thick sample. However FDS can not simulate the impeding effort of the upper char layer on heat and pyrolysis product transfer

Values of the mixture fraction at ignition time were monitored at various locations. It was found that the highest mixture fraction value was obtained at the centre of the sample surface. Information for the mixture fraction will be useful for the investigation of the ignition criteria in the next chapter.

CHAPTER 7 CRITERIA FOR IGNITION AND DISCUSSION

In Chapter 6, several ignition parameters that are commonly used as criteria for wood ignition in the modelled environment were investigated. Selection of these parameters was based on previous review and discussion for the ignition criteria as well as the test and simulation results for the materials studied. The mixture fraction was also monitored in the simulation. In this chapter, all the variables previously mentioned as possible ignition criteria are further examined. The relationship between the mixture fraction and the LFL is investigated. Through comparison and discussion of the variables, the favoured ignition criterion is then suggested.

There are three sections in this chapter. In the first section, judgements of ignition in FDS are critically examined. Limitations of these methods are presented and discussed. A comparison between the simulated results and experimental data is carried out for the major ignition parameters in Section 7.2. In Section 7.3, analysis and discussion is performed for the mixture fraction to develop a suggested criterion for wood ignition in the cone calorimeter situation.

7.1 Further Discussion of Ignition in FDS

As discussed in Chapter 6, two commonly adopted methods in FDS for visual determination of ignition are HRRPUV and mixture fraction. By applying different settings of the critical value for those parameters, the observation results may vary a lot. There are some limitations to apply these two parameters and further discussions of them are given as followings.

Since the ignition phenomenon aimed to predict in the current research is a sustained combustion, as discussed in Chapter 2 and 5, the HRRPUV is not a suitable criterion for this purpose. Shown in Figure 7.1 are HRR curves for the mountain ash under various radiative fluxes. The ignition time determined from the cone calorimeter tests are marked as solid

stars in the graphs and an “apparent ignition” time is also marked as a hollow star for the 30 kW/m².

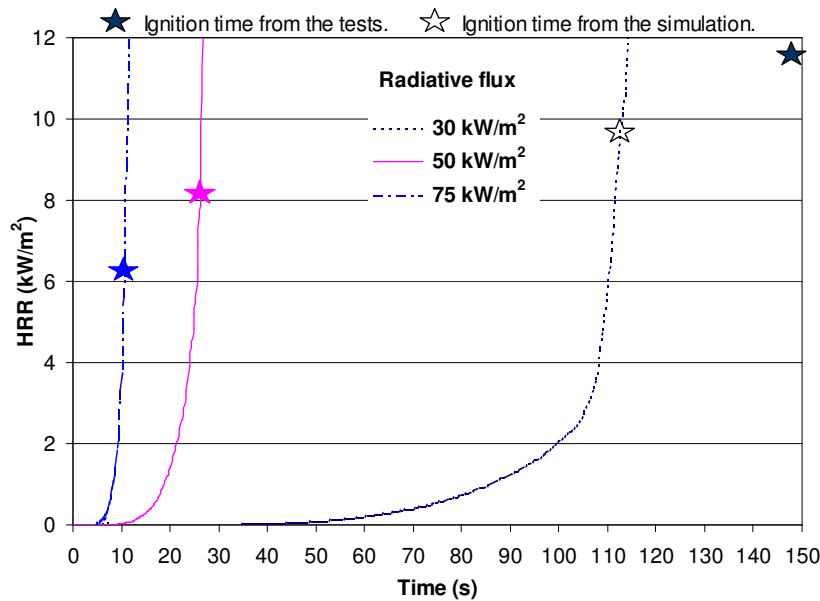


Figure 7.1 HRR curves and the ignition times for mountain ash

It can be seen that the values of HRR at which ignition occurred varied at different radiative fluxes. It is impossible to find a universal value of the HRR as the criterion of ignition, even it's related to another suggested gas phase criterion, critical energy density. As discussed by Lyon (2004), this critical HRR for ignition of solids in a dynamic environment can be calculated from the critical energy density as follow.

$$HRR_{cr} = \frac{H_{remove}}{\rho_{air} c_{air}} Q''' \quad (7.1)$$

where:

H_{remove} : rate of heat removed from solid surface, 10 W/m²·K in a controlled fire calorimeter;

ρ_{air} : density of air, 1 kg/m³;

c_{air} : heat capacity of air, 1 kJ/kg·K;

Q''' : critical energy density, 1900 kJ/m³ for vapors of hydrocarbons containing oxygen, nitrogen, etc.

The critical HRRs for polymers are reported from 10 to 40 kW/m² (Lyon and Janssens 2005), and also varied under various external conditions. Even if the critical HRR values

under different radiative fluxes are similar, when different values were chosen, the ignition times determined will vary greatly. It is noticed that under low radiative flux (30 kW/m^2) the value of HRR at ignition ($150.3 \pm 63 \text{ s}$ which was from the cone calorimeter test) is extremely high. This is because a huge variation exists in the experimental ignition time (from 90 to 216 s) under the low radiative flux (see Table 5.2). The pyrolysis rate in the simulation is much quicker than the average value in the tests and the “ignition” in FDS occurred much earlier (as the hollow star at around 110 s).

The mixture fraction curves obtained at the location of the spark plug are shown in Figure 7.2 for the mountain ash under various radiative fluxes. The critical values of the mixture fraction under radiative fluxes of 50 and 75 kW/m^2 are similar (around 0.02 g/g). Similar to that in HRR graphs (Figure 7.1), an odd value of mixture fraction (above 0.1 g/g) was also observed under 30 kW/m^2 , which was caused by the earlier ignition in FDS. In FDS, both HRR and mixture fraction increased quickly after the “apparent ignition” occurred. Therefore, the value of the mixture fraction at the moment of ignition determined by FDS is also presented for comparison. Shown in Table 7.1 is critical mixture fraction at different locations at ignition. The one monitored at the centre of the solid surface, marked as Z_{surface} and representing the highest value in the domain, as noted in Chapter 6. Another value was simulated at the location of the height of the spark plug, which marked as Z_{plug} . It is noticed that the values of the HRR and mixture fraction under 30 kW/m^2 were extracted at the moment ignition occurred in FDS.

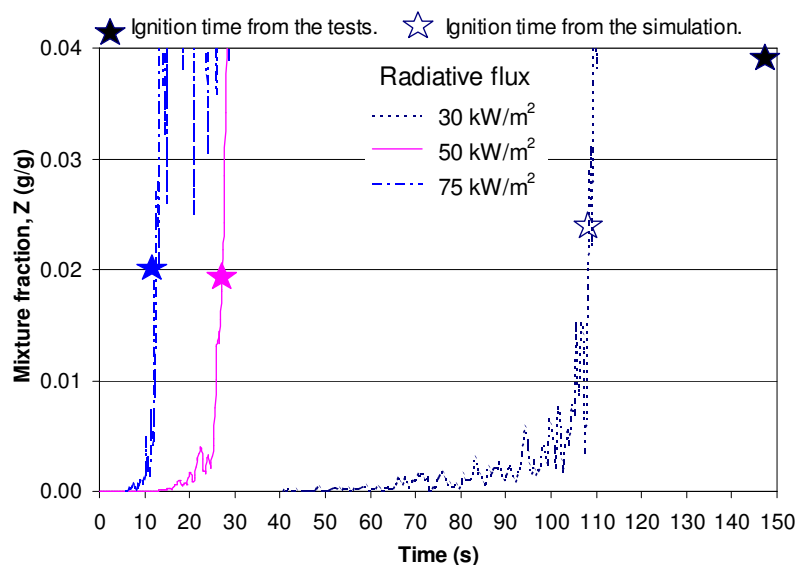


Figure 7.2 Mixture fraction at spark plug and the ignition times for the mountain ash

Table 7.1 Values for the critical parameters at ignition for the mountain ash

External Radiation (kW/m ²)	t _{ig} (s)	T _{ig} (°C)	Mass Flux _{cr} (g/m ² s)	Z _{-surface} (g/g)	Z _{-plug} (g/g)
30	110.0 [#]	326	1.0	0.027	0.020
50	26.7	334	1.3	0.024	0.018
75	11.4	343	1.6	0.030	0.023

Note: [#]: ignition time determined from the simulation.

It can be seen that the critical mixture fractions at the two locations are relatively similar under various radiative fluxes at the different “ignition” times. This provides basis for adopting the mixture fraction as an ignition criterion. However there is still a limitation in applying those values directly.

In reality, the fuel or pyrolysis product is not consumed before ignition. However, due to the mixing and burning controlling mechanism in FDS, the fuel was consumed or burnt before the “apparent ignition”. This can be verified from existing HRR curves before the “apparent ignition” (from Figure 7.1). Therefore the concentration and distribution of fuel were altered by the combustion. The corresponding mixture fraction distribution was not the “true” distribution prior to the “apparent ignition”. In fact, the obtained mixture fraction is the sum of fuel generation rate (pyrolysis rate) and fuel consumption rate. Therefore applying the mixture fraction as an ignition criterion, the effort from this consumption of fuel should be investigated. One may obtain the mixture fraction without the “apparent ignition” presence. Alternatively, one may assume that the burning process prior to the apparent ignition did not significantly alter the fuel distribution. Based on the relatively low HRR values before the “apparent ignition” (in Figure 7.1), as well as the fact that the ignition time (from the tests) and the “apparent ignition” time are very close above a radiative flux of 30 kW/m² (shown in Table 6.8), the latter assumption will apply with a certain degree of accuracy.

7.2 Comparison Between the Simulation and Experimental Data

To evaluate the applicability of these possible ignition criteria, comparison between the simulation results and experimental data must be carried out. In this section the simulated values are compared with experimental data from previous cone calorimeter tests as well as the modelling and experimental data from other researchers.

7.2.1 Critical surface temperature

The simulated surface temperatures of the studied timbers at ignition range from around 326 to 343 °C for the various radiative fluxes. The test results for the mountain ash show a range from 290 to 335 °C. The slightly higher prediction in simulations for the surface temperature is not unusual (Zhou *et al.* 2002). Therefore the values of simulated critical surface temperatures match with the cone calorimeter test data reasonably well.

When compared with the experimental results of others, the simulated values from current study fall into an acceptable range. For example, Tzeng *et al.* (1990) reported a range from 580 to 660 K (307 to 387 °C) for maple, red oak, poplar and mahogany, under tested radiative fluxes from 21 to 36 kW/m². Yang *et al.* (2003) obtained surface temperatures for ignition from 572 to 603 K (299 to 330 °C) for cherry wood with a thickness between 9 and 18 mm. In their tests, the radiation level ranges from 30 to 50 kW/m². Under the same radiative conditions, the surface temperatures for beech wood are from 563 to 593 K (290 to 320 °C).

7.2.2 Critical mass flux

The simulated critical mass fluxes for the mountain ash range from 1.0 to 1.6 g/m²·s under radiation levels from 30 to 75 kW/m². These values are lower than those measured in the cone calorimeter tests. The release of moisture and other inert gases in the real fire scenarios may contribute to the higher experimental values. As reviewed in Section 2.4.3, the composition of the pyrolysis products of timber is very complex. There are still a number of unknowns for these gaseous products. Therefore it is either impossible or unnecessary to include all inert gases into current modelling.

When the simulated critical mass flux is compared with data from other research, it is still within a range, 0.6 to 8 g/m²·s, which has been widely reported (see review in Section 2.4.3.3). Compared with the typical values for timber obtained by others, the current simulated value is slightly lower. However the peak mass fluxes presented in Section 6.3.4 are similar to some values obtained by others, as shown below. For example, Yang *et al.* (2003) reported 2 to 4 g/m²·s for the mass flux for cherry wood. A trend that shows a higher

critical mass flux under higher radiation levels (which was found in the current simulation) was also reported by those researchers. Meanwhile the peak values that they provide are around 6 to 7 $\text{g/m}^2\cdot\text{s}$ under 30 to 50 kW/m^2 radiation, which is slightly lower than the results for the mountain ash but similar to that for pine wood in the current simulations, as shown in Section 6.3.5. The reason for a lower critical mass flux range in the current simulation, apart from the explanation in previous paragraph, may be the determination method adopted here. Generally the simulated mass fluxes match other researchers' experimental data reasonably well.

7.2.3 Critical mixture fraction

Normally the concentration of pyrolysis products, especially the fuel concentration from the pyrolysis, is very difficult to measure in the cone calorimeter test. There is very little data of mixture fraction for timber materials in a cone calorimeter environment at this time. Therefore only the simulation data that are available from others' research are presented here for some kind indirect comparison.

Tsai *et al.* (2001) performed simulations for the auto-ignition problem of PMMA in the cone calorimeter. From their simulation results, the fuel concentration before ignition reached 0.3 to 0.5 g/g (mass fraction) at the centre point of the cone heater's bottom section. The ignition criterion in this simulation was the critical mass flux. The kinetics used for the pyrolysis calculation were obtained by a specified ignition temperature. It is noticed that simulation results for the critical mixture fraction vary from different material properties as well as the ignition criteria chosen. Therefore a direct comparison between values obtained by Tsai *et al.* and that from the current study is not available.

Another example can be found in a numerical analysis carried out by Zhou *et al.* (2002), again for PMMA. The physical problem was based on tests conducted on a FIST apparatus and details have been presented in Chapter 2. In simulating ignition a spark plug was positioned 0.5 to 1.5 mm above the PMMA plate. The mixture fraction between the solid and the igniter ranged from 0.03 to 0.07 g/g (mass fraction) under 35 kW/m^2 radiation and 1 m/s flow velocity. This range of values is slightly lower than current simulated data.

7.3 Special Consideration for the Critical Mixture Fraction

Acceptable agreement has been achieved between the simulated results and the experimental data for the surface temperature and the mass flux. However no direct comparison is available for the mixture fraction at this time. More theoretical analysis is thus required for evaluating this possible ignition criterion.

7.3.1 Relationship between the critical mixture fraction and the LFL

It is found from Chapter 6 and the first section of current chapter that for mountain ash the average mixture fraction values under various radiations at the ignition is about 0.020 and 0.027 g/g (at the spark plug and centre of surface). These average values will be checked for possible relation to a LFL value which was based on the previously mentioned lean flammability theory (Section 2.4.3.3). To perform this checking, the LFL value for timber was calculated first. A comparison between the mixture fraction and the LFL of timber was then carried out.

7.3.1.1 Calculation of LFL for timber

Although it is still difficult to obtain all details for the pyrolysis products of timber, there are some simplified expressions suggested by other researchers (see Section 2.3.3). As provided by Klose *et al.* (2000) from test results for three kinds of timbers, (Aspen, Beech, and Larch), typically representative ratios for the major gases as mole fractions are: 42%, 25%, 8.3% and 24.7% for H₂, CO, CH₄, and CO₂ respectively.

Applying the method shown in Section 2.4.3.3 (Equation (2.25)), the LFL of the pyrolyses products from timber can be evaluated from the *LFL* of pyrolysis composites. It is also known from the SFPE Handbook (Beyler and Hirschler 2002) that the *LFLs* for H₂, CO, and CH₄ are 4.0%, 12.5%, and 5.0% in volume respectively. Therefore the lower flammable limit at ambient temperature and pressure (room temperature and atmospheric pressure) for the wood pyrolysis products, *LFL_{py}*, can be calculated as follows:

$$LFL_{py} = \frac{100}{\left(\frac{8.3}{5} + \frac{42}{4} + \frac{25}{12.5}\right)} = 7.06\% \quad (7.2)$$

It is known that for a wide range of fuels containing carbon, hydrogen and oxygen, the adiabatic flame temperature at the *LFL* is approximately 1600 K, except for hydrogen (900 K) and carbon monoxide (1300 K) (Beyler 2002). Therefore the *LFLs* for H₂, CO and CH₄ at an initial mixing temperature from pyrolysis (200 °C or 473 K for timber materials) are calculated based on Equation (2.28) as follows:

$$\begin{aligned} \text{For H}_2, \quad LFL_{473K} &= LFL_{273K} \frac{T_{f,LFL(H_2)} - 473K}{T_{f,LFL(H_2)} - 293K} \\ &= 4 \times \frac{900 - 473}{900 - 293} = 2.8\% \end{aligned} \quad (7.3)$$

$$\begin{aligned} \text{For CO,} \quad LFL_{473K} &= LFL_{273K} \frac{T_{f,LFL(CO)} - 473K}{T_{f,LFL(CO)} - 293K} \\ &= 12.5 \times \frac{1300 - 473}{1300 - 293} = 10.3\% \end{aligned}$$

$$\begin{aligned} \text{For CH}_4, \quad LFL_{473K} &= LFL_{273K} \frac{T_{f,LFL(CH_4)} - 473K}{T_{f,LFL(CH_4)} - 293K} \\ &= 5\% \times \frac{1600 - 473}{1600 - 293} = 4.3\% \end{aligned}$$

Applying Equation (2.25) again, the *LFL* for wood pyrolysis products at initial mixing temperature of 200 °C is calculated as:

$$LFL_{py} = \frac{100}{\left(\frac{8.3}{4.3} + \frac{42}{2.8} + \frac{25}{10.3}\right)} = 5.2\%$$

7.3.1.2 Converting the mixture fraction into volume fraction

Suppose a mixture fraction value at which ignition occurs is determined from the FDS simulation. Since the “mixing is combustion” mechanism is adopted in FDS, it represents a similar situation as the piloted ignition in the cone calorimeter, i.e. ignition will occur when a certain level of fuel concentration is reached at the location where the spark is present. Therefore this mixture fraction can be related to a lean fuel concentration limit for ignition.

According to the definition of the mixture fraction, which was discussed in Chapter 6, a volume fraction of the pyrolysis combustibles, VF , which is comparable to the LFL , can be calculated by the mixture fraction (mass fraction as a ratio of gas phase fuel to total gas) via the following equation.

$$VF_{Fuel} = \frac{Volume_{Fuel}}{Volume_{Fuel} + Volume_{air}} \quad (\text{volume fraction}) \quad (7.4)$$

$$= \frac{\frac{Z}{MW_{Fuel}}}{\frac{Z}{MW_{Fuel}} + \frac{1-Z}{MW_{air}}} \quad (\text{molar fraction})$$

where:

VF_{Fuel} : volume fraction of the gas phase fuel;

Z : mixture fraction, g/g;

MW_{Fuel} : molecular weight of the gas phase fuel, g/mol;

MW_{air} : molecular weight of air, g/mol.

For the timber material, the molecular weight of its gas phase fuel, i.e. combustible gases in the pyrolysis products, MW_{Fuel} , equals

$$MW_{Fuel} = 42\% \times 2 \text{ (for H}_2\text{)} + 25\% \times 28 \text{ (for CO)} + 8.3\% \times 16 \text{ (for CH}_4\text{)}$$

$$= 9.17 \text{ g/mol}$$

Molecular weight of the air, MW_{air} , equals

$$MW_{air} = 21\% \times 32 \text{ (for O}_2\text{)} + 79\% \times 28 \text{ (for N}_2\text{)}$$

$$= 28.8 \text{ g/mol}$$

Therefore the volume fraction for the gas phase fuel, VF_{Fuel} , is calculated from Equation (7.4) as:

$$VF_{Fuel} = \frac{Z_{Fuel} / MW_{Fuel}}{Z_{Fuel} / MW_{Fuel} + (1 - Z_{Fuel}) / MW_{air}} \quad (7.5)$$

and then the volume fractions of fuel at the spark plug and the centre of solid surface can be calculated from following:

$$VF_{Fuel,plug} = \frac{\frac{0.02}{9.17}}{\frac{0.02}{9.17} + \frac{0.98}{28.8}} = 6.1\%$$

$$VF_{Fuel,surface} = \frac{\frac{0.027}{9.17}}{\frac{0.027}{9.17} + \frac{0.973}{28.8}} = 8.0\%$$

It can be seen that the volume fractions of pyrolysis products, which were calculated from the mixture fraction values, are slightly above the lower flammable limit (5.2% volume) for the timber pyrolysis products. This is an indication that the critical mixture fraction is related to the lower flammable limit to some degree. The value of the critical mixture fraction for the timber can be calculated from Equation (7.4) as 0.017 g/g, which is just below the simulated minimum critical mixture fraction value shown in Table 7.1.

Calculation results for the *LFL* and *VF* may vary when adopted pyrolysis gas composition changed. Reported gas composition varies depending on species of timber, decomposition environment, and testing/measuring equipments, etc. (Chembukulam *et al.* 1981; Lucon 1997; Klose *et al.* 2000). However the relationship between the *LFL* and *VF* is maintained. For example, by using a set of ratios provided by Yao *et al.* (Yao *et al.* 2006), as $CH_4:H_2:CO:CO_2 = 24.0:25.8:38.3:11.9$ (v/v %), following result can be obtained. At 200 °C, *LFL_{py}* is 5.0%, and *VF_{Fuel,surf}* calculated from the mixture fraction of 0.027 g/g is 5.1%, which is still slightly above the *LFL*.

7.3.2 Discussion for the suggested criterion

Among the three criteria for ignition of solid materials, critical surface temperature may be normally considered the most useful since it can be conveniently related to fire spread (Atreya 1983). Some models use this criterion reasonably well, but only in certain situations. Critical surface temperature is an empirical criterion and there is plenty of experimental data available for modelling and validating. However the surface temperature at ignition will be affected by several factors, such as external radiation and oxidizer flow conditions, which are still not fully understood. Meanwhile, as indicated in the literature review, there is great

variation for the reported value of this parameter. This makes it difficult to adopt test data and widely apply it, especially in complex gas flow conditions.

Critical mass flux, as a primary index for pyrolysis progress, is another important criterion for ignition. It is a useful one, specially under some given flow conditions, such as certain quasi-steady periods, and has been suggested by a number of researchers (Bamford *et al.* 1946; Drysdale and Thomson 1989). The limitation of this parameter as a criterion is that the critical mass flux varies under various radiation and air flow conditions. An example of varied critical mass flux under varying radiative fluxes has been given in Table 6.7 which has been also reported by other researchers (Zhou *et al.* 2002; Yang *et al.* 2003).

The mixture fraction is the third potential candidate as the criterion of wood ignition in a cone calorimeter environment. As discussed early in this section, relationship between this criterion and the lower flammable limit has been found. This enables the fourth element in the combustion tetrahedron (discussed in Section 2.4.3) to be met. While a spark exists in a piloted ignition and fresh air was supplied into the space above the specimen in a cone calorimeter environment, satisfying of the fourth element at the spark plug will lead to ignition occurring immediately. Considering other two parameters, critical surface temperature and mass flux, they just satisfy one leg of the tetrahedron separately and then do not necessarily result in ignition. From previous simulation results, it is observed that the mixture fraction criterion works quite well under either various radiation levels (shown in Table 7.1) or various gas velocities (shown in Table 6.7). Therefore it may be expected that this mixture fraction will be useful for prediction of ignition under complicated conditions.

There are still much to be done before the mixture fraction becomes a robust and solid criterion. Most will come from obtaining appropriate pyrolysis information, especially the kinetics, and validating it under a wide range of environment conditions. On the other hand, the computed LFL or mixture fraction should be ideally validated through measurement of fuel concentration at the location of the igniter (spark plug) and at the time of ignition in a cone calorimeter environment. While it is difficult to obtain such measurement with the available technology and resources, further improvement for the numerical scheme, which was used alternatively to obtain the fuel concentration at the igniter, should be carried out. The most critical one may be improvement of the ignition controlling mechanism in the FDS model. The “mixed is burnt” mechanism may affect the accuracy of computation of the

mixture fraction. Meanwhile this mechanism makes FDS suitable to model the piloted ignition where the gas phase time delay can be ignored, according to the basic analysis for ignition controlling mechanism performed in Section 2.4. When the real mixture fraction (generated from pyrolysis of solid) can be obtained accurately, the ideal methodology to predict ignition phenomena will rely on a set of criteria, including the critical mixture fraction, local temperature and oxygen concentration. While the latter two conditions are relatively easy to be verified, this approach of ignition prediction can be applied onto wider and complex fire scenarios, such as non-piloted ignition in the cone calorimeter and flame spread over non-adjacent objects.

In summary, critical mixture fraction is a potentially useful ignition criterion. Compared with the other two commonly adopted criteria, critical surface temperature and critical mass flux, it has several significant advantages. First, it is able to present the gas phase fuel distribution and predict ignition based on the LFL theory in a piloted cone calorimeter condition. Secondly, it is relatively stable in various radiation and gas flow conditions. However, to apply this criterion relies on accurate and applicable kinetics for the studied material. This remains a major task not just for FDS but also for all pyrolysis models with pyrolysis flux calculation function since the available kinetic information of various materials is still very limited. Suggested approach from current research shows a possibility for all the pyrolysis models to produce a more accurate prediction of ignition and wider application of modelling in complicated fuel configurations and environments.

CHAPTER 8 CONCLUSIONS AND RECOMMENDATIONS FOR FURTHER RESEARCH

8.1 Conclusion

Quantitative analysis of the pyrolysis and ignition processes of the studied furnishing materials has been achieved to varying degrees. By improving the testing and computational scheme for the pyrolysis kinetics, the obtained “effective” kinetics have been applied into a comprehensive CFD model, FDS, and the pyrolysis process of the studied timber in a cone calorimeter has been simulated with reasonable accuracy. Through the modelling, a gas phase fuel concentration parameter, the mixture fraction, has been monitored in a cone calorimeter environment. Validating the mixture fraction at ignition against with lower flammable limit (LFL), it is found that the critical mixture fraction is a potential and robust ignition criterion. It has the advantage that it can be applied to complicated environments.

Different decomposition behaviours of the studied materials under various heating conditions have been observed. The testing method and computational scheme of TGA for acquiring the kinetics were then improved to reflect the different decomposition behaviours. By applying the high heating rate combined with the linear shifting relationship of the reaction rate, the obtained “effective” kinetics are capable to describe the decomposition under environmental conditions similar to real fires. These observations and improvements are also useful and applicable for modelling decomposition of some other complex solid materials by an overall scheme. However how to model the sub-reactions from multiple composites in various heating conditions remains as a challenge.

The pyrolysis and ignition processes for the materials have been experimentally studied in a cone calorimeter. The major measured parameters matched the experimental data of others. Some interesting phenomena related to charring were observed. A small peak value was observed in the mass loss rate curves before ignition for charring materials under lower radiation levels. This seldom reported phenomenon matches Atreya’s theoretical analysis that the thicker char layer, if formed before ignition, will slow down the pyrolysis rate. A

data processing technique for the gas yield measurements has been improved. The errors in measurement have been reduced by an integral method.

A CFD model, FDS, which is based on Atreya's one-step overall pyrolysis model, was used for performing numerical simulations. By applying the kinetics from the scheme, which this researcher modified, the simulated major ignition parameters matched the experimental data reasonably well. A gas phase parameter, the mixture fraction, was monitored at desired locations. This successfully extended the application areas of FDS into detailed pyrolysis and ignition processes with engineering accuracy.

The critical mixture fractions for mountain ash under various conditions were found approximately 0.020 g/g at the plug or 0.027 g/g at the center of solid surface. The calculated values are just above the lower flammable limit (LFL) computed for the timber (0.017 g/g). This establishes a relationship between the critical mixture fraction and lean fuel concentration limit for ignition. The mixture fraction is thus suggested by the author to be a suitable gas phase ignition criterion. Compared with other commonly accepted criteria this parameter is able to predict ignition in the simulated environment more accurately and reliably. The existed theoretical basis makes the mixture fraction as a robust criterion and indicates a wider application.

8.2 Further Research Recommendations

There are many aspects of the modelling of pyrolysis and ignition of solid fuels that are required for further research. Generally, two types of tasks still remain: (1) to obtain more basic details about the pyrolysis and ignition processes and to model them effectively, (2) to validate the ignition criteria to apply fire models onto wider and more complex geometries. For example, complex pyrolysis products for commonly used materials are still not fully understood; some phenomena, such as crack and shrink for timber and melt for PU foam, must be taken into consideration in modelling, etc. This research work has shown an engineering approach to combining more phenomena into modelling and to generate more accurate prediction based on a solid theory of ignition controlling mechanism. To perfect this approach, it is recommended that the further development of pyrolysis and ignition should involve the following aspects:

1. The carrying out of TG type tests under even higher heating rate conditions. Since it has been found that there are different thermal decomposition behaviours and kinetics in low and high heating rate ranges, extending the heating rate to those closer to real fire conditions is naturally the next step. Meanwhile such test results can be used to validate the shifting pattern in that higher heating rate range.
2. More details of wood pyrolysis should be included in the current pyrolysis model. These details may include phenomena such as shrinkage and cracking. While the current simulation has not included a relationship between pyrolysis and surface oxidant concentration that theoretically exists, further research may be necessary for extending the modelling ability of FDS on such phenomena.
3. Measurement of fuel concentration at spark plug location in a cone calorimeter environment is desired. Such experimental data will approve the relationship between the critical mixture fraction and the LFL directly.
4. In FDS, some type of modelling should be performed for investigating individual pyrolysis compounds. More and more kinetic parameters from multi-reaction or sub-reaction of complex decompositions are being studied by many researchers to obtain detailed understanding of pyrolysis and combustion, especially for toxic gaseous products. However, such complicated reactions are still unable to be modelled in most of current fire models. Such improved simulations will be helpful to evaluate the mixture fraction criterion proposed by this author.
5. Another major improvement for the FDS model may be the modification of the current ignition controlling mechanism. As discussed in Chapter 6 and 7, functions such as to “turn off” the combustion and to control reaction rate by local oxygen concentration may be helpful to obtain a more accurate and meaningful mixture fraction generated from pyrolysis.
6. Apply the suggested mixture fraction criterion to other environments. Combined with other criteria, like local gas temperature, one may predict ignition in more complicated scenarios, such as non-piloted ignition and non-adjacent flame spread.

APPENDIX A. TGA TEST SETTINGS AND RESULTS

Listed in this chapter are whole set of major experimental settings and testing results of TGA tests for the studied materials.

Table A1 to A6 show the settings and raw results for each testing material. For the dynamic (DYN) tests, the heating rate was quoted and a constant stable environmental temperature was listed for the isothermal (ISO) tests.

The test codes were given as following rules:

TG XX mm

where:

TG: the TGA test;

XX: type of material, CT: cotton;

CP: cotton and polyester;

PI: pine;

MA: mountain ash;

SA: Stamina PU foam;

SD: Standard PU foam;

mm: test order number.

The “-s” in the mass column for the timbers represents saw dust, at a size of around 100 meshes. The parameter WT refers to sample weight for tested materials.

Table A1 TGA tests for the cotton and polyester

Test code	Mass (mg)	Working gas	Test type	Heating rate (K/min)	T _{max,1} (°C)	MLR _{max,1} (mg/min)	WT _{max,1} (%)	T _{max,2} (°C)	MLR _{max,2} (mg/min)	WT _{max,2} (%)
TGCP01	5.27	air	DYN	10	355	0.42	69.2	431	0.42	33.0
TGCP02	5.35	air	DYN	20	365	0.94	68.6	449	0.73	34.0
TGCP03	4.72	air	DYN	30	394	0.74	77.1	489	1.00	38.8
TGCP04	3.33	air	DYN	30	376	0.73	71.4	451	0.77	37.8
TGCP05	2.58	air	DYN	50	412	0.73	75.5	485	1.08	40.6
TGCP06	3.11	air	DYN	100	454	1.85	76.7	559	1.76	36.2
TGCP07	4.50	air	DYN	200	476	7.60	66.7	560	3.30	33.6
TGCP08	2.85	N ₂	DYN	20	394	0.43	66.4	461	0.40	36.0
TGCP09	3.53	N ₂	DYN	30	372	0.74	66.8	462	0.67	30.7

Table A2 TGA tests for the cotton

Test code	Mass (mg)	Working gas	Test type	Heating rate (K/min)	Constant Temp. (°C)	T _{max} (°C)	MLR _{max} (mg/min)	WT _{max} (%)
TGCT01	3.49	air	DYN	10		367	1.10	43.5
TGCT02	6.99	air	DYN	10		368	1.30	50.2
TGCT03	5.25	air	DYN	20		377	7.20	35.8
TGCT04	6.94	air	DYN	20		370	3.67	42.8
TGCT05	6.10	air	DYN	30		385	10.80	36.7
TGCT06	4.55	air	DYN	50		447	329.00	36.6
TGCT07	4.36	air	DYN	75		476	372.80	42.8
TGCT08	3.71	air	DYN	100		500	524.00	44.8
TGCT09	3.95	air	DYN	150		520	1085.20	43.0
TGCT10	3.88	air	DYN	200		540	1731.00	46.0
TGCT11	3.95	N ₂	DYN	10		382	3.60	46.7
TGCT12	5.18	N ₂	DYN	20		400	1.60	52.9
TGCT13	7.40	N ₂	DYN	30		383	3.61	44.6
TGCT14	4.07	N ₂	DYN	75		503	245.40	47.8
TGCT15	3.73	N ₂	DYN	150		535	799.50	49.1
TGCT16	6.09	air	ISO		335		0.38	95.2
TGCT17	5.73	air	ISO		340		0.43	95.1
TGCT18	6.36	air	ISO		350		0.69	95.3
TGCT19	6.09	air	ISO		360		1.20	90.0
TGCT20	6.00	air	ISO		380		2.96	83.7

Table A3 TGA tests for the mountain ash

Test code	Mass (mg)	Working gas	Test type	Heating rate (K/min)	Constant Temp. (°C)	T _{max} (°C)	MLR _{max} (mg/min)	WT _{max} (%)
TGMA01	4.81	Air	DYN	5		320	1.60	59.5
TGMA02	3.36	Air	DYN	10		339	0.48	54.0
TGMA03	2.16	Air	DYN	20		343	10.50	56.1
TGMA04	3.14	Air	DYN	30		353	52.50	56.4
TGMA05	3.59	Air	DYN	50		470	76.90	50.0
TGMA06	5.60	Air	DYN	100		505	433.70	47.2
TGMA07	4.32	Air	DYN	200		516	1,272.90	45.6
TGMA08	2.65	N ₂	DYN	10		367	0.33	41.0
TGMA09	3.00	N ₂	DYN	30		369	1.21	45.0
TGMA10	2.70-s	Air	DYN	10		380	3.29	50.1
TGMA11	4.37-s	Air	DYN	30		411	40.90	49.6
TGMA12	3.40-s	Air	DYN	75		437	188.00	45.7
TGMA13	4.81-s	N ₂	DYN	10		409	4.10	48.3
TGMA14	4.13-s	N ₂	DYN	30		438	30.50	45.2
TGMA15	2.65	Air	ISO		320		0.82	90.1
TGMA16	2.48	Air	ISO		340		1.39	85.0
TGMA17	2.57	Air	ISO		350		1.61	85.1
TGMA18	2.44	Air	ISO		375		1.96	80.5

Table A4 TGA tests for the pine

Test code	Mass (mg)	Working gas	Test type	Heating rate (K/min)	T _{max} (°C)	MLR _{max} (mg/min)	WT _{max} (%)
TGPI01	4.70	Air	DYN	10	359	0.77	52.7
TGPI02	7.50	Air	DYN	20	381	1.70	41.1
TGPI03	2.20	Air	DYN	30	390	0.72	37.7
TGPI04	3.48-s	Air	DYN	30	425	1.08	48.0
TGPI05	3.83-s	Air	DYN	75	449	2.79	46.4
TGPI06	1.40	N ₂	DYN	10	364	2.30	44.9
TGPI07	3.20	N ₂	DYN	20	410	0.72	40.8
TGPI08	3.60	N ₂	DYN	30	391	1.20	39.1
TGPI09	3.76-s	N ₂	DYN	30	452	0.95	50.8

Table A5 TGA tests for the stamina PU foam

Test code	Mass (mg)	Working gas	Test type	Heating rate (K/min)	T _{max,1} (°C)	MLR _{max,1} (mg/min)	WT _{max,1} (%)	T _{max,2} (°C)	MLR _{max,2} (mg/min)	WT _{max,2} (%)
TGSA01	2.37	air	DYN	10	284	0.26	76.4	352	0.22	23.9
TGSA02	3.10	air	DYN	20	283	0.72	78.2	348	0.50	29.4
TGSA03	2.84	air	DYN	30	287	0.76	80.8	370	0.71	20.8
TGSA04	1.50	air	DYN	50	379	0.50	76.7	457	0.57	26.3
TGSA05	1.48	air	DYN	100	397	0.89	74.8	484	0.96	28.2
TGSA06	0.80	N ₂	DYN	20	341	0.19	41.8			
TGSA07	1.76	N ₂	DYN	30	294	0.57	77.1	354	0.46	28.8
TGSA08	1.25	N ₂	DYN	50	398	0.24	76.4	498	1.10	25.1
TGSA09	1.97	N ₂	DYN	100	391	0.67	82.7	517	3.28	29.4

Table A6 TGA tests for the standard PU foam

Test code	Mass (mg)	Working gas	Test type	Heating rate (K/min)	Constant Temp. (°C)	T _{max,1} (°C)	MLR _{max,1} (mg/min)	WT _{max,1} (%)	T _{max,2} (°C)	MLR _{max,2} (mg/min)	WT _{max,2} (%)
TGSD01	1.19	air	DYN	5		277	0.12	59.2			
TGSD02	1.92	air	DYN	10		286	0.33	62.6	318	0.21	27.3
TGSD03	2.44	air	DYN	20		293	0.72	69.3	344	0.51	19.9
TGSD04	2.44	air	DYN	30		297	0.90	73.3	361	0.75	20.9
TGSD05	1.50	air	DYN	50		381	0.63	71.3	453	0.54	21.2
TGSD06	0.77	air	DYN	100		416	0.74	64.6	456	0.83	27.1
TGSD07	1.04	air	DYN	150		423	1.43	64.4	461	1.61	31.1
TGSD08	0.91	air	DYN	200		474	1.78	26.7			
TGSD09	1.39	N ₂	DYN	20		311	0.22	78.4	389	0.47	28.4
TGSD10	1.24	N ₂	DYN	30		313	0.31	76.0	359	0.42	38.7
TGSD11	1.78	N ₂	ISO		250		0.10	98.5			
TGSD12	2.14	N ₂	ISO		300		0.56	96.7			
TGSD13	1.49	N ₂	ISO		300		0.41	95.5			

APPENDIX B. CONE CALORIMETER TEST SETTINGS AND RESULTS

Listed in this appendix are whole set of major experimental settings and testing results for the tested materials in the cone calorimeter.

Table B1 to B6 show the settings and results from the tests for each tested material, including those tests for the surface temperature measuring, individually.

The test codes were given as following:

For the woods and polyurethane foams,

X-mm-nn-Y-Z

X is the type of material, where:

MA: mountain ash;

PI: Pine;

SD: Standard PU foam;

SA: Stamina PU foam

mm is the sample thickness, mm

nn is external radiation, kW/m²

Y is the pilot method, where:

P: piloted; and

N: non-piloted.

Z is the order number.

For the fabrics,

XX-0-nn-Y-Z

where XX is material,

CP: cotton and polyester; and

CT: cotton

0 means single layer of the fabrics tested.

All lefts have same meanings as above.

In the result columns, following parameters are used:

t_{ig} : ignition time, s

HRR_{max} :	maximum heat release rate, kW/m ²
THR :	total heat released, MJ/m ²
EHC_{ave} :	average effective heat of combustion, MJ/kg

Generally, “Smouldering” represents a status of combustion, smouldering. “NC” means no combustion, includes the smouldering, observed.

Table B1 Cone calorimeter tests for the mountain ash

Test code	Settings			Results				Note
	Thickness (mm)	Radiation (kW/m ²)	Piloted	t _{ig} (s)	HRR _{max} (kW/m ²)	THR (MJ/m ²)	EHC _{ave} (MJ/kg)	
MA3230P1	32	30	Y	133	155.9	220.2	13.0	
MA3230P2	32	30	Y	154	159.6	212.5	5.2	
MA3230P3	32	30	Y	248	150.2	239.0	10.8	
MA3230P4	32	30	Y	77	152.4	208.6	11.2	
MA3230N1	32	30	N		85.3	129.8	10.6	Smoulding
MA3230N2	32	30	N		32.2	103.8	11.4	Smoulding
MA3240P1	32	40	Y	52	178.1	219.5	11.2	
MA3240P2	32	40	Y	46	176.7	210.9	11.6	
MA3240P3	32	40	Y	61	171.9	230.0	11.5	
MA3240N1	32	40	N	68	169.1	212.3	11.4	
MA3240N2	32	40	N	60	180.1	206.2	11.7	
MA3240N3	32	40	N	56	183.2	210.8	11.6	
MA3250P1	32	50	Y	23	234.3	204.1	11.0	
MA3250P2	32	50	Y	26	226.4	205.9	11.5	
MA3250P3	32	50	Y	29	223.4	209.6	11.9	
MA3250P4	32	50	Y	30	261.3	210.0	11.7	
MA3250N1	32	50	N	29	224.1	202.9	11.0	
MA3250N2	32	50	N	37	201.3	204.1	11.2	
MA3250N3	32	50	N	46	194.7	253.2	12.1	
MA3250N4	32	50	N	45	203.5	203.7	11.5	
MA3250N5	32	50	N	24	243.6	213.8	11.7	
MA3275N1	32	75	N	13	353.5	259.9	13.2	
MA3275N2	32	75	N	10	345.8	246.4	12.6	
MA3275N3	32	75	N	9	326.0	250.0	12.9	
MA1430P1	14	30	Y	89	186.4	94.2	11.6	
MA1430P2	14	30	Y	111	176.3	98.1	11.3	
MA1430P3	14	30	Y	95	192.6	102.5	11.7	
MA1450P1	14	50	Y	30	191.9	100.8	12.1	
MA1450P2	14	50	Y	27	198.3	110.5	12.3	
MA1450P3	14	50	Y	31	204.9	98.7	12.5	
MA1450N1	14	50	N	45	202.3	106.1	12.2	
MA1450N2	14	50	N	51	197.7	112.0	12.0	
MA1450N3	14	50	N	69	212.8	103.8	12.8	

Table B2 Cone calorimeter tests for the pine wood

Test code	Settings			Results				Note
	Thickness (mm)	Radiation (kW/m ²)	Piloted	t _{ig} (s)	HRR _{max} (kW/m ²)	THR (MJ/m ²)	EHC _{ave} (MJ/kg)	
PI3230P1	32	30	Y	129	160.4	191.4	12.4	
PI3230P2	32	30	Y	92	155.2	196.7	12.5	
PI3230P3	32	30	Y	101	151.0	182.2	12.4	
PI3230P4	32	30	Y	63	167.3	186.5	12.3	
PI3230N1	32	30	N		150.0	120.8	7.9	Smoulding
PI3230N2	32	30	N		39.1	86.2	5.8	Smoulding
PI3230N3	32	30	N		30.4	64.6	4.4	Smoulding
PI3240P1	32	40	Y	34	158.8	161.2	12.0	
PI3240P2	32	40	Y	37	163.5	160.2	11.5	
PI3240P3	32	40	Y	34	162.7	168.5	11.8	
PI3240N1	32	40	N	92	158.8	160.8	12.5	
PI3240N2	32	40	N	40	163.1	179.3	12.3	
PI3240N3	32	40	N	65	162.1	165.1	11.8	
PI3250P1	32	50	Y	21	180.3	175.5	11.7	
PI3250P2	32	50	Y	21	152.7	191.3	12.4	
PI3250P3	32	50	Y	18	171.8	176.1	11.6	
PI3250P4	32	50	Y	17	191.2	182.9	11.9	
PI3250N1	32	50	N	37	180.1	158.3	12.0	
PI3250N2	32	50	N	29	179.3	164.6	12.0	
PI3250N3	32	50	N	31	184.0	209.7	12.1	
PI3250N4	32	50	N	25	199.5	176.8	12.3	
PI3275N1	32	75	N	7	233.1	162.2	12.0	
PI3275N2	32	75	N	8	245.0	173.8	12.3	
PI3275N3	32	75	N	9	228.7	169.5	12.6	

Table B3 Cone calorimeter tests for the cotton and polyester

Test code	Settings			Results			
	Layer	Radiation (kW/m ²)	Piloted	t _{ig} (s)	HRR _{max} (kW/m ²)	THR (MJ/m ²)	EHC _{ave} (MJ/kg)
CP020P1	1	20	Y	34	199.6	7.1	16.6
CP020P2	1	20	Y	34	210.3	7.0	17.1
CP020P3	1	20	Y	36	210.3	7.0	17.4
CP030P1	1	30	Y	17	249.6	7.4	16.7
CP030P2	1	30	Y	16	275.2	7.6	16.3
CP030P3	1	30	Y	19	257.4	7.6	17.2
CP030N1	1	30	N	18	246.6	7.2	16.3
CP030N2	1	30	N	17	249.5	7.0	17.3
CP030N3	1	30	N	20	254.0	7.3	16.9
CP040P1	1	40	Y	10	296.6	7.6	17.2
CP040P2	1	40	Y	9	310.5	7.7	17.9
CP040P3	1	40	Y	7	320.8	7.2	17.3
CP040N1	1	40	N	12	271.4	7.8	16.8
CP040N2	1	40	N	13	270.8	7.1	17.4
CP040N3	1	40	N	13	296.6	7.3	17.9
CP050P1	1	50	Y	6	361.9	7.7	16.3
CP050P2	1	50	Y	6	344.0	7.8	17.4
CP050P3	1	50	Y	7	360.1	7.5	16.6
CP050N1	1	50	N	5	326.8	7.6	16.5
CP050N2	1	50	N	9	305.5	7.5	17.8
CP050N3	1	50	N	9	322.6	7.6	17.7
CP075N1	1	75	N	5	486.2	8.6	17.2
CP075N2	1	75	N	5	413.9	8.8	16.2
CP075N3	1	75	N	6	433.5	8.5	17.1

Table B4 Cone calorimeter tests for the cotton fabric

Test code	Settings			Results				Note
	Layer	Radiation (kW/m ²)	Piloted	t _{ig} (s)	HRR _{max} (kW/m ²)	THR (MJ/m ²)	EHC _{ave} (MJ/kg)	
CT020P1	1	20	Y	54	137.8	5.9	14.5	
CT020P2	1	20	Y	67	143.9	6.3	15.8	
CT020P3	1	20	Y	56	148.7	6.1	14.8	
CT020N1	1	20	N		36.3	3.2	5.0	Smoulding
CT020N2	1	20	N		3.3	3.1	0.4	Smoulding
CT020N3	1	20	N		29.4	3.4	4.8	Smoulding
CT030P1	1	30	Y	24	214.8	7.0	14.2	
CT030P2	1	30	Y	21	233.5	6.8	14.6	
CT030P3	1	30	Y	22	227.6	7.4	15.5	
CT030N1	1	30	N	26	193.3	6.5	14.5	
CT030N2	1	30	N	24	203.1	7.0	14.8	
CT030N3	1	30	N	35	134.6	5.2	17.8	
CT040P1	1	40	Y	16	257.6	7.6	15.2	
CT040P2	1	40	Y	14	290.7	7.4	15.6	
CT040P3	1	40	Y	16	231.1	7.5	14.6	
CT040N1	1	40	N	21	189.5	5.5	15.2	
CT040N2	1	40	N	16	251.4	7.4	14.9	
CT040N3	1	40	N	18	232.5	6.1	15.1	
CT050P1	1	50	Y	13	272.0	7.5	15.9	
CT050P2	1	50	Y	11	336.2	7.0	16.0	
CT050P3	1	50	Y	10	305.6	7.8	15.6	
CT050N1	1	50	N	13	277.1	7.6	15.9	
CT050N2	1	50	N	12	293.2	7.3	15.4	
CT050N3	1	50	N	11	275.8	7.5	15.5	
CT075N1	1	75	N	7	402.0	8.4	13.1	
CT075N2	1	75	N	8	387.9	8.6	15.0	
CT075N3	1	75	N	7	412.5	7.9	14.6	

Table B5 Cone calorimeter tests for the standard PU foam

Test code	Settings			Results				Note
	Thickness (mm)	Radiation (kW/m ²)	Piloted	t _{ig} (s)	HRR _{max} (kW/m ²)	THR (MJ/m ²)	EHC _{ave} (MJ/kg)	
SD5020P1	50	20	Y	12	398.7	33.1	26.7	
SD5020P2	50	20	Y	5	366.5	33.3	25.8	
SD5020P3	50	20	Y	6	386.7	34.5	27.3	
SD5020P4	50	20	Y	9	395.9	33.7	26.1	
SD5020N1	50	20	N		4.3	0.2	1.0	Smoulding
SD5020N2	50	20	N		6.4	2.0	1.6	Smoulding
SD5020N3	50	20	N		8.7	3.1	2.4	Smoulding
SD5030P1	50	30	Y	3	426.2	32.0	25.7	
SD5030P2	50	30	Y	4	499.1	33.1	26.4	
SD5030P3	50	30	Y	3	419.7	32.9	27.1	
SD5030N1	50	30	N		4.0	0.3	0.3	Smoulding
SD5030N2	50	30	N	27	485.5	30.0	27.5	
SD5030N3	50	30	N	18	457.1	31.1	26.5	
SD5030N4	50	30	N	18	454.2	30.1	26.7	
SD5040P1	50	40	Y	3	459.1	32.2	25.7	
SD5040P2	50	40	Y	2	471.6	32.5	26.5	
SD5040P3	50	40	Y	1	448.2	33.3	26.6	
SD5040N1	50	40	N	14	477.7	29.7	25.7	
SD5040N2	50	40	N	6	425.3	32.5	26.9	
SD5040N3	50	40	N	4	436.9	32.2	26.0	
SD5050P1	50	50	Y	2	515.5	35.3	26.4	
SD5050P2	50	50	Y	1	481.6	34.6	27.2	
SD5050P3	50	50	Y	2	486.1	32.9	26.8	
SD5050N1	50	50	N	8	497.8	33.6	27.1	
SD5050N2	50	50	N	4	546.1	39.1	26.3	
SD5050N3	50	50	N	3	503.8	33.6	26.2	
SD5050N4	50	50	N	3	507.2	33.5	26.5	
SD5075N1	50	75	N	1	656.7	37.5	28.4	
SD5075N2	50	75	N	1	627.7	35.0	27.3	
SD5075N3	50	75	N	2	633.0	36.2	28.1	

Table B6 Cone calorimeter tests for the stamina PU foam

Test code	Settings			Results				Note
	Thickness (mm)	Radiation (kW/m ²)	Piloted	t _{ig} (s)	HRR _{max} (kW/m ²)	THR (MJ/m ²)	EHC _{ave} (MJ/kg)	
SA5010P1	50	10	Y	38	126.4	6.2	22.2	
SA5010P2	50	10	Y	45	168.1	6.9	22.2	
SA5010P3	50	10	Y	41	145.2	6.7	22.6	
SA5020P1	50	20	Y	7	389.5	43.1	25.2	
SA5020P2	50	20	Y	6	329.8	43.7	25.9	
SA5020P3	50	20	Y	11	367.1	43.0	25.6	
SA5020N1	50	20	N		1.4	0.0	0.1	NC
SA5020N2	50	20	N		6.1	1.4	1.3	Smoulding
SA5020N3	50	20	N		6.0	0.3	1.3	Smoulding
SA5030P1	50	30	Y	8	433.2	44.4	25.9	
SA5030P2	50	30	Y	6	412.7	42.9	25.6	
SA5030P3	50	30	Y	4	396.8	44.8	25.7	
SA5030N1	50	30	N	32	440.7	41.1	26.1	
SA5030N2	50	30	N	31	386.4	41.1	25.9	
SA5030N3	50	30	N	17	404.7	43.3	24.9	
SA5040P1	50	40	Y	5	391.5	46.3	25.9	
SA5040P2	50	40	Y	4	438.7	43.7	25.4	
SA5040P3	50	40	Y	3	410.8	44.3	25.5	
SA5040N1	50	40	N	21	501.3	45.0	27.3	
SA5040N2	50	40	N	19	491.1	42.1	25.2	
SA5040N3	50	40	N	11	391.4	43.7	25.6	
SA5050P1	50	50	Y	1	386.2	43.9	25.1	
SA5050P2	50	50	Y	1	393.8	43.6	25.2	
SA5050P3	50	50	Y	1	442.7	44.1	25.0	
SA5050N1	50	50	N	12	497.3	46.4	25.8	
SA5050N2	50	50	N	15	398.3	42.6	25.1	
SA5050N3	50	50	N	4	493.1	45.1	25.7	
SA5075N1	50	75	N	3	579.7	44.8	25.2	
SA5075N2	50	75	N	3	573.1	43.7	25.5	
SA5075N3	50	75	N	2	584.3	44.5	25.9	
SA2530P1	25	30	Y	5	495.4	25.4	27.0	
SA2530P2	25	30	Y	6	349.9	18.6	26.9	
SA2530P3	25	30	Y	12	398.4	23.5	25.3	
SA2530N1	25	30	N	63	411.1	19.6	28.1	
SA2530N2	25	30	N	45	423.4	20.4	26.3	
SA2530N3	25	30	N	31	463.0	24.2	25.7	
SA2550P1	25	50	Y	4	617.1	24.5	26.8	
SA2550P2	25	50	Y	2	576.6	20.9	21.6	
SA2550P3	25	50	Y	5	539.4	21.4	22.6	
SA2550N1	25	50	N	4	578.1	26.8	27.3	
SA2550N2	25	50	N	4	621.8	25.3	27.0	
SA2550N3	25	50	N	6	609.4	25.9	27.3	

APPENDIX C. ANALYSIS AND COMPUTATION OF ATREYA'S PYROLYSIS MODEL

All the non-dimensional parameters marked with [*] in this appendix have the same meaning with the corresponding dimensional parameters shown in the Notation.

For a physical heating model described in Section 3.2, following assumption is applied to further simplify the boundary conditions. The thermal conductivity is proportional to the density, i.e., $\lambda^* = \rho^* k$, where $k = \text{constant} = \lambda_\infty / \rho_\infty$. Therefore, the non-dimensional basic equations for the pyrolysis model of a wood material can be written as follows:

$$\text{Energy:} \quad \rho^* \frac{\partial T^*}{\partial t^*} = \frac{\partial}{\partial y^*} \left(\rho^* \frac{\partial T^*}{\partial y^*} \right) \quad (\text{C. 1})$$

$$\text{Decomposition:} \quad \frac{\partial \rho^*}{\partial t^*} = -A^* (\rho^* - \delta^*) e^{-E^* / T^*} \quad (\text{C. 2})$$

$$\text{Mass:} \quad \frac{\partial m^*}{\partial y^*} = \frac{\partial \rho^*}{\partial t^*} \quad (\text{C. 3})$$

Boundary and initial conditions:

$$\begin{aligned} T^*(y^*, 0) = \rho^*(y^*, 0) = T^*(\infty, t^*) = 1 \\ -\rho^* \frac{\partial T^*}{\partial y^*}(0, t^*) = 1 - \Gamma(T_s^* - 1) \end{aligned} \quad (\text{C. 4})$$

Here, following non-dimensional parameters defined:

$$T^* = T / T_\infty$$

$$\rho^* = \rho / \rho_\infty$$

$$y^* = y / L \quad (L = \rho_\infty k T_\infty / F)$$

$$t^* = t / \tau \quad (\tau = L^2 / \alpha_\infty), \quad \alpha_\infty = \lambda_\infty / \rho_\infty c_p$$

$$E^* = E / RT_\infty$$

$$A^* = A \tau$$

$$\delta^* = \overline{\rho_c} / \rho_\infty \quad \text{For char yield}$$

Γ is the linearized heat loss term, containing the effects of convective and linearized radiative heat losses from the surface.

$$\Gamma = hT_\infty / F + (\sigma T_\infty^4 / F)(\overline{T_s^*} + 1)(\overline{T_s^{*2}} + 1)$$

Here, $\overline{T_s^*}$ is an average surface temperature, chosen to match the heat losses to their actual values over the appropriate temperature range.

Defined $D = A^* \exp(-E^* / T_p^*)$ as the Damkohler number, thereby Equation (C. 2) can be rewritten as:

$$\frac{\partial \rho^*}{\partial t^*} = -D(\rho^* - \delta^*) \exp\left[-E^* / T_{py}^* \left(\frac{T_{py}^*}{T^*} - 1\right)\right]$$

For large values of E^* , $\frac{\partial \rho^*}{\partial t^*}$ will be very small until T^* is very close to the pyrolysis temperature. Then $\rho^* = 1$ is used as approximate solution for the density for the stage 1 (inert heating stage). Therefore, inert temperature can be obtained from equation (C. 1) and (C. 4).

$$T_{inert}^* = 1 + \frac{1}{\Gamma} \left\{ \operatorname{erfc}\left(\frac{y^*}{2\sqrt{t^*}}\right) - e^{\Gamma y^* + \Gamma^2 t^*} \times \operatorname{erfc}\left(\Gamma\sqrt{t^*} + \frac{y^*}{2\sqrt{t^*}}\right) \right\} \quad (\text{C. 5})$$

When t^* reaches the pyrolysis time t_{py}^* , the surface temperature $T_{inert}^*(0, t^*)$ equals T_{py}^* .

Assuming t_{py}^* as a known parameter, for the condition $x^* \ll O(1)$ and $t^* - t_{py}^* \ll O(1)$,

Equation (C. 5) gives

$$T^* \cong T_{py}^* - ay + b(t^* - t_{py}^*) + \dots \quad (\text{C. 6})$$

and

$$\frac{\partial T^*}{\partial y^*} \cong -a + b[y^* + \Gamma(t^* - t_{py}^*)] + \dots \quad (\text{C. 7})$$

where:

$$a = \left(-\frac{\partial T_{inert}^*}{\partial y^*} \right)_{y^*=0, t^*=t_{py}^*} = e^{\Gamma^2 t_{py}^*} \operatorname{erfc}\left(\Gamma\sqrt{t_{py}^*}\right) \quad (\text{C. 8})$$

$$b = \left(\frac{\partial T_{Inert}^*}{\partial t^*} \right)_{y^*=0, t^*=t_{py}^*} = \frac{1}{\sqrt{\pi a_{py}^*}} - \Gamma a \quad (C. 9)$$

and

$$T_{py}^* = T_{Inert}^*(0, t_{py}^*) = 1 + \frac{1}{\Gamma}(1-a) \quad (C. 10)$$

Since pyrolysis always occurs on the surface first, $\rho^* = 1$, and most of changes of ρ^* occur near T_{py}^* , the expressions in Equations (C. 5) and (C. 6) were used into Equation (C. 2). By integrating over t^* in the limit $E^* \rightarrow \infty$, following asymptotic evaluation result is achieved.

$$\rho_{py}^* \cong 1 - \frac{A^*(1-\delta)}{bE^*/T_{py}^{*2}} e^{-E^*/T_{py}^*} \quad (C. 11)$$

For the second stage (initial pyrolysis), the basic equations (C. 1) to (C. 4) can be rewritten as following by introducing a new item $T^* = T_{Inert}^* + \theta$:

$$\begin{aligned} (a) \quad & \frac{\partial \theta}{\partial t^*} = \frac{\partial^2 \theta}{\partial y^{*2}} + \frac{1}{\rho^*} \frac{\partial \rho^*}{\partial y^*} \left(\frac{\partial T_{Inert}^*}{\partial y^*} + \frac{\partial \theta}{\partial y^*} \right) \\ (b) \quad & \frac{\partial \rho^*}{\partial t^*} = -D(\rho^* - \delta^*) \exp \left[\left(-\frac{E^*}{T_{py}^*} \right) * \left(\frac{T_{py}^*}{T_{Inert}^* + \theta} - 1 \right) \right] \\ (c) \quad & -\frac{\partial \theta}{\partial y^*}(0, t^*) = \frac{(1-\rho^*)}{\rho^*} \left(-\frac{\partial T_{Inert}^*}{\partial y^*} \right) - \frac{\Gamma \theta}{\rho^*} \\ (d) \quad & \rho^*(y^*, 0) = 1 \\ & \theta(y^*, 0) = \theta(\infty, t^*) = 0 \end{aligned} \quad (C. 12)$$

Similar calculation theme applied to the other stages, following expressions will be obtained.

For the initial pyrolysis stage:

$$t_c^* = t_{py}^* + (bE^*/T_{py}^{*2})^{-1} [s^*(\delta^*) - \ln D_0] \quad (C. 13)$$

where:

$$\begin{aligned} s^* &= s_{\max} \Big|_{m^* = \max} \\ s &= (bE^*/T_{py}^{*2})(t^* - t_{py}^*) + \ln D_0 - (aE^*/T_{py}^{*2}) y^* \end{aligned} \quad (C. 14)$$

$$D_o = D / (b E^* / T_{py}^{*2})$$

Numerical solution shows that s depends only on δ^* and the relation between them was given in Figure C1. For $\delta^* = 0.3$, $s^*(\delta^*) = 0.6$.

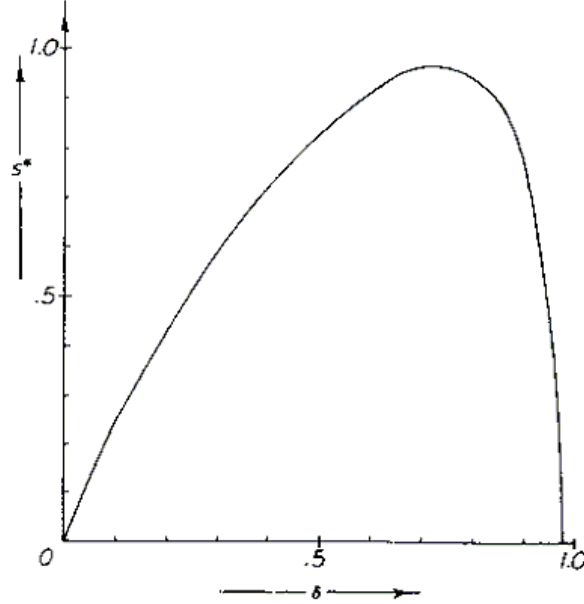


Figure C1 Plot of $s^*(\delta^*)$ versus δ^*

$$m''^* \cong \frac{A^*(1-\delta^*)}{aE^*/T_{py}^{*2}} e^{-E^*/T_{py}^* + (bE^*/T_{py}^{*2})(t^* - t_{py}^*)} \quad (C. 15)$$

$$m''_{\max} = (b/a)(1-\delta^*) \quad (C. 16)$$

The thickness of the pyrolysis zone is given as following:

$$\Delta y^* \cong \frac{3.1}{aE^*/T_{py}^{*2}} \quad (C. 17)$$

For the thin-char stage, following equations can be obtained:

$$\begin{aligned} a_c &= \left(-\frac{\partial T_c^*}{\partial y^*} \right)_{y^*=0, t^*=t_c^*} \quad (C. 18) \\ &= e^{\Gamma^2 t_c^*} \operatorname{erfc}(\Gamma \sqrt{t_c^*}) + \left(\frac{1-\delta}{\delta} \right) a \end{aligned}$$

$$b_c = \left(\frac{\partial T_c^*}{\partial t^*} \right)_{y^*=0, t^*=t_c^*} \quad (C. 19)$$

$$= \frac{1}{\sqrt{\pi t_c^*}} - \Gamma e^{\Gamma^2 t_c^*} \operatorname{erfc}(\Gamma \sqrt{t_c^*}) + \left(\frac{1-\delta}{\delta} \right) b$$

$$m''_{\max} = \left(\frac{J_c^*}{1+J_c^*} \right)^2 \frac{A^*(1-\delta^*)}{(-\partial T^*/\partial y^*)_{t^*=t_c^*}} T_c^{*2} e^{-E^*/T_c^*} \quad (C. 20)$$

where:

$$J_c^* = \frac{4.3}{3.1} \frac{a}{a_c} \left(\frac{T_c^*}{T_{py}^*} \right)^2 \quad (C. 21)$$

For the thick char stage, the reaction is assumed infinitely thin compared to the length scale L . The surface temperature in this stage is assumed close to its maximum value as follows.

$$T_{s,\max}^* = 1 + 1/\Gamma \quad (C. 22)$$

Analysing mass balance across the reaction layer, below equation can be obtained.

$$m''^* = (1-\delta^*) \frac{dy_R^*}{dt^*} = (1-\delta^*) v_R^* \quad (C. 23)$$

where $v_R^* = dy_R^*/dt^*$ is the velocity of the reaction layer.

Since the advance of a constant-temperature front into a solid is proportional to $t^*-0.5$, its rate of advance varies as $t^*-0.5$. Then m''^* is also proportional to $(1-\delta^*)t^*-0.5$. The constant of the proportionality, Ω , is solved by below equation.

$$\text{For small } \Omega \quad \Omega = \frac{\sqrt{\pi\delta^*}}{2} \left(\frac{T_{\max}^* - T_c^*}{T_c^* - 1} \right) \quad (C. 24)$$

Thus,

$$m''^* = \frac{(1-\delta^*)\Omega}{\sqrt{t^*}} \quad (C. 25)$$

For a given set of input value, following parameters have been obtained from Atreya's model, shown in Table C1. The values from numerical calculation are also listed. Excepting the mass flux m''^* , difference between modelling and numerical results is within 20%.

The major calculation results for the mass flux by the given set of inputs were shown in Figure C2.

Table C1 Atreya's modelling results (input: $A^* = 10^{11}$, $E^* = 40$, $\delta^* = 0.3$, $\Gamma = 0.4$)

Quantity	Modelling results	Numerical value	Notes
T_{py}^*	1.5		
t_{py}^*	0.27		
a	0.80		
b	0.76		
t_c^*	0.61	0.7	
m''_{max} (initial pyrolysis)	0.66	0.825	
Δy^*	0.22		
a_c	2.58		$t_c^* = 0.7$ used
b_c	2.16		$t_c^* = 0.7$ used
T_c^*	1.76	1.97	$t_c^* = 0.61$ used
J_c^*	0.74		$T_c^* = 1.97$ used
m''_{max} (thin char)	0.73	0.825	$T_c^* = 1.97$ used
m''^*	$0.2/\sqrt{t^*}$	$0.52/\sqrt{t^*}$	

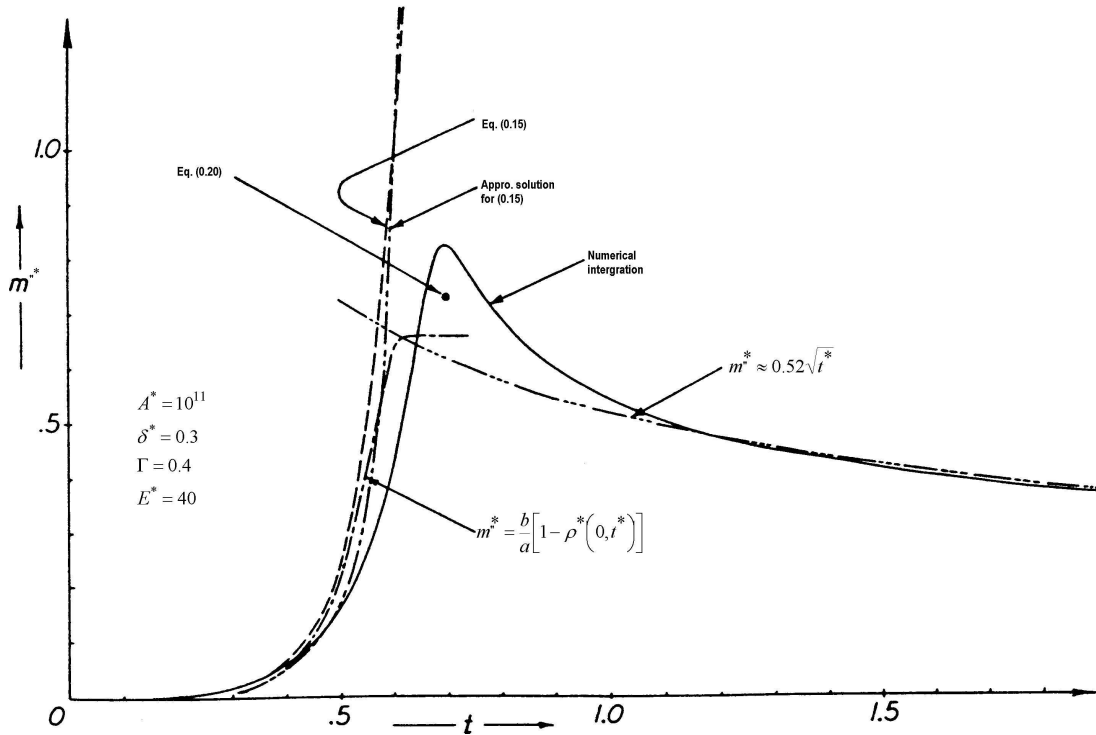


Figure C2 Mass fluxes from Atreya's model

Preparation calculation for one of the testing materials, mountain ash, was shown in Table C2. The analytical calculation results for the mass loss fluxes were given in Chapter 3, Section 3.5.4.

Table C2 Calculation results from applied Atreya's model

Quantity	Modelling Results	Modified Value
T_{py}^*	1.8	
t_{py}^*	0.51	
a	0.65	
b	0.6	
t_c^*	1.91	2.16
m_{max}^{**} (initial pyrolysis)	0.74	0.85
m^{**}	$1.62 \times 10^7 \times e^{-29.7+9.64(t^*-0.5)}$	
Δy^*	0.3	
a_c	2.08	
b_c	1.56	
T_c^*	2.04	2.28
J_c^*	0.53	
m_{max}^{**} (thin char)	0.88	1.02
m^{**}	$0.68/\sqrt{t^*}$	$0.86/\sqrt{t^*}$

REFERENCES

ABCB (1996), "Performance-Based Building Code of Australia", Australian Building Codes Board. Canberra, Australia.

Abu-Zaid, M. (1988), "Effect of water on piloted ignition of cellulosic materials". E. Lansing, MI, Michigan State University.

Agrawal, R. K. (1992), "Analysis of non-isothermal reaction kinetics: Part s. Complex reactions", *Thermochimica Acta*, **203**: 111-125.

Alves, S. S. and J. L. Figueiredo (1989), "A model for pyrolysis of wet wood", *Chemical Engineering Science*, **44**: 2861-2869.

Antal, M. J. and G. Varhegyi (1995), *Ind. Eng. Chem. Res.*, **34(3)**: 703-717.

Arpaci, V. S. and P. S. Larsen (1984), "Convection Heat Transfer", Englewood Cliffs, NJ, Prentice-Hall Inc.

AS/NZS_3837 (1998), "Method of test for heat and smoke release rates for materials and products using an oxygen consumption calorimeter", Standards Australia & Standards New Zealand.

ASTM (1983), "Proposed method for room fire test of wall and ceiling materials and assemblies", *ASTM Annual Book of Standards*, **04.07**: 958-978.

ASTM (1990), "Report to ASTM on Cone Calorimeter Inter-laboratory Trials", Task Group E5.21 T.G. 60.

ASTM_E176 "Standard Terminology of Fire Standards", *Annual Book of ASTM Standard*, ASTM. West Conshohocken, PA., **Vol. 4.07**.

ASTM_E1321-90 (1990), "Standard method for determining material ignition and flame spread properties", ASTM. West Conshohochen, PA.

ASTM_E1354-04 (2004), "Standard test method for heat and visible smoke release rates for materials and products using an oxygen consumption calorimeter", American Society for Testing and Materials. West Conshohocken, PA.

ASTM_E1582 (2000), "Standard Test Method for Rubber-Compositional Analysis by Thermogravimetry (TGA)".

Atreya, A. (1983), "Pyrolysis, ignition and fire spread on horizontal surface of wood". Cambridge, MA, Harvard University.

Atreya, A. (1984), "Pyrolysis, Ignition and Fire Spread on Horizontal Surface of Wood", NBS-GCR-83-449, National Bureau of Standard.

- Atreya, A., C. Carpentier and M. Harkleroad (1986), "Effect of sample orientation on piloted ignition and flame spread", Fire Safety Science - Proc. 1st Intl. Symp., Hemisphere, Washington.
- Babrauskas, V. (1984), "Development of the Cone Calorimeter - A Bench-Scale Heat Release Rate Apparatus Based on Oxygen Consumption", Fire and Materials, **8**: 81-95.
- Babrauskas, V. (1992), "Generation of CO in Bench-Scale Fire Tests and the Prediction for Real-Scale Fires", Fire and Materials Int. Conf., Arlington, VA, Interscience Communications Ltd.
- Babrauskas, V. (1996), "Fire Modelling Tools for FSE: Are They Good Enough?" Journal of Fire Protection Engineering, **8(2)**: 87-96.
- Babrauskas, V. (2001), "Ignition of wood A review of the state of the art", Interflam 2001.
- Babrauskas, V. (2002), "Extended Abstracts and Presentations from the Workshop on Fire Growth and Spread on Objects, March 4-6, 2002, National Institute of Standards and Technology", Workshop on Fire Growth and Spread on Objects, National Institute of Standards and Technology.
- Babrauskas, V., J. Lawson, W. Walton and W. Twilley (1982), "Upholstered furniture heat release rates measured with a furniture calorimeter", NBSIR 82-2604, National Bureau of Standard.
- Babrauskas, V. and R. D. Peacock (1992), "Heat Release Rate: the Single Most Important Variable in Fire Hazard", Fire Safety Journal, **18**: 255-272.
- Baker, R. R. (1978), "Kinetic parameters from the non-isothermal decomposition of a multi-component solid", Thermochemica Acta, **23**: 201-212.
- Bamford, C. H., J. Crank and D. H. Malan (1946), "On combustion of wood", Proc. Cambridge Phil. Soc., **42**: 166-182.
- Barooah, J. N. and V. D. Long (1976), Fuel, **55**: 116.
- Baum, H. R. (2002), "Extended Abstracts and Presentations from the Workshop on Fire Growth and Spread on Objects, March 4-6, 2002, National Institute of Standards and Technology", Workshop on Fire Growth and Spread on Objects, National Institute of Standards and Technology.
- Beard, A. (1992), "Limitations of Computer Models", Fire Safety Journal, **18**: 375-391.
- Beard, A. N. (1997), "Fire models and design", Fire Safety Journal, **28**: 117-138.
- Beck, J. V. and K. J. Arnold (1977), "Parameter estimation in engineering and science", New York, John Wiley & Sons.
- Beck, V. (1998), "CESARE-RISK: a tool for performance-based fire engineering design", 1998 Pacific Rim Conference and Second International Conference on Performance-Based Codes and Fire Safety Design Methods, Maui, Hawaii.

- Beyler, C. (2002), "Flammability Limits of Premixed and Diffusion Flames", The SFPE Handbook of Fire Protection Engineering: 2-173.
- Beyler, C., S. P. Hunt and N. Iqbal (1997), "A computer model of upward flame spread on vertical surface", Fire Safety Science - Proc. 5th Interl. Symp., International Association of Fire Safety Science.
- Beyler, C. L. and M. M. Hirschler (2002), "Thermal Decomposition of Polymer", The SFPE Handbook of Fire Protection Engineering: 1-110.
- Bhargava, A., B. Z. Dlugogorski and E. M. Kennedy (2001), "Emissions from Fires of Wood Chips", Interflam 2001.
- Bilbao, R., J. F. Mastral, M. E. Aldea, J. Ceamanos and J. A. Lana (2001), "Experimental and theoretical study of the ignition and smoldering of wood including convective effects", Combustion and Flame, **126**: 1363-1372.
- Blasi, C. D., S. Crescitelli, G. Russo and A. C. Fernandez-Pello (1989), 2nd Int. Symp. on Fire Safety Science, Hemisphere Pub. Co.
- Bonnefoy, F., P. Gilot and G. Prado (1993), "A three-dimensional model for the determination of kinetic data from the pyrolysis of beech wood", Journal of Analytical and Applied Pyrolysis, **25**: 387-394.
- Bradbury, A. G. W., Y. Sakai and F. Shafizadeh (1979), "A kinetic model for pyrolysis of cellulose", Journal of Appl. Polym. Sci., **23**: 3271-3280.
- Brannigan, V. M. (1999), "Fire Scenarios or Scenario Fires? Can Fire Safety Science Provide the Critical Inputs for Performance Based Fire Safety Analysis?" Fire Safety Science, Proc. 6th Inter. Symp., Poitiers, France, International Association for Fire Safety Science.
- Brauman, S. K. (1988), "Polymer degradation during combustion", Journal of Polymer Science, **26(B)**: 95-105.
- Brown, M. E. (1988), "Introduction to Thermal Analysis: Techniques and Applications", London, New York, Chapman and Hall.
- Bukowski, R. W. and V. Babrauskas (1990), "Developing rational, performance-based fire safety requirements in model building codes", Fire and Materials, **18**: 173-191.
- Burgess, M. J. and R. V. Wheeler (1911), J. Chem. Soc., **99**: 2013.
- Carrasco, F. (1993), "The evaluation of kinetic parameters from thermogravimetric data: comparison between established methods and the general analytical equation", Thermochimica Acta, **213**: 115-134.
- Carslaw, H. S. and J. C. Jaeger (1959), "Combustion of Heat in Solids", London, Oxford University press.
- Chang, T. C., W. S. Shen, Y. S. Chiu and S. Y. Ho (1995), "Thermo-oxidative Degradation of Phosphorus-containing Polyurethane", Polymer Degradation and Stability, **49**: 353-360.

- Chembukulam, S. K., A. S. Dandge, N. L. Kovllur, R. K. Seshagiri and R. Vaidyeswaran (1981), "Smokeless Fuel from Carbonized Sawdust", *Ind. Eng. Chem. Prod. Res. Dev.*, **20**: 714-719.
- Chow, W. K. and R. Yin (2002), "Discussion on Two Plume Formulae with Computational Fluid Dynamics." *Journal of Fire Sciences*, **20**(3).
- Cleary, T. G., T. J. Ohlemiller and K. M. Villa (1992), "Influence of ignition source on the flaming fire hazard of upholstered furniture", NISTIR 4847, National Institute of Standard and Technology.
- Cordero, T., F. Garcia and J. J. Rodriguez (1989), "A Kinetic Study of Holm Oak Wood Pyrolysis from Dynamic and Isothermal TG Experiments", *Thermochimica Acta*, **149**: 225 - 237.
- Cordero, T., J. M. Rodriguez_Maroto, F. Garcia and J. J. Rodriguez (1991), "Thermal decomposition of wood in oxidizing atmosphere", *Thermochimica Acta*, **191**: 161-178.
- Cordero, T., J. M. Rodriguez-Maroto, J. Rodriguez-Mirasol and J. J. Rodriguez (1990), "On the kinetic of thermal decomposition of wood and wood components", *Thermochimica Acta*, **164**: 135-144.
- Cordova, J. L., D. C. Walther, J. L. Torero and A. C. Fernandez-Pello (2001), *Combustion Science and Technology*, **164**: 253.
- Coward, H. F., C. W. Carpenter and W. Payman (1919), *J. Chem. Soc.*, **115**: 27.
- Cox, G. (1994), "The challenge of fire modelling", *Fire Safety Journal*, **23**: 123-132.
- Cox, G., R. Chitty and S. Kumar (1989), "Fire modelling and the King's Cross fire investigation", *Fire Safety Journal*, **15**: 103-106.
- Cox, G. and S. Kumar (2002), "Modeling Enclosure Fires Using CFD", *The SFPE Handbook. Section Three*: 3-194.
- Deepak, D. and D. Drysdale (1983), "Flammability of solids: an apparatus to measure the critical mass flux at firepoint", *Fire Safety Journal*, **5**: 167-169.
- DeHaan, J., "Our Changing World: Fires, Fuels, Investigations and Investigators. Part 1: Furnishings", <http://www.interfire.org/features/ourchangingworld.asp>, InterFire Online.
- Delichatsios, M. A. (1999), "Ignition times for thermally thick and intermediate conditions in flat and cylindrical geometries", 6th International Symposium Fire Safety Science, IAFSS.
- Delichatsios, M. A. (1999), "A new interpretation of data from LIFT (Lateral Ignition and Flame Transport) apparatus and modifications for creeping flame spread", *Interflam '99*.
- Delichatsios, M. A. and K. Saito (1991), "Upward fire spread: Key flammability properties, similarity solutions and flammability indices", *Fire Safety Science - Proceedings of the 3rd International Symposium*.

- Dembsey, N. A., P. J. Pagni and R. B. Williamson (1995), "Compartment fire experiments: comparison with models", *Fire Safety Journal*, **25**: 187-227.
- DiBlasi, C. (1993), *Combustion Science and Technology*, **90**: 315-340.
- DiBlasi, C., B. Carmen and F. Enzo (1999), "Non-isothermal kinetics of wood degradation and combustion", *Interflam'99*.
- Doyle, C. D. (1962), *Applied Polymer Science*, **6**: 639.
- Drysdale, D. (1999), "An Introduction to Fire Dynamics", Suffolk, John Wiley & Sons.
- Drysdale, D. and H. E. Thomson (1989), "Flammability of plastics II: Critical mass flux at the firepoint", *Fire Safety Journal*, **14**: 179-188.
- Durbetaki, P., T. X. Phuoc, M. P. Mathur and J. M. Ekmann (1995), *J. Numeric. Methods in Fluids*, **20**: 507-522.
- Ellis, R. C. (1981), "Building Contents, the Real Fire Problem in the Room", *Building Contents - The Real Fire Problem*. Fall Conference, Philadelphia, PA.
- Fernandez-Pello, A. C. (1977), *Combustion Science and Technology*, **17**: 1.
- Fernandez-Pello, A. C. (1995), "The solid phase", *Combustion Fundamentals of Fire*. G. Cox, Academic Press. **Chapter 2**.
- Fernando, A. E. (2000), "Modelling of Fire Spread and the Growth of Fire in Buildings Using Computational Fluid Dynamics", Centre for Environmental Safety and Risk Engineering, Victoria University of Technology, Australia.
- Flesischmann, C. M. and F. F. Chen (2001), "Radiant Ignition of Upholstered Furniture", *The International Conference on Engineered Fire Protection Design*, San Francisco, CA, SFPE & NIST.
- Floyd, J. E., K. B. McGrattan, S. Hostikka and H. R. Baum (2003), "CFD fire simulation using mixture fraction combustion and finite volume radiative heat transfer", *Journal of Fire Protection Engineering*, **13**: 11-36.
- Flynn, J. H. and I. A. Wall (1966), *J. Res. Nat. Bur. Stand.*, **70A**: 487.
- Forney, G. P. and K. B. McGrattan (2004), "User's Guide for Smokeview Version 4 - A Tool for Visualizing Fire Dynamics Simulation Data", NIST Special Pub. 1017, NIST.
- Fredlund, B. (1988), "A Model for Heat and Mass Transfer in Timber Structures during Fire, A Theoretical, Numerical and Experimental Study", LUTVDG/(TVBB-1003), Dept. of Fire Engineering, Lund University, Sweden.
- Friday, P. and F. W. Mowrer (2001), "Comparison of FDS model predictions with FM/SNL fire test data", NIST GCR 01-810, National Institute of Standards and Technology.
- Friedman, R. (1992), "An International Survey of Computer Models for Fire and Smoke", *Journal of Fire Protection Engineering*, **4**(3): 81-92.

- FTT (1998), "User's Guide for the Cone Calorimeter", CONE WPD, Fire Testing Technology Limited.
- Gijsman, P., J. Hennekens and J. Vincent (1993), "The mechanism of the low-temperature oxidation of polypropylene", *Polymer Degradation and Stability*, **42**: 95-105.
- Goos, A. (1952), "The thermal decomposition of wood", *Wood Chemistry*, **2**.
- Grexa, O., E. Horvathova and A. Osvald (1997), "Cone calorimeter studies of wood species", ISFST '97.
- Grexa, O., M. Janssens, R. White and M. Dietsberger (1996), "Fundamental Thermophysical Properties of Materials Derived from the Cone Calorimeter Measurements", 3rd International Scientific Conference Wood & Fire Safety, The High Tatras Hotel Patria, Slovakia.
- Gullet, B. K. and P. Smith (1987), *Combustion and Flame*, **67**: 143.
- Haessler, W. M. (1974), "The tetrahedron of fire", *The Extinguishment of Fire*. M. A. Quincy, National Fire Protection Association.
- Hakkarainen, T. and M. A. Kokkala (2001), "Application of a one-dimensional thermal flame spread model on predicting the rate of heat release in the SBI test", *Fire and Materials*, **25**: 61-70.
- Hall, G. S., R. G. Saunders, R. T. Allcorn, P. E. Jackman, M. W. Hickey and R. Fitt (1972), "Fire Performance of Timber - A Literature Survey", Timber Research and Development Association.
- Hamins, A., A. Maranghides, K. B. McGrattan, E. Johnsson, T. J. Ohlemiller, M. Donnelly, J. Yang, G. Mulholland, K. Parasad, S. Kukuck, R. Anleitner and T. McAllister (2004), "Report on Experiments to Validate Fire Dynamic and Thermal-Structural Models for Use in the World Trade Center Investigation", NIST Special Publication in preparation, NIST.
- Harada, T. (2001), "Time to ignition, heat release rate and fire endurance time of wood in cone calorimeter test", *Fire and Materials*, **25**: 161-167.
- He, Y. (1996), "Further development and modification of the NRCC fire growth model", CESARE Report IR96-002, CESARE, Victoria University of Technology, Australia.
- He, Y., Y. Jiang, M. Luo, V. Dowling, P. Bowditch and J. Leonard (1999), "Heat release and product yields of polyurethane foams under fabric cover (Abstract)", Interflam '99.
- He, Y., I. Morre, M. Luo and V. Beck (1998), "Doorway Calorimetry for Heat Release Rate Measurement in Building Fires", *Combustion Science and Technology*, **132**: 365-389.
- Heskestad, G. (2002), "Plumes, Flame Height and Air Entrainment", *The SFPE Handbook of Fire Protection Engineering*, 3rd edition, National Fire Protection Association.
- Hietaniemi, J., S. Hostikka and J. Vaari (2004), "FDS Simulation of Fire Spread - Comparison of Model Results with Experimental Data", Technical Report VTT Working Paper 4, VTT Building and Transport.

- Hostikka, S. (2002), "Kinetic Modelling of Wood Pyrolysis in FDS2.2", Workshop on Fire Growth and Spread on Objects, NIST.
- Hostikka, S. (2004), Personal communication, Email.
- Huggett, C. (1980), "Estimation of the rate of heat release by means of oxygen consumption measurements", *Fire and Materials*, **4**: 61-65.
- Ierardi, J. A. and J. R. Barnett (2003), "A quantitative method for calibrating CFD model calculations", CIB-CTBUH International conference on Tall Buildings, International Council for Research and Innovation in Building and Construction (CIB).
- ISO_5660-1 (2002), "Fire tests - Reaction to Fire - Part 1: Rate of heat release from building products (Cone Calorimeter method)", ISO, **Technical Committee ISO/TC 92**.
- ISO_9705 (1993), "Full-scale room fire test for surface products", International Organization for Standardization. Geneva.
- Janssens, M. (1991), "Fundamental thermophysical characteristics of wood and their role in enclosure fire growth". Washington DC, National Forest Products Association.
- Janssens, M. (1992), "Determining flame spread properties from cone calorimeter measurements", *Heat release in fires*. V. Babrauskas and S. J. Grayson. London and New York, Elsevier Applied Science. **1**: 265-281.
- Janssens, M. (1994), "Thermo-physical properties for wood pyrolysis models", Pacific Timber Engineering Conference, Gold Coast, Australia.
- Janssens, M. (2002), "Calorimetry", *The SFPE Handbook of Fire Protection Engineering*, 3rd edition, SFPE. **Section 3/Chapter 2**.
- Janssens, M. L. (2004), "Modeling of the thermal degradation of structural wood members exposed to fires", *Fire and Materials*, **28**: 199-207.
- Janssens, M. L., S. E. Dillon and S. Allwein (2001), "Characterizing the thermal environment of the cone calorimeter for analyzing ignition data of materials", *Interflam 2001*.
- Jones, W. and G. Forney (1990), "A programmer's reference manual for CFAST, the unified model of fire growth and smoke transport", NIST Technical Note 1283, National Institute of Standards and technology.
- Jones, W. W. (1983), "A review of compartment fire models", NBSIR 83-2684, National Bureau of Standards.
- Jones, W. W. (2000), "Modeling Fires - the next generation of tools", 15th Meeting of the UJNR Panel on Fire Research and Safety, NIST.
- Jones, W. W. (2001), "State of the art in zone modeling of fires", 9th International fire Protection Seminar, Munich, Germany.

- Jonsson, R. and O. Pettersson (1985), "Timber Structures and Fire - A Review of the Existing State of Knowledge and Research Requirements", Swedish Council for Building Research.
- Kanury, A. M. (1994), *Combustion Science and Technology*, **97**: 469-491.
- Kanury, A. M. (2002), "Flaming Ignition of Solid Fuels", *The SFPF Handbook of Fire Protection Engineering*, 3rd edition: 2.229-2.245.
- Kanury, M. A. (1995), "Flaming Ignition of Solid Fuels", *The SFPF Handbook of Fire Protection Engineering*: pp 2-190 to 2-204.
- Kanury, M. A. and P. L. Blackshear (1970), "Some considerations pertaining to the problem of wood-burning", *Combustion and Technology*, **1**: 339-356.
- Kashiwagi, T. (1974), *Combustion Science and Technology*, **8**: 225.
- Kashiwagi, T., T. Hirata and J. E. Brown (1985), "Thermal and oxidative degradation of Poly(methyl methacrylate), molecular weight", *Macromolecules*, **18**: 131-138.
- Kashiwagi, T. and H. Nambu (1992), "Globe kinetic constants for thermal oxidative degradation of a cellulosic paper", *Combustion and Flame*, **88**: 345-368.
- Kashiwagi, T. and A. Omori (1988), "Effects of thermal stability and melt viscosity of thermoplastics on piloted ignition", 22nd Symp. Int. Combustion.
- Kashiwagi, T., A. Omori and H. Nanbu (1990), *Combustion and Flame*, **81**: 188-201.
- Kissinger, H. E. (1957), *Analytical Chemistry*, **29**: 1702.
- Klose, W., S. Damm and W. Wiest (2000), "Pyrolysis and activation of different woods - thermal analysis (TG/EGA) and formal kinetics (Oral presentation)", 4th Int. Symp. Catalytic and Thermochemical Conversions of Natural Organic Polymers, Krasnoyarsk.
- Kung, H. C. (1972), "A mathematical model of wood pyrolysis", *Combustion and Flames*, **18**: 185-195.
- Launder, B. E. and D. B. Spalding (1974), "The Numerical Computation of Turbulent Flows", *Computer Methods in Applied Mechanics and Engineering*, **3**: 269-289.
- Lawson, J. R. and T. A. Pinder (2000), "Estimates of Thermal Conductivity for Materials Used in Fire Fighters' Protective Clothing", NISTIR 6512, National Institute of Standards and Technology.
- Lee, C., R. Chaiken and J. M. Singer (1976), "Soot and hydrocarbon formation in a turbulent diffusion flame", 16th Symp. (Int.) Comb.
- Lee, C. K., R. F. Chaiken and J. M. Singer (1977), "Charring in Pyrolysis of Wood in Fires by Laser Simulation", 6th Symp. (Int.) Comb., The Combustion Institute.
- Li, Y. and D. Drysdale (1992), "Measurement of the ignition temperature of wood", *Fire Science and Technology - Proc. 1st Asian Conf. Intl.*, Beijing, Academic Publishers.

- Liu, N. and W. Fan (1998), "Modelling the Thermal Decomposition of Wood and Leaves Under a Nitrogen Atmosphere", *Fire and Materials*, **22**(3): 103-108.
- Liu, N., B. Wang and W. Fan (2003), "Kinetic Compensation Effect in the Thermal Decomposition of Biomass in Air Atmosphere", *Fire Safety Science*, 7th IAFSS, Worcester, MA, IAFSS.
- Liu, N. A. (2000), "Kinetics of thermal decomposition for biomass and relevant kinetic analysis method", *Uni. Sci. Tech. China*.
- Lucon, O. S. (1997), "Preliminary Environmental Performance Analysis of a Small-scale Combined Heat and Power System Attached to a Wood Chips Gasification Unit", Department of Chemical and Process Engineering, University of Newcastle.
- Luo, M. and V. R. Beck (1996), "Effects of Air-handling System on Fire Spread in a Full-scale Building", 6th Australian Heat and Mass Transfer Conference.
- Luo, M. and Y. He (1997), "Kinetics of pyrolysis and combustion of polyurethane foams under fire conditions", Fifth Inter. Symp. Fire Safety Science, Tsukuba, Japan.
- Lyon, R. E. (2004), "Fire Safety", Highlights 2004, Federal Aviation Administration, U.S. Department of Transportation.
- Lyon, R. E. and M. L. Janssens (2005), "Polymer Flammability", DOT/FAA/AR-05/14, Federal Aviation Administration, U.S. Department of Transportation.
- Martin, S. (1965), "Diffusion-controlled Ignition of Cellulosic Materials", 10th Symp. (Inter.) on Comb., The Combustion Institute.
- Martin, S. (1975), "Characterization of the Stanford Research Institute Large-Scale Heat-Release Rate Calorimeter", NBS-GCR 76-54, National Bureau of Standards.
- McGrattan, K. and G. Forney (2005), "Fire Dynamics Simulator (Version 4) User's Guide", NIST Special Publication 1019, National Institute of Standard and Technology.
- McGrattan, K. B. (2004), Personal communication, Conversation.
- McGrattan, K. B. (2004), "Fire Dynamics Simulator (Version 4) Technical Reference Guide", NIST Special Publication 1018, Fire Research Division, Building and Fire Research Laboratory, NIST.
- McGrattan, K. B., H. R. Baum and R. G. Rehm (1998), "Large Eddy Simulations of Smoke Movement", *Fire Safety Journal*, **30**: 161-178.
- McGrattan, K. B., H. R. Baum, R. G. Rehm, A. Hamins and G. P. Forney (2000), "Fire Dynamics Simulator, Technical Reference Guide", Technical Report NISTIR 6467, National Institute of Standards and Technology.
- Messerschmidt, B., P. V. Hees and U. Wickstrom (1999), "Prediction of SBI (Single Burning Item) test results by means of cone calorimeter test results", *Interflam '99*.

- Mierlo, R. v. (1997), "SBI Round-Robin: general information", TNO Building and Construction Research.
- Mierlo, R. v. (1998), "Development of the SBI test method (Volume 1)", TNO-report 98-CVB-R1067, TNO Building and Construction Research.
- Mikkola, E. (1991), Fire Safety Science - 3rd Int. Symp.
- Mitler, H. E. (1985), "The HARVARD fire model", Journal of Fire Safety, **9**: 7-16.
- Mitler, H. E. and J. A. Rockett (1987), "Users guide to FIRST", NBSIR 87-3595, National Bureau of Standards.
- Moghtaderi, B. (2001), "Pyrolysis of Char Forming Solid Fuels: A Critical Review of the Mathematical Modelling Techniques", 5th AOSFST, Newcastle, Australia.
- Moghtaderi, B., B. Z. Dlugogorski, E. M. Kennedy and D. F. Fletcher (1998), "Effects of the structural properties of solid fuels on their re-ignition characteristics", Fire and Materials, **22**: 155-165.
- Moghtaderi, B., V. Novozhilov, D. F. Fletcher and J. H. Kent (1997), "An integral model for the transient pyrolysis of solid materials", Fire and Materials, **21**(1): 7-16.
- Moghtaderi, B., V. Novozhilov, D. F. Fletcher and J. H. Kent (1997), "A new correlation for bench-scale piloted ignition data of wood", Journal of Fire Safety, **29**: 41-59.
- Mukaro, R., M. Gasseller, C. Kufazvinei, L. Olumekor and B. M. Tael (2003), "Microcontroller-based Multi-sensor apparatus for temperature control and thermal conductivity measurement", Measurement Science and Technology, **14**: N45-N49.
- Niioka, T. (1981), "Gas-phase ignition of a solid fuel in a hot stagnation-point flow", 18th Symp. Int. Combust.
- Nurbakhsh, S. (1989), "Thermal decomposition of charring materials". E. Lansing, MI, Michigan University.
- Ohlemiller, T. J. and J. R. Shields (1995), "Behavior of mock-ups in the California Technical Bulletin 133 test protocol: fabric and barrier effects", NISTIR 5653, National Institute of Standard and Technology.
- Ohlemiller, T. J. and M. Summerfield (1971), 13th Symp. Int. Combust.
- Omrane, A., F. Ossler, M. Alden, U. Goransson and G. Holmstedt (2003), "Surface temperature measurement of flame spread using thermographic phosphors", Fire Safety Science - Proceedings of the 7th International Symposium.
- Ozawa, T. (1970), Journal of Thermal Analysis, **2**: 301.
- Pape, P., T. E. Waterman and T. V. Eichler (1981), "Development of a fire in a room from ignition to full room involvement - fires", NBS-GCR-81-301, National Bureau of Standards.

- Parker, W. and M. Long (1972), "Development of a Heat Release Rate Calorimeter at NBS", ASTM.
- Parker, W. J. (1985), "Development of a model for the heat release rate of wood - A status report", NBSIR 85-3163, National Bureau of Standards.
- Parker, W. J. (1985), "Prediction of heat release rate of wood", Fire Safety Science - 1st Int. Symp.
- Parker, W. J. (1988), "Determination of input data for a model of the heat release rate of wood", Mathematical modeling of fires. J. R. Meheffey. Philadelphia, PA, ASTM: 105-115.
- Parker, W. J. (1989), "Prediction of the heat release rate of Douglas Fir", 2nd Int. Symp. Fire Safety Science.
- Parker, W. J. (1992), "Prediction of the heat release rate from basic measurements", Heat Release in Fires. V. Babrauskas and S. J. Grayson. London and New York, Elsevier Applied Science. **2**: 333-356.
- Parker, W. J. and S. L. LeVan (1989), "Kinetic properties of the components of Douglas-fir and the heat of combustion of their volatile pyrolysis products", Wood and Fiber Science, **21**(3): 289-305.
- Peacock, R. D., G. P. Forney, P. Reneke, R. Portier and W. W. Jones (1993), "CFAST, the Consolidated Model of Fire Growth and Smoke Transport", NIST Tech. Note 1299, National Institute of Standards and Technology.
- Peacock, R. D., W. W. Jones, R. W. Bukowski and C. L. Forney (1991), "Technical Reference Guide for the HAZARD I Fire Hazard Assessment Method", NIST Hbbk 146, National Institute of Standards and Technology.
- Perkin_Elemer (1991), "TGA 7 Thermogravimetric Analyzer Operator's Manual", Perkin Elemer Corporation.
- prEN_13823 (2002), "Reaction to fire tests for building products - Building products excluding floorings exposed to the thermal attack by a single burning item", European Committee for Standardization. Brussels.
- Quintiere, J. G. (1977), "Growth of fires in building compartments", ASTM STP 614, American Society for Testing and Materials.
- Quintiere, J. G. (1981), "A simplified theory for generalized results from a radiant panel rate of flame spread apparatus (LIFT)", Fire and Materials, **5**(2): 52-60.
- Quintiere, J. G. (1988), "The application of flame spread theory to predict material performance", Journal of Research of the NBS, **93**(1): 61-70.
- Quintiere, J. G. (1993), "A simulation model for fire growth on materials subject to a room-corner test", Fire Safety Journal, **20**: 313-339.
- Quintiere, J. G. (1995), "Surface Flame Spread", SFPE Handbook. **Section 2, Chapter 14**: 2-205.

- Quintiere, J. G. (2002), "Compartment fire modeling", The SFPE Handbook of Fire Protection Engineering, 3rd edition. **Section 3, Chapter 5:** 3-125.
- Quintiere, J. G. and M. Harkleroad (1984), "New Concepts for Measuring Flame Spread Properties", NBSIR 84-2943, US. Department of Commerce.
- Quintiere, J. G. and B. Rhodes (1994), "Fire growth models for materials", NIST-GCR-94-647, National Institute of Standards and Technology.
- Raithby, G. D. and E. H. Chui (1990), "A Finite-Volume Method for Predicting Radiant Heat Transfer in Enclosures with Participating Media", Journal of Heat Transfer, **112**(2): 415-423.
- Ramiah, M. V. (1970), "Thermogravimetric and differential thermal analysis of cellulose, hemicellulose, and lignin", Journal of Appl. Polym. Sci., **14**: 1323-1337.
- Rasbash, D. J., D. D. Drysdale and D. Deepak (1986), "Critical heat and mass transfer at pilot ignition of a material", Fire Safety Journal, **10**: 1-10.
- Richardson, J. K. (1994), "Moving towards performance-based codes", NFPA Journal, **88**(May/June): 70-78.
- Ritchie, S. J., K. D. Steckler, A. Hamins, T. G. Cleary and J. C. Kashiwagi (1997), "Effect of Sample Size on the Heat Release Rate of Charring Materials", Fire Safety Science. Proc. 5th Inter. Symp., Melbourne, Australia.
- Roberts, A. F. (1970), "A Review of Kinetics Data for the Pyrolysis of Wood and Related Substances", Combustion and Flame, **14**: 261-272.
- Sauer, F. (1956), "The charring of wood during exposure to thermal radiation: correlation analysis for semi-infinite solids", Intrim, T. AFSWP-868, Forest Service.
- Schaffer, E. L. (1967), "Charring rate of selected woods - transverse to grain", Research Paper FPL 69, U.S. Department of Agriculture, Forest Products Laboratory.
- Schneider, H. A. (1992), "Thermogravimetric kinetics of polymer degradation: science or fiction?" Polymer Engineering and Science, **32**(17): 1309-1315.
- Schultz, T. P., G. D. McGinnis and D. Nicholas, Eds. (1989), "Effect of crystallinity and additives on the thermal degradation of cellulose", Fire and Polymers Hazard Identification and Prevention, American Chemical Society.
- Seungdo, K. and J. K. Park (1995), "Characterization of thermal reaction by peak temperature and height of DTG curves", Thermochemica Acta, **264**: 137-156.
- SFPE (2002), "SFPE Handbook of Fire Protection Engineering".
- Simms, D. L. (1963), "On the pilot ignition of wood by radiation", Combustion and Flame, **7**: 253.
- Smith, E. (1972), "Heat Release Rate of Building Materials", ASTM.

- Snell, J. E., V. Babrauskas and A. J. Fowell (1993), "Elements of a framework for fire safety engineering", Interflam '93, London, Interscience Communications Ltd.
- Spearpoint, M. J. and J. G. Quintiere (2000), "Predicting the burning of wood using an integral model", *Combustion and Flame*, **123**: 308-324.
- Spearpoint, M. J. and J. G. Quintiere (2001), "Predicting the Piloted Ignition of Wood in the Cone Calorimeter Using an Integral Model - Effect of Species, Grain Orientation and Heat Flux", *Fire Safety Journal*, **36**: pp 391 - 415.
- Staggs, J. E. J. (1999), "Modelling thermal degradation of polymers using single-step first-order kinetics", *Fire Safety Journal*, **32**: 17-34.
- Staggs, J. E. J. and R. H. Whiteley (1999), "Modelling the combustion of solid-phase fuels in cone calorimeter experiments", *Fire and Materials*, **23**: 63-69.
- Stanmore, B. R. (1991), "Use of the Differential Thermal Gravimetric Analyser for Carbon/Oxygen Reactivity Measurement", *Fuel*, **70**: 1485-1487.
- Steckler, K. D., A. Hamins and T. Kashiwagi (1994), "A model for the burning of a horizontal slab of wood: status report", NISTIR 5499, NIST.
- Stroup, D. W. (2002), "Using Field Modeling to Simulate Enclosure Fires", Boston, MA, Society of Fire Protection Engineers.
- Tanaka, T. (1983), "A model of Multicompartment Fire Spread", NBSIR 83-2718, National Bureau of Standards.
- Tang, W. K. (1972), "Forest Products", *Differential Thermal Analysis*. R. C. Mackenzie, Academic Press, New York. **2**: 523-553.
- Tewarson, A. (1982), "Experimental evaluation of flammability parameters of polymeric materials", *Flame retardant polymeric materials*. E. M. Pearce. New York, London, Plenum Press. **3**: 97-153.
- Tewarson, A., W. Chin and R. Shuford (1999), "An exploratory study on a high-energy flux (HEF) calorimeter to characterize flammability of advanced engineered polymers: phase 1 - ignition and mass loss rate", ARL-TR-2102.
- Thompson, N. and E. Cousins (1959), "The FM Construction Materials Calorimeter", *NFPA Quarterly*, **52**: 186-192.
- Thomson, H. E. and D. D. Drysdale (1989), "Flammability of plastics II Critical mass flux at the firepoint", *Fire Safety Journal*, **14**(3): 179-188.
- Thornton, W. (1917), "The Relation of Oxygen to the Heat of Combustion of Organic Compounds", *Philosophical Magazine and J. of Science*, **33**.
- T'ien, J. S. (2002), "Detailed modeling of flame spread processes over solid: progress and prospect", Workshop on Fire Growth and Spread on Objects, March 4-6, 2002, National Institute of Standards and Technology.

- Tran, H. C. (1992), "Experimental data on wood materials", Heat release in fires. V. Babrauskas and S. J. Grayson. New York, Elsevier Applied Science. **Chapter 11**.
- Tsai, T., M. Li, I. Shih, R. Jih and S. Wong (2001), "Experimental and numerical study of autoignition and pilot ignition of PMMA plates in a cone calorimeter", *Combustion and Flame*, **124**: 466-480.
- Tzeng, L., A. Atreya and I. S. Wichman (1990), "A one-dimensional model of piloted ignition", *Combustion and Flame*, **80**: 94-107.
- Urbas, J. and W. J. Parker (1993), "Surface temperature measurements on burning wood specimens in the cone calorimeter and the effect of grain orientation", *Fire and Materials*, **17**: 205-208.
- Urbas, J. and W. J. Parker (2005), "Surface Temperature Measurement in a Fire Environment Using an Infrared Pyrometer", *Fire Safety Science - Proceedings of the 8th International Symposium*.
- Urbas, J., W. J. Parker and G. E. Luebbers (2004), "Surface temperature measurements on burning materials using an infrared pyrometer: accounting for emissivity and reflection of external radiation", *Fire and Materials*, **28**: 33-53.
- Vervisch, L. and T. Poinso (1998), "Direct numerical simulation of non-premixed turbulent flames", *Ann. Rev. Fluid Mech.*, **30**: 655.
- Vovelle, C., R. Akrich and J. L. Delfau (1984), 20th Smpy. (Int.) Comb.
- VTT (1997), "Development of the Single Burning Item test - results of the SBI Round Robin tests", VTT Building Technology, Fire Technology.
- Vyazovkin, S. and C. A. Wight (1998), "Isothermal and non-isothermal kinetics of thermally stimulated reactions of solids", *International Reviews in Physical Chemistry*, **17**(3): 407-433.
- Wagoner, C. L. and A. F. Duzy (1976), "Burning Profiles of Solid Fuels", ASME Paper 67-WA/FU-4, ASME.
- Walther, D. C., R. A. Anthenien and A. C. Fernandez-Pello (2000), "Smolder ignition of polyurethane foam: effect of oxygen concentration", *Fire Safety Journal*(34): 343-359.
- Walton, W. D. (1985), "ASET-B A room fire program for personal computers", NBSIR 85-3144, National Bureau of Standards.
- Wang, G. G. and J. T. Yang (1992), "Convective thermal ignition of an individual polymethylmethacrylate particle", *Journal of Thermophysics and Heat Transfer*, **6**(2): 326-332.
- Watt, S. D., J. E. J. Staggs, A. C. McIntosh and J. Brindley (2001), "A theoretical explanation of the influence of char formation on the ignition of polymers", *Fire Safety Journal*, **36**: 421-436.

- White, R. and E. Nordheim (1992), "Charring rate of wood for ASTM E119 exposure", *Fire Technology*, **28**: 5-30.
- Wichman, I. S. (1986), *Combustion and Flame*, **63**: 217-229.
- Williams, F. A. (1976), "Mechanisms of fire spread", 16th Symp. Int. Combustion.
- Williams, F. A. (1985), "Combustion Theory", The Benjamin/Cummings Co. Inc.
- WPI, "Cone Calorimeter Data", <http://www.wpi.edu/Academics/Depts/Fire/Lab/Cone/Data>, Accessed May 1, 2005, Fire Protection Engineering & Center for Firesafety Studies.
- Xue, H., J. C. Ho and Y. M. Cheng (2001), "Comparison of different combustion models in enclosure fire simulation", *Fire Safety Journal*, **36**: 37-54.
- Yang, L., X. Chen, X. Zhou and W. Fan (2003), "The pyrolysis and ignition of charring materials under an external heat flux", *Combustion and Flame*, **133**: 407-413.
- Yao, Y. B., C. Ryu, D. Poole, P. Gilbert, A. Khor, V. Sharifi and J. Swithenbank, "Mathematical Modelling of Biomass Pyrolysis and Gasification in Lab-scale Packed-bed Systems", Mathematical Modelling Workshop, SUWIC, Sheffield University.
- Yuen, R., R. Casey, G. d. V. Davis, E. Leonardi, G. H. Yeoh, V. Chandrasekaran and S. J. Grubits (1997), "Three-dimensional mathematical model for the pyrolysis of wet wood", *Fire Safety Science - Proc. 5th Interl. Symp.*, International Association of Fire Safety Science.
- Zhou, X., K. H. Luo and J. J. R. Williams (2000), "Dynamic behaviour in reacting plumes", 28th Symposium (International) on Combustion, Pittsburgh, Combustion Institute.
- Zhou, Y. Y., D. C. Walther and A. C. Fernandez-Pello (2002), "Numerical Analysis of Piloted Ignition of Polymeric Materials", *Combustion and Flame*, **131**: 147-158.